



Aptamer-mediated transport of microRNAs into cells of the cardiovascular system

Dissertation

zur Erlangung des Doktorgrades

der Naturwissenschaften

vorgelegt beim Fachbereich Biowissenschaften (FB15)

der Johann Wolfgang Goethe-Universität

in Frankfurt am Main

von

Jan-Hendrik Rohde

aus Leer, Deutschland

Frankfurt 2016

(D 30)

vom Fachbereich Biowissenschaften (FB15) der
Johann Wolfgang Goethe-Universität als Dissertation angenommen.

Dekan: Prof. Dr. Meike Piepenbring
Gutachter: Prof. Dr. Stefanie Dimmeler
Prof. Dr. Beatrix Süß

Datum der Disputation: 17.08.2016

Table of Contents

1. Introduction.....	7
1.1 The mammalian cardiovascular system	7
1.2 Cardiovascular disease	10
1.2.1 Atherosclerosis	11
1.2.2 Cardiac remodeling after acute myocardial infarction	12
1.3 MicroRNAs.....	18
1.3.1 Biogenesis and function	19
1.3.2 MicroRNAs in the cardiovascular system	22
1.3.3 MiR-126	23
1.3.4 miRs in reprogramming.....	31
1.4 Aptamers	32
1.4.1 SELEX	33
1.4.2 Delivery of RNAi by aptamers.....	35
1.4.3 Chemical modifications of aptamers.....	36
1.5 Objective of the thesis.....	39
2. Material and Methods.....	40
2.1 Isolation of adult murine cardiac fibroblasts	40
2.2 Cell culture ³⁸⁹	41
2.3 Aptamer acquisition ³⁸⁹	42
2.4 Gel purification of Pool DNA ³⁸⁹	42
2.5 RNA extraction using trizol ³⁸⁹	43
2.6 Ethanol precipitation of DNA/RNA ³⁸⁹	43
2.7 <i>In vitro</i> transcription of DNA using T7 Durascribe kit ³⁸⁹	43
2.8 Aptamer and chimera construct folding ³⁸⁹	44
2.9 Cell treatment with aptamers and chimeras to harvest RNA ³⁸⁹	44
2.10 RNA samples of microRNA overexpression using liposomal transfection ³⁸⁹	45
2.11 Isolation of total and internal RNA using QIAgen kit and qPCR analysis ³⁸⁹	45
2.12 Aptamer visualization ³⁸⁹	45
2.13 VCAM-1 Western Blot ³⁸⁹	46
2.14 HUVEC Spheroid Assay ³⁸⁹	46
2.15 Cell counting kit 8 (Cck8) Proliferation assay ³⁸⁹	47
2.16 HUVEC recruitment assay ³⁸⁹	47
2.17 Reprogramming using a microRNA cocktail	47
2.18 SELEX Pool amplification	48

2.19 Cell SELEX for RNA pool with 20 randomized nucleotides	49
2.20 Cell SELEX for RNA pool with 52 randomized nucleotides	52
2.21 Bioinformatics analysis of SELEX round 5-7	53
2.22 Testing candidate AMCF aptamers	53
2.23 Statistics and figures.....	54
3 Material	55
3.1 Consumables	55
3.2 Equipment	56
3.3 Chemicals and reagents.....	58
3.4 Kits	61
3.5 Enzymes.....	61
3.6 Cell culture solutions and supplements	62
3.7 Antibodies.....	63
3.8 Custom Primers	64
3.9 Taqman primers	65
3.10 microRNA mimics	65
3.11 customized oligonucleotides and libraries.....	66
3.12 Primary cells and cell lines.....	68
3.13 software.....	68
4. Results	69
4.1 Analysis of candidate aptamers	69
4.1.1 Internalization of the transferrin receptor aptamer (TRA) and the general internalizing RNA motif (GIRM) detected via qPCR ³⁸⁹	69
4.1.2 Fluorescent microscopy analysis of TRA and GIRM internalization ³⁸⁹	72
4.1.3 Fluorescent microscopy analysis of TRA localization	72
4.1.4 Analysis of transferrin receptor expression	74
4.2 Chimeras of transferrin receptor aptamer and microRNA-126	74
4.2.1 Design of TRA-miR-126 chimeras ³⁸⁹	74
4.2.2 Comparison of TRA and TRA-stick constructs	77
4.2.3 Internalization of the chimeras into ECs detected via qPCR ³⁸⁹	77
4.2.4 miR-126 delivery by the chimeras ³⁸⁹	79
4.2.5 Effect of chimeras on VCAM-1 expression in HUVEC ³⁸⁹	81
4.2.6 Effect of Chimeras on EC spheroid sprouting assay ³⁸⁹	82
4.2.7 Internalization of chimeras into two breast cancer cell lines detected via qPCR ³⁸⁹	84
4.2.8 Effect of Chimeras on breast cancer viability ³⁸⁹	85

4.2.9 Effect of Chimeras on EC recruitment by breast cancer cells ³⁸⁹	86
4.3 Analysis of adult murine cardiac fibroblasts in the context of candidate aptamers, chimeras and reprogramming	87
4.3.1 Isolation of adult murine cardiac fibroblasts	87
4.3.2 Internalization of GIRM and TRA into adult murine cardiac fibroblasts	90
4.3.3 Internalization of chimera 4 into AMCF and effect on miR-1a-3p ³⁸⁹	91
4.3.4 Reprogramming of cardiac fibroblasts	93
4.4 Cell-SELEX for aptamers binding to adult murine cardiac fibroblasts.....	95
4.4.1 Using a pool containing 20 randomized nucleotides	95
4.4.2 Using a pool 52 randomized nucleotides	97
4.4.3 Bioinformatics Analysis	99
4.4.4 Analysis of candidate aptamers via qPCR.....	106
5. Discussion	110
5.1 Candidate aptamers internalize into all cell types tested ³⁸⁹	110
5.1.1 Method of GIRM internalization	111
5.1.2 TRA internalization and possible mechanism.....	111
5.1.3 Choosing TRA for further experiments ³⁸⁹	112
5.2 Design and effects of Chimeras of TRA and miR-126.....	113
5.2.1 Chimera design ³⁸⁹	113
5.2.2 Internalization of chimeras into HUVEC and MEC ³⁸⁹	113
5.2.3 Increase of miR levels after chimera treatment in EC ³⁸⁹	114
5.2.4 Functional effects of the chimeras in HUVEC ³⁸⁹	115
5.2.5 Ch3 in breast cancer cell lines ³⁸⁹	117
5.2.6 A chimera of TRA and miR-1 ³⁸⁹	120
5.2.7 Implications for therapy and experimental work ³⁸⁹	120
5.3 Inefficient reprogramming of AMCF using a microRNA cocktail.....	122
5.3.1 Differences in cell types used for reprogramming	122
5.3.2 Possible methodological inaccuracies.....	124
5.3.3 Consideration for human use	124
5.4 Cell SELEX to select aptamers binding to AMCF.....	124
5.4.1 Performance of the aptamer pool with 20 variable nucleotides	125
5.4.2 SELEX using an aptamer pool with 52 variable nucleotides.....	125
5.4.3 Evaluation of the 10 AMCF aptamer candidates.....	125
6. Conclusion and Outlook	127
7. Zusammenfassung.....	129

8. References	135
9. Glossary	159
10. Eidesstattliche Erklärung	162
11. Copyright permission	163
12. Acknowledgements	Error! Bookmark not defined.
13. Curriculum Vitae	Error! Bookmark not defined.

1. Introduction

1.1 The mammalian cardiovascular system

In the mammalian cardiovascular system the heart pumps blood through the vessel network all throughout the body. This circulation provides the means of essential and efficient distribution of oxygen, nutrients and other metabolites while allowing removal of carbon dioxide and other waste products and providing access of the immune system to all tissues. The circulation can be split into the pulmonary and systemic circulation. In the pulmonary circulation blood enters the heart from the veins of the body and is pumped by the right ventricle through the lungs, saturating it with oxygen. In the systemic circulation this oxygen-rich blood then enters the left ventricle and is pumped through the arteries into the body. Nutrients are absorbed and waste products are excreted in specialized organs in the systemic circulation through the smallest vessels named capillaries, which form the link between veins and arteries. Capillaries consist of a single layer of endothelial cells (EC) above a basement membrane of extracellular matrix (ECM), supported by pericytes. Larger vessels contain three distinct layers: the tunica intima, media and externa. The tunica intima contains a highly functional layer of EC deposited on ECM. The tunica media is made of elastic fibers and vascular smooth muscle cells (VSMC), which can contract and dilate to increase the resistance of the vessel to blood flow. This is a major regulator of the blood pressure in the vascular system and can mediate distribution of blood through the body. The tunica externa contains fibroblasts, pericytes and components of the ECM; it serves to stabilize the vessel and connect it to the surrounding tissue ¹.

Ischemia is the result of a failure of efficient perfusion of blood in parts of the body and belongs to the cardiovascular diseases (CVD). The lack of nutrients and oxygen in concert with the accumulation of waste products leads the onset of cell death and tissue damage; depending on the organ, this damage may be irreversible. After ischemia or in case of wound regeneration, new vessels have to be formed to ensure blood supply. There are three major mechanisms by which vessels can be formed: Vasculogenesis, arteriogenesis and angiogenesis (Figure 1.1) ². Vasculogenesis takes place mainly during embryonic development and involves *de novo* formation of vessels from progenitor cells ^{2,3}. Arteriogenesis is enlargement of preexisting smaller vessels to compensate for the occlusion

or degeneration of larger vessels ⁴. The main mechanism by which blood supply is re-established after ischemia is angiogenesis, discussed in more detail in the next chapter.

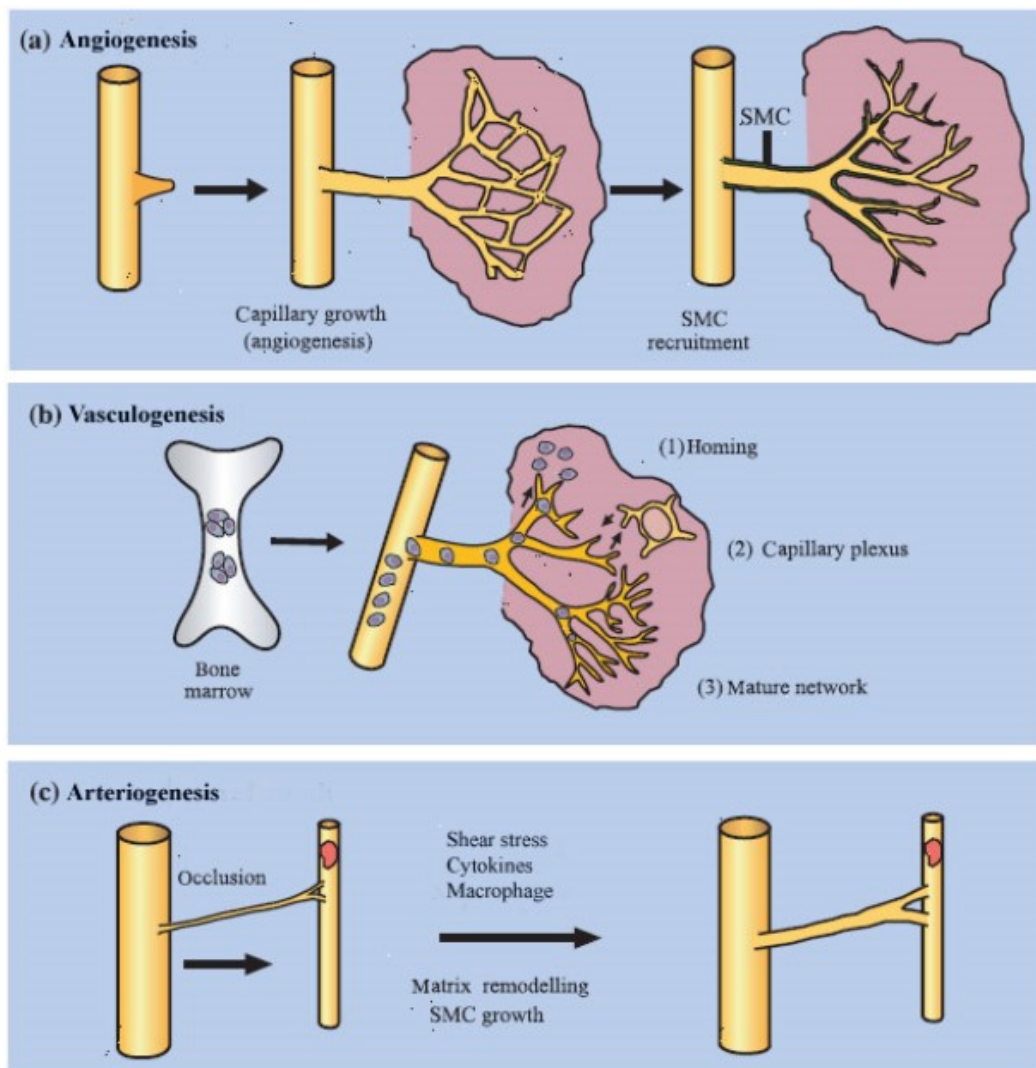


Figure 1.1. Mechanisms of vessel growth in the adult

Vessel formation can be classified into three modes: angiogenesis, vasculogenesis and arteriogenesis. Angiogenesis involves proliferation and migration of EC from pre-existing vessels into avascular regions. The vessels mature upon recruitment of mural cells. b) Vasculogenesis is the process of de novo formation of vessels from progenitor cells during development. In adult, precursor cells released from bone marrow integrate into preexisting vessels and contribute to vessel growth. c) Arteriogenesis describes the formation of collateral vessel growth in the event of vessel occlusion of a main vessel. SMC: smooth muscle cell. Figure from 2

1.1.1 Angiogenesis

Angiogenesis is signified by sprouting of vessels from pre-existing ones, which plays a major role in the later stages of development and in adult blood vessel formation. In healthy

vessels EC are in a quiescent stage, but they retain the ability to quickly adapt to changes in the environment. EC can initiate sprouting angiogenesis in response to angiogenic cues such as vascular endothelial growth factor (VEGF) or hypoxia (Figure 1.1.1). In adults, this mainly happens to promote wound healing or remodeling after ischemia, but it can also have negative consequences for example during tumor angiogenesis⁵. An impairment of angiogenesis has been implicated to play a major role in several CVD and the metabolic syndrome^{6,7}. Despite the large insight gained about the angiogenic process, it is an intricate process mediated by a plethora of factors and signaling pathways and still a subject of ongoing research⁸. During the initiation of sprouting angiogenesis, the major factor influencing the selection of tip and stalk cells is VEGF and its receptors VEGFR1 and VEGFR2 as well as the Notch signaling pathway. Upon detecting a VEGF gradient or hypoxia, tip cells begin to form filopodia and increase expression of VEGFR2 and Delta like 4, which in turn induces neighboring EC to adopt a stalk cell phenotype by increasing notch signaling⁹⁻¹². Tip cells express receptors which allow them to respond to attractive and repulsive cues to guide the sprouting vessel towards the area of ischemia¹³⁻¹⁵. The stalk cells meanwhile proliferate to elongate the sprout, interconnect with each other, secrete ECM components and ultimately form the lumen of the vessel, which allows blood flow⁸. The tip and stalk cell phenotypes are notably plastic and EC may transition between them during the sprouting process^{9,16}. Eventually tip cells of different sprouts meet and merge, forming cellular junctions between them. The newly formed vessels then mature, which involves the deposition of mural cells, including pericytes, and deposition of ECM to form a basal membrane^{17,18}. The newly formed vessel also adapts to the surrounding tissue to meet its homeostatic demands¹⁹. Another crucial step in the maturation of the vessels is the initiation of blood flow and resulting shear stress, which induces a more quiescent phenotype in EC better suited to a stable blood vessel^{14,20,21}.

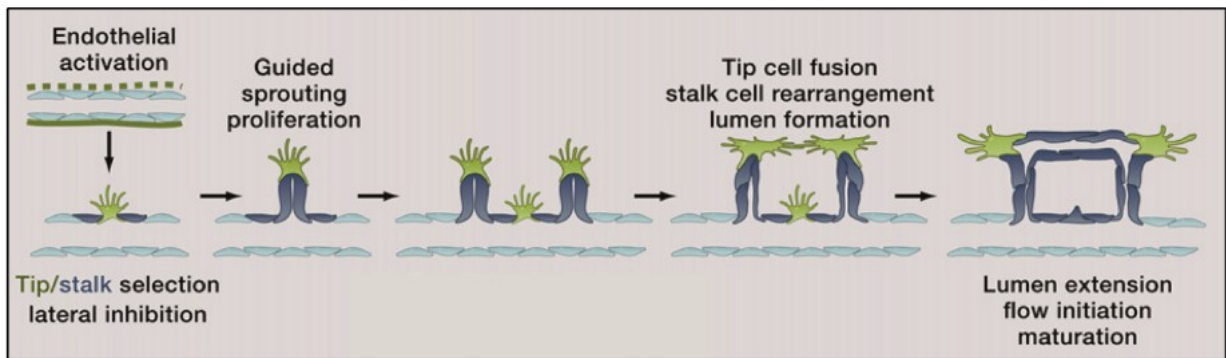


Figure 1.1.1 Current model of vessel sprouting

First tip/stalk cells are selected. The tip cell navigates towards the angiogenic stimulus, guiding the stalk cell proliferation and the direction of sprouting. Neighboring sprouts then coordinate their branching. Stalk cells elongate and re-arrange to form the lumen of the new vessel. Finally, the vessel can mature if it is properly perfused by blood. Adapted from ⁸

1.2 Cardiovascular disease

CVD, especially ischemic heart diseases, are still the most common cause of death worldwide, despite a drastic improvement in treatment options ²² (Figure 1.2). In the USA more than one third adults are estimated to suffer from CVD and a third of all deaths are attributed to CVD ²³. The incidence of CVD is also rising in developing countries however; in India for example 27% of recent premature deaths are reportedly being caused by CVD ²⁴. Two of the most common and devastating vascular disorders are acute myocardial infarction (AMI) and atherosclerosis.

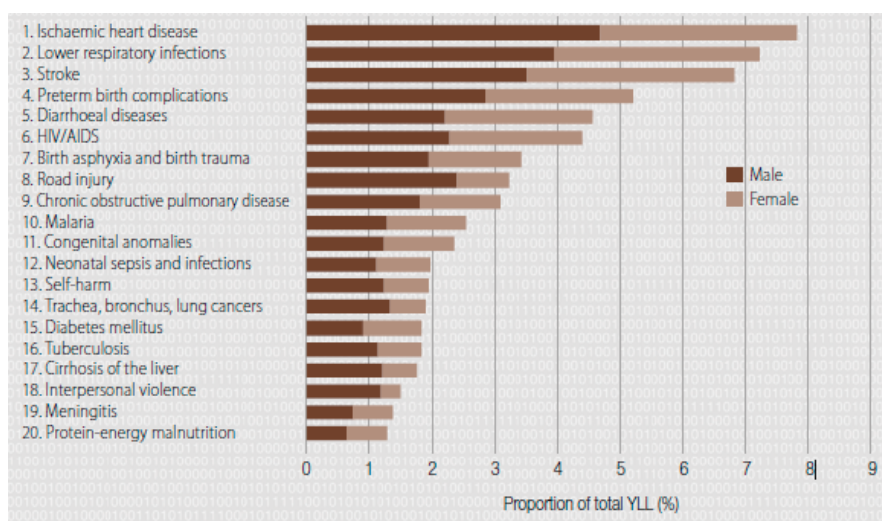


Figure 1.2 The 20 leading causes of yearly loss of life in the world at 2012 according to the WHO ²²

1.2.1 Atherosclerosis

Atherosclerosis is signified by pathological thickening in the intima of blood vessels. It starts with asymptomatic fatty streak lesions during the first decades of life²⁵ which accumulate cholesterol containing low-density lipid particles (LDL) and grow in size, especially in areas of disturbed blood flow (Figure 1.2.1)^{26,27}. Due to compensatory remodeling of the vessel growing lesions may remain asymptomatic for years²⁸. The LDL retained in atherosclerotic lesions are prone to oxidation²⁹, which can be counteracted by high-density lipoproteins³⁰. If excess oxidation of LDL occurs, the overlying EC are activated and begin to express surface receptors and cytokines, for example vascular cell adhesion molecule 1 (VCAM-1), to attract leukocytes, including monocytes. Monocytes transmigrate into the intima and differentiate into macrophages which absorb the oxidized LDL, becoming foam cells in the process^{25,31}. Foam cells taking up large amount of LDL may die and release lipids, forming a lipid or necrotic core in the atherosclerotic lesion site^{31,32}. Foam cells also exacerbate the inflammatory reaction, recruiting cells like T-cells and macrophages to the lesion²⁵. The macrophages produce matrix metalloproteases degrading the ECM at the site of the lesion and destabilizing it³³. Inflammatory cells begin recruiting VSMC, which secrete matrix components forming a fibrous cap above the lesion³⁴. The lesion begins to grow towards the lumen of the vessel and may partially or completely occlude it, forming a plaque. Atherosclerotic plaques can be classified as either stable or unstable, depending on the composition of the plaque, the mass of the necrotic core and the thickness of the fibrous cap³⁵. Large plaques may initiate an angiogenic response, inducing microvessel growth. These vessels can lead to hemorrhages into the necrotic core, swelling it in size and destabilizing the plaque³⁶. Unstable atherosclerotic plaques can rupture and release a thrombus which can enter the blood stream³¹. This thrombus can occlude smaller vessels for example in the brain, leading to a stroke, or the heart, leading to an acute myocardial infarction^{25,31,37}. Major risk factors for the generation of mature atherosclerotic plaques from asymptomatic fatty streaks include high blood pressure as well as levels of cholesterol and LDL^{32,38}. Despite extensive research and development of therapies to combat atherosclerosis, it remains a major culprit of symptoms and mortality arising from CVD^{25,32,39,40}.

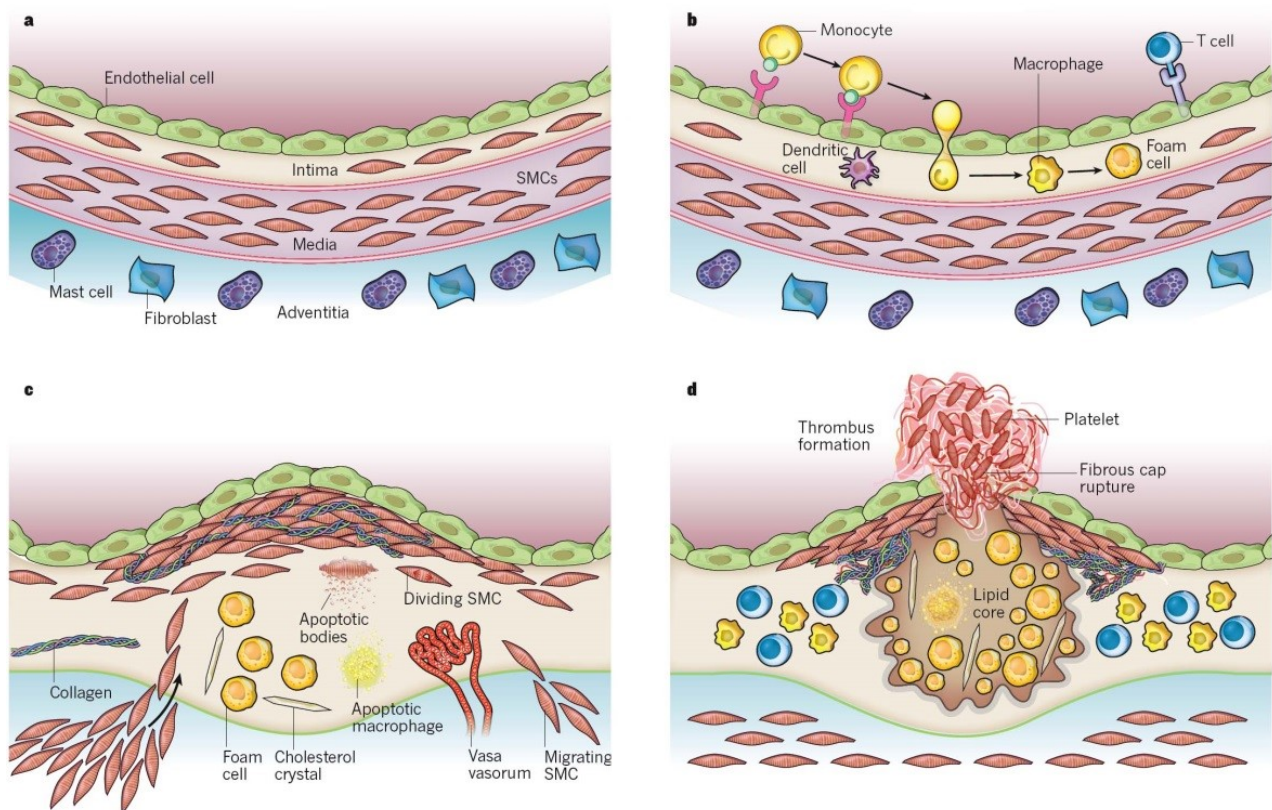


Figure 1.2.1 Progression of atherosclerosis

a) The normal artery is composed of three layers. The inner layer, the tunica intima, is lined by a single layer of endothelial cells (EC), contacting the blood flow and overlying a basement membrane. The human intima also contains vascular smooth muscle cells (VSMC). The middle layer, or tunica media, contains VSMC as well, which are embedded in a complex extracellular matrix (ECM). The adventitia is the outer layer of arteries and contains mast cells, nerve endings and microvessels. **b)** The initial steps of atherosclerosis are comprised of adhesion of blood leukocytes to activated EC, directed migration of the bound leukocytes into the intima, maturation of monocytes into macrophages, and their uptake of lipids, turning them into foam cells. **c)** Lesion progression involves recruitment of VSMCs from the media to the intima, the proliferation of resident intimal VSMC and media-derived VSMC, and increased synthesis of ECM macromolecules. Plaque macrophages and VSMC can die in advancing lesions and lipids derived from dead and dying cells can accumulate in the central region of a plaque, often denoted the lipid or necrotic core. Advancing plaques also contain cholesterol crystals and microvessels. **d)** Thrombosis is the main cause of concern for atherosclerosis. The fibrous cap ruptures, enabling blood coagulation components to come into contact with tissue factors in the plaque's interior. This triggers a thrombus that extends into the vessel lumen, from where it can migrate and/or impede blood flow. Adapted from ³²

1.2.2 Cardiac remodeling after acute myocardial infarction

During an AMI a cardiac vessel is obstructed, often by blood clots originating from atherosclerotic lesions. This leads to cardiac ischemia: loss of blood supply in the area of the heart perfused by the obstructed vessel. The main therapy implemented in an AMI is

primary percutaneous coronary intervention, which removes the obstruction on the coronary arteries and leads to a reperfusion of the infarcted area in most, but not all patients^{41,42}. However, even if reperfusion is established, AMI leads to a profound loss of cardiomyocytes (CM) in the area and vicinity of the infarction; the loss is increased the longer the infarcted area remains without perfusion⁴³⁻⁴⁶. While zebrafish and neonatal mice are able to regenerate a loss of up to 15-20% of the heart's ventricle^{47,48}, in adult mammals the ischemia triggers a response called cardiac fibrosis or remodeling (Figure 1.2.2)⁴⁹⁻⁵¹. In response to the death of CM, mast cells, macrophages and monocytes are also recruited to the site of injury, initiating an inflammatory response⁵²⁻⁵⁵. Dead cell debris and ECM is cleared away by macrophages. Myofibroblasts are major contributors to cardiac fibrosis the main source of which are cardiac fibroblasts (CF)^{56,57}. Myofibroblasts proliferate and deposit ECM components to form mature scar tissue⁵⁰. While the scar maintains the structural integrity of the heart, it lacks the ability to contract and cannot support its pumping function. To maintain cardiac output, the remaining CM contract faster and harder, which subjects them to stress, damaging them further and resulting in cardiac hypertrophy. CM deterioration leads to significant impairments in the quality of life and loss in life expectancy for the patients^{43,58-60}. Enhancing the recovery of the infarcted area during the repair phase after cardiac ischemia could significantly improve the prospects of patients as well as alleviating the cost of required post-ischemic treatments.

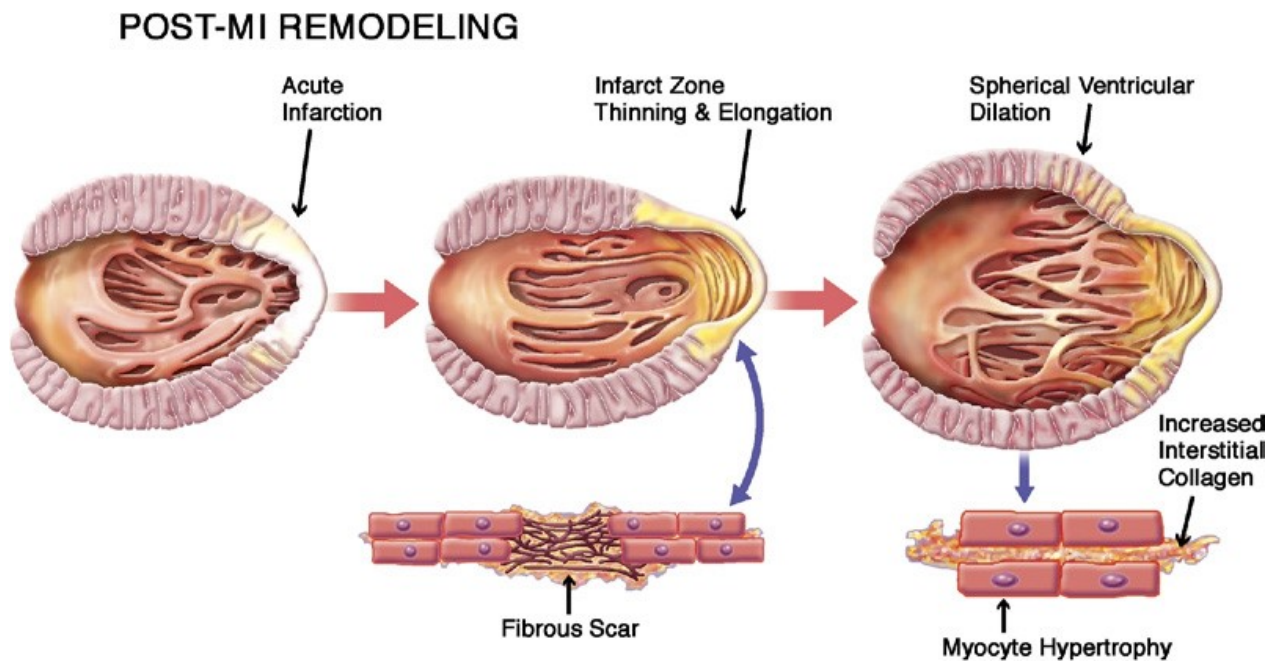


Figure 1.2.2 Post-AMI remodeling

Schematic representation of post-myocardial infarction left ventricular remodeling. The early phase is characterized by thinning and elongation of the fibrous scar within the infarcted zone. Subsequent left ventricular dilation, with transition from an elliptical to a more spherical configuration, is driven principally by diffuse myocyte hypertrophy associated with increased apoptosis and increases in interstitial collagen. Figure illustration by Craig Skaggs from ⁶⁰.

1.2.2.1 Post-AMI therapy

The main objective of therapy after an adverse cardiac event is the regeneration of cardiac contractive tissue to restore the heart's contractile capabilities. The underlying idea is to influence the cells in the infarcted area to reform functional tissue or to insert cells or tissue fragments to prevent scar formation. There are several approaches to overcome the mammalian heart's inability to regenerate on its own ⁶¹. A recently emerging approach involves the reprogramming of cardiac fibroblasts and will be discussed in more detail in 1.2.2.2 below.

An approach which has been extensively researched in the clinic since 2001 is cell therapy ^{46,62}. Different cell types have been used in this therapy, including endothelial progenitor cells (EPC) ^{63,64}, mesenchymal stem cells ⁶⁵, adipose stem cells ⁶⁶, pluripotent stem cells ⁶⁷,

cardiac stem cells^{68,69} and induced pluripotent or embryonic stem cell derived CM⁷⁰⁻⁷³; however most trials use autologous bone marrow derived mononuclear cells⁷⁴⁻⁷⁸. In nearly all trials a very small, but significant positive effect on recovery after AMI could be observed⁷⁸⁻⁸¹. Proposed mechanisms by which cells improve the remodeling process, dependent on the specific cell type, are through inducing angiogenesis in the infarcted area, reducing the formation of rigid scar tissue, reducing the rate of CM apoptosis, inducing generation of new CM or integrating into the infarcted area^{46,62}. The stem cells could achieve this possibly by incorporating into the damaged tissue themselves and/or through releasing paracrine factors which influence the cells already present in the infarcted area⁸².

Another approach to influence the remodeling is to use paracrine factors either on their own or in a co-treatment with cell therapy. As the remodeling is accompanied by a large immune reaction, modulating this reaction might prove beneficial as might ensuring an increase in angiogenesis⁸³⁻⁸⁵. Among such factors influencing the performance of cell therapy and remodeling are microRNAs (miRs), which will be discussed in more detail in chapter 1.3⁸⁶⁻⁹¹.

There have also been attempts to engineer heart tissue grafts, containing CM or cardiac progenitor cells for implantation into mammalian hearts with the attempt to provide viable and functional CM, which have met with some success in rodent models so far⁹²⁻⁹⁴.

1.2.2.2 Reprogramming of cardiac fibroblasts to induced cardiomyocytes

In the last couple of years several combinations of specific factors have been described to induce cardiac fibroblasts to transdifferentiate into a cell type similar to CM, which could help retain contractility after ischemic heart injury (Figure 1.2.2.2). The first described method was published by Ieda and colleagues, who used viral transfection of murine dermal and cardiac fibroblasts with the three transcription factors Gata4, Myocyte-specific enhancer factor 2C (Mef2c) and T-box transcription factor TBX5 (Tbx5), in short called GMT, to transdifferentiate fibroblasts into induced CM (iCM) in the course of several weeks *in vitro*⁹⁵. These iCM can spontaneously contract and express CM-specific marker proteins (e.g. cardiac troponin T (cTnT) and myosin heavy chain 6/ α -myosin heavy chain (Myh6)). 20% of all transfected cells could be turned into this iCM phenotype and the expression of CM markers remained detectable in the iCM even after implantation into murine hearts. Two similar viral delivery approaches succeeded in producing iCM in a mouse model of AMI^{96,97}. There was a

slight improvement in the recovery of the mice, but the amount of reprogrammed CF was small. Later studies showed that the expression levels of each of the three transcription factors play major roles in the efficiency; a high expression of Mef2c and Gata 4 over Tbx 5 promotes reprogramming^{98,99}. However, Chen et al reported in 2012 that using inducible lentiviral GMT vectors identical to the ones used by Ieda et al in 2010 did not lead to an efficient transdifferentiation of CF to CM *in vitro* or in a murine AMI model¹⁰⁰.

GMT based transdifferentiation can apparently be improved by incorporating additional factors. In mice treated with GMT after coronary ligation, the hormone thymosin β 4, ascribed to improve CM growth, enhanced the effects of GMT on AMI recovery⁸⁵. In a rat model of AMI, VEGF increased GMT mediated recovery⁹⁵. Adding the factor *Hand 2* to GMT (GHMT) led to an increased efficiency in transdifferentiating CF to iCM *in vitro* and *in vivo*¹⁰¹, although only a small number showed organized muscle cell structures¹⁰². *In vitro* GHMT treated fibroblast generated roughly equal numbers of CF-subtypes: atrial, ventricular and pacemaker cells¹⁰², while iCM generated by GMT are reportedly mainly of the atrial subtype¹⁰³. Further addition of Nkx2.5 to the GHMT cocktail (HNGMT) resulted in more efficient induction of iCM than either GMT or GHMT¹⁰⁴. Further research with this cocktail indicated that inhibiting transforming growth factor β (TGF- β) via the small molecule SB431542 before treatment with HNGMT could further increase the generation of iCM¹⁰⁵. The influence of microRNAs on the transdifferentiation will be discussed in more detail in chapter 1.3.4

Apart from the direct route established by GMT, there have been efforts to apply the cocktail of four transcription factors (Oct4, Klf2, Sox2 and c-Myc, also called Yamanaka factors), used in the creation of induced pluripotent stem cells¹⁰⁶ and adapt the procedure to interrupt the regression into pluripotency and differentiate into iCM instead¹⁰⁷. Treatment with Oct4, Klf2 and Sox2 led to generation of immature iCM from murine embryonic fibroblasts (MEF)¹⁰⁸. Co-treating the cells with Jak-inhibitor 1 (Ji1), bone morphogenic protein 4 (BMP4) and vitamin C could enhance the reprogramming process^{108,109}. It was later found that Klf2 and Sox2 could be substituted by a cocktail of small molecules¹¹⁰. Based on this work and reports on the creation of iPS cells using only chemicals^{111,112}, it was reported that a cocktail of small molecules could generate beating clusters of cells from MEF and murine tail-tip-derived fibroblasts¹¹³. While these reports are

encouraging and show a relatively high efficiency, it should be noted that due to the intricate protocols involved it is not possible to use such methods *in vivo* as of yet.

Unfortunately, it would appear that transdifferentiation of human CF to CM is even more complicated than in murine cells since both GMT and GHMT alone do not lead to an efficient reprogramming^{114,115}. However, a transfection with GHMT and co-treatment with miRs initiated reprogramming in human cardiac fibroblasts *in vitro*¹¹⁴. Also, when Mef2c is omitted (leaving GHT) and myocardin (MyocD) was added a small number of immature iCM was observed¹¹⁴. Also, treatment with GMT, MyocD and Mesp1 (GMTMM) was able to induce a small number of iCM¹¹⁵. Addition of estrogen-related receptor γ and zinc finger protein 2 to GMTMM was found to enhance the transdifferentiation¹¹⁶. Additional treatment of the cells with TGF- β during reprogramming could more than double the number of cells turning positive for Myh6, while inhibition of TGF- β had the opposite effects¹¹⁶. This is interesting since the opposite of what was reported for murine CF to CM transdifferentiation¹⁰⁵, which might point at fundamental differences in signaling between human and murine cells during reprogramming into iCM.

The disparity of these results shows that reprogramming of CF to CM is not a simple task and due to the low efficiency can be hard to initiate and detect. Notably, in all these reports the CF reprogrammed *in vivo* showed a stronger resemblance to endogenous CM than cells transdifferentiated *in vitro* and the beneficial effects on the recovery of rodents after AMI was larger than could be anticipated from the *in vitro* data^{96,117-119}. This can probably be attributed to environmental factors in the heart, which support maturation of CM after transdifferentiation has been initiated. If this is true in humans as well, therapies aiming at generating iCM in the heart after injury are promising indeed.

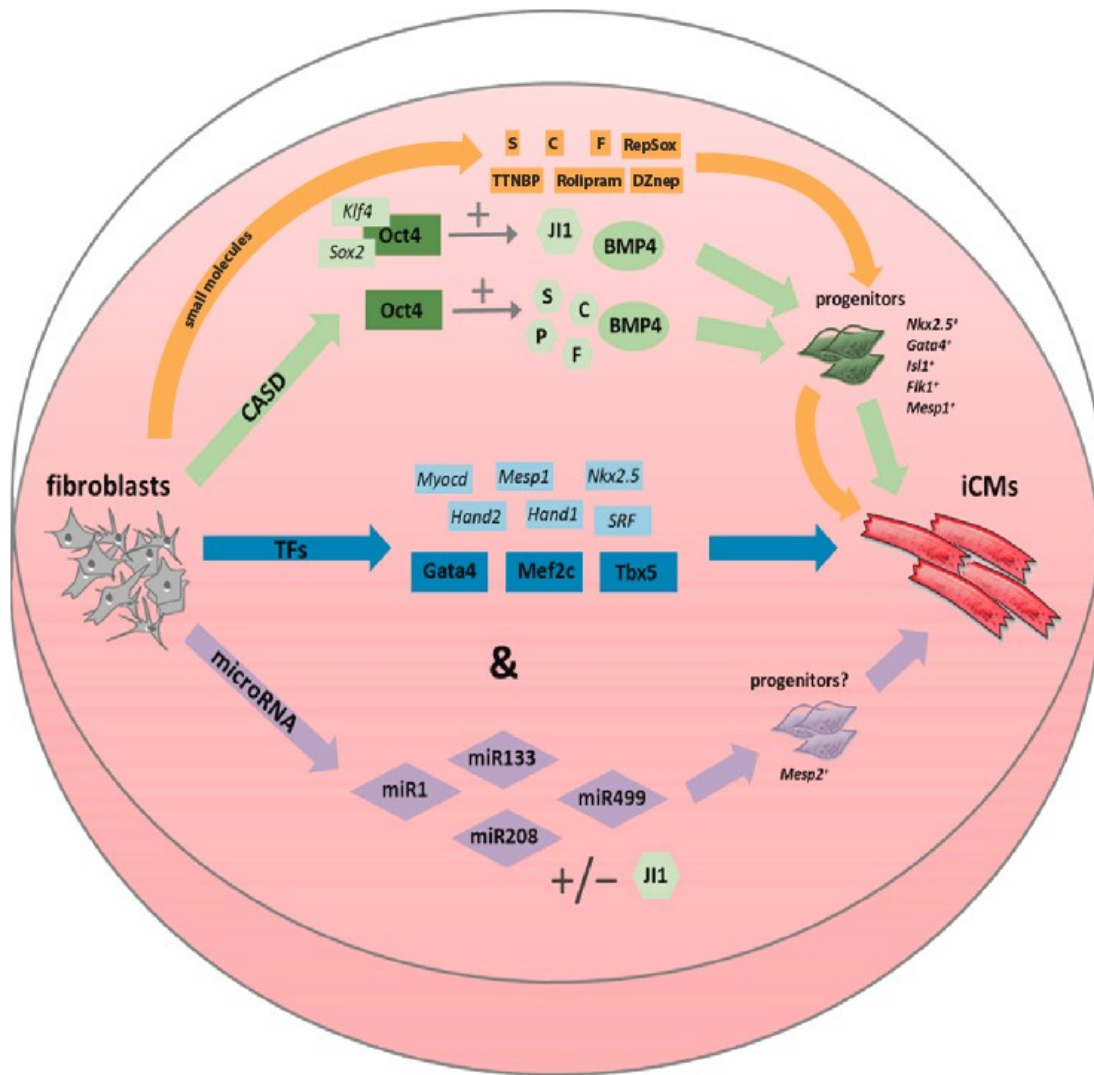


Figure 1.2.2.2 *In vitro* approaches for direct reprogramming of fibroblasts into induced cardiomyocytes (iCMs).

The CASD lineage conversion method tries to directly convert fibroblasts into iCMs by a transient overexpression of pluripotency factors in combination with lineage specific soluble signals. Other, more direct approaches use transcription factors (TFs), microRNAs, or a combination of both (&) to achieve iCMs. Abbreviations: CASD: Cell activation and signaling-directed; TF: transcription factor; miR: microRNA; iCM: induced cardiomyocyte; JI1: JAK inhibitor JI1; BMP4: bone morphogenic protein 4; S: SB431542 (ALK4/5/7 inhibitor); C: CHIR99021 (GSK3 inhibitor); P: parnate (LSD1/KDM1 inhibitor); F: forskolin (adenylyl cyclase activator). Adapted from ¹²⁰.

1.3 MicroRNAs

MicroRNAs (miRs) are endogenous, short (about 20 nucleotides), non-coding RNA fragments which can block the transcription of complementary messenger RNAs (mRNA) and/or induce their degradation ^{121,122}. It is estimated that more than half of all mRNA can be targeted by miR-repression ^{123,124}. Since one miR can target multiple mRNAs, a single miR can

significantly influence the gene expression pattern of cells ^{122,125–127}, for example during the maturation of stem cells ¹²⁸.

By targeting multiple miRNAs in the same signaling cascade, miRs can also circumvent compensation by other genes for a target gene, which can be a problem when using single targeted small interfering RNAs (siRNA) to achieve a knockdown. Because of this, miRs have been researched as potential targets for the therapy of a wide selection of pathologies. It should be noted that different miRs can have different effects in different cell types. Therefore, a target (cell) specific delivery of the therapeutic miR might be necessary; one possible approach to achieve this is by using aptamers (see 1.4). Also, when designing synthetic miRs or inhibitors of miRs, it is generally advisable to acquaint oneself with the biogenesis and processing of miRs to allow maximum efficiency.

1.3.1 Biogenesis and function

Most mammalian miR loci are close to other miRs and transcribed in larger transcription units, so called transcriptional clusters ¹²⁹. About 40% of miRs are located in introns of non-coding transcripts, 40% are in introns of coding transcripts and 10% are within exons of non-coding transcripts while for the rest alternative splicing determines whether they are located exonic or intronic ¹²³. The transcription of miRs is mediated by RNA polymerase II ¹³⁰, although a small set is transcribed by polymerase III ¹³¹. The primary miR transcripts (Pri-miR) transcribed by RNA polymerase II are several kilobases long and contain prominent stem loop structures (Figure 1.3). There is a canonical pathway through which most miRs are processed, although a small number of miRs are processed via alternative pathways ^{124,132}. Usually Pri-miR are processed via Drosha in the nucleus into one or more precursor-miRs (Pre-miR) which usually possess a single stem-loop structure ^{133,134}. In humans Drosha processing of miRs requires the cofactor DiGeorge syndrome critical region 8 ¹³⁵. This cofactor recognizes and binds to the stem loop and the single stranded RNA (ssRNA) stretches of the Pri-miR and facilitates its cleavage by Drosha about 11 bases from the ssRNA-dsRNA junction (Figure 1.3) ^{136,137}. Drosha can process the Pri-miR in introns before splicing without impairing the transcription of the host mRNA sequence ¹³⁸ but processing of Pri-miRs located in the exon of a protein-coding transcript can reduce protein synthesis ¹³⁹. It should be noted that the cleavage by Drosha creates a two nucleotide (nt) long overhang at the 3'-end of the Pre-miR, which predetermines the 5'-end of the 5p and the 3'-end of the

3p mature miR-strand^{123,133,137}. Exportin 5 also recognizes these overhangs and facilitates the export of the Pre-miR into the cytoplasm via the nuclear pore (Figure 1.3)^{140–143}. The Pre-miR is cleaved by dicer ~22 nt from the 5'- and 3'-ends to release a duplex of mature miRs^{123,124,144,145}. The mature-miR-duplex is then incorporated into the RNA-induced silencing complex (RISC) (Figure 1.3). One of the strands is then typically degraded, while the other strand guides an Argonaut protein (AGO), part of the RISC, to a target mRNA^{121,124,146}. The major determinant of AGO binding to its target is a 6-8 nt short seed sequence at the 5'-end of the miR, which is structurally rearranged by its binding to AGO¹⁴⁷. This rearrangement is necessary for the seed binding to the complementary sequence of the target mRNA^{124,148,149}. These target sequences in the mRNA can occur anywhere within the mRNA, but are most often found in the 3' untranslated region^{150,151}. It has been shown that an extensive complementarity between the miR and target sequence can lead to degradation of the miR along with the target mRNA^{124,152,153} by facilitating AGO2-mediated mRNA cleavage (Figure 1.3)^{154,155}. The majority of miRs however recognize their targets mainly by the seed sequence, possessing only partial complementarity with the rest of their target mRNA. This precludes the possibility of AGO2 cleavage and consequent mRNA degradation. However, correlation of protein and mRNA expression, based on ribosome profiling, strongly imply that degradation of mRNA by miRs is common in most miRs (> 80%), although for many miRs the repression of the protein levels seems to exceed those observed for the mRNA^{156,157}. One proposed mechanism to mediate this degradation is deadenylation of the poly-A-tail of the mRNA, which promotes de-capping and turnover of the mRNA through classical degradation pathways^{158–160}. However, it has been reported for several miRs in fish and flies that mutated targets lacking a poly-A-tail can be repressed by miRs or that their target mRNAs retain their poly-A-tail after translational repression^{161,162}. Also, these publications unveiled that the onset of translational repression precedes the degradation of the mRNA, endorsing a model of miRs interfering with the initiation of translation which subsequently leads to a destabilization and degradation of the target mRNA, though the precise mechanisms still need to be elucidated^{161–163}.

It is possible to inhibit the actions of miRs through anti-miR treatment. Several compounds have been used *in vitro* and *in vivo* some have even entered the phase of clinical trials. General, inhibition of miRs is achieved by blocking the interaction of miR and target mRNA, either by steric hindrance or by hybridization of the miR to the inhibitor substance^{164–170}.

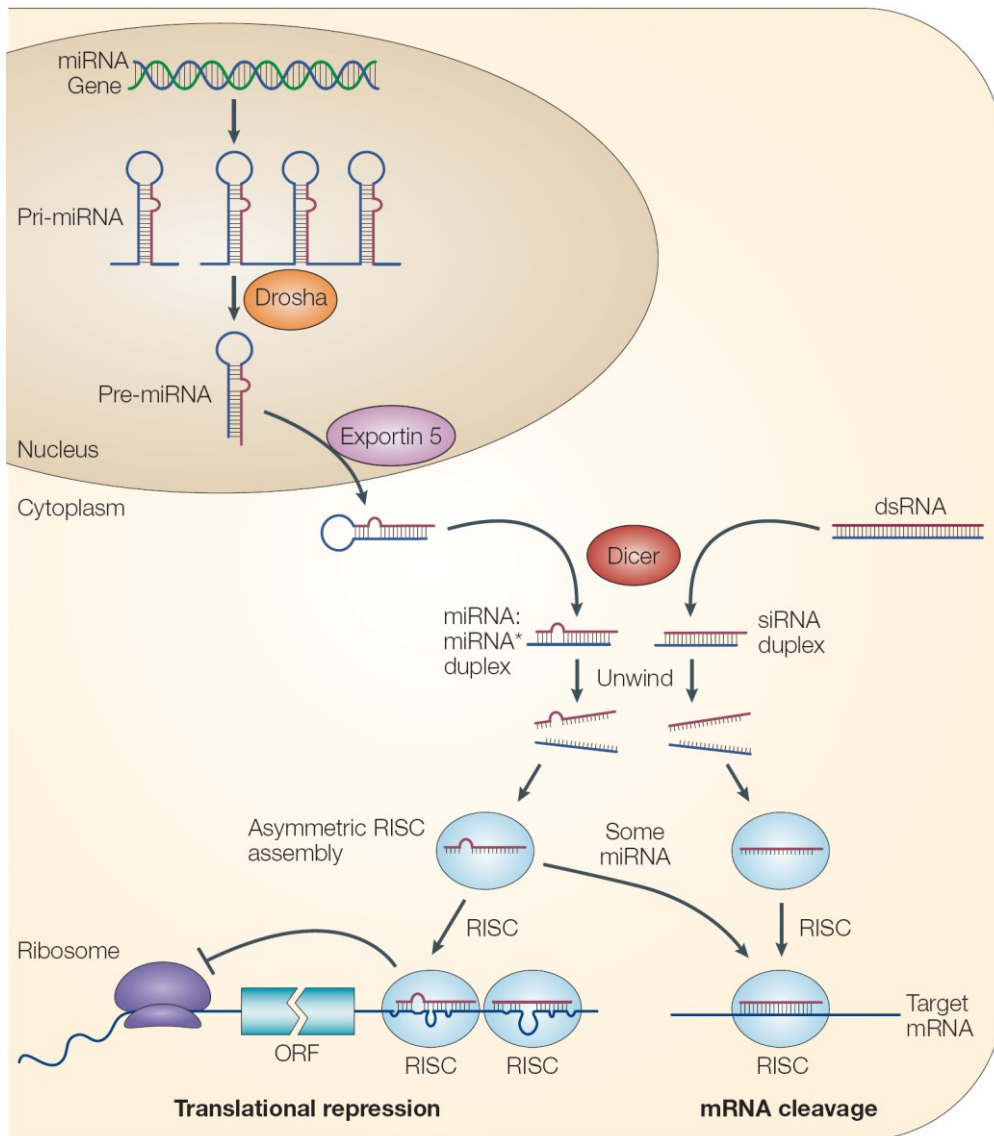


Figure 1.3 Model for the biogenesis and post-transcriptional suppression of microRNAs and small interfering RNAs.

The nascent primary microRNA (pri-miR) transcripts are first processed into ~70-nucleotide pre-miRs by Drosha inside the nucleus. Pre-miRs are transported to the cytoplasm by Exportin 5 and are processed into miR:miR* duplexes by Dicer. Dicer also processes long double stranded RNA molecules into small interfering RNA (siRNA) duplexes. Only one strand of the miR:miR* duplex or the siRNA duplex is preferentially assembled into the RNA-induced silencing complex (RISC), which subsequently acts on its target by translational repression or mRNA cleavage, depending, at least in part, on the level of complementarity between the small RNA and its target. ORF, open reading frame. Image from ¹⁴⁶

1.3.2 MicroRNAs in the cardiovascular system

A multitude of miRs have been described to play an important role in the vascular system^{86,88,171}. MiR-1, miR-21, miR-29a, miR-129, miR-133, miR-210, miR-211, miR-320, miR-423 and miR-let-7c have been implicated to play a role in the fetal development of the mammalian cardiovascular system, especially the heart, and an absence of dicer leads to a lethally abnormal cardiac development in murine models¹⁷²⁻¹⁷⁶. Maybe the most prominent miR in the cardiovascular system is miR-126, discussed separately in chapter 1.3.3. This chapter will discuss some of the many other miRs involved in the cardiovascular system and should illustrate the potential of miRs in the treatment of CVD.

1.3.2.1 MicroRNAs in the heart

Even in adult mammalian hearts, inhibition of miRs by deletion of dicer is lethal¹⁷⁷. miR-1, miR-16, miR-27b, miR-30d, miR-133, miR-143, miR-208 and the let-7 family are highly expressed, indicating a role in cardiac maintenance^{86,178}. miR-34a has been implied to play a major role in the regulation of cardiac ageing and CM death after AMI¹⁷⁹⁻¹⁸¹. Inhibition of miR-21, miR-24, miR-92a or the cluster consisting of miR-329, miR-487b, miR-494, and miR-495 has been reported to increase recovery and neovascularization after cardiac ischemia^{90,182-185}. Recently, inhibition of miR-25 was shown to increase cardiac function in failing hearts¹⁸⁶. Also, miR-199 and miR-208 enhance cardiac fibrosis and hypertrophy and elevated miR-208 levels correlate with adverse outcomes in cardiomyopathy¹⁸⁷⁻¹⁸⁹. The muscular miR-1 and miR-133 were shown to negatively regulate cardiac hypertrophy¹⁹⁰⁻¹⁹². Cardiac arrhythmias have also been tied to reduction of miR-1 as well as elevation of miR-228, miR-328 and miR-664¹⁹³⁻¹⁹⁶. In hypertension, the miR-143/145 was implicated to exacerbate symptoms in mice¹⁹⁷.

1.3.2.2 microRNAs in the vasculature

VSMC, major players in atherosclerosis, are strongly influenced by miR-145; overexpression was shown to increase the stability of plaques and reduce neointima formation¹⁹⁸⁻²⁰⁰. EC were also shown to secrete miR-143/145 to modulate VSMC behavior, leading to atheroprotection²⁰¹. On the lipid metabolic side of atherosclerosis, miR-122 and miR-33 were shown to mediate levels of cholesterol and high-density lipoproteins, indicating their inhibition as a potentially therapeutically beneficial^{167,202-204}. MiR-29a has been shown to reduce the integrity of the vascular ECM, which might predispose them to the formation of aneurysms²⁰⁵. MiR-503 was shown to be tied to diabetic EC dysfunction and its inhibition

improved recovery in murine models of hindlimb ischemia²⁰⁶ Also, inhibition of miR-200b increased production of VEGF thereby increasing angiogenesis^{207,208}.

1.3.2.3 MiRs as biomarkers in plasma

Low levels of miRs can be detected in human plasma²⁰⁹. Dysregulation of specific miRs in the plasma of CVD patients has been reported, making them potential biomarkers^{210,211}. For example, plasma levels of miR-126, miR 197 and miR-223 were shown to be predictive of AMI in CVD patients²¹² while miR-1, miR-133, miR-208 and miR-499 plasma levels are enriched shortly after an AMI^{213–215}.

Over all, miRs play a major role in the generation and homeostasis of the cardiovascular system, which makes them an interesting target for treatment or prevention of CVD.

1.3.3 MiR-126

miR-126 lies in the intron of the epidermal growth factor like 7 gene (EGFL7), highly expressed in EC²¹⁶. It is comprised of miR-126-3p and miR-126-5p (also known as miR-123 and miR-126* respectively) which are processed from Pre-miR-126. In EC, miR-126 is one of the most highly expressed miRs²¹⁷. Both of the mature strands have been described to play prominent roles in the (patho-) physiology of vertebrates (Figure 1.3.3), affecting various targets sometimes with overlapping, sometimes with distinct functions (for an exhaustive list of targets, see tables 1.3.3a+b). In the following chapter, the term miR-126 will be used if it was not possible from the source to determine between Pre-miR-126, miR-126-3p or miR-126-5p, otherwise the appropriate specific term is used.

As Pre-miR-126 lies in intron-9 of EGFL7, they are usually transcribed together. Knockdown of EGFL7 by siRNA does not affect pre-miR-126 transcription and vice versa, suggesting that Pre-miR-126 is excised in the nucleus as would be expected^{218–220}. MiR-126-5p was shown to increase EGFL7 levels however, most likely mediated through inhibition of factors blocking EGFL7 transcription, indicating a positive feedback loop²²¹. Methylation of the EGFL7 promoter correlated with a reduction of Pre-miR-126 expression, indicating that miR-126 shares the promotor²²². Pre-miR-126 is embedded within a 287 base pairs long CpG island within EGFL7 and expression of both miR-126-3p and -5p is negatively correlated with the methylation of this CpG island in acute myeloid leukemia (AML) cells²²³. However, there have also been reports of EGFL7 independent regulation of miR-126 expression²²⁴. About 20% of the expression of miR-126 is regulated by the transcription factor E26

transformation-specific sequence 2 and 15% by E26 transformation-specific sequence 1²²⁵. A single nucleotide polymorphism was discovered by analyzing a cell line known for deficient miR-126-3p levels. It is comprised of an A to G substitution 24 bases from the 3' end results in reduced efficiency in the processing of the Pri-miR-126 to ~20% of the canonical A-allele²²⁶. This aberrant A allele is associated with severe diabetic retinopathy²²⁷.

The main role of miR-126 described so far is in the vascular system and in various forms of cancer, which are discussed in detail below. It has also been implicated in various other physiological and pathological processes however, including kidney injury²²⁸, lung cystic fibrosis,²²⁹ hepatic fibrosis²³⁰⁻²³³, nicotine metabolism²³⁴ and type 2 diabetes mellitus²³⁵⁻²³⁹ (see Fig 1.3.3).

Cardiovascular System

- Embryonic vascular development
- Enhanced EC response to VEGF
- Reduced EC expression of VCAM-1
- Maintenance of endothelial progenitor cell function
- EC to VSMC communication

miR-126

Cancer

- Breast cancer
- Leukemia
- Renal cancer
- Lung cancer
- Cutaneous melanoma
- Bone cancer
- Gastric cancer
- Tumor angiogenesis
- Tumor cell signalling

Cardiovascular Disease

- Cardiac remodeling
- Atherosclerosis
- Preeclampsia
- Ischemia reperfusion Injury

Other functions

- Kidney injury
- Hepatic fibrosis
- Lung Cystic fibrosis
- Type 2 Diabetes mellitus

Figure 1.3.3 MicroRNA-126 is implicated in various pathophysiological processes

Target	Validation	References
Spred-1	WB, qPCR, RA	223,238,240,241
PIK3R2	WB, qPCR, RA	242–245
VCAM-1	WB, RA	233,246–251
VEGF-a	WB, qPCR, RA	232
IRS-1	WB, RA	252–254
CRK	WB, qPCR, RA, NGS	255
EGFL7	WB, qPCR, RA	220,221
SOX2	WB, qPCR, RA, MA	256,257
DNMT1	WB, qPCR, RA, MA	219
IGFBP2	WB, qPCR, Elisa, RA, MA	258
PITPNC1	WB, qPCR, Elisa, RA, MA	258
MERTK	WB, qPCR, Elisa, RA, MA	258
ADAM9	WB	259
MMP7	WB	259
SDF-1/CXCL12	WB, RA	222
PLK2	qPCR, RA	223
PTPN9	WB, RA	260
TOM1	WB, qPCR, RA	229
DNMT1	WB, RA	219
HOXA9	WB	261
KRAS	WB, RA	262

Table 1.3.3a: List of validated targets for miR-126-3p taken from miRTarBase 7.0²⁶³ and updated to include all referenced data. WB = Western Blot; qPCR = quantitative RT-PCR (only if the mRNA levels are regulated); RA = Reporter assay (e.g. luciferase); NGS = Next generation sequences; MA = microarray

Target	Validation	References
SIRT1	WB, RA	264
ADAM9	WB	259
MMP7	WB	259
MMP13	WB, qPCR, RA	265
PTHrP	WB, qPCR, RA, Elisa	266
Klotho	WB, qPCR	267
SDF-1/CXCL12	WB, RA	222
SLC45A3/Prostein	WB, RA	218
EGFL7*	protein	221

Table 1.3.3b List of validated targets for miR-126-5p taken from miRTarBase 7.0 ²⁶³ and updated to include all referenced data. WB = Western Blot; qPCR = quantitative RT-PCR; RA = Reporter assay (e.g. luciferase); NGS = Next generation sequences; MA = microarray; *EGFL7 levels are indirectly increased by miR-126-5p

1.3.3.1 MiR-126 in the (cardio-) vascular system

The first role ascribed to miR-126 was in angiogenesis, both in embryos and in adults. Both EGFL7 and miR-126 expression are induced during day four of embryoid body formation and increase together with the expression of EC markers ²⁶⁸. The response of EC to the angiogenic factors VEGF and basic fibroblast growth factor is enhanced by miR-126-3p ^{268,269}. MiR-126-3p modulates VEGF effects by targeting sprouty-related, EVH1 domain-containing protein 1 (SPRED-1) ²⁴¹ and phosphatidylinositol-4,5-bisphosphate 3-kinase (PIK3) regulatory subunit 2/ β (PIK3R2) ^{220,242}, which inhibit the Mitogen-activated protein (MAP) kinase and PIK3 pathways respectively (Figure 1.3.3.1). In both mammals and zebrafish, miR-126 is essential for the formation of the vasculature in the embryo ^{241,268}, partly mediated by inhibition of PIK3R2 and the resulting increase of angiotensin 1 signaling ^{220,243}. In zebrafish, but not mammals, the crucial shear stress response to blood flow in newly formed vessels is also dependent on miR-126 ^{201,270,271}.

Aberrant levels of miR-126 might be of use as diagnostic markers in patients suffering from CVD ^{272,273}. miR-126-3p levels increase after an AMI in the blood ²⁷⁴, while a lower plasma level of miR-126 can be detected in patients suffering from peripheral artery disease ²³⁶. In mice levels of miR-126-3p drop in the heart during ischemia ²⁷⁵ and knocking out miR-126

reduces AMI recovery, increases mortality and decreases neovascularization ²⁴¹. Also, mesenchymal stem cells overexpressing miR-126 perform better when used in cell therapy for AMI (see 1.2.2.1) ²⁷⁶. In ischemia reperfusion injury of the kidneys mir-126 overexpression in hematopoietic cells has been found to increase the recruitment of progenitor cells and increases re-vascularization ²⁷⁷. This indicates that miR-126-3p might be of therapeutic relevance to treat ischemic disorders.

Despite its many pro-angiogenic attributes, miR-126 has also been described to inhibit the secretion of stromal derived growth factor 1 (SDF-1) by EC and thus block the recruitment of pro-angiogenic progenitor cells from the blood ^{248,278}. It was proposed that miR-126 expression levels in the ischemic endothelium could be reduced to enable SDF-1 secretion, while at the same time inhibiting the migration and expansion of the damaged EC ²⁷⁸.

Through its suppression of VCAM-1 and resulting attenuation of leukocyte adherence miR-126-3p also plays a role in inflammation, a hallmark of many lifestyle diseases ^{246,268}. During acute renal inflammation, increased miR-126-3p expression in the EC of glomeruli prevents an increase of VCAM-1 protein. In the neighboring arterioles there is no increase in miR-126-3p and so VCAM-1 is upregulated which leads to increased recruitment of leukocytes and consequently to exacerbation of the inflammation in the arterioles ²⁴⁷. A drop in miR-126-3p levels was also registered in rats having undergone an injury of the spinal cord ²⁷⁹ and miR-126-3p was found to both enhance vascularization and reduce inflammation ^{232,240,243}. Antiatherogenic triglyceride rich lipoproteins also regulate the expression of VCAM-1 via miR-126-3p ²⁵¹. In EC subjected to shear stress, miR-126-5p, but not miR-126-3p, increases the proliferation, conferring protection from atherosclerosis ²⁷¹.

miR-126 can also be secreted by EC in vesicles or bound to Argonaute 2 ^{236,280,281}. VSMC can take up this secreted miR-126, which suppresses their apoptosis and increases proliferation, leading to increased neointima formation ²⁸¹. EC can also increase miR-126-3p levels in osteoblasts by cell-to-cell contact, which inhibit osteoblast migration ²⁸². In adipose patients, a deficiency of miR-126 was detected in adipose tissue derived vesicles. The miR-126 derived from these adipose cell vesicles was shown to have the expected angiogenic effects on EC ²⁸³.

In rat early EPC miR-126 increases migration and colony and tube formation as well as a reduction in apoptosis and increased viability^{238,244,245}. It is known that EPC of coronary artery disease and preeclampsia patients are functionally impaired and their miR-126 levels are reduced^{245,284–288}. In rats miR-126 inhibition significantly reduced the size of the fetus and placenta as well as placental vascularization, while miR-126 mimics had the opposite effects²⁴⁵. EPC have also been described to infiltrate thrombi in deep vein thrombosis, which significantly enhances their resolution^{289,290}. In a rat model miR-126-3p significantly reduced the size of the thrombus while increasing EPC homing as well as recanalization and resolution of the thrombus²⁴⁴. This indicates that miR-126 plays a role not only in the mature endothelium but also in the homeostasis of EPC under physiological and pathological conditions.

It has been reported that miR-126-5p, through inhibition of PIK3R2, reduces proliferation of hematopoietic stem cells²⁹¹. miR-126-3p and -5p also reduce the number of erythroid cells during erythroid body formation²⁶⁰. Also, overexpression of both strands of mir-126 in bone-marrow derived mononuclear cells significantly increased their colony forming potential, which might improve their ability to enhance recovery after AMI when used for cell therapy (see 1.2.2.1)²²³. Together this might indicate that miR-126 is involved in inducing an EC fate instead of hematopoietic state in stem and progenitor cells.

An increase of miR-126-3p expression was observed in human plasma during ageing; this was attributed to an increase in extracellular and intracellular endothelial cell miR-126-3p levels in the onset of senescence²³⁹.

Therapeutically, it is also possible to use the high EC expression of miR-126-3p to construct vectors specifically inactive in these cells. Santulli *et al.* recently reported an elegant treatment strategy to prevent restenosis without impairing reendothelization in rat arterial injury²⁹². An adenoviral vector carrying the cyclin dependent kinase inhibitor p27^{kip1} was shown to inhibit restenosis by inhibiting VSMC proliferation²⁹³. By introduction of miR-126-3p binding sites, the vector was inhibited efficiently in EC, which significantly abolished its negative side effects on these cells²⁹². Comparable use of endogenous miRs to selectively inactivate vectors might provide useful therapeutic tools in the future.

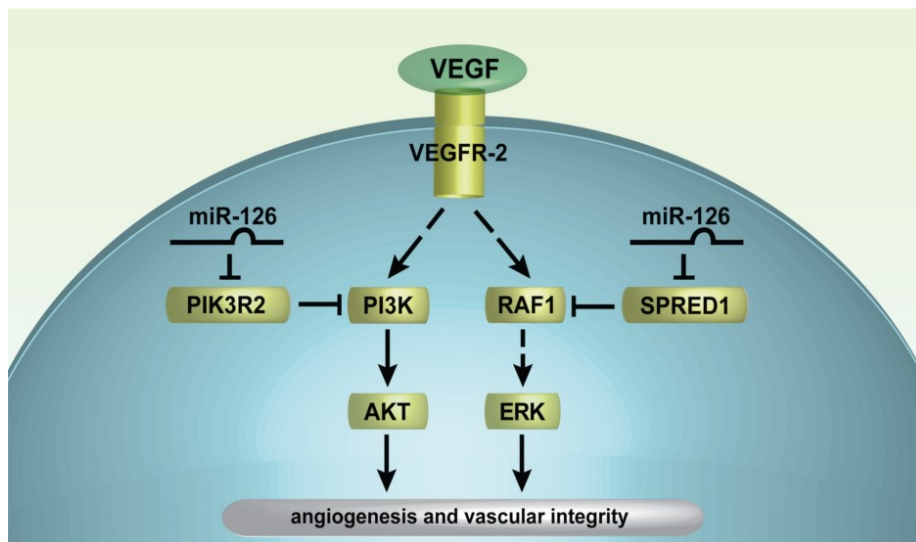


Figure 1.3.3.1 Model of miR-126 function in endothelial cells

MiR-126 represses SPRED1 and PIK2R2, which negatively regulate VEGF signaling (and possibly other growth factor signaling pathways) via the MAP kinase and PIK3 pathways, respectively. Thus, miR 126 promotes VEGF signaling, angiogenesis and vascular integrity by inhibiting protein production of endogenous VEGF repressors within endothelial cells. Adapted from ²⁶⁸

1.3.3.2 miR-126 in cancer

miR-126 has also been implicated to play a role in cancer, both due to its involvement in tumor angiogenesis and by direct effects on the cancer cells ^{294,295}. Reduction of miR-126-3p was reported in tumors of the pancreas ²⁶², cervix ²⁹⁶, breasts ^{222,253,297} and stomach ²⁹⁸. In lung ²⁹⁹, colon ^{242,300} and prostate cancer ^{218,301} both miR-126-3p and 5p are downregulated. The proto-oncogene tyrosine-protein kinase Src significantly inhibits miR-126-3p in various tumor cells, which enhances tumor migration in for example mammary carcinoma cells ^{255,302}.

In breast cancer, miR-126-3p reduces cell proliferation by arresting cells in the G1/G0-phase which is mediated by inhibition of insulin receptor substrate-1 ^{253,303}. The recruitment of EC by breast cancer cells is also inhibited by miR-126-3p through inhibition of the secretion of angiogenic factors ²⁵⁸. By reducing secretion of SDF-1, miR-126-3p and -5p also reduce the recruitment of mesenchymal cells to breast tumors ²²².

In acute myeloid/lymphoid lymphoblastic leukemia a loss of miR-126-3p has been reported and reconstitution of miR-126-3p led to a partial rescue of the B-cell differentiation disorder ²⁵².

In hepatocellular and clear cell renal carcinoma, miR-126 levels are reduced and miR-126-3p reconstitution inhibits proliferation and increases the carcinomas susceptibility to apoptosis^{256,304–307}.

In prostate cancer, miR-126-5p is reduced which promotes invasiveness and motility²¹⁸.

In non-small cell lung carcinoma, miR-126-5p overexpression led to a decrease in cell proliferation and colony formation *in vitro* while tumor size was significantly smaller in nude mice²²¹. This effect of miR-126-5p was attributed to the increase in EGFL7 levels²²¹.

In cutaneous melanoma, miR-126-3p and miR-126-5p levels negatively correlate with the severity of the melanoma. Both strands were shown to inhibit viability as well as migratory and invasive abilities^{259,308}.

In three forms of bone cancer, miR-126 was reduced. In giant cell tumor of the bone, miR-126-5 reduces tumor cell proliferation and prevents the degradation of healthy bone tissue^{265,266,309–311}. In chondrosarcoma, inhibition of VCAM-1 by miR-126-3p reduces migratory and invasive capabilities of the tumor cells²⁵⁰. In Osteosarcoma both miR-126-3p reduces viability, migration and invasiveness of cancer cells while miR-126-5p reduces their proliferation and resistance to apoptosis^{264,312–314}.

In gastric cancer there are conflicting reports about the effects of miR-126. On the one hand, miR-126-3p reduction in tumor cells correlates with increased severity^{298,315,316} and overexpression of Pre-miR-126 was reported to reduce metastasis, proliferation and tumor vascularization^{298,315}. On the other hand, Pre-miR-126 was described to increase viability and colony forming capacity of gastric cancer cell lines²⁵⁷.

In AML, increased levels of miR-126-3p and -5p have been detected^{223,267}, especially in treatment resistant leukemic stem cells^{317,318}. The current hypothesis is that miR-126-3p is crucial in maintaining these cells stemness and self-renewal while miR-126-5p inhibits apoptosis in all AML cells^{223,267,318}.

Cancer cells can also use miR-126-3p as a means of cellular communication. A chronic myelogenous leukemia cell line has been found to secrete miR-126-3p in exosomes, which are taken up by EC. In the EC, miR-126-3p then lowers the adhesion of the leukemic cells as

well as their short term ability to pass through the EC-layer, while enhancing this ability on the long term ²⁴⁹.

1.3.4 miRs in reprogramming

It has also been reported that miRs can facilitate reprogramming of CF to iCM (see 1.2.2.2). When cells transfected with GMT were also treated with miR-133a, the efficiency of transformation was increased drastically ¹⁰³, primarily, but not solely, through inhibition of the Zinc finger protein Snai1 ¹⁰³. Interestingly, treatment of human CF with miR-133a as well as GMTMM also increased the reprogramming efficiency, indicating that miR-133a plays a comparable role in human and murine CF transdifferentiation: suppression of the fibroblast phenotype ^{103,118}. In 2012, Jayawardena *et al.* used a cocktail of four miRs (miR-1a, -133a, -208a, -499a) to cause a transdifferentiation of neonatal murine CF to iCM *in vitro* and in adult mice *in vivo* ^{119,319}. Treatment of neonatal CF with the miR cocktail *in vitro* led to the expression of CM markers in 1-5% of the cells as early as three days after treatment. Co-treatment with JI1 increased the number of cells to 13-28%. However, it should be noted that treatment of MEF with the four miR-cocktail did not lead to an induction of CM genes, indicating that cells more distantly related to CM are not reprogrammed efficiently by the cocktail ¹⁰³. *In vivo* treatment of the infarction area with four separate lentivirus containing the miRs after permanent coronary artery ligation in mice led to a very small number (1-3%) of CF adapting an iCM phenotype ³¹⁹. In a follow-up *in vivo* study, about 12% of cells expressed CF and CM markers concomitantly (compared to 4% in hearts treated with control vector) in the infarcted area 7 weeks after infarction (Figure 1.3.4) ¹¹⁹. iCM isolated from the infarcted hearts 5-6 weeks after surgery showed excitation-contraction coupling and action potential characteristics comparable to CM. Furthermore, mice treated with the lentiviral miR-combination showed an increased recovery of the fractional shortening as well as a drastic reduction of fibrosis in the heart ¹¹⁹.

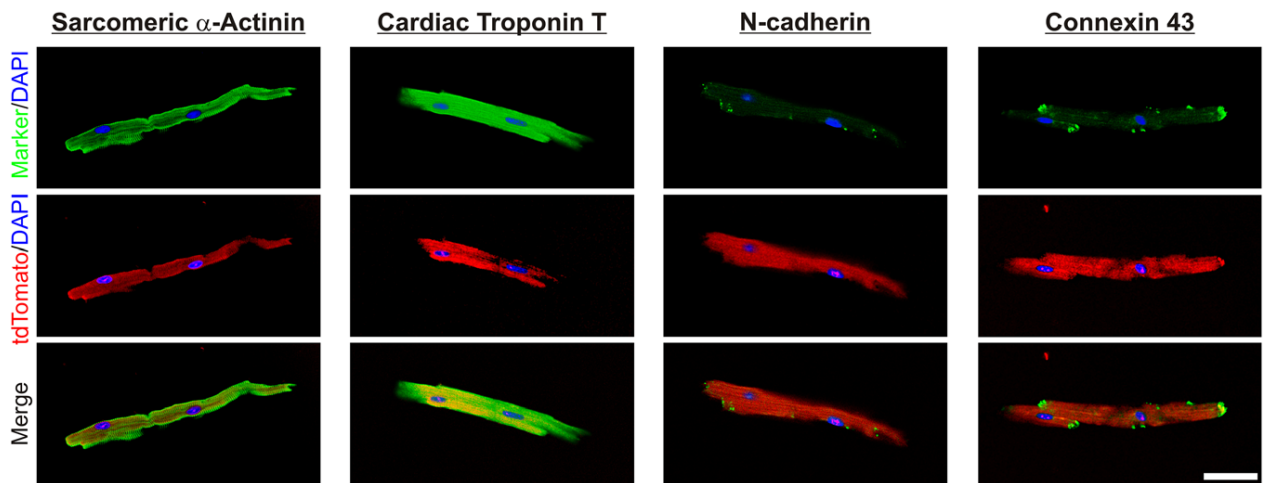


Figure 1.2.4 A specific combination of microRNAs (miR combo) reprogrammed cardiac myocytes express mature cardiac markers.

Images of purified tandem dimer Tomato (tdTomato)+ cardiac myocytes immunostained for sarcomeric α -actinin, cardiac troponin-T, N-cadherin, and Connexin-43 (green), together with tdTomato (red), and DAPI (4',6-diamidino-2-phenylindole; blue). For each cardiac marker, images shown include overlay of cardiac marker and DAPI (top), tdTomato and DAPI (middle), and merged image of marker, tdTomato, and DAPI (bottom). Scale bar, 100 μ m. Image from ¹¹⁹

1.4 Aptamers

In the last years aptamers have emerged as tools which enable a specific transport of molecules into cells or allow the detection of specific biomarkers ^{320,321}. Aptamers are nucleotide chains which fold into specific and stable three dimensional structures ³²². This allows aptamers to fit into or attach onto target molecules (from Greek aptus = to fit, meros = a region), much in the same manner as antibodies (Figure 1.4) ^{323,324}. Aptamers have also been shown to bind to their targets agonistic, antagonistic or independent of the usual binding partners of their targets, depending on the antibody ³²⁵⁻³²⁸. Aptamers do have some advantages over antibodies however, since they are smaller, providing better tissue penetration and are more easily and cheaply synthesized and stored ^{320,326}. Also, to date aptamers have been shown to be neither toxic nor eliciting any immune response in vivo ^{326,329}. Using a technique called systematic evolution of ligands by exponential enrichment (SELEX) developed in the 1990s, it is possible to select aptamers for specific target molecules *in vitro* ³²³. The SELEX is described in more detail in 1.3.2. Aptamers have been developed against a plethora of targets, for example against VEGF. This aptamer has since then been approved by the Food and Drug administration and is used under the name of Macugen to

treat age related macular degeneration^{328,330-332}. A thorough discussion of the various applications and targets of aptamers and ways to modify them chemically is outside the scope of this thesis, which will therefore focus on the discoveries in the field most relevant to this project.

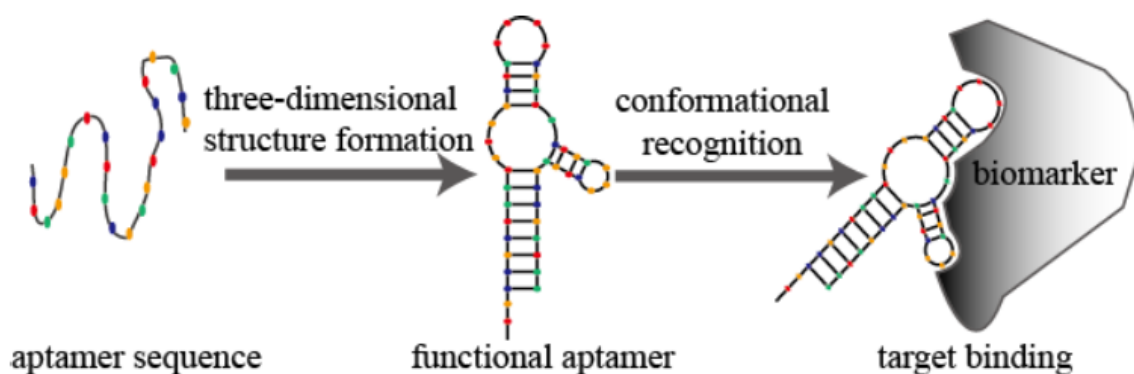


Figure 1.4 Schematic diagram of aptamer conformational recognition of targets to form an aptamer-target complex.

The DNA or RNA aptamer strand is linearized and allowed to fold into a specific 3-dimensional structure. This conformation of the aptamer then recognizes its target molecule, in this case a biomarker for diagnostics, and binds with high affinity. Picture from³²⁶.

1.4.1 SELEX

In the SELEX (Figure 1.4.1), aptamers are selected from a pool of different species of DNA or RNA for their ability to bind to purified molecules (most often proteins, potentially also other oligonucleotides, drugs or sugars)^{323,324,333-335}. Each species usually consists of conserved primer binding sites at either ends of the oligonucleotide and 20-60 randomized nucleotides, leading to more than 10^{12} species in the pool. The pool is then allowed to fold into specific three-dimensional structures and subsequently incubated with the target molecule. Through different methods, the easiest of which is washing with buffer, oligonucleotides not binding to the target are then removed from the pool^{327,336,337}. The remaining oligonucleotides are then amplified using a common polymerase chain reaction (including reverse transcription steps if an RNA-pool is used). After amplification, the pool is ready for a repeat of the selection procedure. In many cases a counterselection step is applied before or after the incubation with the target to eliminate species that bind non-specifically³³⁸. After 8-20 rounds, usually taking many weeks or months, the pool now enriched in species binding to the target is sequenced to determine likely aptamer candidates. These species are then further tested for the strength and specificity of their interaction with the target molecule

^{326,327}. High throughput sequencing can also be used to increase the speed and efficiency of the screening process. By analyzing multiple rounds of SELEX at once, species which are highly enriched during the early rounds of SELEX can be discovered. This has the advantage of minimizing the bias of the PCR reaction to amplify some species more than others while reducing the number of rounds and thus time needed for the SELEX ^{339–342}. Using nonequilibrium capillary electrophoresis of equilibrium mixtures it is also possible to perform a non-SELEX, which does not involve the repeated amplification steps used in the traditional approach and enables selection of binding partners in a lower number of rounds, but requires more expert equipment and handling ^{343,344}.

In 2001 the first of now many articles has been published which screened aptamers for their ability to adhere to cells instead of purified molecules using an adapted protocol named cell SELEX ³⁴⁵. This approach allows selection of aptamers specific for a certain cell type without knowledge of a surface marker molecule on the cellular membrane. It also has the benefit of selecting for molecules in their native formation on the cellular surface. This precludes the possibility of the aptamer binding to a motif on the purified molecule that might be inaccessible when encountered on the cell, a problem occasionally occurring with the traditional SELEX method ^{326,346}. In cell SELEX, specificity is achieved by using a second, different population of cells to perform counterselection to eliminate non-specific binders. Often the other cell population is closely related to the target cell line, for example healthy leukocytes can be used when selecting for aptamers specific for leukemic cells ³⁴⁷. Aptamers identified using a cell SELEX are often internalized into their target cells, allowing them to deliver therapeutics specifically into their target cell lines ^{348–350} and the protocol can be adapted to specifically select for internalizing aptamers by degrading or detaching aptamers attached to the cell surface, for example by RNase treatment ³⁵¹ or washing with concentrated saline solutions ^{339,352}. Both procedures effectively exclude aptamers which do not internalize into the cells in the timespan allotted during selection. More recently, whole living animals were used as targets for SELEX. The underlying rationale is comparable to cell SELEX, but the pool is applied to living animals and the organ which is supposed to be targeted by the aptamers is excised after some time. The pool is then purified, sequenced and amplified from the tissue sample and then amplified. The whole process is then repeated over several rounds as with traditional SELEX until the pool converges onto

promising candidates^{353,354}. This approach is suited even better to select for aptamers binding in living organisms, but it is also cumbersome, expensive and ethically questionable.

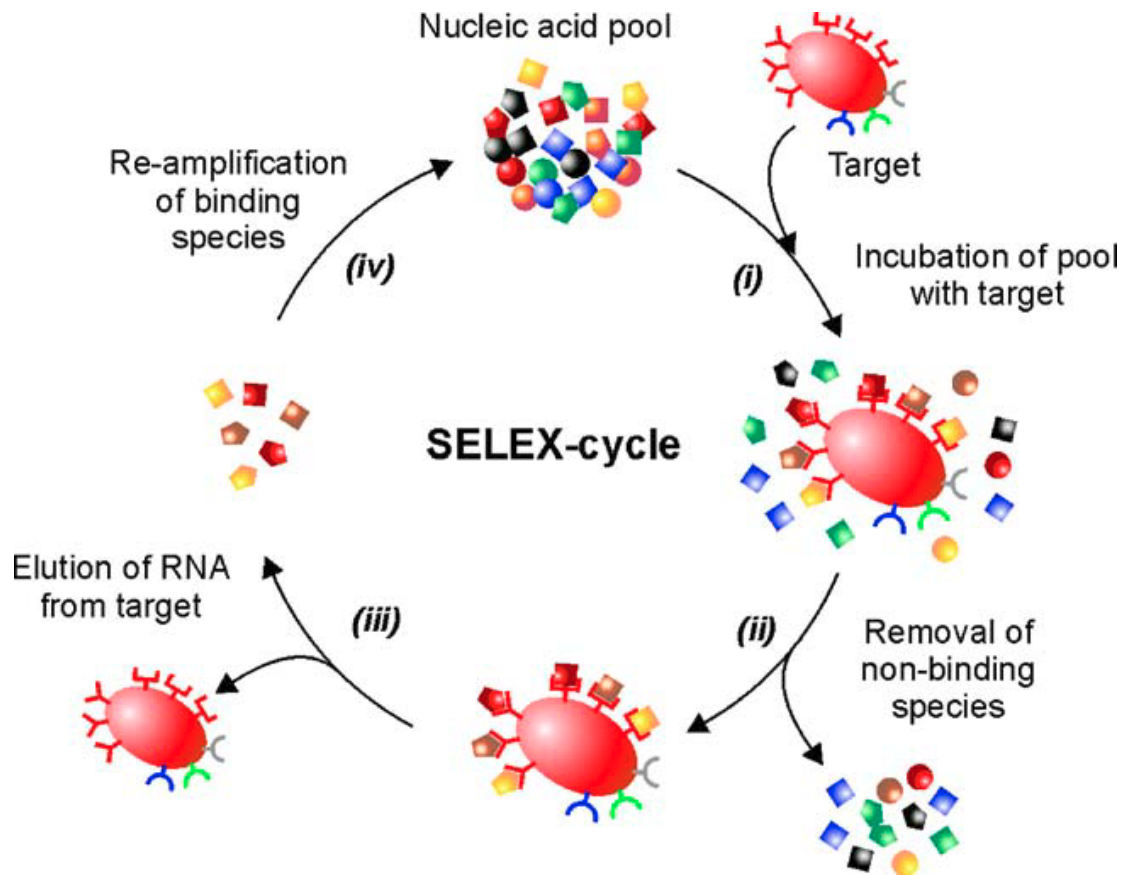


Fig. 1.4.1 General scheme of the SELEX procedure

(i) A pool of 3-D folded, random DNA/RNA oligonucleotides flanked by constant primer sites is incubated with the target. (ii) Unbound sequences are partitioned away. (iii) Binding sequences are eluted from the target and (iv) amplified by PCR and to yield an enriched pool with respect to binding to the corresponding target. Over 8-20 rounds, highly affine and specific aptamers are selected. Adapted from³²⁷

1.4.2 Delivery of RNAi by aptamers

In the last few years different research groups have successfully used the ability of some aptamers to internalize into cells by using them to transport siRNA into cells to cause a knockdown of specific genes. The first reports of such successful transports were published in 2005/2006^{349,355} and many groups have since used similar approaches (reviewed in^{325,356,357}). An example is the use of an aptamer which binds specifically to the membrane protein gp120, highly expressed on T-cells infected by HIV³⁵⁸. By attaching a siRNA against an HIV gene needed for the multiplication of the virus, it was possible to almost completely

stop the spread of HIV in a mouse model ³⁵⁸. Other examples include the use of a general RNA internalization motif (GIRM) ³⁵¹ or an aptamer for the ubiquitously expressed transferrin receptor (TRA) ³⁵⁹, which are not cell specific and therefore allow delivery into most cell types, for the delivery of siRNA.

Recently, it was reported that aptamers can also be used to deliver miRs into cells. An aptamer which preferentially binds to tumor expressed mucin 1 was conjugated to miR-29b and inhibited the growth of xenograft tumors ^{360,361}. The miR let-7g was attached to the aptamer GL21.T. GL21.T binds to and antagonizes the oncogenic receptor tyrosine kinase Axl, and was able to efficiently deliver let-7g to target cells. The treatment significantly reduced tumor growth in a murine xenograft model of lung adenocarcinoma ³⁶². Moreover, polymers conjugated to the TD05 immunoglobulin heavy mu chain aptamer ³⁶³ were used to deliver miR-15a and miR-16 to prostate cancer cells ³⁶⁴.

1.4.3 Chemical modifications of aptamers

As promising as aptamers for delivery of therapeutics are, they face a major problem. Most aptamers are made of oligonucleotides, which are vulnerable to degradation by nucleases abundant in living animals. Their small size also leads to a fast renal filtration ^{325,327,365}. Therefore, many chemical modifications or incorporation of unnatural nucleotides have been applied to increase the bioavailability and stability of aptamers (Figure 1.4.3) ^{326,366–368}.

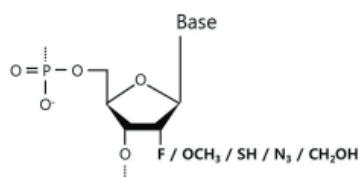
RNA nucleases usually attack the 2'-OH group of RNA for degradation, which is why this group or the RNA backbone is often chemically modified to enhance resistance to nucleases ³²⁷. The most common modification is 2'-O-methoxy replacement of the OH group, which as an added benefit prevents the aptamers to interact with the Toll-like receptors of the immune system ^{369–371}. Another common pyrimidine substitution is a 2'-Fluor modification (2'-F), also applied to Macugen ³³² and has since been used to enhance the nuclease resistance of aptamers ^{358,372–375}. Another approach is the use of RNA Spiegelmers®, which are built from L-ribose units and not recognized by nucleases ^{376–379}. Although DNA aptamers are more stable due to the lack of an 2'-OH group, their biostability and that of RNA aptamers can be drastically enhanced by incorporating locked nucleic acids into the sequence ^{346,380}.

To increase the half-life of aptamers *in vivo*, they can be attached to larger materials, slowing renal clearance by increasing the aptamers mass above the renal filtration threshold ^{368,381}.

The most commonly attached material is polyethylene glycol, which has been used to increase the half-life of Macugen in humans ^{331,382} as well as the *in vivo* stability of numerous aptamers in animal models. This modification has also been reported to increase nuclease resistance and decrease accumulation of aptamers in non-target tissue ^{371,383–385}. Other possible materials to attach to aptamers include gold particles and lipid tails ^{386,387}.

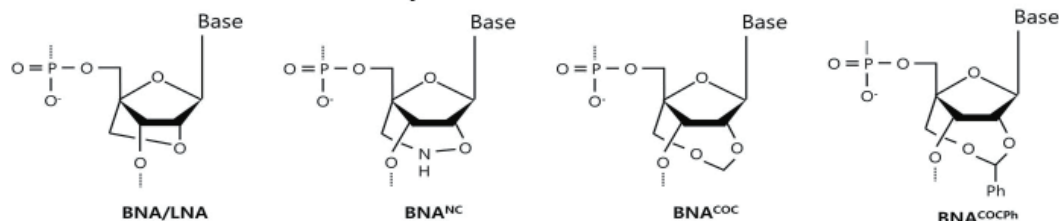
It should be noted that such post-SELEX modifications of aptamers can confer additional benefits apart from their main goal, such as an increase in binding affinity, but especially larger modifications can also interfere with the aptamer-target interaction thus rendering the compound useless. Therefore, there is no widely recognized optimal modification strategy; the extent and nature of post-SELEX modifications has to be tailored to the specific aptamer of interest ^{326,356,368}.

Ribose Modification – 2'-modification

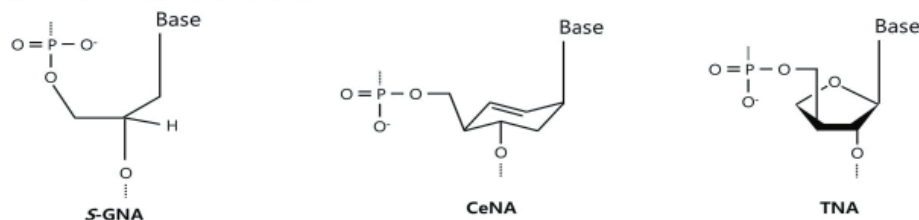


2'-fluor (F), 2'-methoxy (OCH₃), 2'-thio (-SH), 2'-azido (-N₃), 2'-hydroxymethyl (-CH₂OH) nucleotide

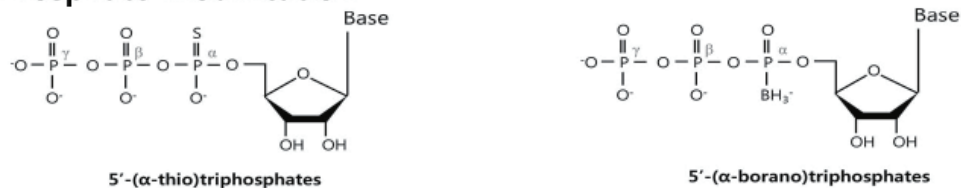
Ribose Modification – BNA/LNA



Ribose Modification – Others



Phosphate Modification



Base Modification

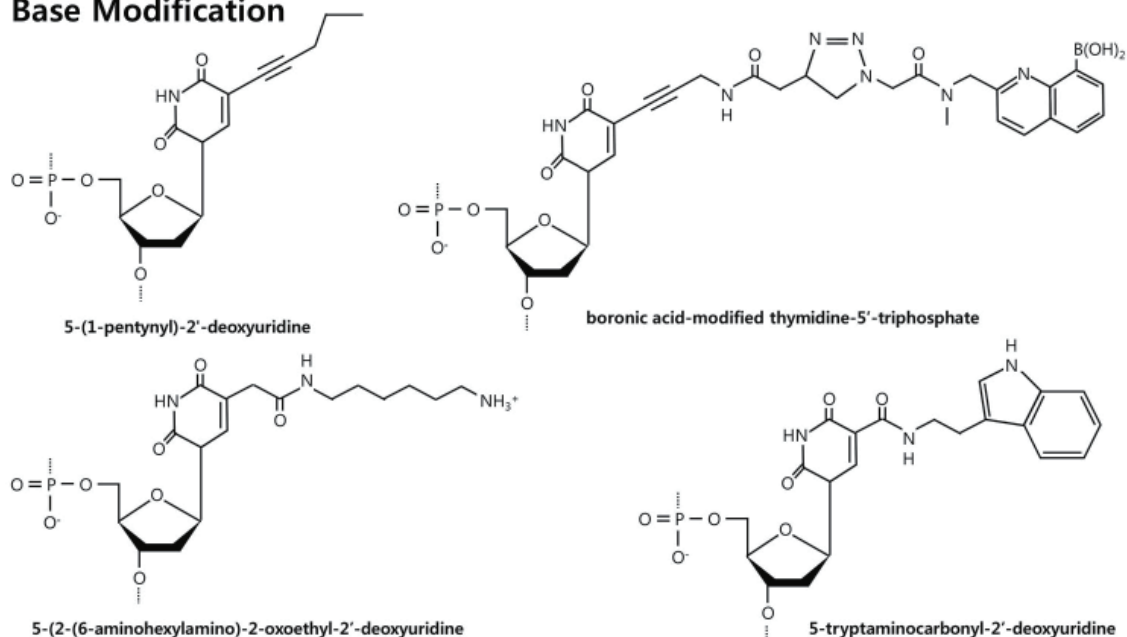


Figure 1.4.3 Examples of structures of chemically modified nucleotides.

The simplest ribose 2' modification is widely used to increase aptamer stability in vivo. Phosphate and base modification are also used for this purpose. Substitution of F, OCH₃, SH or CH₂OH for 2'-OH (H) is widely used. BNA/LNA was designed to structurally protect 2' site. In addition, thiol (S) or borane (BH₃) group is introduced to α phosphate to strengthen oligonucleotide backbone. Functional groups can also be introduced into the base. Modified from ^{368,388}.

1.5 Objective of the thesis

The long term goal of our research is the specific transport of microRNAs into cardiac fibroblasts after cardiac ischemia or other adverse cardiac events to initiate transdifferentiation into cardiomyocytes. Based on prior research mentioned above, this should lead to a drastic increase in regeneration as well as long term prognosis and symptoms after cardiac events. To achieve this, we have determined three major intermediate goals of the thesis, which could then be combined to reach the primary objective.

1. Delivery of functional microRNA into cells of the cardiovascular system. For this, we intend to use non-specific aptamers, as there are none reported to be specific for any cells of the vasculature. As proof of concept, we plan to develop aptamers to deliver miR-126, which is a well-studied microRNA, which may be useful for treating cardiovascular disease or cancer (see 1.3.3).
2. Reproduce, adapt and optimize the reprogramming protocol to initiate the conversion of adult murine cardiac fibroblasts to cardiomyocytes. This step should establish the microRNAs that should be used in later steps to induce cardiac reprogramming in vivo
3. Selection of aptamers specific for adult murine cardiac fibroblasts. This would allow specific in vivo delivery of the miRs used for reprogramming without causing unwanted side effects in other cell types of the heart.

2. Methods

Some of the methods described hereafter have already been described in ³⁸⁹, which will be noted next to the heading of the section. The methods section of that manuscript has been written exclusively by the first author, Jan-H. Rohde.

2.1 Isolation of adult murine cardiac fibroblasts

Two methods were used to isolate fibroblasts from the hearts of adult C57Bl/J6 mice.

1. **Langendorff-Perfusion** ³⁹⁰: *Wildtype* C57Bl/J6 mice were treated with 50 units (U) heparin to prevent coagulation and then sacrificed using isoflurane. Hearts were then excised and a cannula was inserted into the aorta. The heart was then hung onto a Langendorff-perfusor and flushed first with a physiological buffer solution adapted to increase CM survival (see material section), then with digestive enzyme 420 U/ml Collagenase II (Worthington, Lakewood, NJ, USA) in this buffer with 1 mM CaCl₂ for 7-11 minutes (min) until the heart became white and flaccid. The hearts were then dissected in digestive enzyme in buffer for 1 min, after which medium containing 15% fetal bovine serum (FBS, Lonza, Basel, Switzerland) was used to inactivate the collagenase. The tissue was minced further and sheared using pipettes, and then the cell suspension was passed through a 100 µM cell strainer. The leftover tissue fragments were plated on a 6 cm culture dish. The cell suspension was centrifuged at 22 x g for 3 min to remove the large cardiomyocytes and then the supernatant was centrifuged again for 300 x g to pellet the adult murine cardiac fibroblasts (AMCF). The pellet was resuspended in AMCF-medium and seeded in culture containers.
2. **Extravasation** ⁹⁵: *Wildtype* C57Bl/J6 mice were treated with 50 U heparin, and then anesthetized using isoflurane. Hearts were then excised and a cannula was inserted into the aorta. The heart was then flushed with Dulbecco's Phosphate Buffered Solution (DPBS) using a syringe to remove residual blood, which could impair the digestive process. Subsequently, hearts were transferred into 3.5 cm cell culture dishes and cut into fragments using shears and scalpels. The heart fragments were then digested using 420 U/ml per ml Collagenase II (Worthington, Lakewood, NJ, USA) for ~5 min. Digestion was then stopped by taking up the fragments in AMCF medium and cells were seeded in culture flasks. During the course of several weeks,

fibroblasts migrated from the tissue fragments to the culture containers. Tissue fragments were usually removed after 2-4 weeks, depending on the observable amount of extravasated AMCF.

For both procedures, the antifungal Nystatin was added to the medium for the first 2-4 weeks of culture, as both procedures exposed the hearts to airborne yeast and fungi.

2.2 Cell culture ³⁸⁹

Human umbilical cord-derived venous endothelial cells (HUVEC) were purchased from Lonza and cultured in endothelial cell basal medium (EBM, Lonza, Basel, Switzerland). Medium was supplemented with 10% FBS (Lonza, Basel, Switzerland), rather than the 1% suggested by Lonza, and endothelial cell growth medium (EGM) SingleQuots™ supplements, (Lonza, Basel, Switzerland) without adding the supplied ascorbic acid; these are the optimal conditions determined by people in our laboratory. For the functional assays, HUVEC of passage two (for the spheroid sprouting assay) or three (HUVEC recruitment assay) were used.

Murine endothelial cells (MEC) of the immortalized strain H5V were provided by Dr. E. Dejana (Department of Biomolecular Sciences and Biotechnologies, School of Sciences, University of Milan, Italy). MEC were cultured in Dulbecco's modified Eagle medium (DMEM, Sigma-Aldrich, St. Louis, MI, USA) supplemented with 10% FBS and a penicillin and streptomycin solution (P/S, Roche, Mannheim, Germany) diluted according to the manufacturer's instructions.

Murine embryonic fibroblasts (MEF) were grown in DMEM (Sigma-Aldrich, St. Louis, MI, USA) supplemented with 20% Medium-199 (M-199, Sigma-Aldrich, St. Louis, MI, USA), 15% FBS and P/S or DMEM with 10% FBS and P/S; the composition seemed to have little impact on the cells so whatever medium was readily available at the time was used.

Prof. Dr. M.A. Rieger (LOEWE Center for Cell and Gene Therapy, Goethe-University, Frankfurt am Main, Germany) was kind enough to provide the MCF7 and SK-BR3 breast cancer cell lines. These were cultured in DMEM (high glucose, no glutamine, Gibco, Carlsbad, CA, USA) supplemented with 10% FBS, 1% Insulin-Transferrin-Selenium solution in Earle's balanced salt solution (EBSS, Gibco, Carlsbad, CA, USA) and P/S.

2.3 Aptamer acquisition ³⁸⁹

2'-F (2'-deoxy-2'-fluoro)-modified RNA aptamers as well as chimera constructs were acquired from Dharmacon, Lafayette, USA (sequences see Table 1). Secondary structures of the aptamers and Precursor-microRNA (pre-miR) were predicted by the RNAstructure software (<http://rna.urmc.rochester.edu/RNAstructure.html>; Figure 4.3. 1a-c) and the sequences were designed to not interfere with their native folding.

A scrambled version of the TRA was designed to act as a control construct and ordered as single stranded DNA (ssDNA) from Sigma-Aldrich (St. Louis, MI, USA). The ssDNA was then amplified using standard PCR reagents with 2mM MgCl₂ (Sigma-Aldrich, St. Louis, MI, USA). The run protocol used was: 93 °C for 3 min, 15 rounds heating to 94 °C for 1 min, 37 °C for 2 min, 72 °C for 3 min, followed by a final annealing step at 72 °C for 7 min. The control aptamer was then run on an agarose gel, purified (see 2.4), transcribed *in vitro* using T7 Durascribe kit (Epibio, Madison, WI, USA) and precipitated using trizol and ethanol (details see 2.7).

2.4 Gel purification of Pool DNA ³⁸⁹

DNA was run on a gel made by dissolving 3% agarose (Lonza, Basel, Switzerland) in 1 millimolar (mM) lithium tetraborate (LB, Sigma-Aldrich, St. Louis, MI, USA) buffer; this buffer has enhanced conductivity compared to more widely used Tris/Acetic acid/EDTA or Tris/Borate/EDTA buffers and allows a much faster run with equally clear resolution. The gel was placed in the buffer and DNA was loaded using a loading buffer made from glycine and Orange G (Sigma-Aldrich, St. Louis, MI, USA) since the sodium salts in commercially available loading dyes can react with the LB, leading to a blurring of the bands on the gel. DNA was run through the gel at 200 Volt (V) for 15-30 min along with the GeneRuler ultra low range ladder (10-300 bp; Thermo Fisher Scientific, Carlsbad, CA, USA). Bands of appropriate size (68 nucleotides for the Rossi pool, 124 bp for the Süß Pool, see 3.1.11) were excised. The DNA was then purified from the gel using the QIAquick gel extraction (QIAGEN, Venlo, the Netherlands) or Zymoclean Gel recovery kits (Zymo Research, Freiburg, Germany). Briefly, the gel was dissolved in dissolving buffer belonging to the kit and applied to the columns. The DNA retained in the columns was then washed two times with washing buffer containing ethanol (EtOH) and eluted using water treated with 1,2-dimyristoyl-sn-glycero-3-phosphocholine (DMPC). The DNA concentration was determined using a Nanodrop

spectrophotometer (Thermo Scientific, Waltham, MA, USA) by measuring the amount of ultraviolet light absorbed by the bases of the DNA³⁹¹.

2.5 RNA extraction using trizol³⁸⁹

One volume (Vol) trizol was added directly to cells or to RNA in solution. After a brief incubation 0.2 Vol of chloroform was added, the solution was shaken rapidly for 15 seconds (sec) and incubated at room temperature for 3 min. The solution was then centrifuged at 12.000 x g for 15 min. The RNA is located in the aqueous upper phase after centrifugation and was carefully removed from the remaining trizol and the precipitated, white DNA layer. RNA was subsequently submitted to EtOH-precipitation (see 2.6) to reduce volume and remove salts.

2.6 Ethanol precipitation of DNA/RNA³⁸⁹

0.1 Vol of 3 M sodium acetate and 1 µl of GenElute-Linear Polyacrylamide (Sigma-Aldrich, St. Louis, CA, USA) was added to DNA or RNA in solution and vortexed. 2.5 Vol of 99% EtOH were then added, followed by vortexing and 2 h incubation on ice. The solution was centrifuged at maximum speed on a tabletop centrifuge (< 20.000 x g) for at least one hour. The pelleted DNA/RNA was then washed at least once with 70% ethanol and centrifuged again at maximum speed. The ethanol was then decanted off and the pellet was dried then reconstituted in DMPC-treated water. The DNA/RNA concentration was determined using a Nanodrop spectrophotometer (Thermo Scientific, Waltham, MA, USA).

2.7 *In vitro* transcription of DNA using T7 Durascribe kit³⁸⁹

DNA was transcribed to RNA *in vitro* using the Durascribe T7 kit (Epibio, Madison, WI, USA). Briefly, the DNA was linearized by heating it to 65°C for 10 min, then it was incubated with 5mM dithiothreitol (DTT), 2.5mM Adenosine triphosphate, Guanine triphosphate, 2'-F modified CTP and 2'-F modified UTP with RNase-inhibitor (Life Science Technologies, Paisley, UK) in a buffered solution 6 h (for the control aptamer and the Rossi Pool) or overnight (for the Süß Pool) at 37 °C. The DNA was then digested with DNase 1 (Epibio, Madison, WI, USA) for 15 min, followed by trizol extraction of the remaining RNA. The aqueous phase of the extraction was subjected to another DNase 1 (Sigma-Aldrich, St. Louis, CA, USA) digestion for 1 h to remove traces of DNA, followed by another trizol extraction of the RNA. RNA was purified from the aqueous phase using 2 h of EtOH-precipitation (see 2.6) and washed with 70% EtOH to remove salts. RNA was then passed through BD30 columns (Becton Dickinson,

East Rutherford, NJ, USA) to remove nucleotide fragments of less than 30 kilodalton mass (cut DNA, single nucleotides etc.). The RNA was run on a 20% acrylamide gel using TBE buffer to analyze the purity and size of the RNA-pool.

2.8 Aptamer and chimera construct folding ³⁸⁹

Before use, aptamers and chimeras were folded and then annealed by separately heating all RNA fragments at a concentration of 5 μ M in DPBS containing $MgCl_2^+$ and $CaCl_2^+$ (Sigma-Aldrich, St. Louis, MI, USA) at 70 °C for 5 min, followed by 10 min cooling at room temperature. The constructs were subsequently incubated at 37 °C for 10 min to allow folding. The individual components of the chimeras were then mixed and incubated at 37 °C for 10 min to anneal them. In case of chimera 2 (Ch2), which is made of three separate components, the mature hsa-miR-126-3p was added to the mature-126-5p-stick construct and allowed to anneal for 5 min at 37 °C before the TRA-stick construct was added and allowed to anneal for another 10 min at 37 °C. The constructs were then diluted to working concentration in medium appropriate to the cell type used. Annealing of the constructs was examined by running them on 12-20% acrylamide gel containing urea in TBE buffer. Briefly, samples were mixed with RNA loading dye (New England Biolabs, Ipswich, MA, USA) and linearized at 95 °C for 5 min, then loaded onto the gel together with a low range RNA ladder (New England Biolabs, Ipswich, MA, USA) and run at low (≤ 80) voltage (V) for 3-5 h. The gel was then stained using Midori Green (Nippon Genetics, Tokyo, Japan) in TBE buffer for 15-30 min and visualized using UV-light on a Fluorchem M (Proteinsimple, St. Jose, CA, USA) or Chemidoc Touch imaging system (Bio-Rad, Hercules, CA, USA).

2.9 Cell treatment with aptamers and chimeras to harvest RNA ³⁸⁹

Cells were seeded in 12-well culture plates (Greiner, Kremsmünster, Austria) and grown to 50-90% confluence. Cells were then blocked with 0.1 mg/ml yeast transfer RNA (tRNA, Sigma, St. Louis, MI, USA) in medium appropriate to the cells for 30 min to inhibit unspecific binding. Afterwards, cells were treated with aptamers at concentrations ranging from 50 to 500 nM in 200 μ l cell appropriate medium for 1 h. Then cells were either directly used for detecting early aptamer up-take at 1 h or 1.5 ml medium was added for prolonged incubation (commonly 24 h).

2.10 RNA samples of microRNA overexpression using liposomal transfection³⁸⁹

Cells were seeded in 12-well culture plates (Greiner, Kremsmuenster Austria) and grown to 50-90% confluence. Pre-miR™ microRNA mimics (Ambion/Life Technologies, Carlsbad, CA, USA) were mixed with 2.5 µl Lipofectamine® RNAiMAX (Life Technologies, Carlsbad, CA, USA) in 500 µl OptiMEM at a concentration of 30 nM and incubated at room temperature for 15 min. Cells were washed with 1.5 ml OptiMEM (Gibco, Carlsbad, CA, USA) and then transfected by adding the Pre-miR solution and 1 ml OptiMEM to the wells, leading to a final concentration of 10 nM miR-mimic. Cells were incubated for 4 h, and then the OptiMEM was replaced with 1.5 ml of the appropriate medium.

2.11 Isolation of total and internal RNA using QIAgen kit and qPCR analysis³⁸⁹

RNA was isolated from cells by adding trizol (QIAgen, Venlo, the Netherlands) and removing the aqueous phase (see 2.5). The phase was then applied to miRNAeasy kit columns (QIAgen, Venlo, the Netherlands) according to the manufacturer's protocol. To isolate only internal RNA (iRNA), cells were detached from culture dishes using trypsin. It should be noted that trypsin also digest most membrane bound proteins and releases any RNA bound to these proteins in the process. Then, cells were suspended in 100 µl DPBS and subjected to digestion with 10 U of Riboshredder RNase cocktail (EpiBio, Madison, WI, USA) for 15 min at 37 °C (Gibco, Carlsbad, CA, USA) prior to addition of trizol. Aptamer levels were analyzed using custom made primers (sequences see table 3.8) and SYBR green reagents (Life Technologies, Carlsbad, CA, USA), both on a StepOne thermo cycler (Applied Biosystems, Carlsbad, CA, USA). Copy numbers were calculated based on a standard curve using recombinant miR-126-3p (Life Technologies, Carlsbad, CA, USA).

2.12 Aptamer visualization³⁸⁹

Fluorescin-conjugated GIRM was purchased from Dharmacon (Lafayette, CO, USA). The TRA and control aptamer were labelled with Cy3 using the LabelIT™ siRNA tracker kit (Mirus, Madison, WI, USA) according to the manufacturer's protocol. Cells on 8-chamber glass slides were grown to confluence, then treated with 150 µl of 500 nM aptamer in medium (see 2.8) and fixed 1 h after treatment using 4% formaldehyde (FA) in PBS. The cell nuclei were stained with 4',6-diamidino-2-phenylindole (DAPI) and cells were subsequently mounted with coverslips. The slides were immediately used to take images with an AxioObserver

microscope (Zeiss, Oberkochen, Germany) or kept in the fridge for analysis on the same microscope later.

2.13 VCAM-1 Western Blot ³⁸⁹

48 h after lipofection with miR-126-3p mimics or treatment with the chimera, ice-cold RIPA buffer (Sigma, St. Louis, MI, USA) containing protease inhibitor cocktail (Roche, Mannheim, Germany) was used to lyse the cells and protect the protein samples. 30 µg protein per sample were run on a 10% acrylamide gel (AppliChem, Darmstadt, Germany), blotted to a methylcellulose membrane and blocked with 5% non-fat milk or 3% bovine serum albumin (BSA) in Tris-buffered saline solution containing 1% Tween20 (TBST). The membranes were then stained with primary antibodies for VCAM-1 (abcam, Cambridge, UK) or α-tubulin (Neomarkers, Fremont, CA USA) in TBST, containing 5% non-fat milk or 3% BSA respectively, overnight. Membranes were washed and secondary anti-rabbit-horseradish peroxidase (HRP) or anti-mouse-HRP antibodies (GE Healthcare, Buckinghamshire, UK) in TBST were applied to the membranes for 2 h. The blots were then treated with Immobilon Western substrate (Millipore, Billerica, MA, USA) and imaged using a Fluorchem M (Proteinsimple, St. Jose, CA, USA) or Chemidoc Touch (Bio-Rad, Hercules, CA, USA) imaging system. Relative amounts of proteins were calculated using Fiji software ³⁹² to analyze images of the blots .

2.14 HUVEC Spheroid Assay ³⁸⁹

HUVEC in 12-well plates were transfected with miR-126-3p or control RNA or treated with aptamers/chimeras (see 2.9). After 24 h, HUVEC were harvested and 400 cells per well were seeded in 96-well plates in EBM (Gibco, Carlsbad, CA, USA) containing methylcellulose (Sigma-Aldrich, St. Louis, CA, USA) for 24 h. Under these conditions the cells from spheroid clusters, which were harvested and divided in two wells of a 24-well plate and seeded in a mixture of collagen solution and medium containing methylcellulose. One half of the spheroids were left under basal conditions. The other half was treated with 50 ng/ml VEGF-A to stimulate endothelial sprouting (Peprotech, Rocky Hill, CO, USA). After 24 h, cells were fixed with 4% FA in DPBS and images were taken using an AxioObserver microscope (Zeiss, Jena, Germany). The sprout length observed in the microscopic images was measured manually using Fiji software ³⁹².

2.15 Cell counting kit 8 (Cck8) Proliferation assay ³⁸⁹

MCF7 and SK-BR3 breast cancer cells were seeded as triplicates in a 96 wells plate and grown overnight. The next day, cells were then treated with 10 nM miR-126-3p or -5p (150 μ l OptiMEM with Lipofectamine[®] RNAiMAX) or 500 nM of the chimeras (30 μ l/well; see 2.8). 72 h after the treatment, medium was replaced and cells were incubated in medium containing Cck8 assay reagent (Dojindo, Kumamoto, Japan) for 3 h according to the manufacturer's protocol. The absorption of light of each well at a wavelength of 450 nm was then measured using a Synergy HT plate reader (BioTek, Winooski, VT, USA).

2.16 HUVEC recruitment assay ³⁸⁹

5 x 10⁵ MCF7 or SK-BR3 breast cancer cells were seeded in 24-well plates and incubated overnight before treatment with 10nM Pre-miR-126-3p and -5p, 500nM TRA or 500nM Ch3 for 72 h (see 2.9). 16 h prior to the analysis medium was replaced by DMEM containing 0.5% BSA, since the FBS in the serum is known to induce EC recruitment. Boyden chambers with transwell membranes (pore size of 8 μ m, Millipore, Billerica, MA, USA) containing 50.000 HUVEC in EBM without FBS or SingleQuots[™] were then placed atop of the wells containing breast cancer cells. Both cell types were then co-cultured for 5 h. The inserts with the HUVEC were removed and cells were fixed in 4% FA. Subsequently, HUVEC adherent to the upper part of the membrane were removed using cotton swabs. The HUVEC on the bottom were stained with DAPI and pictures were taken using an AxioObserver microscope (Zeiss, Oberkochen, Germany). The number of migrated cells visible on the bottom of the membrane in the microscopic images were automatically counted using Fiji software ³⁹².

2.17 Reprogramming using a microRNA cocktail

AMCF were seeded in 6-well culture plates (Greiner, Kremsmuenster, Austria) or 6 cm dishes and grown to 50-90% confluence. Pre-miR[™] microRNA mimics (Ambion/Life Technologies, Carlsbad, CA USA) for mature murine miR-1a-5p, -133a-3p, -208b-3p and -499-3p (mature miR-1-3p, 133-3p, 208b-3p and 499-3p are conserved between mice and humans) were mixed with 2.5 μ l Lipofectamine[®] RNAiMAX (Life Technologies, Carlsbad, CA, USA) in 500 μ l OptiMEM at a concentration of 30 nM and incubated at room temperature for 15 min. Cells were washed with 1.5 ml OptiMEM (Gibco, Carlsbad, CA, USA) and then transfected by adding the Pre-miR mimic solution and 1 ml OptiMEM to the wells, leading to a final concentration of 10-100 nM (single or cocktails of multiple) miR-mimics or the same amount of a control construct called negmiR (Ambion/Life Technologies, Carlsbad, CA, USA). The cells

were incubated for 4 h before the OptiMEM was replaced with 1.5 ml AMCF medium. The AMCF were cultivated for 3 days after which RNA was isolated to check for the overexpression of the miRs. To analyze reprogramming, AMCF were 5 to 21 days post-transfection after which RNA was isolated using the miRNAeasy kit from Qiagen (Venlo, the Netherlands; see 2.11 for procedure) and expression of markers for stemness and cardiomyocytes was analyzed via qPCR using custom primers (see table 3.1.8) with SYBR green reagents (Life Technologies, Carlsbad, CA, USA) on a StepOne cycler (Applied Biosystems, Carlsbad, CA, USA).

Due to the inefficacy of the reprogramming using only miRs, we altered the reprogramming protocol in accordance with previously published works (see below). Firstly, a specific cardiac reprogramming medium (DMEM GlutaMAX™ with 15% FBS, P/S and 0.1 mM β-mercaptoethanol) was used after miR-treatment to facilitate reprogramming into a CM state. Furthermore, some of the cells were treated with growth factors and small molecules to enhance the actions of the miR-cocktail. Specifically, 20 ng/ml BMP4^{393,394} and 1 nM JAK-inhibitor 1^{319,393} was used. The AMCF were cultivated for 5 to 21 days after which RNA was isolated using the miRNAeasy kit from Qiagen (Venlo, the Netherlands; see 2.11) and expression of markers for stemness and cardiomyocytes was analyzed via qPCR using custom primers (see table 3.1.8) with SYBR green reagents (Life Technologies, Carlsbad, CA, USA) on a StepOne thermocycler (Applied Biosystems, Carlsbad, CA, USA).

2.18 SELEX Pool amplification

For the sequences of both aptamer pools, please consult table 3.11. A pool, with a sequence of 20 randomized nucleotides (identical to the one used at the lab of Prof. John J. Rossi, Beckman Research Institute of City of Hope, Duarte, CA, USA) was ordered from integrated DNA Technologies (Coralville, IA, USA). The protocol for the amplification and SELEX was kindly provided by Dr. Jiehua Zhou (Beckman Research Institute of City of Hope, Duarte, CA, USA). The pool was amplified using 10X PCR buffer (Sigma-Aldrich, St. Louis, CA, USA), 200 nM dNTP mix, 2 mM MgCl₂, 2 μM forward and reverse primer and 50 U/ml Taq-Polymerase (Sigma-Aldrich, St. Louis, CA, USA). Another DNA template for an RNA aptamer pool consisting of 2 stretches with 26 randomized nucleotides was kindly received from Prof. Dr. Beatrix Süß (TU Darmstadt, Germany) and a protocol for the amplification and SELEX was kindly provided by Mr. Florian Groher (TU Darmstadt, Germany). The DNA template was

amplified using optimized PCR buffer (50 mM KCl, 10 mM Tris, pH 9, 0.1% Triton^{X100}), 200 nM dNTP mix, 1.5 mM MgCl₂, 2 μM forward and reverse primer and 50 U/ml Taq-Polymerase (Sigma-Aldrich, St. Louis, CA, USA) on a Tprofessional basic gradient thermocycler (Biometra, Göttingen, Germany). The purity and size of the pool DNA was analyzed by running it on a 3% agarose gel using 1 mM LB buffer. The aptamer pools were then transcribed *in vitro* (see 2.7).

2.19 Cell SELEX for RNA pool with 20 randomized nucleotides

During the cell SELEX, the aptamer pool was applied in conditions increasingly unfavorably for binding to the AMCF. Please refer to tables 2.19a+b for the specific conditions of each round. Before the cell SELEX, cells were washed three times to remove extracellular matrix proteins, blocked with 0.1 mg/ml yeast tRNA (Sigma-Aldrich, St. Louis, CA, USA) to prevent unspecific RNA binding. The RNA Pool in DPBS+ (containing MgCl₂ and CaCl₂, Sigma-Aldrich, St. Louis, CA, USA) was heated to 70 °C for 5 min to linearize the species, then cooled for 10 min at room temperature and consequently incubated at 37 °C for 10 min to facilitate proper folding. Cells were then incubated with the pool in AMCF-medium for 30 or 90 min (30 min for the 1st attempted SELEX, 90 for the 2nd), then washed with DPBS as often as indicated in tables 2.19a and b.

The following actions were taken only during those rounds of SELEX denoted in table 2.19a and b. For negative selection, the pool was pre-incubated with human or murine endothelial cells (EC) prior to the incubation with AMCF and only species not binding to the EC were then incubated with the AMCF to clear binders unspecific to fibroblasts. To remove any aptamers that have not internalized into the AMCF, the cells were treated with trypsin to digest membrane proteins. After 7 min the digestion was stopped through addition of AMCF-medium (containing trypsin-inhibitors in the 15% FBS) and cells were scraped off the culture container and spun down at ~230 x g for 10 min. Cells were resuspended in 100 μl DPBS and treated with 10 μl Riboshredder RNase cocktail for 15 min at 37 °C to remove any RNA traces bound to the cellular membrane.

After the selection procedure, AMCF were taken up in trizol and RNA was extracted. The RNA was purified and washed by EtOH-precipitation, then reverse transcribed into cDNA using the Thermoscript RT kit (Life Science Technologies, Paisley, UK). After cDNA synthesis the cDNA was digested using RNase H from the kit to remove the 2'F-labeled RNA species.

Scout PCRs were then performed to determine how much cDNA would be necessary to allow optimal amplification without producing unwanted contaminating products (such as DNA without promotor or elongated sequences of aptamers sticking to another). Briefly, a PCR using the conditions described above was run for 15 rounds using 2, 0.2, 0.02 and 0.002 μ l cDNA and products were run on a 3% agarose gel to visualize them. When necessary, ran additional scout PCR's to determine the optimal conditions. The cDNA was then amplified using the scouted conditions and transcribed to RNA again (as described in 2.7) for the next round of cell SELEX.

Round	Cardiac Fibroblasts Number/culture dish/DPBS (ml)	Neg cells/number/culture dish/DPBS (ml)/ratio	Ribo Shredder	RNA pool	RNA conc.	Competitor tRNA during incubation	wash
1	1.5*10 ⁶ / T75 / 10	HUVEC/7*10 ⁶ /T75/10/1:7	No	4nmol	400nM	0	2*10ml
2	1.5*10 ⁶ / T75/ 10	MEC/28*10 ⁶ /T75/10/1:28	No	4nmol	400nM	100 µg	2*10ml
3	5*10 ⁵ / T25 / 5	HUVEC/7*10 ⁶ /T75/5/1:14	Yes	2nmol	400nM	200 µg	4*5ml
4	5*10 ⁵ / T25 / 5	MEC/28*10 ⁶ /T75/5/1:48	Yes	2nmol	400nM	400 µg	4*5ml
5	5*10 ⁵ / T25 / 5	HUVEC/7*10 ⁶ /T75/5/1:14	No	2nmol	400nM	400 ng	6*5ml
6	5*10 ⁵ / T25 / 5	MEC/28*10 ⁶ /T75/5/1:48	No	2nmol	400nM	400 ng	6*5ml
7	5*10 ⁵ / T25 / 5	HUVEC/7*10 ⁶ /T75/5/1:14	Yes	2nmol	400nM	400 ng	6*5ml

Table 2.19a: First SELEX protocol used for the pool with 20 randomized nucleotides

Round	Cardiac Fibroblasts Number/culture dish/DPBS (ml)	Neg cells/number/culture dish/DPBS (ml)/ratio	Ribo Shredder	RNA pool	RNA conc.	Competitor tRNA during incubation	wash
1	2.5*10 ⁶ / T125 / 10	-/-	yes	2nmol	200nM	1mg/10ml	3*15ml
2	2.5*10 ⁶ / T125 / 10	-/-	yes	2nmol	200nM	1mg/10ml	3*15ml
3	2.5*10 ⁶ / T125 / 10	MEC/47*10 ⁶ /T125/10/1:19	Yes	2nmol	200nM	1mg/10ml	3*15ml

Table 2.19b: Second SELEX protocol used for the pool with 20 randomized nucleotides

2.20 Cell SELEX for RNA pool with 52 randomized nucleotides

During the cell SELEX, the aptamer pool was applied in conditions increasingly unfavorably for binding to the AMCF. Please refer to table 2.20 for the specific conditions of each round. Before the cell SELEX, cells were washed three times to remove extracellular matrix proteins, then blocked with 0.1 mg/ml yeast tRNA (Sigma, St. Louis, CA, USA) to prevent unspecific RNA binding. The RNA Pool in DPBS+ (containing MgCl₂ and CaCl₂, Sigma, St. Louis, CA, USA) was heated to 70 °C for 5 min to linearize the species, then cooled for 10 min and consequently incubated at 37 °C for 10 min to facilitate proper folding. Cells were then incubated with the pool in DPBS+ for 30 or 90 min and washed as indicated in table 2.20. If indicated in table 2.20, the pool was pre-incubated with EC prior to the incubation with AMCF and only species not binding to the EC were then incubated with the AMCF to clear binders unspecific to fibroblasts. After the incubation, AMCF were taken up in trizol and RNA was extracted. The RNA was purified and washed by EtOH-precipitation, then reverse transcribed into cDNA using the Thermoscript RT kit (Life Science Technologies, Paisley, UK). After cDNA synthesis the cDNA was digested using RNase H from the kit to remove the 2'-F-labeled RNA species. Scout PCRs were then performed to determine how many cycles of PCR would be necessary to allow optimal amplification without producing unwanted contaminating products (such as DNA without promotor or elongated sequences of aptamers sticking to another). Briefly, a PCR using the conditions described above was run for 12-30 rounds. Samples were taken every 3 rounds and run on a 3% agarose gel to

visualize the products. When necessary, ran additional scout PCR's to determine the optimal conditions. The cDNA was then amplified using the scouted conditions and transcribed to RNA again (see 2.7) for the next round of cell SELEX. Gel-purified DNA (see 2.4) from Süß rounds 5-7 were taken to GenXPro (Frankfurt a.M., Germany) for sequencing.

Round	AMCF/culture dish/DPBS+ (ml)	Neg cells/number/culture/ratio	RNA pool	RNA conc.	Competitor tRNA	wash
1	6*10 ⁶ / T175 /10	none	2nmol	200nM	100ng/ml	3*15ml
2	6*10 ⁶ / T175 /10	none	2nmol	200nM	100ng/ml	3*15ml
3	6*10 ⁶ / T175 /10	HUVEC/12*10 ⁶ /T175/1:5	2nmol	200nM	10µg/ml	3*15ml
4	6*10 ⁶ / T175 /10	MEC/47*10 ⁶ /T175/1:19	2nmol	200nM	10µg/ml	3*15ml
5	1.5*10 ⁶ / T75 / 5	MEC/47*10 ⁶ /T175/1:31	1nmol	200nM	50µg/ml	4*10ml
6	1.5*10 ⁶ / T75 / 5	HUVEC/12*10 ⁶ /T175/1:8	1nmol	200nM	50µg/ml	4*10ml
7	1.5*10 ⁶ / T75 / 5	HUVEC/12*10 ⁶ /T175/1:8	1nmol	200nM	100µg/ml	6*10ml

Table 2.20: Second SELEX protocol used for the pool with 2x26 randomized nucleotides

2.21 Bioinformatics analysis of SELEX round 5-7

Sequences in the data from GenXPro (Frankfurt a.M., Germany) were sorted according to the number of reads. Since the DNA was amplified before sequencing, it contained the sense and antisense sequences of the candidate aptamers. The antisense reads were removed and the 1000 sequences with the most reads were analyzed. Using MEME and DREME³⁹⁵⁻³⁹⁷, these 1000 candidates were analyzed for conserved sequence motifs. The data also included a list with the 10.000 most plentiful sequences for each round (sense and antisense), which was used to further confirm the conserved motifs discovered by MEME and DREME.

2.22 Testing candidate AMCF aptamers

The ten chosen potential AMCF aptamer candidates were synthesized as ssDNA strands (Sigma-Aldrich, St. Louis, MI, USA). The ssDNA was then amplified using standard PCR reagents with 2mM MgCl₂ (Sigma-Aldrich, St. Louis, MI, USA). The run protocol used was: 93 °C for 3 min, 15 rounds heating to 94 °C for 1 min, 37 °C for 2 min, 72 °C for 3 min, followed

by a final annealing step at 72 °C for 7 min. DNA was run on a 3% agarose gel to analyze size and little contaminating DNA was found; consequently, unpurified DNA was used for *in vitro* transcription. DNA was transcribed in vitro using mutant T7 polymerase (see 2.7); 10µg DNA were used per T7 reaction. The RNA was run on a 12% acrylamide gel using TBE buffer to analyze the purity and size of the RNA-pool. The RNA concentration of the candidates was measured and they were diluted to 20nM in DMPC-water.

To assess the binding and internalization of the AMCF aptamer candidates AMCF, HUVEC and MEC were treated with 2 nM solutions of the aptamers. First, aptamers were folded (see 2.8) while cells were blocked with 0.1 mg/ml yeast tRNA, then aptamers solution was applied for 90 minutes (See 2.9) before total or internal RNA was isolated and used for qPCR analysis (see 2.11). The initial aptamer pool and TRA served as comparative controls.

2.23 Statistics and figures

Statistical analysis was performed with the Prism 5 software (Graphpad, La Jolla, CA, USA) using student's t-test or ANOVA. All bar graphs represent the mean ± the standard error of the mean (SEM). Adobe Illustrator software (Adobe systems, San José, CA, USA) was used to compile the figures and create the schematic images of the aptamers, chimeras and candidates (4.1.1a+b, 4.3.3, 4.4.3).

3. Material

3.1 Consumables

Item	Manufacturer
96 well cell culture plates, U bottom	Greiner Bio-one GmbH (Frickenhausen, Germany)
Cell culture dishes (3.5,6 or 10cm)	Greiner Bio-one GmbH (Frickenhausen, Germany)
Cell culture flasks (T25, T75, T175)	Greiner Bio-one GmbH (Frickenhausen, Germany)
Cell scraper	Greiner Bio-one GmbH (Frickenhausen, Germany)
Cell scraper (25cm)	Sarstedt (Newton, NC, USA)
Cell strainer (100µm)	BD Biosciences (Erembodegem, Belgium)
Color fixed pH indicator strips	Macherey-Nagel GmbH (Düren, Germany)
CoStar Multiwell cell culture plates (96 well)	Sigma-Aldrich (St.Louis, MO, USA)
Culture Inserts (for migration assays)	Ibidi (Martinsried, Germany)
Biopur Combitips (0.1, 0.2, 0.5, 2.5, 5, 10 ml)	Eppendorf (Hamburg, Germany)
Cotton Swabs, 4-5mm	Noba Danz GmbH (Wetter, Germany)
Costar stripette serological pipettes	Corning (Big flats, NY, USA)
Filter Tips TipOne RPT (10, 100, 1000µl)	Starlab (Ahrensburg, Germany)
Filter Tips SureOne (10, 100, 1000µl)	Thermo Fisher Scientific (Waltham, MA, USA)
Hybond Nitrocellulose membrane (100µm)	GE Healthcare (Little Chalfont, UK)
Immobilon-FL transfer membrane (PVDF)	Millipore (Billerica, MA, USA)
Lab-Tek II chamber glass slides (8 well)	Nalge Nunc International (Naperville, IL, USA)
Membrane Insert Costar T-well 6,5x8µm	Corning (Big flats, NY, USA)
Micro Bio-Spin 30 Columns	BioRad (Hercules, CA, USA)
Microtubes 2ml, polypropylene	Sarstedt (Newton, NC, USA)
Multiwell cell culture plates (6, 12, 24 and 96 well)	Greiner Bio-one GmbH (Frickenhausen, Germany)
Multiwell cell culture plates (12, 24 and 96 well)	Corning (Big flats, NY, USA)
Optical 96 well reaction plates	Applied Biosystems (Foster City, CA, USA)
Optical 384 well reaction plates	Applied Biosystems (Foster City, CA, USA)
Optical adhesive covers	Applied Biosystems (Foster City, CA, USA)
Pasteur Pipette	Carl Roth (Karlsruhe, Germany)
PCR tubes/strips of 8 tubes (0.2ml)	Biozym Scientific GmbH (Oldendorf, Germany)
Polypropylene falcon tubes (15ml and 50ml)	Greiner Bio-one GmbH (Frickenhausen, Germany)
Safe lock tubes (0.5, 1.5 and 2ml)	Eppendorf (Hamburg, Germany)
Steriflip sterilization kits (50 and 500ml)	Corning (Big flats, NY, USA)
Surgical Scalpels	Feather (Osaka, Japan)
Whatman paper	Macherey-Nagel GmbH (Düren, Germany)
µ-slide 8 chamber, glass bottom	Ibidi (Martinsried, Germany)

3.2 Equipment

Instrument	Model/type	Manufacturer
8 channel multipipette		Eppendorf (Hamburg, Germany)
Adjustable volume pipettes		Eppendorf (Hamburg, Germany)
Cell Cooler		Biocision (San Rafael, CA, USA)
Cell counting chamber	Neubauer, 0.1mm depth	Paul Marienfeld GmbH & Co. KG (Lauda-Königshofen, Germany)
Centrifuge (falcons, plates)	Multifuge 3S-R	Heraeus Instruments (Osterode, Germany)
Centrifuge benchtop	Biofuge Primo R	Heraeus Instruments (Osterode, Germany)
CO₂ Incubator	Heracell	Heraeus Instruments (Osterode, Germany)
Confocal Microscope	LSM 780, Axio Observer	Zeiss (Jena, Germany)
Confocal Microscope	DMI6000B	Leica microsystems (Wetzlar, Germany)
Digital heat block	949307	VWR (Leuven, Belgium)
Digital heat block		Liebisch Labortechnik (Bielefeld, Germany)
FACS	Canto II	BD Biosciences (Franklin Lakes, NJ, USA)
Fine Balance (1mg – 110g)		Denver Instrument (Bohemia, NY, USA)
Homogenizer	FastPrep24	MP Biomedicals (Solon, OH, USA)
Imaging system	Chemidoc Touch	Bio-Rad (Hercules, CA, USA)
Imaging system	FluorChem M system	Proteinsimple (Santa Clara, CA, USA)
Magnetic stirring rod		Carl Roth (Karlsruhe, Germany)
Microplate reader	Synergy HT	Biotek (Winooski, VT, USA)
Microscope	Axio Observer Z1	Zeiss (Jena, Germany)
Microscope	Axiovert 100	Zeiss (Jena, Germany)
Microscope	Primovert	Zeiss (Jena, Germany)
Microwave		Severin (Sundern, Germany)
Mini gel electrophoresis setup	Protean Tetra	Bio-Rad (Hercules, CA, USA)
Mini Trans Blot Cell setup		Bio-Rad (Hercules, CA, USA)
Multipipette	XStream	Eppendorf (Hamburg, Germany)
pH-meter	PB-11	Sartorius (Göttingen, Germany)
Pipette	Pipetboy	Integra Biosciences AG (Zizers, Switzerland)
Pipette	ErgoOne FAST	Starlab (Ahrensburg, Germany)
Powersupply	Powerpac HC	BioRad (Munich, Germany)
QIACube		Qiagen (Venlo, the Netherlands)
Real time PCR system	StepOnePlus	Applied Biosystems (Foster city, CA, USA)
Real time PCR system	Via-7	Thermo Scientific (Waltham, MA, USA)

Safety cabinet	HeraSafe HS18	Heraeus (Hanau, Germany)
Safety cabinet	Mars Safety Classe 2	Scanlaf (Lyngø, Denmark)
Scales (1-600g)		Ohaus (Parsippany, NJ, USA)
Spectrophotometer	Nanodrop 2000	Thermo Scientific (Waltham, MA, USA)
Thermocycler	TProfessional basic gradient	Biometra (Göttingen, Germany)
UV Trans illuminator	T2201	Sigma-Aldrich (St.Louis, MO, USA)
Vortexer	Vortex Genie 2	Scientific Industries (Bohemia, NY, USA)
Water bath	1008	GFL GmbH (Burgwedel, Germany)

3.3 Chemicals and reagents

Item name	Manufacturer
1,2-dimyristoyl-sn-glycero-3-phosphocholine (DMPC)	Sigma-Aldrich (St.Louis, MO, USA)
2,3-Butanedione monoxime (BDM)	Sigma-Aldrich (St.Louis, MO, USA)
2X Fast SYBR green mix	Applied Biosystems (Foster City, CA, USA)
2x RNA loading dye	New England Biolabs (Ipswich, MA, USA)
3-(4, 5-Dimethylthiazol-2-yl)-2, 5-Diphenyltetrazolium Bromide (MTT)	Sigma-Aldrich (St.Louis, MO, USA)
37% Formaldehyde (FA)	AppliChem (Darmstadt, Germany)
4', 6- diamidin-2-phenylindol (DAPI)	Roche (Indianapolis, USA)
10X PCR buffer	Applied Biosystems (Foster City, CA, USA)
10X PCR buffer	Sigma-Aldrich (St.Louis, MO, USA)
10X PCR buffer (50mM KCl, 10mM Tris, 0.1% TritonX100)	Self-Made (chemicals see list below), used for amplification of n=52 and n=65 Pools
Acrylamide (PAA) 30%	AppliChem (Darmstadt, Germany)
Acetone	Sigma-Aldrich (St.Louis, MO, USA)
Agarose	Sigma-Aldrich (St.Louis, MO, USA)
Ammonium Persulfate (APS)	Carl Roth (Karlsruhe, Germany)
BD 30 Trizol	Sigma-Aldrich (St.Louis, MO, USA)
Bovine Serum Albumin (BSA) Fraction V	PAA laboratories (Pasching, Austria)
Bradford reagent	Bio-Rad (Hercules, CA, USA)
Bromophenol blue	Merck (Darmstadt, Germany)
Calcium dichloride (CaCl₂)	Merck (Darmstadt, Germany)
Chloroform	Sigma-Aldrich (St.Louis, MO, USA)
Collagenase Type II	Worthington Biochemical Corp. (New Jersey, USA)
Dimethyl sulfoxide (DMSO)	Sigma-Aldrich (St.Louis, MO, USA)
Dithiothreitol (DTT)	AppliChem (Darmstadt, Germany)
DMPC-water (RNase-free)	Self-made (treat water with 0.1% DMPC, autoclave twice)
DNase, RNase and protease-free water for injection	B. Braun AG (Melsung, Germany)
2-F dCTP	Jena Bioscience (Jena, Germany)
2-F dUTP	Jena Bioscience (Jena, Germany)
dATP	Jena Bioscience (Jena, Germany)
dGTP	Jena Bioscience (Jena, Germany)
dNTP solution	Sigma-Aldrich (St.Louis, MO, USA)
Ethanol absolute (EtOH)	Sigma-Aldrich (St.Louis, MO, USA)

70-80% Ethanol for disinfection	Carl Roth (Karlsruhe, Germany)
Gelatine, 2% in water	Sigma-Aldrich (St.Louis, MO, USA)
GelElute LPA	Sigma-Aldrich (St.Louis, MO, USA)
Glycerol	AppliChem (Darmstadt, Germany)
HCl	Sigma-Aldrich (St.Louis, MO, USA)
Immobilon western ECL reagent	Millipore (Billerica, MA, USA)
Incidine Plus for disinfection	Ecolab (St. Paul, MI, USA)
Isopropanol	Sigma-Aldrich (St.Louis, MO, USA)
Isoflurane	Abbvie (North Chicago, IL, USA)
Janus Kinase inhibitor 1	EMD Chemicals (San Diego, CA, USA)
KCl	Sigma-Aldrich (St.Louis, MO, USA)
KH₂PO₄	Sigma-Aldrich (St.Louis, MO, USA)
KHCO₃	Sigma-Aldrich (St.Louis, MO, USA)
LE agarose	Lonza (Basel, Switzerland)
Li₂B₄O₇	Sigma-Aldrich (St.Louis, MO, USA)
Low range ssRNA ladder	New England Biolabs (Ipswich, MA, USA)
Magnesium dichloride (MgCl₂)	Applied Biosystems (Foster City, CA, USA)
Magnesium dichloride (MgCl₂)	Sigma-Aldrich (St.Louis, MO, USA)
Manganese dichloride (MnCl₂)	Sigma-Aldrich (St.Louis, MO, USA)
Methanol	Sigma-Aldrich (St.Louis, MO, USA)
Methyl cellulose	Sigma-Aldrich (St.Louis, MO, USA)
MgSO₄·7H₂O	Merck (Darmstadt, Germany)
Midori Green Dye	Nippon Genetics (Tokyo, Japan)
Na₂HPO₄	Merck (Darmstadt, Germany)
NaHCO₃	AppliChem (Darmstadt, Germany)
Orange G	Sigma-Aldrich (St.Louis, MO, USA)
O'Gene Ruler Ultra low range DNA ladder	Thermo Scientific (Waltham, MA, USA)
PCR nucleotide mix	Carl Roth (Karlsruhe, Germany)
Phalloidin AF-488	Molecular Probes (Eugene, OR, USA)
Potassium chloride (KCl)	AppliChem (Darmstadt, Germany)
Protease inhibitor tablets	Roche (Indianapolis, USA)
Protein block buffer, serum free	DAKO (Glostrup, Denmark)
QIAzol (Trizol)	Qiagen (Venlo, the Netherlands)
QR buffer	Qiagen (Venlo, the Netherlands)
Random hexamer primer	Applied Biosystems (Foster City, CA, USA)
RIPA buffer	Sigma-Aldrich (St.Louis, MO, USA)

RNA loading dye	New England Biolabs (Ipswich, MA, USA)
SDS	Carl Roth (Karlsruhe, Germany)
<i>S. cerevisiae</i> transfer RNA	Sigma-Aldrich (St.Louis, MO, USA)
Sodium azide (NaN₃)	Sigma-Aldrich (St.Louis, MO, USA)
Sodium acetate (CH₃COONa)	Sigma-Aldrich (St.Louis, MO, USA)
Sodium chloride (NaCl)	J T Baker (Phillipsburg, NJ, USA)
Sodium hydroxide (NaOH)	Carl Roth (Karlsruhe, Germany)
Nonfat dried milk powder	AppliChem (Darmstadt, Germany)
SYBR Green PCR Mix	Thermo Scientific (Waltham, MA, USA)
Taqman Fast Universal Master Mix	Applied Biosystems (Foster City, CA, USA)
Taurine	Sigma-Aldrich (St.Louis, MO, USA)
TEMED	AppliChem (Darmstadt, Germany)
Tris pure	AppliChem (Darmstadt, Germany)
Triton X-100	Sigma-Aldrich (St.Louis, MO, USA)
Tween 20	Sigma-Aldrich (St.Louis, MO, USA)
Urea	Sigma-Aldrich (St.Louis, MO, USA)

3.4 Kits

Name	Manufacturer
Cell counting Kit 8	Dojindo Molecular Technology (Kumamoto, Japan)
Durascribe T7 kit	Epicentre (Madison, WI, USA)
LabelIT siRNA Tracker Cy3	Mirus Bio LCC (Madison, WI, USA)
MinElute Gel extraction kit	Qiagen (Venlo, the Netherlands)
miRNAeasy RNA isolation kit	Qiagen (Venlo, the Netherlands)
QiaQuick Gel extraction kit	Qiagen (Venlo, the Netherlands)
Taqman Reverse Transcription kit	Thermo Fisher Scientific (Waltham, MA, USA)
Thermoscript RT PCR kit	Life Technologies (Paisley, UK)
Zymoclean Gel recovery kit	Zymo Research (Freiburg, Germany)

3.5 Enzymes

Enzyme name	Manufacturer
Collagenase II	Worthington (Lakewood, NJ, USA)
DNase I	Sigma-Aldrich (St.Louis, MO, USA)
MuLV reverse transcriptase	Applied Biosystems (Foster City, CA, USA)
RNase OUT (inhibitor)	Applied Biosystems (Foster City, CA, USA)
RNase H	Epicentre (Madison, WI, USA)
Riboshredder RNase Mix	Epicentre (Madison, WI, USA)
Taq Polymerase	Sigma-Aldrich (St.Louis, MO, USA)

3.6 Cell culture solutions and supplements

Item name	Manufacturer
0.5% Trypsin/EDTA	Life Technologies (Paisley, UK)
L-Ascorbic Acid/Vitamin C	Sigma-Aldrich (St.Louis, MO, USA)
DFO	Sigma-Aldrich (St.Louis, MO, USA)
DMEM/F-12	Invitrogen (San Diego, CA, USA)
Dulbecco's modified Eagle medium (DMEM), low glucose	Sigma-Aldrich (St.Louis, MO, USA)
DMEM Glutamax/High Glucose	Gibco (Waltham, MA, USA)
Dulbecco's Phosphate Buffer Saline (DPBS)	Life Technologies (Paisley, UK)
Dulbecco's Ph. B. Sal. With MgCl ₂ and CaCl ₂ (DPBS+)	Sigma-Aldrich (St.Louis, MO, USA)
EDTA (dissolved to 1mM in DPBS)	Sigma-Aldrich (St.Louis, MO, USA)
EGM single quotes	Lonza (Verviers, Belgium)
Endothelial Basal Medium (EBM)	Lonza (Verviers, Belgium)
Fetal Bovine Serum	Invitrogen (San Diego, CA, USA)
Fetal Bovine Serum (F2442)	Sigma-Aldrich (St.Louis, MO, USA)
Gelatin from bovine skin	Sigma-Aldrich (St.Louis, MO, USA)
Glucose 40%	B.Braun (Melsungen, Germany)
Glutamax-I (100X)	Life Technologies (Paisley, UK)
HEPES, 1M	Invitrogen (San Diego, CA, USA)
Insulin-Transferrin-Selenium (10x)	Gibco (Waltham, MA, USA)
Lipofectamine RNAimax	Life Technologies (Carlsbad, CA, USA)
M199 medium	Sigma-Aldrich (St.Louis, MO, USA)
Matrigel basement membrane matrix	BD Biosciences (San Diego, CA, USA)
Murine heart perfusion buffer (113mM NaCl, 4,7 mM KCl, 0.6mM KH ₂ PO ₄ , 0.6 mM NA ₂ HPO ₄ , 1.2mM MgSO ₄ , 12mM NAHCO ₃ , 10mM KHCO ₃ , 30mM Taurin, 10mM HEPES, 1mM BDM, 0,01% glucose)	Self-Made, sterilized
Nystatin	Applichem (Darmstadt, Germany)
OptiMEM	Invitrogen (San Diego, CA, USA)
Penicillin-Streptomycin (500X)	Roche (Mannheim, Germany)
Rat tail collagen type I (spheroid assay)	BD Biosciences (San Diego, CA, USA)
Sodium pyruvate	Life Technologies (Paisley, UK)
Unbuffered DMEM base	Sigma-Aldrich (St.Louis, MO, USA)
Vascular endothelial growth factor 165 (VEGF)	Peprtech (Rocky hill, NJ, USA)
Vitamin B12	

3.7 Antibodies

Target	Source	Manufacturer
α-tubulin	Mouse Monoclonal	Neomarkers (Fremont, CA, USA)
Anti-Mouse secondary HRP-Antibody	Goat Polyclonal	GE-Healthcare (Little Chalfont, UK)
Anti-Rabbit secondary HRP-Antibody	Goat Polyclonal	GE-Healthcare (Little Chalfont, UK)
Anti-Rabbit secondary Alexa 647-Antibody	Goat Polyclonal	Invitrogen (San Diego, CA, USA)
Early Endosome Antigen 1	Rabbit Monoclonal	Cell Signaling (Danvers, MA, USA)
Fibroblast specific protein 1	Rabbit Monoclonal	Millipore (Billerica, MA, USA)
Lysosomal-associated membrane protein 1	Rabbit Polyclonal	Abcam (Cambridge, UK)
Vascular cell adhesion molecule-1	Rabbit Monoclonal	Abcam (Cambridge, UK)
Vimentin	Goat Polyclonal	Abcam (Cambridge, UK)

3.8 Custom Primers

Target	Forward Primer	Reverse Primer
Mmu CaCNa1c P1	AATCACCCGAAGGGAGCAAG	CAATGCTTATGCACGCCCTC
Mmu CaCNa1c P2	CGAAGGGAGCAAGAACCACT	GCTGTGTGGAAGTACGGTA
Mmu cardiac troponin T type2	TGAAGAAGCCAAAGATGCTG	CCTGCTGGGCTTGGGTTT
Mmu Collagen 16 alpha-1 P1	AAGGGCAGTGAAGGGATTTCG	GAGGACCAAGATGCCCTGG
Mmu Collagen 16 alpha-1 P2	ATGGTTTACCTGGCCTTCCG	TGTAGCTCAGACAAGGCTGT
Mmu DDR2 P1	ACCCACCACCTATGATCCCA	CGGATCAGTCTGGATGGCTC
Mmu DDR2 P2	TGCCAAATATGGGAGGCTGG	TCGGGTTGCACTGGAATCTC
Mmu GATA4	TGTGCCAACTGCCAGACTAC	GCTCCGTTTTCTGGTTTGA
Mmu Mesp2	CACCACCTCAAGCATGTCC	GCAGGGTTCTGGAGACACA
Mmu Myosine heavy chain 6	GATTGGTCTCCAGCCTCTG	TCTTGTCGAACTTGGGTGGG
Mmu P0	GCGTCTGGCATTGTCTGT	GAAGGCCTTGACCTTTTCAGTAAG
Mmu PI3-kinase regulator 2 (PI3KR2)	CCGGGACATACGTGGAGTTC	AATGGCTTCCACCAGCTTCA
Mmu Snail 1	GTCTGCACGACCTGTGGAAA	AGCCAGACTCTTGGTGCTTG
Mmu SPRED-1, transcript 1	GCCCAGCGTCAAAAAGTGAAG	AGGCCTTGCTGACTGAATGG
Mmu TCF21	GCCAACGACAAGTACGAGAAC	GGTCAGGATGCTGTAGTTCCA
Mmu Tbx5	GAGCACAGCCAAATTTACCA	TAGCCCAGCGATAGAAGGT
Mmu Transferrin receptor P1	GTGCGGAAGGAAGTGACGTA	ATAGCCCAGGTAGCCACTCA
Mmu Transferrin receptor P2	AGAGGCGTCTCCTAGTACTCC	TCATCTCGCCAGACTTTGCT
Mmu Vacular Cell Adhesion Molecule 1 (VCAM-1)	CTGGGAAGCTGGAACGAAGT	GCCAAACACTTGACCCTGAC
Mmu Vimentin	TGGAGCGCCAGATGCGTGAG	AGAAATCCTGCTCTCCTCGCT
Mmu zinc finger E-box binding homeobox 1 (Zeb1)	AGGAGGTGACTCGAGCATTTA	GTCTTGCCAGCAGTTCTTGG
Hsa SPRED-1	ACGGTGAGGGAAAGATGAGC	CAGTGACGCTGCTTAGTCCA
Hsa Transferrin receptor	CTGCTATGGGACTATTGCTGTG	CCGACAACCTTCTCTTCAGGTC
Transferrin receptor aptamer (TRA)	GGGGGATCAATCCAAGG	GGGGTGTAAAGGGAGCGTTT
general RNA internalization motif (GIRM)	TGCGAATCCTCTATCCGTTT	TGCGAAATCATAAAGCGTTT
51bp aptamer Pool	<u>TAA TAC GAC TCA CTA TA</u> GGG GAG GAC GAT GCG G	TCG GGC GAG TCG TCT G
104bp aptamer Pool (used for cand. amplification)	<u>GTA TAA TAC GAC TCA CTA TA</u> GGG AGA CGC AAC TGA ATG AA	GTG ACG CGA CTA GTT ACG GA
Candidates 2,3,5,7-10 (qPCR only)	GGG AGA CGC AAC TGA ATG AA	GTG ACG CGA CTA GTT ACG GA
Candidate 1 (qPCR only)	CGA CAA TCC ATT CTG CTT CGG	GTG ACG CGA CTA GTT ACG GA
Candidate 4 (qPCR only)	GCG CGA AAC ACA ACT AGC TC	GTG ACG CGA CTA GTT ACG GA
Candidate 6 (qPCR only)	GGC TTC CTC GAT TCC TGC TT	GTG ACG CGA CTA GTT ACG GA

All custom primers were ordered from Sigma-Aldrich (St.Louis, MO, USA). T7 promotor sequences in the forward primers are underlined. P1 and P2 are Primer pair 1 and 2, mmu = *mus musculus*, hsa = *homo sapiens*.

3.9 Taqman primers

Target	Manufacturer
Mmu/hsa -miR-1a-2-3p	Applied Biosystems (Foster City, CA, USA)
Mmu-miR-1a-2-5p	Applied Biosystems (Foster City, CA, USA)
Mmu/hsa-miR-126-3p	Applied Biosystems (Foster City, CA, USA)
Mmu/hsa-miR-126-5p	Applied Biosystems (Foster City, CA, USA)
Mmu/hsa-miR-133-3p	Applied Biosystems (Foster City, CA, USA)
Mmu/hsa-miR-208b-3p	Applied Biosystems (Foster City, CA, USA)
Mmu/hsa-miR-208b-5p	Applied Biosystems (Foster City, CA, USA)
Mmu/hsa-miR-499-5p	Applied Biosystems (Foster City, CA, USA)
Small nuclear RNA U6 (snU6)	Applied Biosystems (Foster City, CA, USA)

Note: for many miRs, the mature sequences are conserved between species, hence some of the primers and mimics are cross-reactive between *homo sapiens* and *mus musculus*

3.10 microRNA mimics

Target	Manufacturer
Mmu/hsa -miR-1a-2-3p	Applied Biosystems (Foster City, CA, USA)
Mmu-miR-1a-2-5p	Applied Biosystems (Foster City, CA, USA)
Mmu/hsa-miR-126-3p	Applied Biosystems (Foster City, CA, USA)
Mmu/hsa-miR-126-5p	Applied Biosystems (Foster City, CA, USA)
Mmu/hsa-miR-133-3p	Applied Biosystems (Foster City, CA, USA)
Mmu/hsa-miR-208b-3p	Applied Biosystems (Foster City, CA, USA)
Mmu/hsa-miR-208b-5p	Applied Biosystems (Foster City, CA, USA)
Mmu/hsa-miR-499-5p	Applied Biosystems (Foster City, CA, USA)

3.11 customized oligonucleotides and libraries

Name	Sequence (5' to 3' end)	Manufacturer
Transferrin receptor aptamer (TRA)	S-S GGG GGA UCA AUC CAA GGG ACC CGG AAA CGC UCC CUU ACA CCC C idT	Dharmacon (Lafayette, CO, USA)
General internalizing RNA motif (GIRM)	Fi UGC GAA UCC UCU AUC CGU UCU AAA CGC UUU AUG AUU UCG CA idT	Dharmacon (Lafayette, CO, USA)
Control aptamer (CA)	AUG CCC GAC CAG CCA AGA GCG CCG AGA ACC CUU GUC CCU AAG G	Dharmacon (Lafayette, CO, USA)
mature miR-126-5p_TRA construct (for Ch1)	<u>CAU UAU UAC UUU UGG UAC GCG</u> uu cgc GGG GGA UCA AUC CAA GGG ACC CGG AAA CGC UCC CUU ACA CCC C gcg idT	Dharmacon (Lafayette, CO, USA)
TRA_stick construct (for Ch2 and 3)	<i>GUA CAU UCU</i> AGA <i>UAG CC</i> aac gcg_GGG GGA UCA AUC CAA GGGA CCC GGA AAC GCU CCC UUA CAC CCC C gcg idT	Dharmacon (Lafayette, CO, USA)
Mature-miR-126-5p_stick construct (for Ch2)	<i>GGC UAU CUA GAA UGU AC</i> ggg <u>CAU UAU UAC UUU UGG UAC GCG</u>	Dharmacon (Lafayette, CO, USA)
Mature miR-126-3p (for Ch1 and 2)	<u>UCG UAC CGU GAG UAA UAA UGC G</u>	Dharmacon (Lafayette, CO, USA)
Pre-miR-126_stick construct (for Ch3)	<i>GGC UAUC UAG AAU GUA C</i> aa <u>CAU UAU UAC UUU UGG UAC GCG</u> CUG UGA CAC UUC AAA C UC GUA CCG UGA GUA AUA AUG CG	Dharmacon (Lafayette, CO, USA)
Pre-miR-1a-2_stick construct (for Ch4)	<i>GGC UAU CUA GAA UGU AC</i> aa <u>ACA UAC UUC UUU AUG UAC CCA UA</u> UGA ACA UUC AGU GCU A <u>UG GAA UGU AAA GAA GUA UGU AU</u>	Dharmacon (Lafayette, CO, USA)
Recombinant miR-126-3p	UCG UAC CGU GAG UAA UAA UGC G	Life Technologies, (Carlsbad, CA USA).
51bp aptamer Pool	GGG AGG ACG ATG CGG -N*20- CAG ACG ACT CGC CCG A	Integrated DNA Technologies (Coralville, IA, USA)
104bp aptamer Pool	GGG AGA CGC AAC TGA ATG AA -N*26- CTG CTT CGG CAG -N*26- TCC GTA ACT AGT CGC GTC AC	
Candidate 1	GGG AGA CGC AAC TGA ATG AAC TGA TTC AAA AGC ACG ACA ATC CAT TCT GCT TCG GCA GGT TCT CGT TCT TTT GAA CAG TCG GTG TCC GTA ACT AGT CGC GTC AC	Sigma-Aldrich (St.Louis, MO, USA)
Candidate 2	GGG AGA CGC AAC TGA ATG AAG ATA TTA GCA CCG AAT CTC AGT TCT TCT GCT TCG GCA GCT CAA TCT CCA GTA CAC CGT ATC GTC TCC GTA ACT AGT CGC GTC AC	Sigma-Aldrich (St.Louis, MO, USA)
Candidate 3	GGG AGA CGC AAC TGA ATG AAT ACA CCT AGC AAT GAG TAT CAC CCA TCT GCT TCG GCA GTT TAA GTG ATT CCT CAT TTC GGA TTT ATC CGT AAC TAG TCG CGT CAC	Sigma-Aldrich (St.Louis, MO, USA)
Candidate 4	GGG AGA CGC AAC TGA ATG AAT AAC GCG CGA AAC ACA ACT AGC TCA TTC TGC TTC GGC AGG CTC GTT CTG TTT CGA AGT TAC TGT GTC	Sigma-Aldrich (St.Louis, MO,

	CGT AAC TAG TCG CGT CAC	USA)
Candidate 5	GGG AGA CGC AAC TGA ATG AAC AAT TTC CCC CTC TAT TCC TTT CGA ACT GCT TCG GCA GAT TTC GCC AGC ATA GAG TGA GGG TCA TCC GTA ACT AGT CGC GTC AC	Sigma-Aldrich (St.Louis, MO, USA)
Candidate 6	GGG AGA CGC AAC TGA ATG AAT TCT GCC TTT TCG GCT TCC TCG ATT CCT GCT TCG GCA GTA TCT ACT GGA ACC GTC AAG GTA TGT TCC GTA ACT AGT CGC GTC AC	Sigma-Aldrich (St.Louis, MO, USA)
Candidate 7	GGG AGA CGC AAC TGA ATG AAA TTT CTC GTC TCA ATT TCC AGA ATT CCT GCT TCG GCA GTA TTC GTG GCA ATG AGT CAA CGA ACT TCC GTA ACT AGT CGC GTC AC	Sigma-Aldrich (St.Louis, MO, USA)
Candidate 8	GGG AGA CGC AAC TGA ATG AAG GCA ATA CGT CAG AGC TTA TTC CAA ACT GCT TCG GCA GTT TGA GTC TGT ACG TAT TTC CGG AGG TCC GTA ACT AGT CGC GTC AC	Sigma-Aldrich (St.Louis, MO, USA)
Candidate 9	GGG AGA CGC AAC TGA ATG AAG TAT CAC TCT CCA GAT TCC TTC ACA GCT GCT TCG GCA ACG TCC GGT GCA TTG CGA CAC CGG CCT CCG TAA CTA GTC GCG TCA C	Sigma-Aldrich (St.Louis, MO, USA)
Candidate 10	GGG AGA CGC AAC TGA ATG AAC TTT CAG CCA GAT GAC TCT TCG GAT CCT GCT TCG GCA GTT CAC AAA GGA GCC TCT GGA CGT GAT CCG TAA CTA GTC GCG TCA C	Sigma-Aldrich (St.Louis, MO, USA)

Bold indicates nucleotides with 2'-F modified sugars, italics indicate sequences of the stick structure, small letters indicate nucleotides of the linkers, mature miR sequences are underlined. IdT= inverted dT sequence at the 3' end, S-S = 5'-Disulfide Thiol-Modifier, Fi = 5'-Fluorescein label (for microscopy), N = random nucleotide (manually pipetted, to ensure equal distribution among A, T, G and C)

3.12 Primary cells and cell lines

Name	Species	Source	Manufacturer
HUVEC	<i>Homo sapiens</i>	Umbilical vein	Lonza (Verviers, Belgium)
SK-BR3	<i>Homo sapiens</i>	mammary gland/breast	Prof. M. Rieger (Frankfurt a.M., Germany)
MCF7	<i>Homo sapiens</i>	mammary gland/breast	Prof. M. Rieger (Frankfurt a.M., Germany)
MEC H5V	<i>Mus musculus</i>	Lung endothelium	Prof. W. Claycomb (New Orleans, LA, USA)
AMCF	<i>Mus musculus</i>	Heart	Self-isolated from C57BL/6 mice

3.13 software

Name	Developer
Prism	Graphpad (La Jolla, CA, USA)
Adobe Illustrator	Adobe Systems (San José, CA, USA)
Zen	Zeiss (Jena, Germany)
Axiovision	Zeiss (Jena, Germany)
FIJI/ImageJ	Open Source ³⁹²
MS Office	Microsoft (Redmond, WA, USA)
Mendeley Desktop	Elsevier (Amsterdam, the Netherlands)
Irfanview	Mr. Irfan Skijan (Vienne, Austria)

4. Results

Some of the results presented in the following section have been published previously in ³⁸⁹. The experiments for this manuscript were exclusively performed by the first author Jan-H. Rohde. Copyright permission has been acquired to include data and images from ³⁸⁹, see section 11. If data in a section has been previously published, it will be noted in the header.

4.1 Analysis of candidate aptamers

4.1.1 Internalization of the transferrin receptor aptamer (TRA) and the general internalizing RNA motif (GIRM) detected via qPCR ³⁸⁹

The first aim of the thesis was to establish whether it is possible to deliver miRs into cells of the vasculature using aptamers as carriers. Unfortunately, no endothelial or vascular specific aptamers have been described so far. However, two RNA constructs were reported to internalize into all cell types tested so far: the aptamer for the ubiquitously expressed transferrin receptor aptamer (TRA) and the general internalizing RNA motif (GIRM) (Figure 4.1.1a+b). Both were used to treat adult murine cardiac fibroblasts (AMCF) as well as human umbilical vein endothelial cells (HUVEC) and murine endothelial cells (MEC). Initial experiments showed that a treatment with TRA or GIRM led to detectable levels of both oligonucleotides in reverse transcription (RT) quantitative PCR (qPCR) after 1 h and 24 h in the total cellular RNA (Figure 4.1.1c-h). To isolate the intracellular/internal RNA (iRNA), cells were also digested with trypsin and RNase (Figure 4.2.1i-n), which should strip all RNA on their surface. Both constructs were also detectable in this iRNA in all cell types (Figure 4.1.1i-n). However, treatment with a control aptamer (CA) did not lead to any detectable levels of TRA or GIRM in total or iRNA (Figure 4.1.1). We also calculated the percentage of internalization after 1 h and 24 h for all cell types by dividing the levels of construct in iRNA by the levels in total RNA (Figure 4.1.1e,h,k,n). The internalization of TRA into HUVEC, MEC and MEF after 24 h was 2.5%, 39% and 14% respectively. Of note, it appeared that basically 100% of GIRM was internalized for into MEC after 24 h (the levels detected in iRNA were as high or higher as in total RNA) while in MEF 50% were internalized and only 6% internalization was observed in HUVEC (Figure 4.1.1h+n).

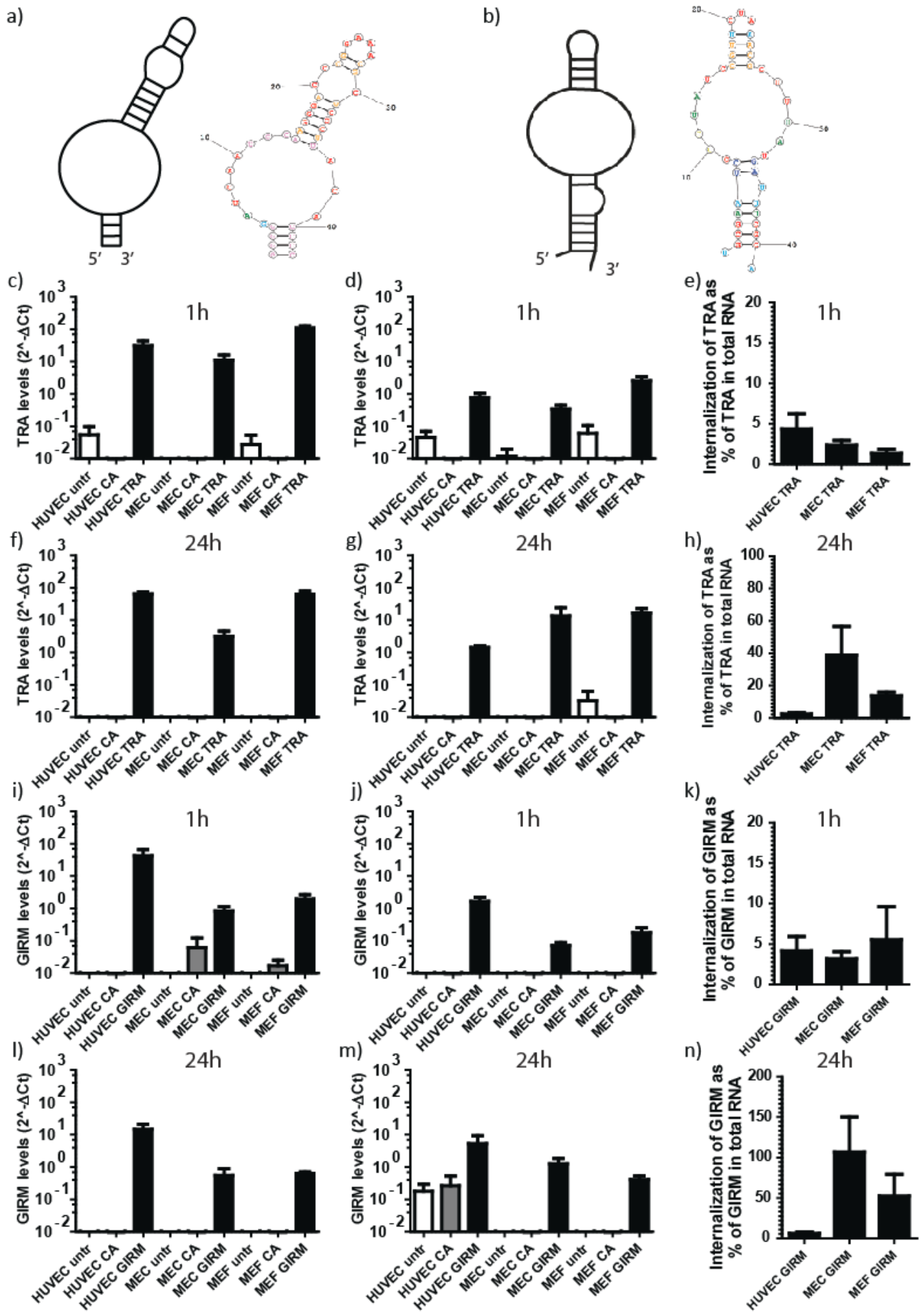


Figure 4.1.1 Aptamer internalization in different cell types

a+b) Schematic illustrations and predictions of the secondary structure of the TRA (a) and GIRM (b) made with RNAstructure 5.6³⁹⁸. Figure c) shows levels of TRA measured in total RNA after treatment of human and murine endothelial cells or murine fibroblasts with 500nM CA or TRA for 1 h while f) shows the same for 24 h treatment. Next to it, the levels of intracellular TRA after 1 h (d) and 24 h (g) are shown. Levels of GIRM in total RNA after 1 h (i) and 24 h (l) as well as internal RNA after 1h (j) and 24 h (m) are shown. The levels of TRA and GIRM were normalized to the expression of the ribosomal protein P0 (RPLP0). Level of internalization was calculated as the ratio of internal divided by total RNA levels and is shown for TRA after 1 (e) and 24h (h) and GIRM after 1 (k) and 24 h (n); this data was not normalized to RPLP0. Data are shown as mean \pm standard error of the mean (SEM), n=3-6 for all graphs. Figures previously published in³⁸⁹.

4.1.2 Fluorescent microscopy analysis of TRA and GIRM internalization³⁸⁹

To validate the internalization observed via qPCR, GIRM labeled with a Fluorescein-Tag as well as CA and TRA labeled with Cyanine 3 (Cy3) were used to analyze internalization via fluorescent microscopy. After 24h treatment with the constructs, both GIRM and TRA could be observed in murine endothelial cells and murine embryonic fibroblasts (MEF) after treatment while CA could not be detected (Figure 4.1.2). Taken together there were no large differences between GIRM and TRA in both qPCR and the microscopic analysis, so it was decided to use TRA for subsequent experiments. This decision was made primarily because the ligand of TRA, the transferrin receptor, is well described in mammalian cells while the ligand of GIRM is not known.

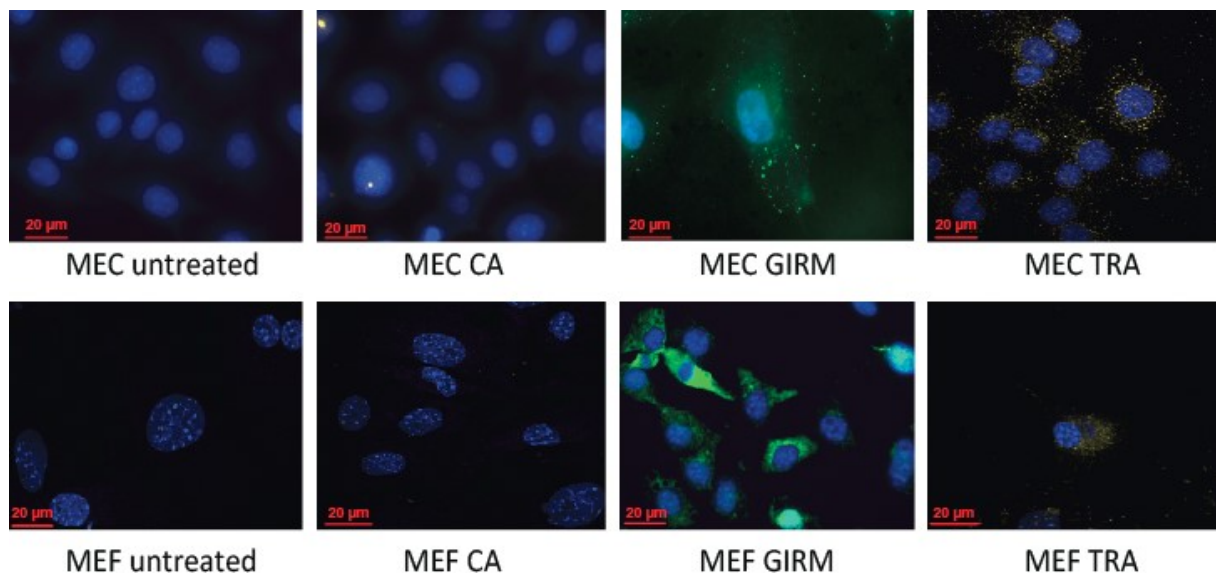


Figure 4.1.2 Fluorescent Images of aptamer internalization in different cell types

MEC and MEF treated with fluorescently labelled CA, TRA or GIRM for 1 hour were used to capture representative fluorescence microscopy images (n=3). Blue = DAPI staining, Green = Fluorescein-tagged GIRM, Yellow = Cy3-labeled TRA/CA. 400x magnification, Scale bar = 20μm. Previously published in³⁸⁹.

4.1.3 Fluorescent microscopy analysis of TRA localization

To analyze the cellular location of TRA, a co-staining using the Cy3-labeled TRA and several markers for cellular compartments was performed using MEC. There was some co-localization of TRA and the early endosome antigen as well as the lysosomal marker LAMP1 (Figure 4.1.3a+b). There was however, no co-localization of TRA and EDC4 (Figure 4.1.3c) or HGS (Figure 4.1.3d), which are markers for P-bodies and multivesicular bodies respectively,

was detected. This indicates that TRA is probably taken up by endosomes and ends up in lysosomes for processing.

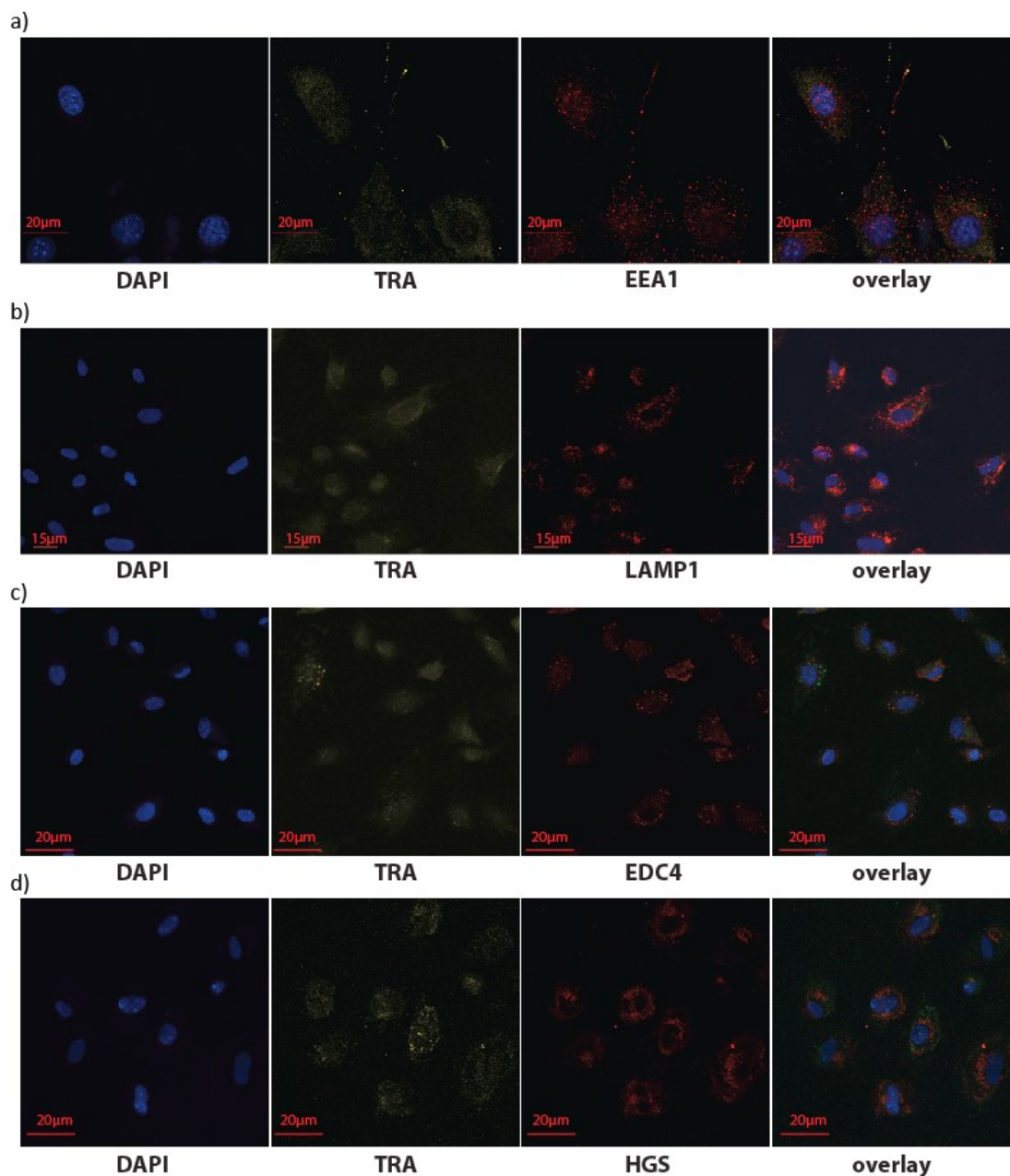


Figure 4.1.3 Fluorescent Images of aptamer localization in MEC

a-d) MEC were treated with TRA labeled with Cy3 (yellow) for 2 h and then fixated with 4% FA. The MEC were then stained using antibodies for EEA1 (a), LAMP1 (b), EDC4 (c) or HGS (d) and secondary antibodies labeled with Alexa 488 or 647 (both depicted as red for convenience) and nuclei were stained with DAPI (blue). Images were taken using a confocal microscope. Scale bar = 15 μm for (b) or 20 μm (a,c,d).

4.1.4 Analysis of transferrin receptor expression

The expression of the target of TRA, the transferrin receptor (TrfRc), was analyzed in two human breast cancer cell lines (MCF7 and SK-BR3), HUVEC (Figure 4.1.4a) as well as MEC and MEF (Figure 4.1.4b) using qPCR. All cell types show a significant and robust expression of TrfRc.

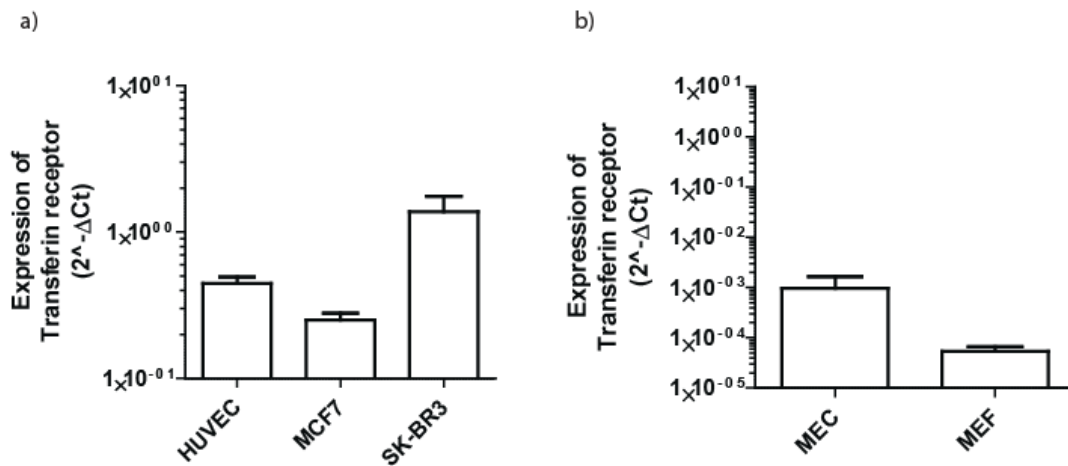


Figure 4.1.4 Expression of the transferrin receptor in different cell types

a+b) Relative expression of transferrin receptor mRNA measured by qPCR in human EC and breast cancer cells (a) as well as murine EC and fibroblasts (b) (n=3-5). Expression levels were normalized to the expression of RPLP0. Data shown as mean ± SEM. Data was referenced, but not shown in ³⁸⁹.

4.2 Chimeras of transferrin receptor aptamer and microRNA-126

4.2.1 Design of TRA-miR-126 chimeras ³⁸⁹

After establishing the ability of TRA to internalize into cells of the vasculature, the next step was to establish whether it can be used to deliver functional miRs as well. Three different approaches were used to create RNA-oligonucleotide chimeras of TRA and microRNA-126. For chimera 1 (Ch1), TRA was directly attached to mature miR-126-5p (Figure 4.2.1a). The 3p strand of miR-126 was ordered as a separate oligo and annealed prior to use (Figure 4.2.1d). Chimera 2 (Ch2) uses a similar approach, but in this case miR-126-5p and TRA bear a complementary sticky bridge structure (Figure 4.2.1b) which is used to anneal them to another ³⁷². This chimera was designed in the case that the close proximity of TRA and miR inhibits the functionality in Ch1. MiR-126-3p was then annealed as in chimera 1 (Figure 4.2.1e). Finally, chimera 3 (Ch3) uses the sticky bridge structure as well, but in this case to attach the Pre-miR-126 (Figure 4.2.1c) to TRA instead of the mature 3p and 5p strands

(Figure 4.2.1f). The rationale for Ch3 was that cells might be able to recognize the two nucleotide overhang at the 3' end and the stem loop of the precursor and thus cleave off the TRA and process Ch3 into functional mature miR-126-3p and 5p. The secondary structure of the constructs was predicted using RNAstructure 5.6³⁹⁸ (Figure 4.2.1a-c) and the schematic figures were drawn according to those predictions (Figure 4.2.1d-f). To analyze the stability of the constructs, they were folded and placed in sterile DPBS for 1 h or 24 h, after which RNA was isolated. Levels of TRA, miR-126-3p and 5p were stable in these RNA samples from 1 h to 24 h (Figure 4.2.1g-i). It should be noted that these constructs were limited by the maximum length that can be manufactured using an RNA synthesizer. It was not possible for example to directly attach Pre-miR-126 to TRA since the resulting construct would have been too long for effective synthesis.

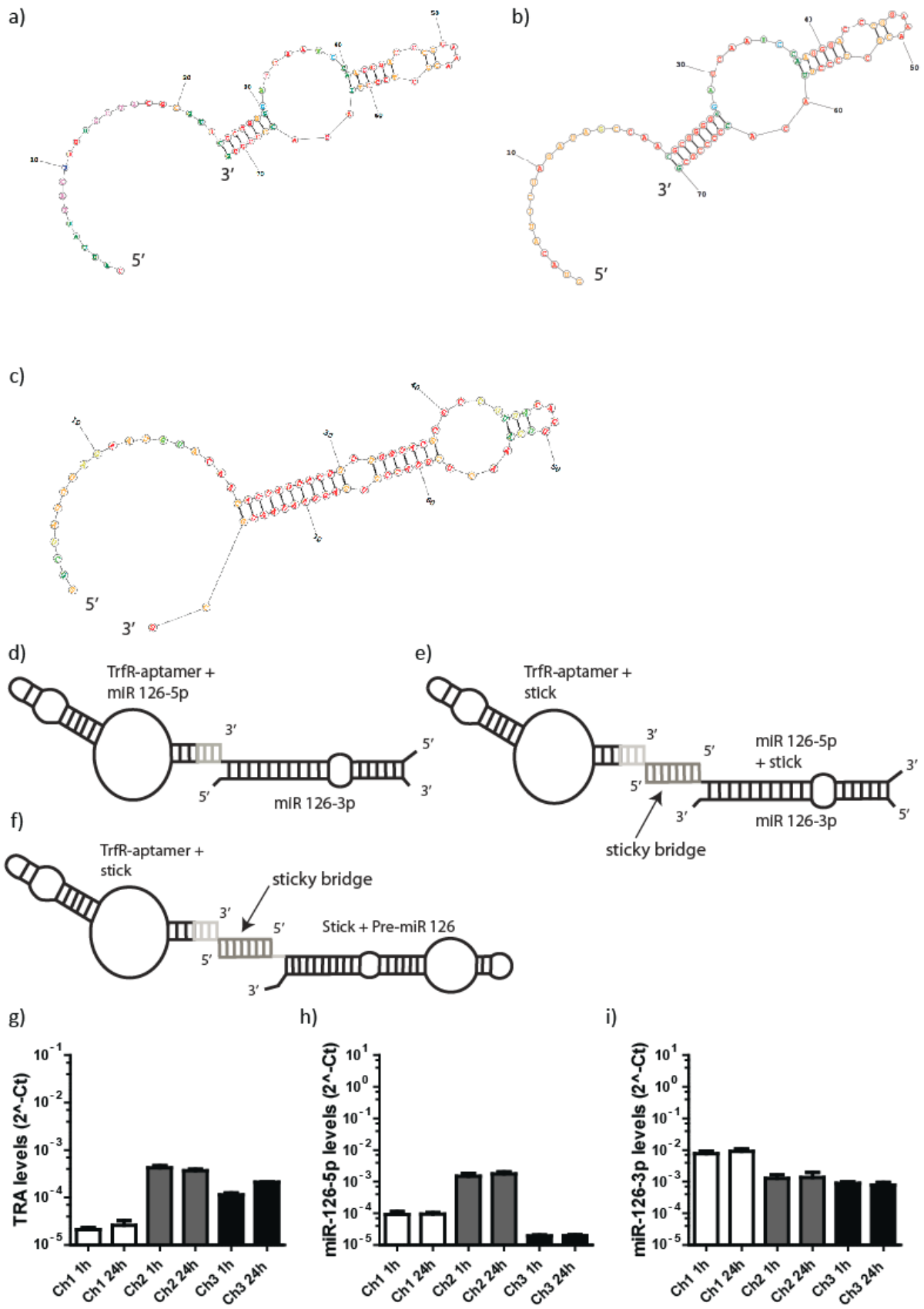


Figure 4.2.1: Chimera structures and stability in PBS

a-c) Predicted secondary structures using RNAstructure 5.6³⁹⁸ of parts of the chimera a) TRA with miR-126-5p (used for Ch1), b) TRA with stick (used for Ch2 and 3) c) Pre-miR-126 with stick (used for Ch3). d-f) Shows schematic illustration of aptamer-miR chimeras 1 (Ch1) (d), 2 (Ch2) (e) and 3 (Ch3) (f) after annealing based on these predicted structures. The TRA and miR sequences are depicted black, the linker sequences are light grey and the sticky bridge is dark grey. Levels of TRA (g), miR-126-3p (h) and 126-5p (i) detected in 500nM chimeras left in sterile PBS for 1 or 24h after folding (n=3). Data depict mean \pm SEM. Previously published in³⁸⁹.

4.2.2 Comparison of TRA and TRA-stick constructs

To determine if the attachment of the stick impairs the ability of TRA to bind to cells, TRA and the TRA-stick construct were compared via qPCR for their ability to attach and internalize into HUVEC. After treatment qPCR of total HUVEC RNA there was no discernible difference between TRA with and without the stick (or Ch3) (Figure 4.2.2). Therefore, for the rest of this thesis TRA and TRA-stick are both used as controls and denominated as TRA for practical reasons.

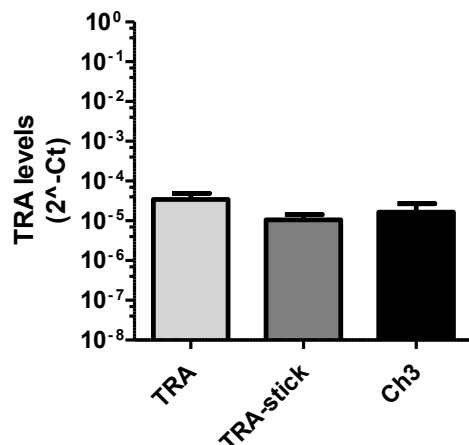


Figure 4.2.2 Comparison of TRA and TRA-stick for attachment and internalization

Levels of TRA, TRA-stick (see Figure 4.2.1b) or Ch3 detected one hour after 500nM treatment in HUVEC total RNA (n=4). Levels are not normalized to RPLP0. Data depict mean \pm SEM.

4.2.3 Internalization of the chimeras into ECs detected via qPCR³⁸⁹

Next, the chimeras were used on cells of the vasculature to determine if they would retain the binding and internalization observed for unmodified TRA. Using qPCR, expression of TRA was detectable in the total RNA of HUVEC (Figure 4.2.3a) and MEC (Figure 4.2.3b) as well as iRNA of HUVEC (Figure 4.2.3c) and MEC (Figure 4.2.3d) 1 and 24 h after treatment with any

of the chimeras. In HUVEC total RNA, there was little difference between TRA and the three chimeras, but in the internal RNA after 1 h and 24 h Chimera 1 treated HUVEC showed a markedly higher level of TRA than the other constructs or unmodified TRA (Figure 4.2.3c). In MEC however, unmodified TRA led to the highest detectable levels of TRA in total RNA 1 h after treatment, while Ch1 showed lower levels than Ch2 and 3 (Figure 4.2.3b). Conversely, 24 h post-treatment unmodified TRA and Ch1 showed similar levels in qPCR while Ch2 and 3 had lower detectable levels of TRA (Figure 4.2.3b). In the internal RNA of MEC, TRA and Ch1 led to the highest levels after 1 h (Figure 4.2.3d). In treated cells 24 h after treatment, Ch1 was hardly detectable in the iRNA of MEC while TRA, Ch2 and Ch3 led to low detectable levels (Figure 4.2.3d).

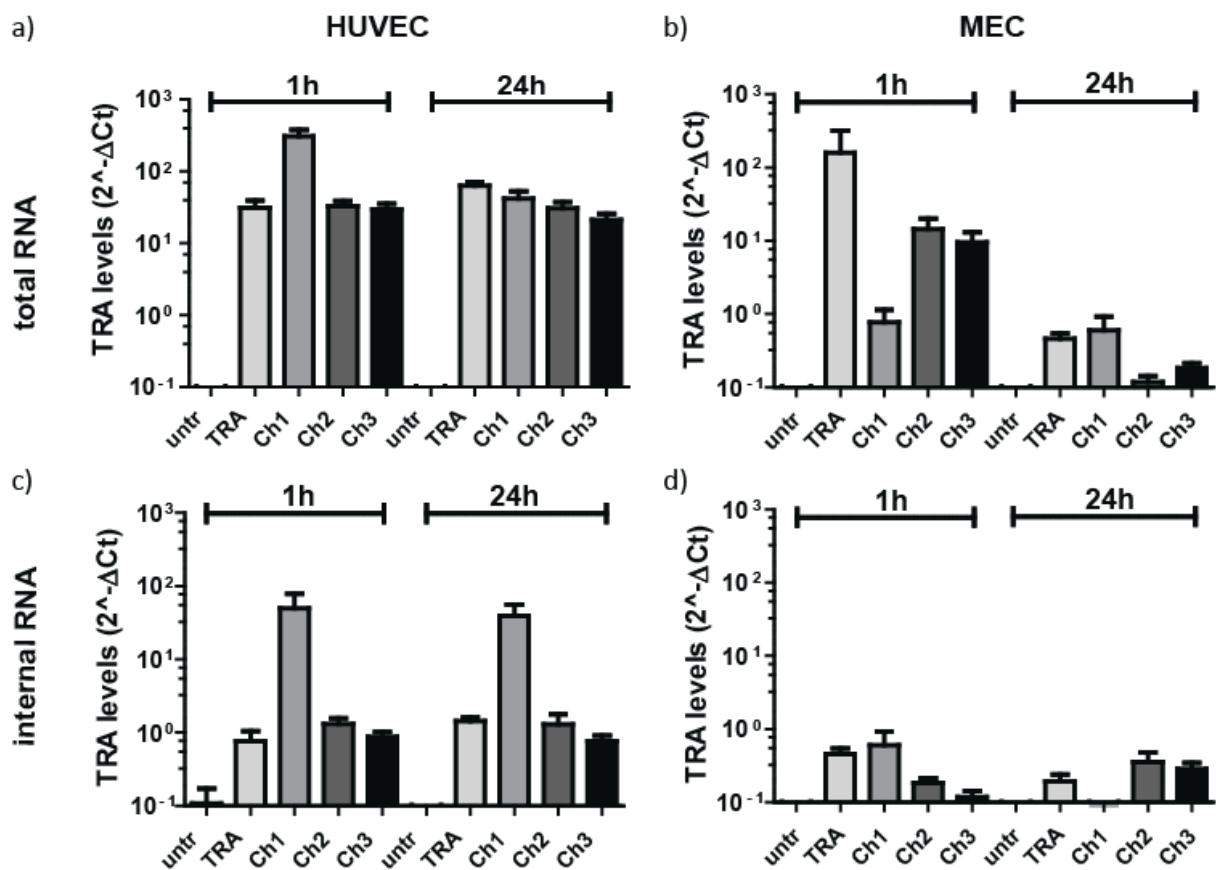


Figure 4.2.3 Aptamer internalization in human and murine endothelial cells

a-d) The levels of the TRA measured with RT-qPCR in total RNA of HUVEC (a) and MEC (b) as well as internal RNA of HUVEC (c) and MEC (d) after treatment with nothing (untr), 500 nM TRA, chimera 1,2 or 3 for 1 h or 24 h (n=3-7). Data depict mean ± SEM. Previously published in ³⁸⁹.

4.2.4 miR-126 delivery by the chimeras ³⁸⁹

RT-qPCR analysis was used to determine if miR-126 levels would be increased after treatment, which would indicate delivery of the miR by the chimeras. Levels of miR-126-3p were significantly increased in total and iRNA of HUVEC treated with any of the three chimeras both 1 h and 24 h after treatment (Figure 4.2.4a+b). The highest levels of intracellular miR-126-3p were detected in Ch2-treated cells (Figure 4.2.4b). Expression levels of miR-126-5p were also significantly increased by Ch1, Ch2 and Ch3 treatment in total RNA after 1 h and after 24 h under treatment with Ch2 and Ch3. Ch2 induced to the most elevated levels in both cases (Figure 4.2.4c). In HUVEC iRNA, Ch1 and Ch2 led to a significant increase in miR-126-5p expression 1 h after treatment while after 24 h an increase was only observable in cells treated with Ch2 (Figure 4.2.4d). Mouse endothelial cells showed a slightly different response to treatment with the chimeras; only a modest increase of miR-125-3p levels was detected in the iRNA of chimera treated cells (Figure 4.2.4e+f). As for miR-126-5p in MEC, the greatest increase in total (Figure 4.2.4g) and internal (Figure 4.2.4h) RNA levels after 1 h was also observed for Ch2. To calculate the increase in copy numbers of miR-126-3p a standard curve of made from synthetic miR-126-3p oligonucleotides was used. In HUVEC, treatment with Ch3 led to the internalization of $1,58 \times 10^6 \pm 0,31 \times 10^6$ copies of miR-126-3p while in MEC $0,44 \times 10^6 \pm 0,24 \times 10^6$ copies were delivered per nanogram iRNA (Figure 4.2.4i).

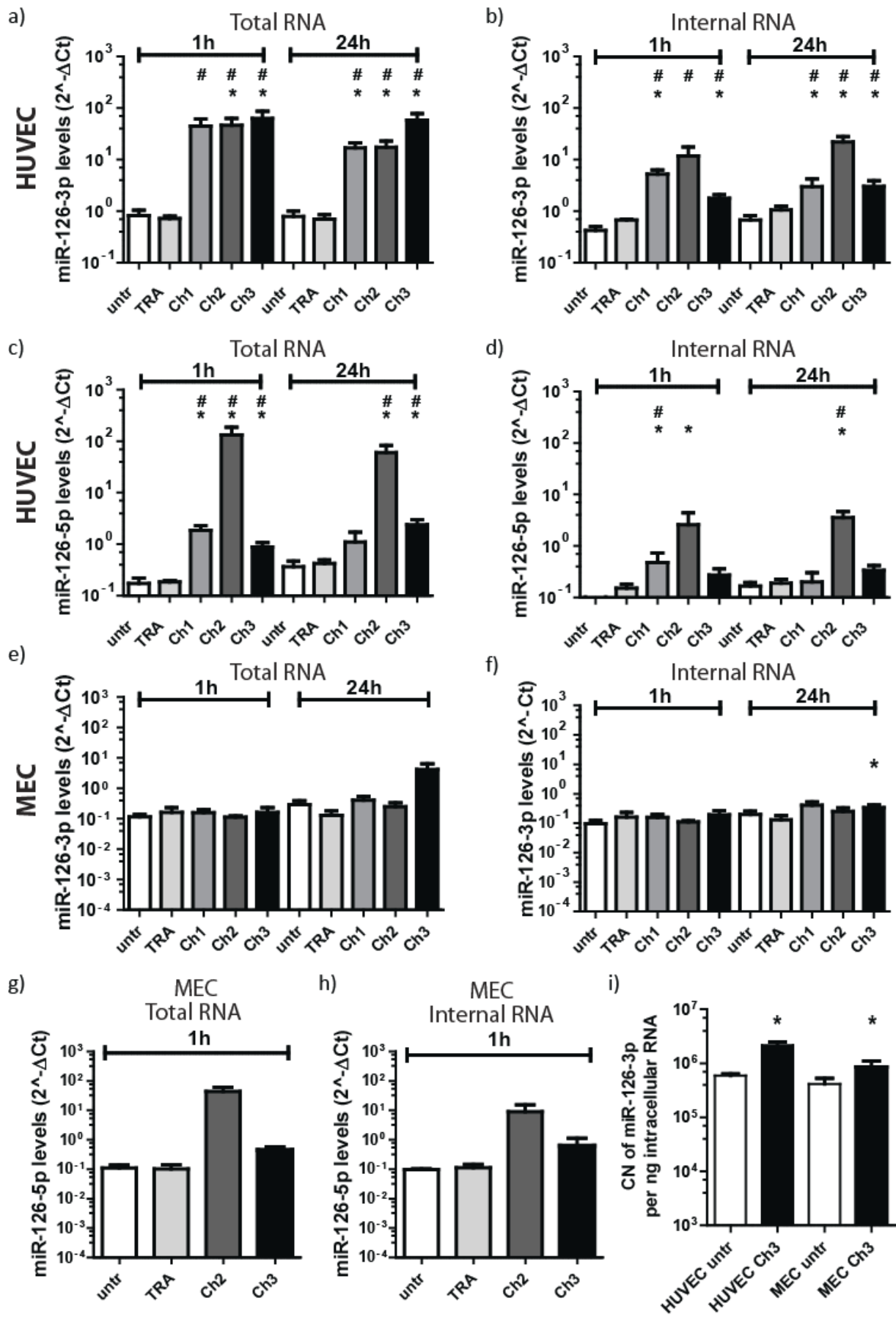


Figure 4.2.4 Chimeras increase levels of miR-126-3 and 5p in EC

a-d) The levels of miR-126-3p (a, b) and miR-126-5p (c, d) expression were measured in total (a, c) or internal RNA (b, d) of HUVEC treated for 1 h or 24 h without (untr) or with 500nM TRA, Ch1, Ch2 or Ch3 using RT-qPCR (n=3-17). e,f) Expression of miR-126-3p in MEC total (e) internal RNA (f) 1 h and 24 h after treatment with 500nM Ch1, Ch2 or Ch3 (n=3-10).g,h) Expression of miR-126-5p in MEC total (g) and iRNA (h) 1 h after treatment with 500nM Ch2 or Ch3 (n=3-10). i) The number of miR-126-3p molecules (copy number/CN) found in 1 ng iRNA of HUVEC and MEC after treatment with 500nM TRA or Ch3 for 1 h. The miR-126-3p copy numbers were normalized to snU6 expression and calculated based on standard curves made using synthetic recombinant miR-126-3p (n=3-4). Data are shown as mean \pm SEM. *p \leq 0.05 vs TRA; #p \leq 0.05 vs untreated. Figures a-d) and f) previously published in ³⁸⁹. Figure i) contains data represented in a different format in ³⁸⁹.

4.2.5 Effect of chimeras on VCAM-1 expression in HUVEC ³⁸⁹

The next step was to analyze whether the chimeras have the same effect on EC as has been reported for overexpression of miR-126 using mimics. Vascular cell adhesion molecule 1 (VCAM-1) is a known target of miR-126-3p in ECs on protein, but not mRNA level and is responsible for the anti-inflammatory effects of miR-126-3p overexpression (see 1.3.3.1) ²⁴⁶. HUVEC were treated with 500nM TRA, Ch1, Ch2, Ch3 or 10nM Pre-miR-126-3p or control mimics. As HUVEC do not express VCAM-1 protein under basal culture conditions, the cells were then stimulated with 1 nM Tumor necrosis factor- α (Tnf- α) for 16 h to simulate an inflammatory environment. Cells treated with Pre-miR-126-3p and Ch3, but not TRA, Ch1 or Ch2, showed a significantly reduced amount of VCAM-1 protein expression (Figure 4.2.5a). A more pronounced effect of the miR-126-3p mimic on the VCAM-1 levels was observed compared to the effect of Ch3. Therefore, the amount of miR-126-3p overexpression caused by these treatments was analyzed. Indeed, transfection with miR-126-3p mimics led to a significantly more pronounced overexpression of miR-126-3p than Ch3 (Figure 4.2.5b).

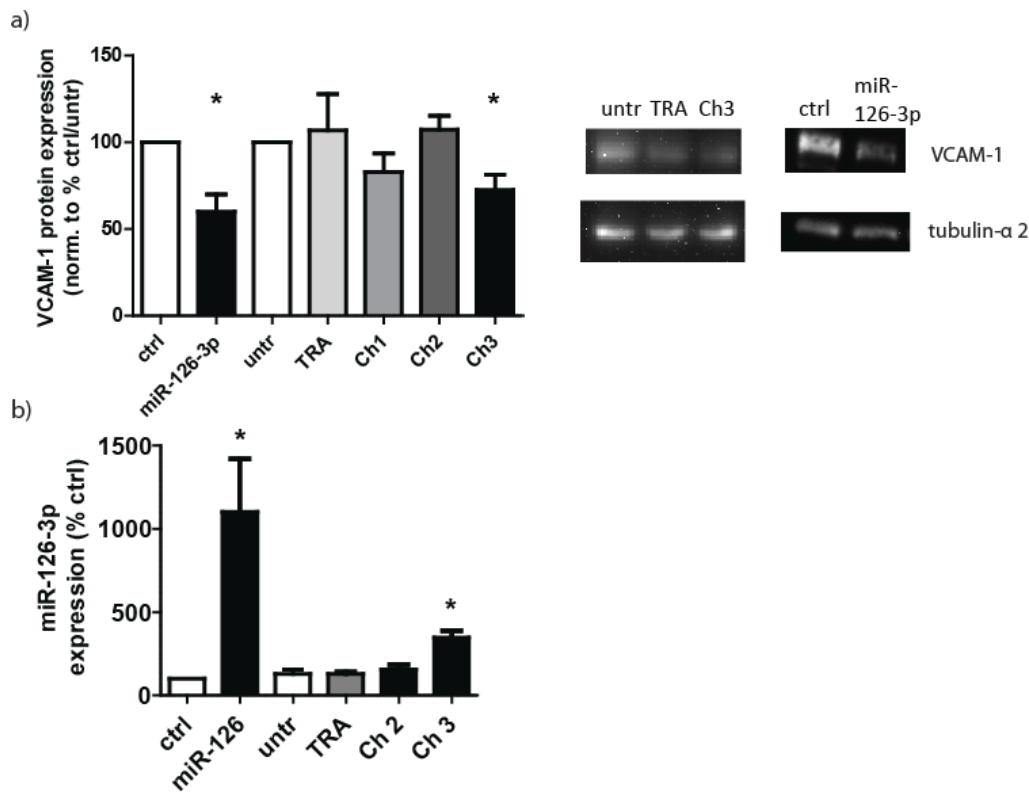


Figure 4.2.5 Chimera effect on VCAM-1 protein expression

a) Protein expression levels of the miR-126-3p target VCAM-1 after treatment with 500nM Ch1, Ch2 or Ch3 or lipofection with miR-126-3p mimic and subsequent stimulation with TNF- α for 16 h. Western blot analysis was used to calculate relative amounts of VCAM-1, which were normalized to tubulin- α 2. The VCAM-1 levels are expressed as percentages of corresponding controls (control RNA for miR-126-3p, untr for TRA and Ch1-3) (n=4-10). To the right, representative images of the Western Blots. b) Comparison of the overexpression in iRNA of HUVEC induced by miR-126-3p mimics or Ch2 and 3 treatment (n=4-5). Data is shown as mean \pm SEM. *p \leq 0.05 compared to controls (ctrl for miR-126-3p; untreated or TRA for Ch1-3). Figures a) and b) previously published in ³⁸⁹.

4.2.6 Effect of Chimeras on EC spheroid sprouting assay ³⁸⁹

The spheroid sprouting assay has been well established as an indicator of angiogenic sprouting of endothelial cells ³⁹⁹. It has been reported, that miR-126-3p overexpression can increase the sprouting of ECs by enhancing the VEGF signaling pathway (see 1.3.3.1) ⁴⁰⁰. To test whether the miR-126-3p transported by the chimeras shows comparable effects on angiogenic sprouting, spheroid sprouting assays were performed using HUVECs treated with 500nM of TRA, Ch1, Ch2, Ch3 or 10 nM ctrl or Pre-miR-126-3p mimics. Under basal conditions all HUVEC showed the same additive length of sprouts (Figure 4.2.6a+c). When HUVEC were co-treated with 50 ng/ml VEGF however, the HUVEC treated with Pre-miR-126-

3p and Ch3, but not TRA, Ch1 or Ch2, showed a significantly increased length of sprouts (Figure 4.2.6b). In line with the results from the Western Blot, this indicates that Ch3, but not Ch1 or 2 has effects comparable to conventional mimic-based miR-126-3p overexpression on endothelial cells.

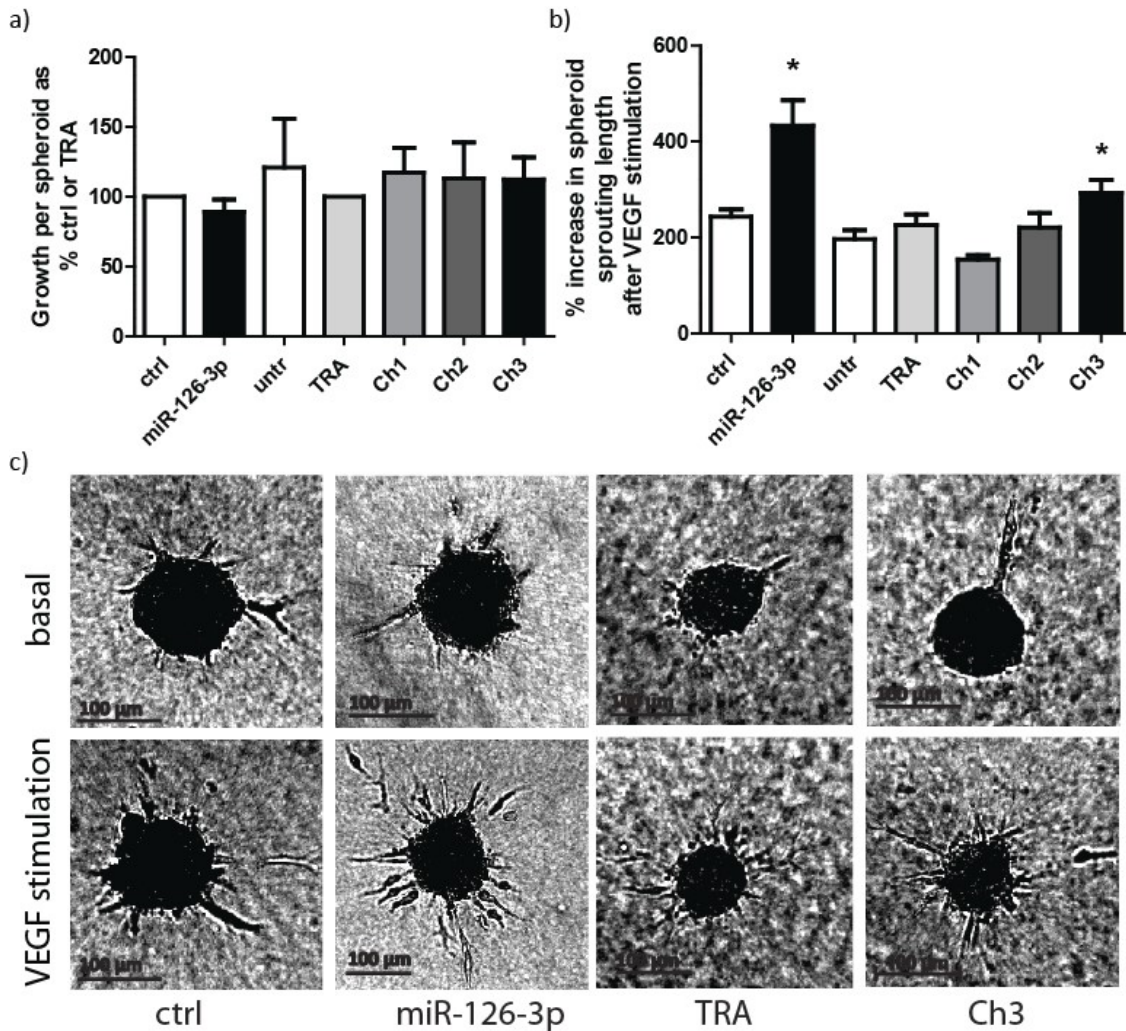


Figure 4.2.6 Effects of chimeras on angiogenesis in HUVEC

The formation of spheroid sprouting was assessed in untreated HUVEC (n=9), HUVEC transfected with 10nM ctrl (n=9) or miR-126-3p (n = 11) as well as HUVEC treated with 500nM TRA (n=19), Ch1 (n = 3), Ch2 (n = 8), Ch3 (n = 16) under basal conditions (a). Sprouting of spheroids was also analyzed in treated HUVEC under the influence of 50 ng/mL vascular endothelial growth factor (VEGF) (b). Values in a) were normalized to the sprouting observed in the corresponding control (ctrl or TRA) while values in b) were normalized to sprouting length of spheroids without VEGF stimulation. (c) Representative images of HUVEC spheroid sprouting under various basal and VEGF stimulated conditions for several treatments. Scale Bar = 100μm. Data is shown as mean ± SEM. *p<0.05 compared to controls (ctrl for miR-126-3p; untreated or TRA for Ch1-3). Figures b) and c) previously published in ³⁸⁹.

4.2.7 Internalization of chimeras into two breast cancer cell lines detected via qPCR ³⁸⁹

In breast cancer cells, miR-126 has been described to inhibit growth, endothelial cell recruitment, migration and metastasis ^{220,258,295,297,298}. Because of this, functional effects of Ch3 on two human breast cancer cell lines were analyzed. The two breast cancer cell lines MCF7 and SK-BR3, showed a very low expression of miR-126-3p and 5p in the untreated and control mimic conditions (Figure 4.5.1a+b). After transfection with 10 nM Pre-miR-126-3p, the levels of miR-126-3p, but not 5p, were significantly increased (Figure 4.5.1a+b). However, treatment with 500 nM Ch3 led to a significantly larger increase in miR-126-3p as well as a 1.000 fold increase in miR-126-5p levels, suggesting that the Pre-miR-126 of Ch3 is processed to both mature strands in breast cancer cells (Figure 4.2.7a+b). We then also calculated the increase in copy number for miR-126-3p and found that treatment with 500 nM Ch3 increases CN by 430.000 ± 390.000 copies per nanogram RNA in MCF7 and 158.000 ± 71.000 copies per nanogram RNA in SK-BR3 cell lines (Figure 4.2.7c). Ch3 increases the copy number of miR-126-3p almost to the number detected in untreated ECs (see Figure 4.2.4i), which are known to show a very high amount of miR-126 expression to the point that miR-126 was initially thought to be EC-specific ²⁶⁹. Notably, a decrease in the mRNA levels of SPRED-1 was visible in SK-BR3 cells treated with Ch3 or Pre-miR-126-3p (Figure 4.2.7d), although it was not statistically significant.

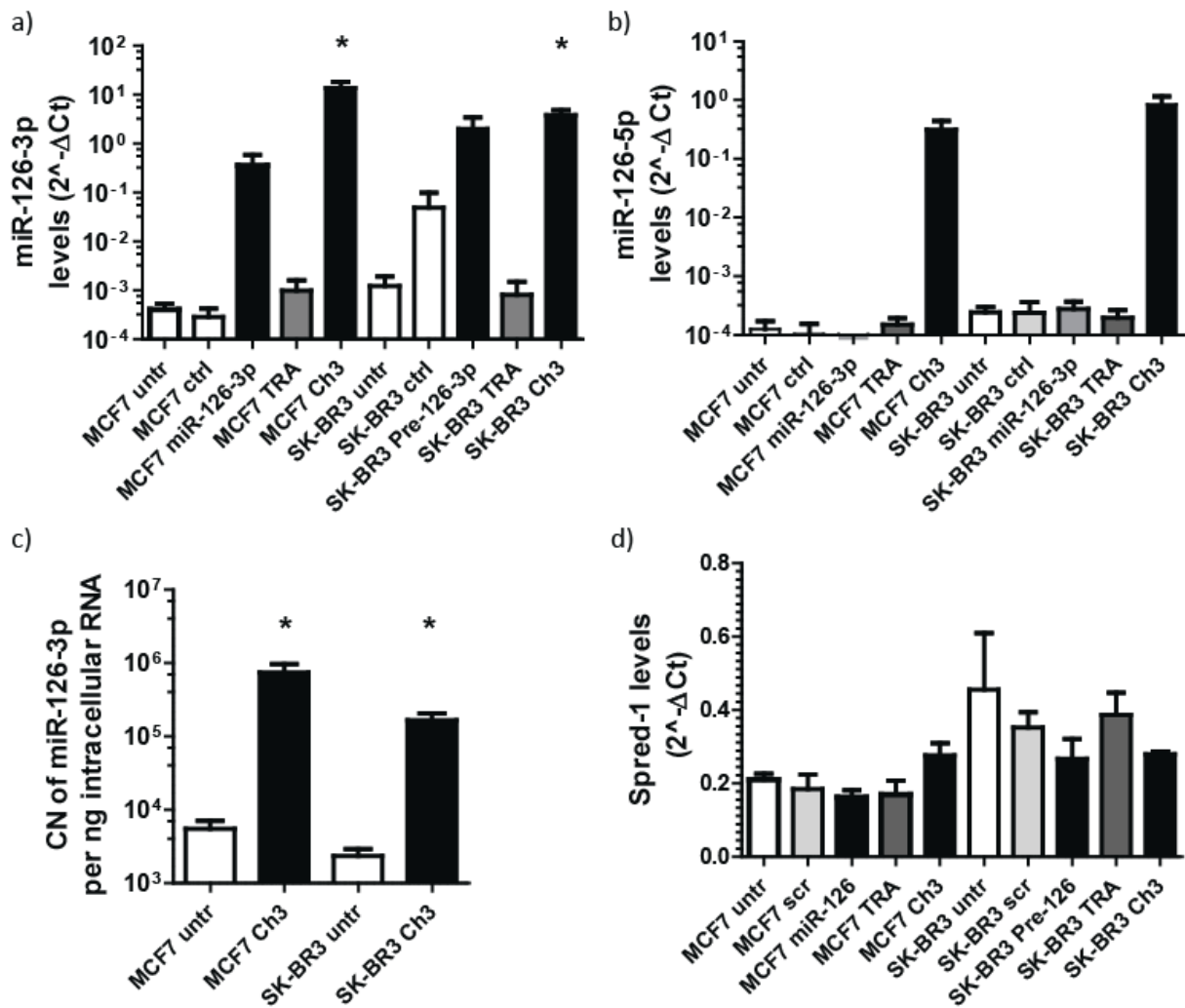


Figure 4.2.7 Delivery of miR-126 to breast cancer cells by Chimera 3

a+b) The levels of miR-126-3p (a) and 5p (b) in internal RNA of breast cancer cells 24 h after treatment with Pre-miR-126-3p, TRA, or Ch3 (n = 3–4). c) Copy number of miR-126-3p in the iRNA of SK-BR3 and MCF7 breast cancer cell lines untreated or treated with 500nM Ch3 for 1 h. miR-126-3p copy numbers (CN) were normalized to snU6 expression and calculated based on standards curves with recombinant miR-126-3p (n = 3–4). d) Expression of the miR-126-3p target Spred-1 in the iRNA of breast cancer cells 24h after treatment with chimeras or miR-126-3p mimic, normalized to the expression of RPLP0 (n=3). Data is shown as mean \pm SEM. *p<0.05 compared to controls (ctrl for miR-126-3p; untreated or TRA for Ch1-3). Figures a) and d) previously published in ³⁸⁹. Figure b) and c) contains data represented also used for the generation of figures in ³⁸⁹, but the figures here contain more datapoints.

4.2.8 Effect of Chimeras on breast cancer viability ³⁸⁹

As miR-126-3p has been described to reduce breast cancer cell viability ²⁹⁵, we analyzed the effect of Ch3 on this parameter where we observed striking differences between the two cell lines. Liposomal transfection with miR-126-3p significantly reduced the viability measured in SK-BR3 cells (74–3,9%), an effects which could also be observed when the cells were treated

with Ch3 (64,5–7,7%), as did conventional (Figure 4.2.8a). However, Ch3 surprisingly increased the viability of MCF7 cells (150,1–9,7%) (Figure 4.2.8b). Similar effects on viability could be observed when miR-126-5p was overexpressed in MCF7 cells (152,1–28,5%) or when cells were treated with TRA (122,4–9,4%). Liposomal overexpression of miR-126-3p however had no effect on the viability of MCF7 cells (Figure 4.2.8b). Together, these data demonstrate that Ch3 inhibits SK-BR3 proliferation, but increases viability of MCF7 cells.

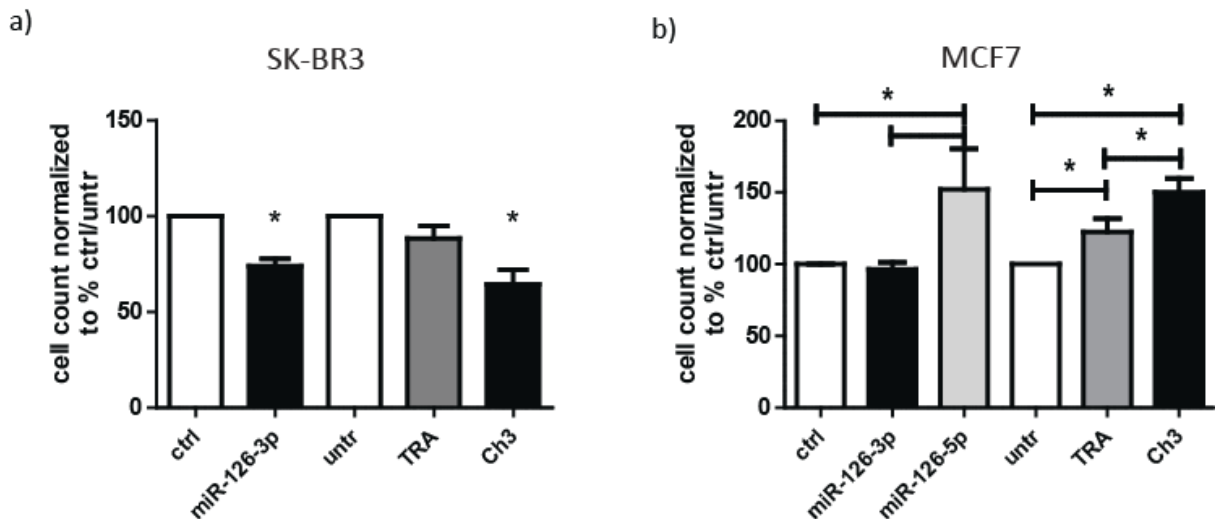


Figure 4.2.8 Effect of miR-126 delivery to breast cancer cells via Ch3 on viability

a+b) A cck8 viability assay was used to assess the viability of SK-BR3 (a) and MCF7 (b) breast cancer cells 72 h after transfection of 10nM miR-126-3p or control precursors or treatment with 500nM TRA or Ch3 (500 nM) (n=7-18). Data is shown as mean \pm SEM. *p<0.05 compared to controls (ctrl for miR-126-3p; untreated or TRA for Ch3). Previously published in ³⁸⁹.

4.2.9 Effect of Chimeras on EC recruitment by breast cancer cells ³⁸⁹

Breast cancer cells recruit ECs to ensure their supply with blood during tumor growth. While SK-BR3 cells showed no difference in their ability to recruit HUVEC when treated with Pre-126-3p or Ch3 (Figure 4.2.9a), MCF7 cells showed a significant reduction (24% and 19% respectively) in their ability to recruit HUVEC through a porous membrane when subjected to the same treatment (Figure 4.2.9b+c). Together with the viability assays this suggests that Ch3 mimics the biological effects of miR-126-3p and miR-126-5p overexpression in breast cancer cells.

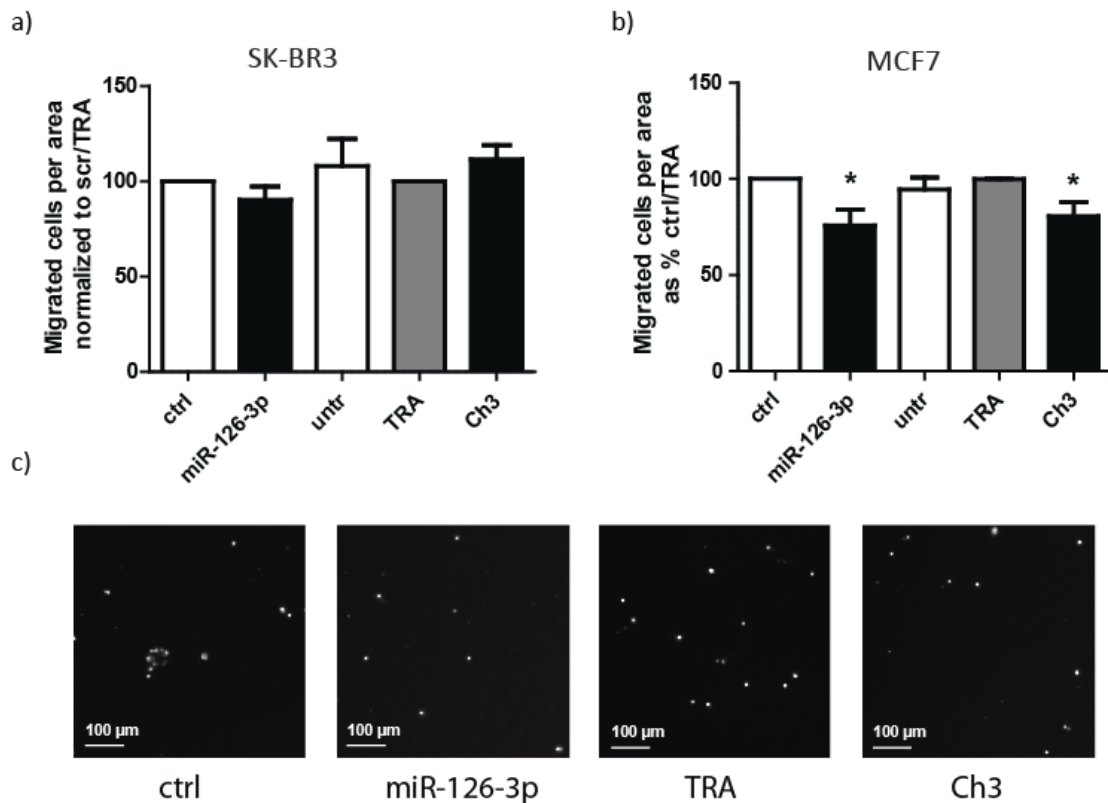


Figure 4.2.9 Effect of miR-126 delivery to breast cancer cells on HUVEC recruitment

a-b) The recruitment of HUVEC by SK-BR3 and MCF7 cell lines untreated or treated with 10nM ctrl or miR-126-3p mimics or 500nM of TRA or Ch3 was analyzed. Automatic counting of DAPP-stained nuclei was used to assess the number of migrated HUVEC, which is expressed as percentage of corresponding controls (control RNA for miR-126-3p, TRA for untr and Ch1-3) (n=3 -11). e) Fluorescent microscopic images representative for the different treatment conditions in the MCF7 recruitment assay. Data are shown as mean \pm SEM. * $p < 0.05$ compared to ctrl (Pre-126-3p+5p) or TRA (Ch3). Previously published in ³⁸⁹.

4.3 Analysis of adult murine cardiac fibroblasts in the context of candidate aptamers, chimeras and reprogramming

4.3.1 Isolation of adult murine cardiac fibroblasts

Having established the possibility of miR-delivery via aptamers in cells of the cardiovascular system, we next endeavored to establish a protocol for the reprogramming of AMCF to induced cardiomyocytes. To do so, we first had to isolate primary AMCF. We were able to isolate viable AMCF from the hearts of C57BL/6 mice using both the Langendorff-Perfusion as well as the extravasation procedure. The morphology of the isolated AMCF was analyzed via the microscope and found to be spindle-shaped (Figure 4.3.1a). Cells could also clearly been observed to grow from tissue fragments during the extravasation (Figure 4.3.1b). In both cases, the time spent from the death of the mouse to the beginning of the isolation

procedure seemed to have the largest impact on the yield of viable cells. The Langendorff-Perfusion isolation procedure resulted in a relatively large yield in some of the cases, but with a lot of variance, to the point that no viable AMCF could be obtained from some of the processed hearts. For the extravasation protocol, a more moderate but stable amount of cells was obtained for each heart processed (Figure 4.3.1c). Since the Langendorff-Perfusion protocol is not only more laborious but also uses five times as much of the rather expensive Collagenase II enzyme, the extravasation method for AMCF isolation was used to obtain the majority of isolated AMCF.

AMCF of up to passage 10 were analyzed for the expression of fibroblast markers vimentin and discoidin domain-containing receptor 2 (DDR2) as well as the endothelial cell marker VE-cadherin and cardiomyocyte markers myosin heavy chain 6 (Myh6) and light chain 2 (Myl2). A strong expression of fibroblast mRNA and very low expression levels of EC or CM mRNA were observed (Figure 4.3.1c). Fluorescent cell staining also revealed a strong expression of vimentin (Figure 4.3.1d) and fibroblast-specific protein 1 (FSP-1) by the AMCF (Figure 4.3.1e). Together, this data indicates that the cells isolated are indeed adult murine cardiac fibroblasts.

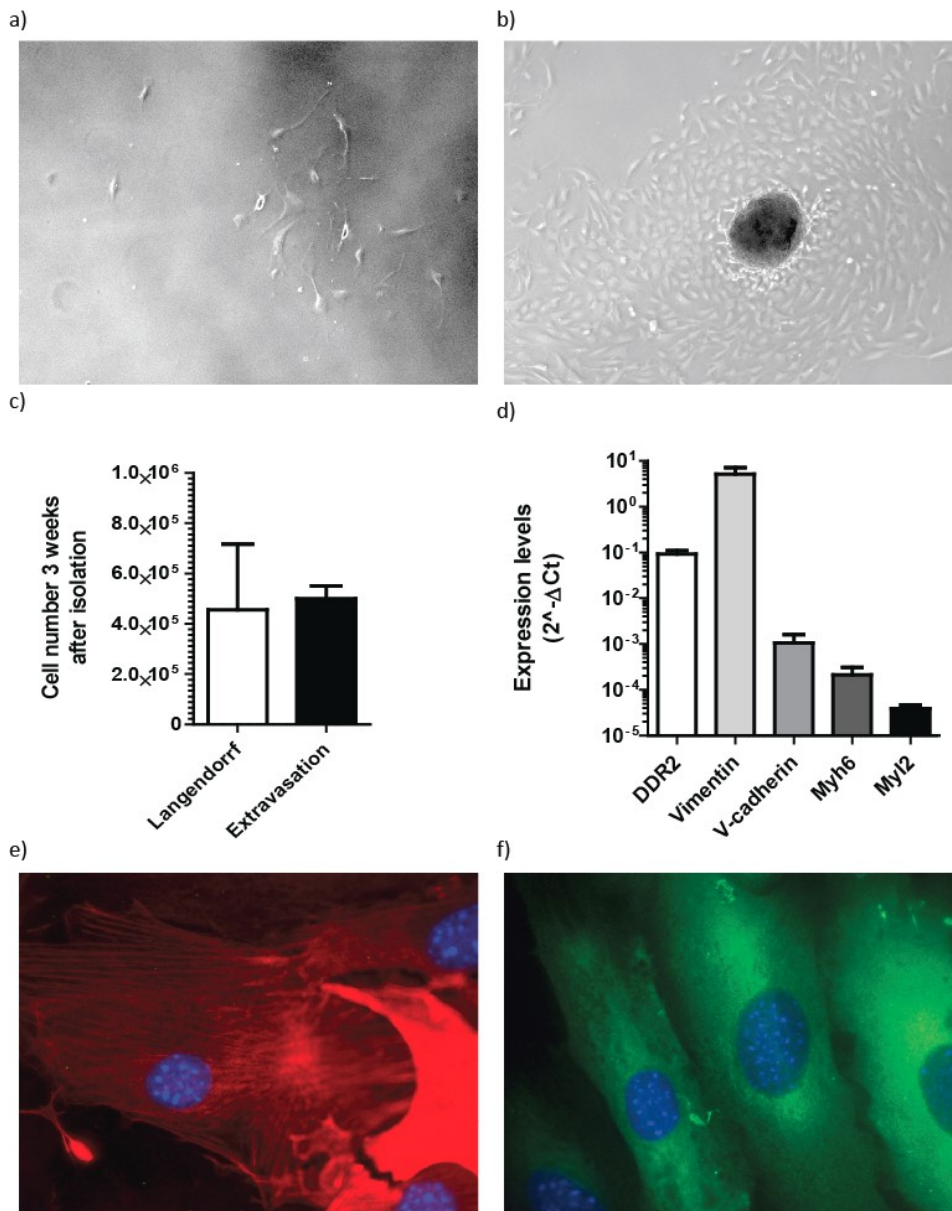


Figure 4.3.1 Characterization of isolated adult murine cardiac fibroblasts

a+b) Representative light microscopic pictures of isolated AMCF, 100 x magnification, ~10 days after isolation. In (b) it can clearly be observed that some cells are migrating from tissue slices onto the culture plate. c) Number viable cells counted 3 weeks after isolation from adult murine hearts with the Langendorff-perfusion or extravasation method (n=6 and 2 respectively). d) Expression levels of markers for fibroblasts (DDR2, vimentin), endothelial cells (V-cadherin) and cardiomyocytes (Myh6, MyI2) in the isolated AMCF, normalized to RPLP0 (n=3-4). Data are shown as mean \pm SEM. e+f) Fluorescence microscopy images of AMCF that were stained for vimentin (d) and FSP-1 (e), 630 x magnification (n=2).

4.3.2 Internalization of GIRM and TRA into adult murine cardiac fibroblasts

As the goal of the thesis was to reprogram AMCF using miRs carried by aptamers, GIRM and TRA were also analyzed for their ability to enter these primary cells. We found that treatment with GIRM or TRA leads to levels of the constructs easily detectable by qPCR in both total and iRNA (Figure 4.3.2a+b). Both fluorescently labeled constructs could also be observed in AMCF using fluorescent microscopy (Figure 4.3.2c).

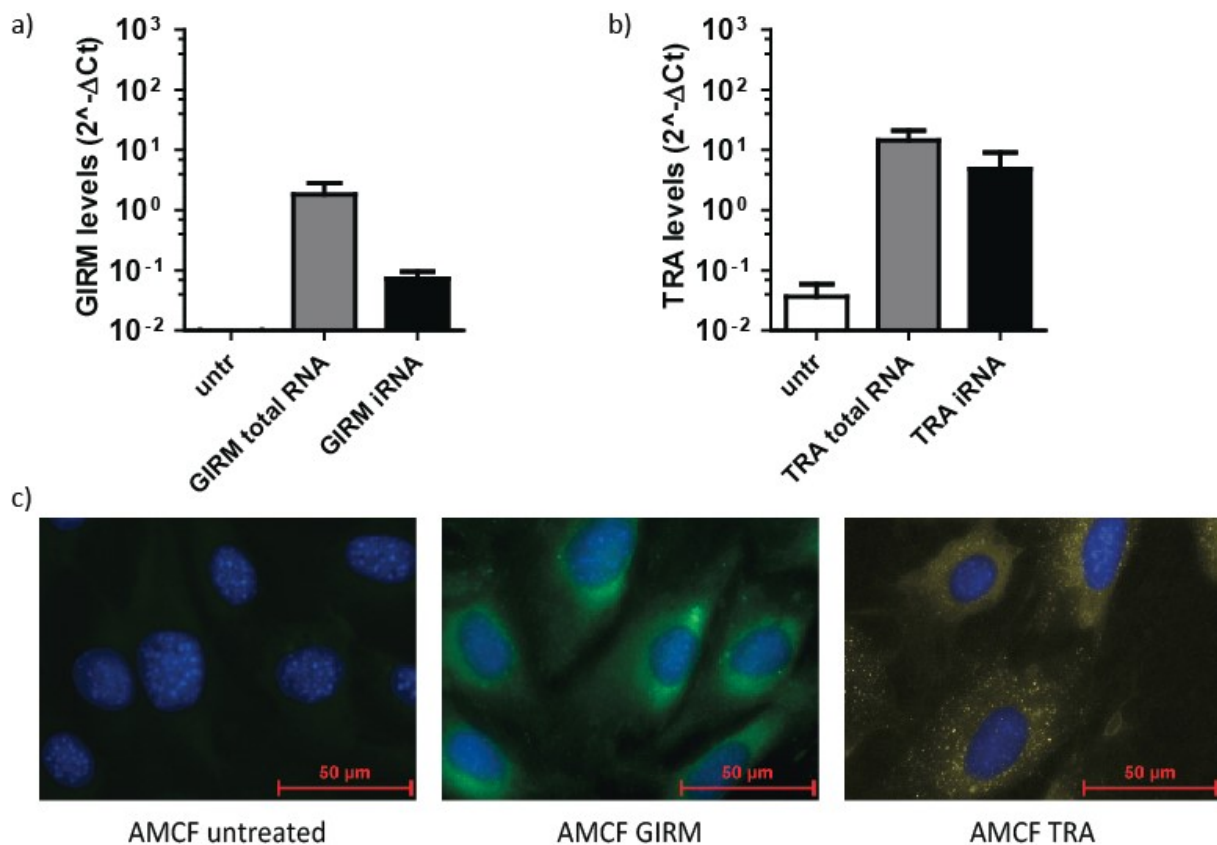


Figure 4.3.2 Candidate aptamers internalize into adult murine cardiac fibroblasts

a+b) Levels of GIRM (a) and TRA (b) in total and internal RNA of AMCF after 1h of treatment with 500nM of the constructs. Data shown as mean \pm SEM. c) Representative fluorescence microscopy images of AMCF that were treated with fluorescein-tagged GIRM (green) or Cy3-tagged TRA (yellow) for 1 hour (n=2). 630x magnification, scale bar = 50 μ m.

4.3.3 Internalization of chimera 4 into AMCF and effect on miR-1a-3p

389

Since it appears that the chimera using a precursor of the target microRNA is the only one functional, it would be interesting to know whether the design can be used to transport other miRs than (Pre-)miR-126. Therefore, a chimera of TRA and murine Pre-miR-1a-2, called chimera 4 (Ch4) was designed (Figure 4.3.3a+b). The intention was to use Ch4 for AMCF to CM reprogramming, as miR-1 was reported to be part of the miR-cocktail used to induce the transition³¹⁹. Indeed, treatment of AMCF with Ch4 for 1 h led to a significant increase in levels of TRA and miR-1a-2-3p (Figure 4.3.3c+d).

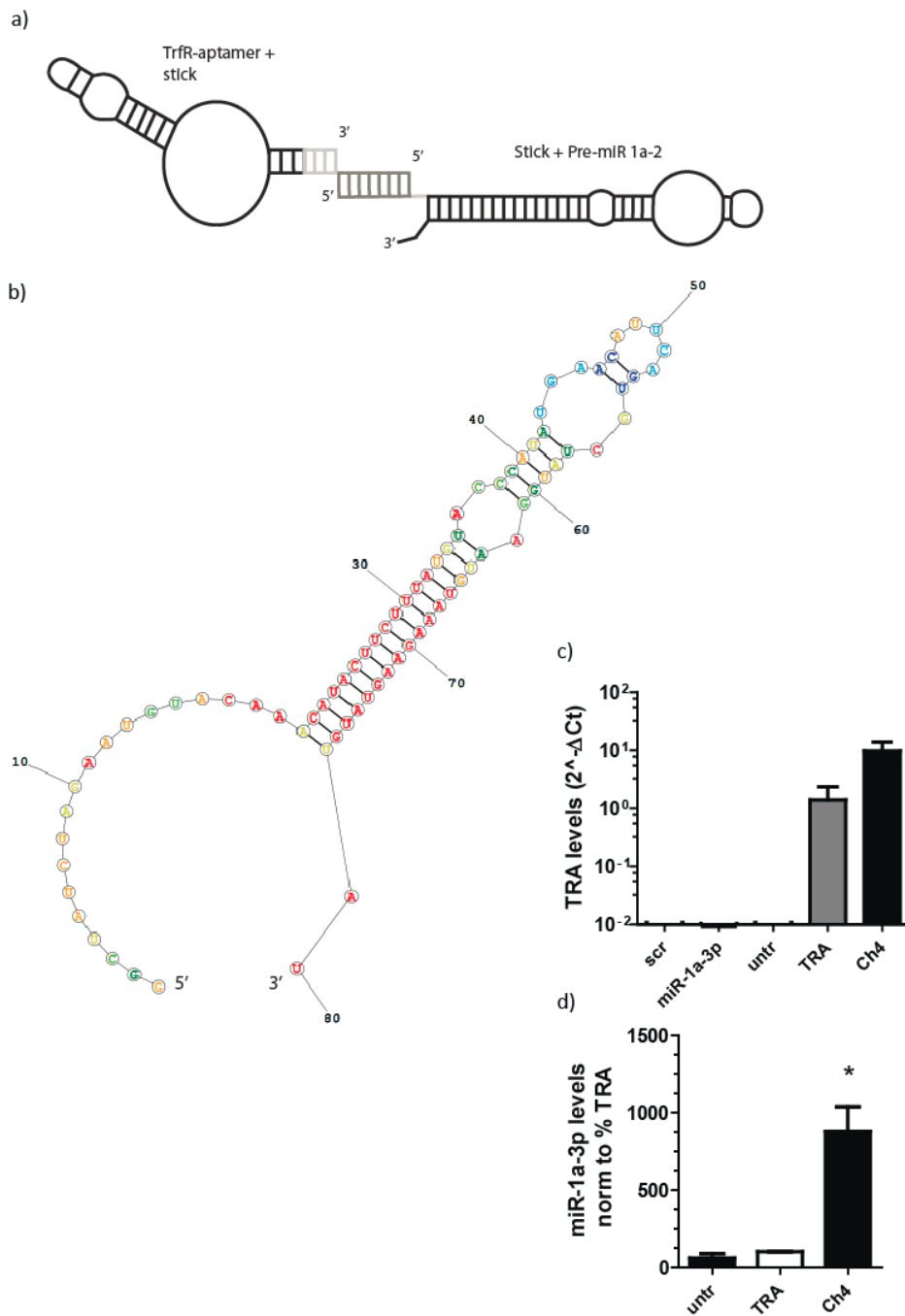


Figure 4.3.3 The TRA-stick construct can also be used to deliver other pre-miRs

a) Schematic illustration of the design of Chimera 3 compared to the TRA-miR-1 chimera (Chimera 4; Ch4). The TRA and miR sequences are shown in black, the linker sequences are shaded light grey and the stick sequence is shaded dark grey. b) Predicted secondary structure (RNAstructure 5.6) of parts of the stick-pre-1a-2 construct. c) Incubation of Ch4 (500 nM, 1 hour) increases total levels of TRA in AMCF. d) Ch4 increases levels of miR-1a-3p in intracellular RNA of AMCF (n=3). Data depict mean \pm SEM. *p<0.05 compared to TRA. Previously published in ³⁸⁹.

4.3.4 Reprogramming of cardiac fibroblasts

Jayawardena et al described a transdifferentiation of neonatal murine cardiac fibroblasts into iCM using a cocktail of miR-1a-2-3p, 133 and 208a³¹⁹. They were also able to induce this reprogramming in a murine model of AMI¹¹⁹. We set out to replicate the results using adult cardiac fibroblasts, as these are more relevant in the context of AMI since it usually occurs in adults, not newborns. To analyze and optimize the reprogramming, isolated primary AMCF were treated with a cocktail of 25nM of each of miR-1a-2-3p, 133 and 208a or 75nM negmiR control (ctrl). The treatment led to a drastic increase in the levels of all three miRs, which had a very low basal expression (Figure 4.3.4a-c). Some of cells were also treated with JI1, reported to facilitate miR-mediated reprogramming of AMCF^{108,109,319}, from day 1 post-treatment until RNA samples were taken 2-21 days later. According to the prior publication these experiments were based on, a decrease in vimentin expression of ~30-50% and at least 300% increase in GATA4 expression should be visible from day 4 onwards, even without JI1³¹⁹. No significant increase in the stem-marker GATA4 (Figure 4.3.4d) or the CM marker Myh6 was observed (Figure 4.3.4e). AMCF also failed to exhibit any significant decrease in the expression of the fibroblast markers vimentin (Figure 4.3.4f). Inclusion of miR-499a into the cocktail also had no impact on the expression of GATA 4 (Figure 4.3.4g) and Myh 6 (Figure 4.3.4h) after 4 days.

Treatment of AMCF with JI1 for 3 days and with 20 ng/ml BMP4 from day 4 onwards (based on^{108,401}) also had no significant effect on the expression of GATA 4 and Myh6 (Figure 4.3.4i+j). Also, the duration of reprogramming (the longest period measured was 21 days) had no significant impact on the levels of GATA4 and vimentin measured (data not shown). Together, it appears that treatment of AMCF with a cocktail of Pre-miR-1a-2-3p, 133, 208a and 499 does not induce the cells to change their expression of fibroblast and CM marker mRNA or their morphology and consequently they do not adapt an iCM phenotype.

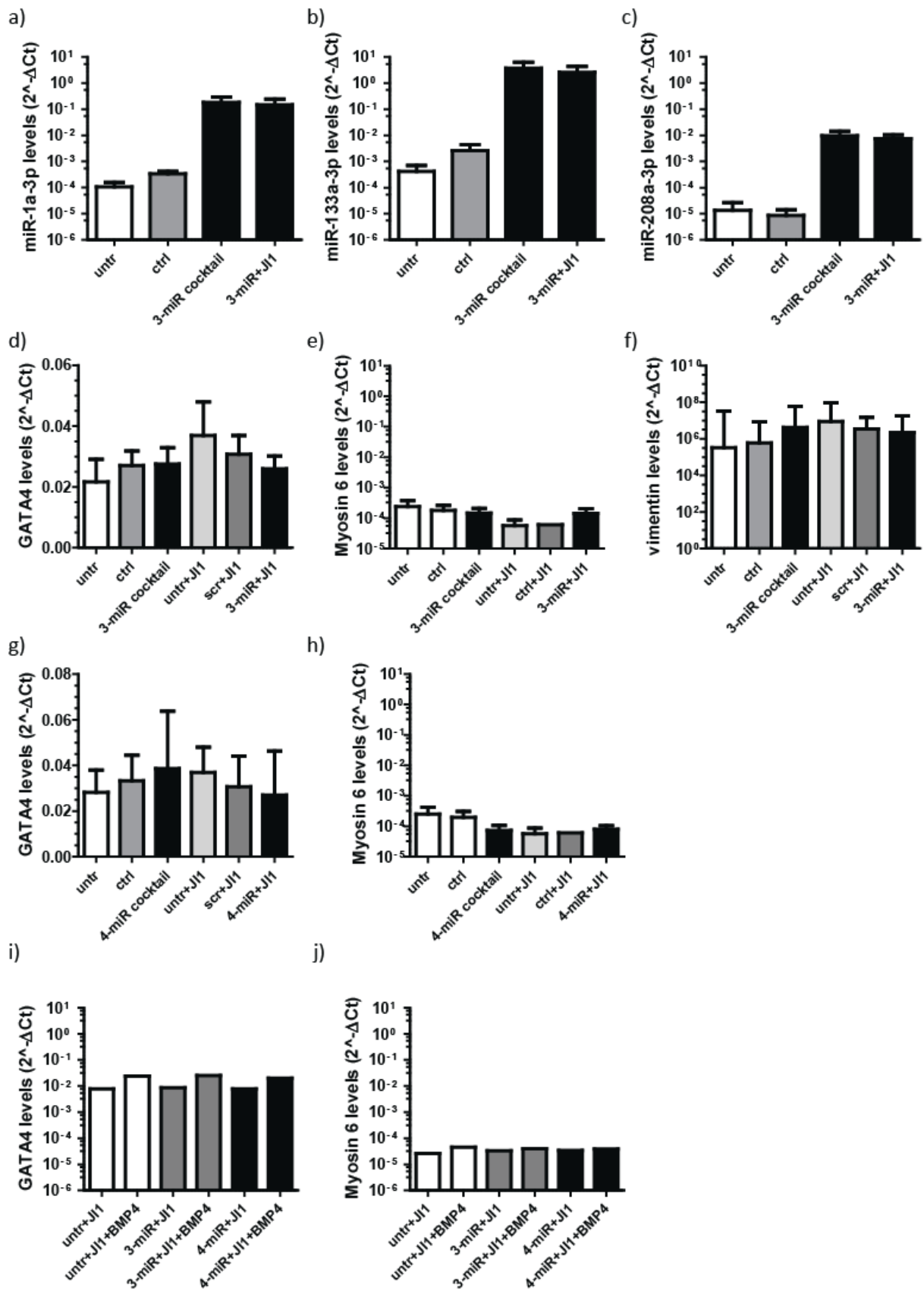


Figure 4.3.4 Attempted reprogramming of AMCF using a miR-cocktail

a-c) Expression levels of miR-1a-3p (a), miR-133a-3p (b) and miR-208a-3p (c) 4 days after transfection with a cocktail of 25nM of each of the 3 Pre-miR mimics (miR-1a, 133a, 208a) or 75nM negmiR control (n = 3). c-h) Expression levels of GATA 4 (d), Myh6 (e) and vimentin (f) in AMCF 2-21 days after transfection with a 25nM cocktail of 3 miRs (n = 4–15). g+h) Expression levels of GATA4 (g) and Myh6 (h) in AMCF 14 days after treatment with a cocktail of 25nM of each of the 4 miRs (3-miR+ miR-499; n=3). In all graphs, half of the samples were also treated with 1nM Jak inhibitor 1 (JI1) daily starting one day post-transfection. i+j) Treating AMCF with BMP starting 7 days after transfection with a cocktail of 3 or 4 miRs does not significantly influence the expression of GATA4 (i) or Myh6 (j; n=1). Data is shown as mean \pm SEM.

4.4 Cell-SELEX for aptamers binding to adult murine cardiac fibroblasts

4.4.1 Using a pool containing 20 randomized nucleotides

The aptamer pool using 20 randomized nucleotides initially proved difficult to amplify, a problem which was ameliorated by using a maximum of 24 samples per PCR-machine. During the first SELEX procedure (see Methods table 2.19a), RNase digestion was postponed until round 7. However, once the RNase selection step was introduced, the amount of recovered pool RNA was too small to continue working (figure 4.4.1a). Also, during the selection there was no visible enrichment of the pool for species attaching to AMCF from one round to the next, indicated by no significant changes in the amount of pool recovered after selection (Figure 4.4.1a).

Another SELEX was therefore started (see Methods table 2.19b), using a larger number of target cells, omitting negative cell selection for the first two rounds and longer incubation of the pool with the AMCF, but introducing RNase digestion from round 1 onwards. While initially the recovered amount of RNA seemed to be sufficient, it soon became apparent that again, no enrichment of the pool could be observed (Figure 4.4.1c). We therefore switched to another pool containing 52 randomized nucleotides and a conserved stem loop sequence.

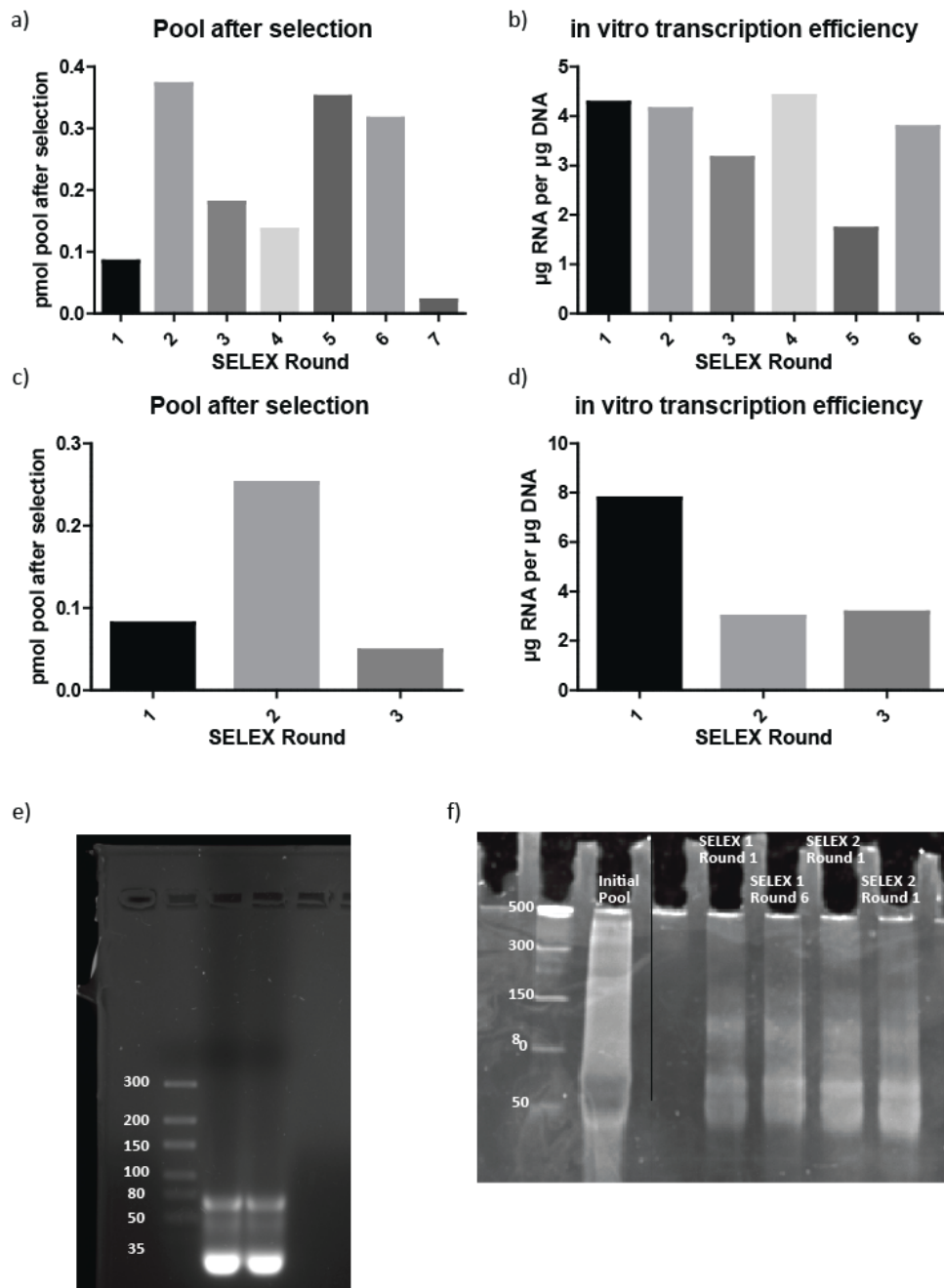


Figure 4.4.1 Cell SELEX Rossi-Pool

a-b) After each SELEX round, the pool was reverse transcribed into cDNA, which was then amplified and purified by EtOH-precipitation. The yield was measured using a Nanodrop and used to calculate the molar amount of pool present in the template in picomol for the first (a) and 2nd attempted SELEX (b). c+d) Efficiency of the T7 Durascribe transcription as µg RNA per µg DNA used for the reaction for the first (c) and 2nd attempted SELEX (d). e) The DNA-gel used to purify DNA from SELEX 1 round 1. The leftmost band is an ultra-low range DNA ladder. f) RNA gel that was used to check the size of RNA produced in the T7 Durascribe reaction for round 4.

4.4.2 Using a pool 52 randomized nucleotides

The protocol for the cell SELEX using the pool containing 52 randomized nucleotides was adapted from Florian Groher (TU Darmstadt, Germany) who worked with this pool selecting aptamers in a conventional protein based SELEX in the lab of Prof. B. Süß (TU Darmstadt, Germany). The first two rounds were run without exposing the pool to EC for negative selection, the pool was applied in DPBS, not medium, which omits selection for FBS-stability and no RNase digestion was used (to allow for aptamers which can attach, but not internalize into AMCF since it might not be possible to find an aptamer which can do both). Using the new pool and selection protocol, an increase in enrichment was observed from round 1 to 2 and 3 to 4 (Figure 4.4.2a). It should also be noted, that the amount of pool remaining after the selection rounds was much greater and the transcription efficiency was increased (Figure 4.4.2b), though this might be due to a slight adaption of the protocol (the reaction time was increased from 6 h to overnight). Round 5, 6 and 7 were sent to GenXPro (Frankfurt, Germany) for sequencing.

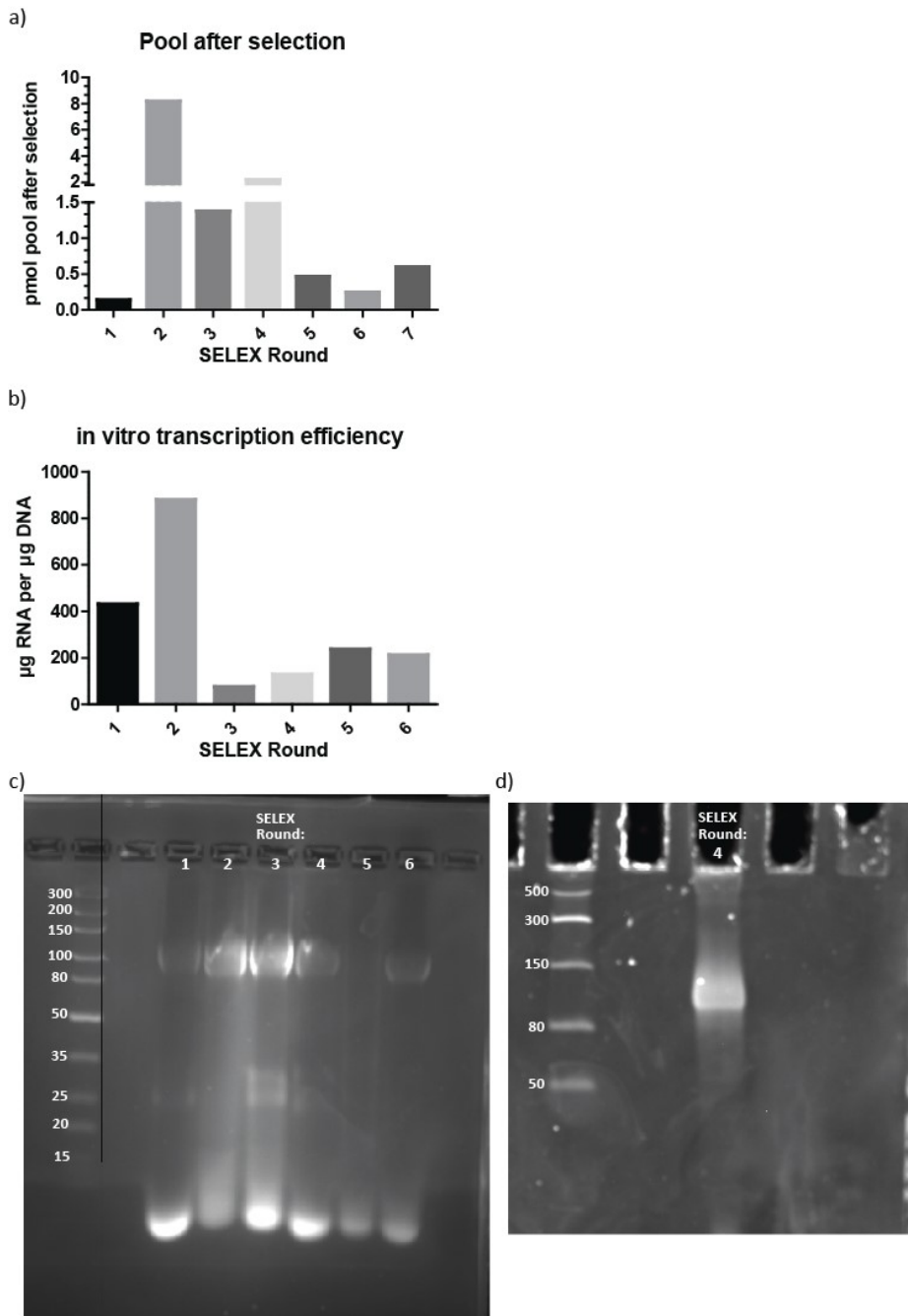


Figure 4.4.2 Cell SELEX Süß-Pool

a) After each SELEX round, the pool was reverse transcribed into cDNA, which was then amplified and purified by EtOH-precipitation. The yield was measured using a Nanodrop and used to calculate the molar amount of pool present in the template in picomol. b) Efficiency of the T7 Durascribe transcription as $\mu\text{g RNA per } \mu\text{g DNA}$ used for the reaction. c) The DNA-gel used to purify DNA from rounds 1-6 for sequencing. The leftmost band is an ultra-low range DNA ladder. d) Example of an RNA gel that was used to check the size of RNA produced in the T7 Durascribe reaction for round 4.

4.4.3 Bioinformatics Analysis

Rounds 5, 6 and 7 of the SELEX were sequenced and the sequences were sorted according to the number of reads. It should be noted that the sequence reads contain both the sense and the antisense variants of all candidates; these were matched and the reads pooled. Table 4.4.3a-c shows the top 10 sense candidates for each of the three rounds. The top 1000 reads from each round were also analyzed for conserved sequence motifs using the MEME^{395,397} and DREME³⁹⁶ algorithms. Motifs which were not present in SELEX rounds 5 and 6 or located in the conserved regions at the ends or the stem loop of the aptamers. The most highly conserved motifs are shown in table 4.4.3d+e together with their number of total reads in each round and their enrichment from round to round. 10 candidates were chosen for further analysis by combining the number of reads and the motif data (see table 4.4.3f and figure 4.4.3).

Rank	Reads	Sequence
1	112583	GTA TAA TAC GAC TCA CTA TAG GGA GAC GCA ACT GAA TGA ACT GAT TCA AAA GCA CGA CAA TCC ATT CTG CTT CGG CAG GTT CTC GTT CTT TTG AAC AGT CGG TGT CCG TAA CTA GTC GCG TCA C
2	105120	GTA TAA TAC GAC TCA CTA TAG GGA GAC GCA ACT GAA TGA AGA TAT TAG CAC CGA ATC TCA GTT CTT CTG CTT CGG CAG CTC AAT CTC CAG TAC ACC GTA TCG TCT CCG TAA CTA GTC GCG TCA C
3	102901	GTA TAA TAC GAC TCA CTA TAG GGA GAC GCA ACT GAA TGA ATA CAC CTA GCA ATG AGT ATC ACC CAT CTG CTT CGG CAG TTT AAG TGA TTC CTC ATT TCG GAT TTA TCC GTA ACT AGT CGC GTC AC
4	93993	GTA TAA TAC GAC TCA CTA TAG GGA GAC GCA ACT GAA TGA ATA ACG CGC GAA ACA CAA CTA GCT CAT TCT GCT TCG GCA GGC TCG TTC TGT TTC GAA GTT ACT GTG TCC GTA ACT AGT CGC GTC AC
5	89791	GTA TAA TAC GAC TCA CTA TAG GGA GAC GCA ACT GAA TGA ACA ATT TCC CCC TCT ATT CCT TTC GAA CTG CTT CGG CAG ATT TCG CCA GCA TAG AGT GAG GGT CAT CCG TAA CTA GTC GCG TCA C
6	77899	GTA TAA TAC GAC TCA CTA TAG GGA GAC GCA ACT GAA TGA ATT CTG CCT TTT CGG CTT CCT CGA TTC CTG CTT CGG CAG TAT CTA CTG GAA CCG TCA AGG TAT GTT CCG TAA CTA GTC GCG TCA C
7	71903	GTA TAA TAC GAC TCA CTA TAG GGA GAC GCA ACT GAA TGA ATT GAT TAC TCA CAG ATT CCT CGA ATC CTG CTT CGG CAG TTT CTT AAG TAT CTA AGT TAG TTT CAA TCC GTA ACT AGT CGC GTC AC
8	64408	GTA TAA TAC GAC TCA CTA TAG GGA GAC GCA ACT GAA TGA ATC CCG CGA ATA TCC AAG TGA TTC CTC CTG CTT CGG CAG GAG TAT CAC CCA ATC TTT AGC GTG GGT CCG TAA CTA GTC GCG TCA C
9	60333	GTA TAA TAC GAC TCA CTA TAG GGA GAC GCA ACT GAA TGA AGC TTG CTA GAG TCG CTT TCG CGA TTC CTG CTT CGG CAG TAT CTA ACG AAA CGC CTA TTG CTG CCT CCG TAA CTA GTC GCG TCA C
10	57158	GTA TAA TAC GAC TCA CTA TAG GGA GAC GCA ACT GAA TGA AAT TTC TCG TCT CAA TTT CCA GAA TTC CTG CTT CGG CAG TAT TCG TGG CAA TGA GTC AAC GAA CTT CCG TAA CTA GTC GCG TCA C

Table 4.4.3a Top 10 sequences measured in SELEX round 7

Rank in	reads	Sequence
Round 7		
13	17224	GTA TAA TAC GAC TCA CTA TAG GGA GAC GCA ACT GAA TGA AGG CAA TAC GTC AGA GCT TAT TCC AAA CTG CTT CGG CAG TTT GAG TCT GTA CGT ATT TCC GGA GGT CCG TAA CTA GTC GCG TCA C
4	10803	GTA TAA TAC GAC TCA CTA TAG GGA GAC GCA ACT GAA TGA ATA ACG CGC GAA ACA CAA CTA GCT CAT TCT GCT TCG GCA GGC TCG TTC TGT TTC GAA GTT ACT GTG TCC GTA ACT AGT CGC GTC AC
17	8923	GTA TAA TAC GAC TCA CTA TAG GGA GAC GCA ACT GAA TGA ATT TGA GTA CTA AGC TGA GCC GTT TAT CTG CTT CGG CAG TTC CTC CAA TTC GAA TGG TCG CCT GAA TCC GTA ACT AGT CGC GTC AC
3	6574	GTA TAA TAC GAC TCA CTA TAG GGA GAC GCA ACT GAA TGA ATA CAC CTA GCA ATG AGT ATC ACC CAT CTG CTT CGG CAG TTT AAG TGA TTC CTC ATT TCG GAT TTA TCC GTA ACT AGT CGC GTC AC
1	5284	GTA TAA TAC GAC TCA CTA TAG GGA GAC GCA ACT GAA TGA ACT GAT TCA AAA GCA CGA CAA TCC ATT CTG CTT CGG CAG GTT CTC GTT CTT TTG AAC AGT CGG TGT CCG TAA CTA GTC GCG TCA C
30	5141	GTA TAA TAC GAC TCA CTA TAG GGA GAC GCA ACT GAA TGA AGC AAA GTT ATT CGT TTC GCA AAT TCC TGC TTC GGC AGT ATT TGT TGC AAC AAT AAA CGA TTC TTT CCG TAA CTA GTC GCG TCA C
11	4804	GTA TAA TAC GAC TCA CTA TAG GGA GAC GCA ACT GAA TGA ACT CAT TCG GAT CTG CCT AAG TCG ACT CTG CTT CGG CAG AGA CCG GCT CAT TCA GAT TGC GGT CCG TAA CTA GTC GCG TCA C
7	4755	GTA TAA TAC GAC TCA CTA TAG GGA GAC GCA ACT GAA TGA ATT GAT TAC TCA CAG ATT CCT CGA ATC CTG CTT CGG CAG TTT CTT AAG TAT CTA AGT TAG TTT CAA TCC GTA ACT AGT CGC GTC AC
14	4287	GTA TAA TAC GAC TCA CTA TAG GGA GAC GCA ACT GAA TGA AGT ATC ACT CTC CAG ATT CCT TCA CAG CTG CTT CGG CAA CGT CCG GTG CAT TGC GAC ACC GGC CTC CGT AAC TAG TCG CGT CAC
10	4219	GTA TAA TAC GAC TCA CTA TAG GGA GAC GCA ACT GAA TGA AAT TTC TCG TCT CAA TTT CCA GAA TTC CTG CTT CGG CAG TAT TCG TGG CAA TGA GTC AAC GAA CTT CCG TAA CTA GTC GCG TCA C

Table 4.4.3b Top 10 sequences measured in SELEX round 6

Rank in	reads	Sequence
Round 7		
4	121	GTA TAA TAC GAC TCA CTA TAG GGA GAC GCA ACT GAA TGA ATA ACG CGC GAA ACA CAA CTA GCT CAT TCT GCT TCG GCA GGC TCG TTC TGT TTC GAA GTT ACT GTG TCC GTA ACT AGT CGC GTC AC
13	115	GTA TAA TAC GAC TCA CTA TAG GGA GAC GCA ACT GAA TGA AGG CAA TAC GTC AGA GCT TAT TCC AAA CTG CTT CGG CAG TTT GAG TCT GTA CGT ATT TCC GGA GGT CCG TAA CTA GTC GCG TCA C
11	85	GTA TAA TAC GAC TCA CTA TAG GGA GAC GCA ACT GAA TGA ACT CAT TCG GAT CTG CCT AAG TCG ACT CTG CTT CGG CAG AGA CCG GCT CAT TCA GAT TGC GGT CCG TAA CTA GTC GCG TCA C
17	83	GTA TAA TAC GAC TCA CTA TAG GGA GAC GCA ACT GAA TGA ATT TGA GTA CTA AGC TGA GCC GTT TAT CTG CTT CGG CAG TTC CTC CAA TTC GAA TGG TCG CCT GAA TCC GTA ACT AGT CGC GTC AC
300	69	GTA TAA TAC GAC TCA CTA TAG GGA GAC GCA ACT GAA TGA AGA CCA TTG TAC CCT TCA ACA CAT TCC TGC TTC GGC AGT ATG AGG TTT AAG GTC GCG TTG CGT GTC CGT AAC TAG TCG CGT CAC
49	62	GTA TAA TAC GAC TCA CTA TAG GGA GAC GCA ACT GAA TGA AAT GCA AGT ATC TGC ACC GCA CGA AAG CTG CTT CGG CAG ATT CCT TGC GCG TTC CGC GTG TAT CCG TAA CTA GTC GCG TCA C
157	60	GTA TAA TAC GAC TCA CTA TAG GGA GAC GCA ACT GAA TGA ACA CTT CCC AAA GGC GCT AAA GCG TTC CTG CTT CGG CAG TAC GTA CAA CTT CTG TTC TTA GCG CAT CCG TAA CTA GTC GCG TCA C
47	59	GTA TAA TAC GAC TCA CTA TAG GGA GAC GCA ACT GAA TGA AGC TAT CTC TCC GCT GGT TCC CCG GTT CCT GCT TCG GCA GTA CCT AGA TGG AAC CAC GCG TCC GTA ACT AGT CGC GTC AC
3	54	GTA TAA TAC GAC TCA CTA TAG GGA GAC GCA ACT GAA TGA ATA CAC CTA GCA ATG AGT ATC ACC CAT CTG CTT CGG CAG TTT AAG TGA TTC CTC ATT TCG GAT TTA TCC GTA ACT AGT CGC GTC AC
30	48	GTA TAA TAC GAC TCA CTA TAG GGA GAC GCA ACT GAA TGA AGC AAA GTT ATT CGT TTC GCA AAT TCC TGC TTC GGC AGT ATT TGT TGC AAC AAT AAA CGA TTC TTT CCG TAA CTA GTC GCG TCA C

Table 4.4.3c Top 10 sequences measured in SELEX round 5

MEME Motif	Sequence	hits top 10k	Est. reads	Hits Rnd 6	Reads Rnd 6	Enr. 6 to 7	Hits Rnd 5	Reads Rnd 5	Enr. 5 to 6
4	CAC TCT CCA GAT TCC TTC ACA GCT GCT TCG GCA ACG TCC GGT GCA TTG CG	20	32223	4	2157	14,93	1	15	143,8
6	TCG TTC TGT TTC GAA GTT ACT	41	63849	11	15897	4,01	2	56	283,8
7	AAC GCG CGA AAC AC A/G ACT AGC	46	65371	10	6178	10,58	2	56	110,3
8	GTG ATT CCT CAT TTC GGA TTT	34	63196	5	3456	18,2	1	25	138,2
9	ACC TAG CAA TGA GTA TCA CCC <i>or</i> ACC TAG CAA TGA GTA TCG CCC	42	64572	6	3199	20,18	1	25	127,9
10	ATT AGC ACC GAA TCT CAG TTC <i>or</i> ATT AGC GCC GAA TCT CAG TT	38	63606	1	1085	58,62	1	14	77,5
11	A/T TT TCT CGT CTC AAT TTC CAG	24	39634	4	2316	17,11	2	14	165,4
12	ATC TCC AGT AC A/G CCG TAT CGT	29	61191	1	1085	56,39	1	14	77,5
13	GTG GCA ATG AGT CA A/G CGA AC <i>or</i> GTG GCA ATG AGT CGA CGA AC	25	40891	6	2368	17,26	2	14	169,1
14	CTC GTT CTT TTG AAC AGT CGG	35	66571	2	2647	25,14	1	13	203,6
15	TCG CCA GCA TAG AGT GAG GGT <i>or</i> TCG CCA GCA TAG AGT AAG GGT	29	51837	2	1384	37,45	1	12	115,3
16	TTT CCC CCT CTA TTC CTT TCG <i>or</i> TTT CCC CCT CTA TTC CTC TCG	36	53482	2	1384	38,64	1	12	115,3

Table 4.4.3f Sequence Motifs present in SELEX round 7 predicted by MEME^{395,397}

Rnd = round, 10k = 10.0000, Est. = estimated, Enr. = enrichment, A/G = either A or G, A/T = A or T

DREME Motif	Sequence	hits top 10k	Est. reads	Site Cons?	Hits Rnd 6	Reads Rnd 6	Enr. 6 to 7	Hits Rnd 5	Reads Rnd 5	Enr. 5 to 6
11	AAC T?A TTC	194	194926	no	101	18143	10,7	45	240	75,5
13	AGT ATC ACC C <i>or</i> AGT ATC ACT C	84	115991	no	12	7600	15,2	5	75	101,3
14	GCA GTT CA <i>or</i> GCA GCT CA	163	120991	no	110	13900	8,70	48	238	58,4
15	AAC AAT TC <i>or</i> AAC AAT TT	95	133136	no	32	7400	17,9	18	120	61,6
16	AAC CTA TTC <i>or</i> AAC CTT TTC	84	65116	no	45	7675	8,48	19	101	75,9
17	GTT CTT TTG A	45	59049	yes	2	2630	22,4	1	13	202,3
18	AGC ACC GAA TC <i>or</i> ATC ACC GAA TC	46	68816	no	3	1800	38,2	2	24	75
20	AAA AGC ACG AC	47	72255	yes	1	2595	27,8	1	13	199,6
22	AAT AAC GCG CGA	47	65743	yes	12	6395	10,2	1	53	120,6
24	GTT CTG TTT CGA	51	68544	yes	12	6368	10,7	1	53	120,1
26	AAT TCT GCC T <i>or</i> AAT TCA GCC T	45	63892	yes	3	2254	28,3	3	23	98
29	ATC TCC AGT ACA	35	62126	yes	1	1085	57,2	1	14	77,5

Table 4.4.3e Sequence Motifs present in SELEX round 7 predicted by DREME^{395,396}

Rnd = round, 10k = 10.0000, Est. = estimated, Enr. = enrichment, ? = any base

Rank	Name	Sequence	MEME	DREME
Rnd			motif	motif
7				
1	Cand 1	GGG AGA CGC AAC TGA ATG AAC TGA TTC AAA AGC ACG ACA ATC CAT TCT GCT TCG GCA GGT TCT CGT TCT TTT GAA CAG TCG GTG TCC GTA ACT AGT CGC GTC AC	14	11+17+20
2	Cand 2	GGG AGA CGC AAC TGA ATG AAG ATA TTA GCA CCG AAT CTC AGT TCT TCT GCT TCG GCA GCT CAA TCT CCA GTA CAC CGT ATC GTC TCC GTA ACT AGT CGC GTC AC	10+12	18+29
3	Cand 3	GGG AGA CGC AAC TGA ATG AAT ACA CCT AGC AAT GAG TAT CAC CCA TCT GCT TCG GCA GTT TAA GTG ATT CCT CAT TTC GGA TTT ATC CGT AAC TAG TCG CGT CAC	8+9	13
4	Cand 4	GGG AGA CGC AAC TGA ATG AAT AAC GCG CGA AAC ACA ACT AGC TCA TTC TGC TTC GGC AGG CTC GTT CTG TTT CGA AGT TAC TGT GTC CGT AAC TAG TCG CGT CAC	6+7	22+24
5	Cand 5	GGG AGA CGC AAC TGA ATG AAC AAT TTC CCC CTC TAT TCC TTT CGA ACT GCT TCG GCA GAT TTC GCC AGC ATA GAG TGA GGG TCA TCC GTA ACT AGT CGC GTC AC	15+16	15+35
6	Cand 6	GGG AGA CGC AAC TGA ATG AAT TCT GCC TTT TCG GCT TCC TCG ATT CCT GCT TCG GCA GTA TCT ACT GGA ACC GTC AAG GTA TGT TCC GTA ACT AGT CGC GTC AC	-	26
9	Cand 7	GGG AGA CGC AAC TGA ATG AAA TTT CTC GTC TCA ATT TCC AGA ATT CCT GCT TCG GCA GTA TTC GTG GCA ATG AGT CAA CGA ACT TCC GTA ACT AGT CGC GTC AC	11+13	-
12	Cand 8	GGG AGA CGC AAC TGA ATG AAG GCA ATA CGT CAG AGC TTA TTC CAA ACT GCT TCG GCA GTT TGA GTC TGT ACG TAT TTC CGG AGG TCC GTA ACT AGT CGC GTC AC	-	33
13	Cand 9	GGG AGA CGC AAC TGA ATG AAG TAT CAC TCT CCA GAT TCC TTC ACA GCT GCT TCG GCA ACG TCC GGT GCA TTG CGA CAC CGG CCT CCG TAA CTA GTC GCG TCA C	4	-
28	Cand 10	GGG AGA CGC AAC TGA ATG AAC TTT CAG CCA GAT GAC TCT TCG GAT CCT GCT TCG GCA GTT CAC AAA GGA GCC TCT GGA CGT GAT CCG TAA CTA GTC GCG TCA C	-	14

Table 4.4.3f Candidate sequences selected for further testing

The 20bp T7 promotor binding sequence (GTATAATACGACTCACTATA) has been removed, since this will not be transcribed into the final RNA construct used for the experiments. Cand = candidate

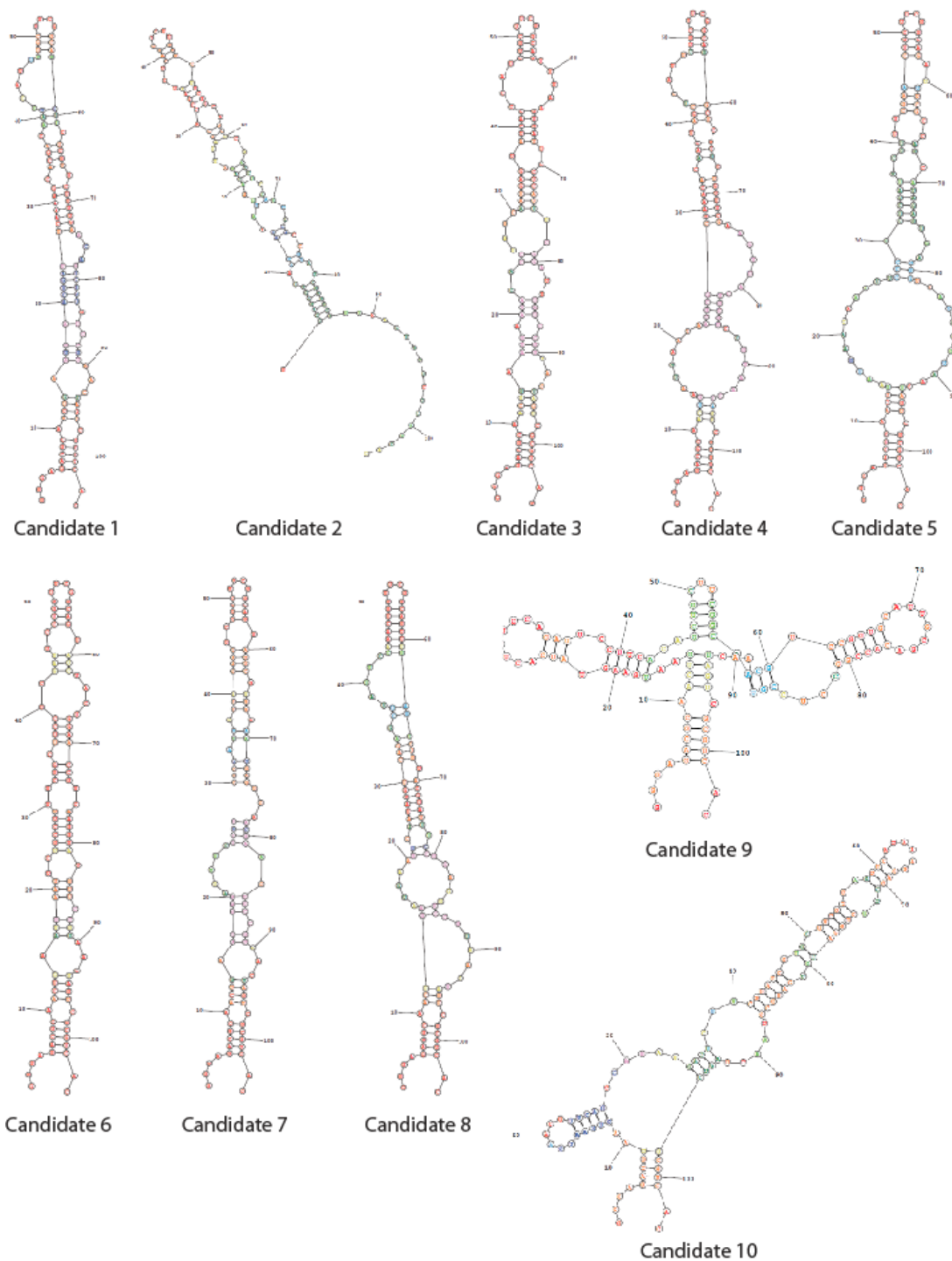


Figure 4.4.3 Predicted secondary structures of the 10 candidate sequences

Secondary structures of all 10 candidates predicted using RNAstructure 5.6³⁹⁸

4.4.4 Analysis of candidate aptamers via qPCR

To analyze the binding abilities of the 10 selected candidates, AMCF, MEC and HUVEC were treated with 2nM solutions of the aptamers, the same concentration used in the SELEX. The levels of candidates in the total RNA of cells was measured with qPCR. Due to the conserved

regions, it was possible to use a general PCR primer set for most candidates. For candidates 1, 4 and 6 better binding forward primers than the general one were predicted and were therefore measured with specific primers (see table 3.1.8). All 10 candidates showed considerable detectable levels in the total RNA of all three cell types (Figure 4.4.4a-c). Next, the copy numbers of the candidates in AMCF and MEC were assessed using the same samples and a standard curve made from pure candidate RNA. The use of this standard curve made it possible to eliminate the influence of primer efficiency on the levels of candidates measured, which allows an easier comparison between the candidates (Figure 4.4.4d). It appeared that candidates 2,3,4,6 and 10 showed the highest detectable amount of copy numbers in total RNA of both AMCF and MEC. It also shows that the candidates bind better to AMCF than MEC by about 10 fold. We then analyzed the internalization of candidates 1 (as it was most highly predicted by the sequencing), 2, 4 and 6 (due to their high levels CN-count in total RNA) into AMCF and MEC by measuring the levels in internal RNA and comparing them to the levels measured for cells treated with 2nM TRA (Figure 4.4.4e+f). Surprisingly, all of the candidates showed higher levels than TRA in the iRNA of both AMCF and MEC. Taken together, the data implies that the candidates bind unspecifically to cells in culture and are partially internalized by them.

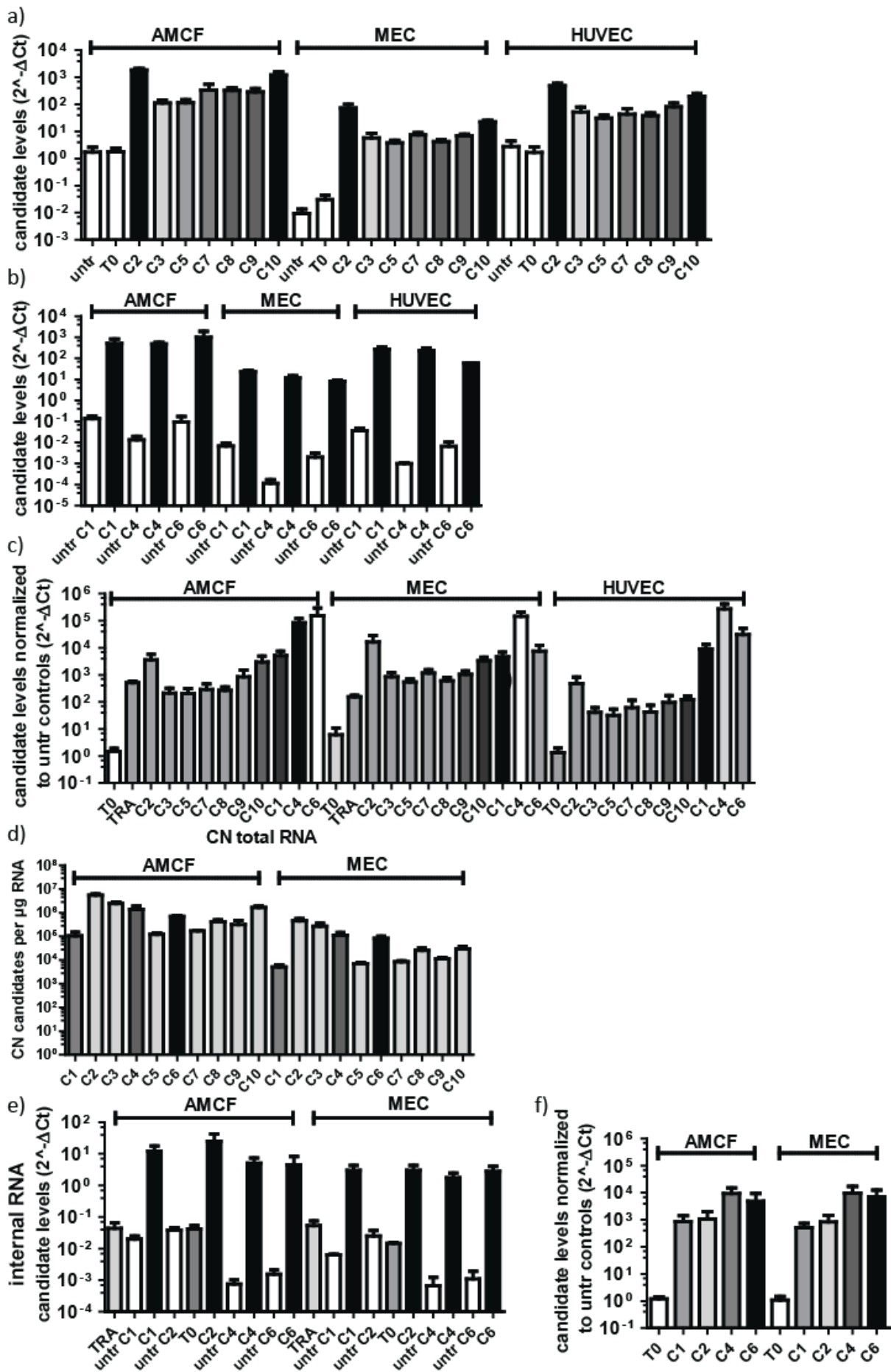


Figure 4.4.4 Candidates attach and internalize into AMCF and EC

a) Levels of candidate aptamers using a general qPCR primer measured in total RNA after treatment of human (HUVEC) and murine endothelial cells (MEC) or adult murine cardiac fibroblasts (AMCF) with 2 nM candidates or the initial T0 pool for 90 minutes. b) Levels of candidates 1,4 and 6 using specific qPCR primers after treatment of human and murine endothelial cells or murine fibroblasts with 2nM candidates for 90 minutes. c) The same expression levels normalized to the levels detected in untreated cells, which eliminates the differences between the primers. d) Copy numbers of the candidates measured in total RNA of the treated cell samples using a standard curve of diluted pure aptamer candidates. e) Levels of candidate aptamers 1,2,4 and 6 measured in internal RNA after treatment of murine endothelial cells (MEC) or adult murine cardiac fibroblasts (AMCF) with 2nM TRA, candidates or the initial T0 pool for 90 minutes. f) The same expression levels normalized to the levels detected in untreated cells, which eliminates the differences between the primers (TRA levels were undetectable in untr, which is why this data is missing). Expression levels were normalized to the expression of the ribosomal protein P0 (RPLP0). Data are shown as mean \pm SEM, n=3-6 for all graphs.

5. Discussion

Some of the findings have been discussed before in less detail in ³⁸⁹. Sections which contain a degree of overlap with the previous work will be marked in the headings.

Our work firmly establishes the feasibility of using aptamers to transport functional oligonucleotides into cells of the vasculature. We were able to show that the transferrin receptor aptamer can be used to shuttle precursor microRNA constructs attached via a sticky bridge structure not only into human and murine endothelial cells, but also into human breast cancer cells and primary adult murine cardiac fibroblasts. We showed an increase in the expression levels of two different microRNAs shuttled into cells in this way and were able to confirm functional biological effects for one of the constructs, chimera 3, in three cell lines. We were also able to select aptamers which can bind to target healthy cells of the cardiovascular system, specifically adult murine cardiac fibroblasts, although regrettably these aptamers proved to be non-specific and also bind to endothelial cells. However, we were unable to reproduce reprogramming of murine embryonic fibroblasts and adult murine cardiac fibroblasts into induced cardiomyocytes using a cocktail of the four microRNAs miR-1a, 133a, 208a and 499 ^{119,319}.

5.1 Candidate aptamers internalize into all cell types tested ³⁸⁹

We found that both of the candidate aptamers (TRA and GIRM) we chose to analyze for their ability to be internalized into cells of the cardiovascular system were able to attach with apparent ease into all cells we tested (Figure 4.1.1). The levels of both constructs detectable in the RNA of cells after digestion with trypsin and Riboshredder also shows that both TRA and GIRM can efficiently internalize into EC and fibroblasts (Figure 4.1.1) It could be argued that qPCR is an insufficient proof of uptake of the oligonucleotide constructs due to the possibility of false positive detection. In order to exclude this possibility the CA was included to address the possible lack of specificity of primers for GIRM and TRA. Indeed, after treatment with CA no levels of TRA or GIRM were detectable in HUVEC, MEC or MEF (Figure 4.1.1). Furthermore, we were able to observe fluorescently labeled TRA and GIRM in microscopic pictures of MEC and MEF (Figure 4.1.2). We are therefore convinced that both TRA and GIRM are internalized into all cell types we tested.

5.1.1 Method of GIRM internalization

For GIRM, the internalization is not surprising as it was shown to internalize, via endocytosis, into several murine and human cell lines³⁵¹. GIRM was originally selected for binding to the human LnCAP carcinoma cell line. In the same study, an internalizing oligonucleotide was selected for human HeLa cells, called otter. GIRM and otter showed remarkably similar sequences and were predicted to form a similar secondary structure. Also, GIRM and otter competed for binding in human Jurkat cells. It seems that GIRM and otter bind to a yet unknown target in both murine and human cell lines to initiate endocytosis. This cellular uptake of GIRM was also shown to be possible in the vaginal mucosa of mice and in human primary lung epithelial cells³⁵¹.

5.1.2 TRA internalization and possible mechanism

TRA was originally selected in a SELEX for its ability to bind a recombinant human transferrin receptor molecule and subsequently to human HeLa cells, which express a high amount of the transferrin receptor³⁵⁹. Surprisingly, we found that TRA attaches to MEC and MEF as well as HUVEC, as can be appreciated from TRA detectable in total cell RNA (Figure 4.1.1c+f). TRA can also be found in the iRNA of all three cell types (Figure 4.1.1d+g), indicating an internalization of the construct regardless of the species from whom the cells are derived. It was reported that TRA acts agonistic on TrfRc and competes with human transferrin³⁵⁹. A likely explanation for the observed internalization would be that the binding motif of TRA to TrfRc is evolutionary conserved; this allows binding and internalization of TRA to the murine TrfRc of MEC and MEF. Considering the origin of TRA one might expect a better binding to the original target, which is the human, not the murine TrfRc. Notably however, there were no significant differences visible for the attachment levels of TRA in human and murine cells (Figure 4.1.1e) but after 24 h the internalization of TRA was significantly higher in murine cells (Figure 4.1.1h). The uptake of TRA is dependent on ATP³⁵⁹ and we have been able to show that it co-localizes with markers for early endosomes (Figure 4.1.3a) and lysosomes (Figure 4.1.3b). Together this strongly indicates an endosomal uptake of TRA. Likely TRA acts like transferrin on TrfRc; both lead to endocytosis and subsequent recycling of TrfRc to the membrane (Figure 5.3)^{359,402}. As GIRM is also internalized via endocytosis, similar internalization ratios when comparing HUVEC and murine cells as for TRA would be expected. Indeed, GIRM also trends to be internalized more efficiently into murine than human cells after 24 h after treatment, although not to a statistically significant degree

(Figure 4.1.1n). The similarities in the uptake of TRA and GIRM are most likely caused by their similar method of internalization (Figure 4.1.1c-n).

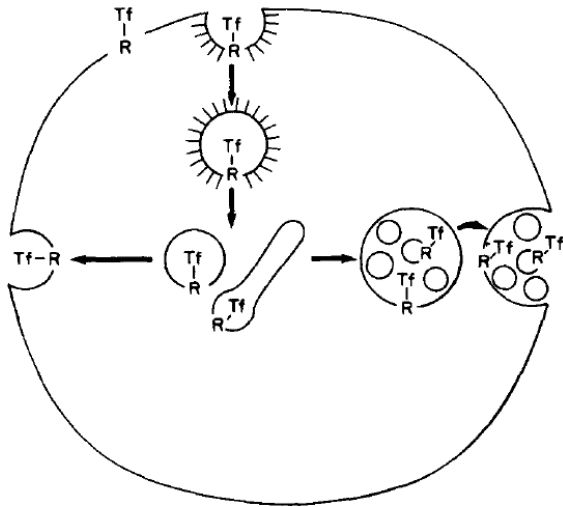


Figure 5.3 Possible routes of transferrin processing in reticulocytes.

Transferrin is internalized via coated pits and vesicles. It rapidly appears inside small vesicles and tubules in the reticulocyte cytoplasm; subsequently it is transferred to multivesicular endosome. Recycling appears to occur from the endosome, but transferrin may also recycle directly from small vesicles or tubules to the cell surface. Image from ⁴⁰².

5.1.3 Choosing TRA for further experiments ³⁸⁹

We ultimately chose TRA as a candidate to create chimeras for miR-transport over GIRM.

Judging from the initial experiments, we anticipated that both TRA and GIRM would be able to deliver functional miRs into their target cells. As stated in 4.1.2, TRA was chosen mainly because its target is well known, whereas the molecular target of GIRM is unknown. In case of unexpected side-effects, the relatively well researched functions of transferrin would allow us to draw conclusions for chimeras containing TRA, but not GIRM. We were also able to validate a robust expression of TrfRc, the target of TRA, in all cell types used, as should be expected for a ubiquitously expressed receptor (Figure 4.1.4). Also, for TRA an ability to shuttle siRNA into cells via stable nucleic acid lipid particles was already established ³⁵⁹.

Because of these reasons and due to the similar performance of both constructs in our initial experiments, we chose to design chimeras using TRA.

5.2 Design and effects of Chimeras of TRA and miR-126

5.2.1 Chimera design ³⁸⁹

When using aptamers to transport siRNAs or miRs into cells, there is an abundance of design options and methods to achieve uptake and efficient knockdown of the targets ^{325–327,356,361,362}. Both TRA and miR-126 are made of RNA, which is why we decided to directly attach them to another to create chimeras of a small size. This would not only make the synthesis relatively easy, but also potentially allow for better tissue penetration *in vivo*. A major hurdle of any RNA-interference based constructs is their ability to be recognized by the cellular machinery (e.g. the RISC). Also, attachment of aptamers to the miR might potentially limit this recognition and inhibit processing partially or even completely. We therefore designed three constructs, two of which contained the mature miR-126-3p and 5p and one of which was made of the Pre-miR-126 (Figure 4.2.1). We were able to show that all parts of the chimeras were stable in DPBS for 24 h when assessed by qPCR (Figure 4.2.1g). However, apparently the primer binding is not equally efficient to all parts of the different chimeras as detectable levels differ even though the same amount of chimeras was used. Notably, levels of all 3 parts were comparatively high in Ch2. Ch1 showed good detection levels of miR-126-3p, but poor detection of TRA while Ch3 showed a markedly reduced propensity for miR-126-5p detection. Overall, the design of the chimeras seems to still allow primer binding and detection by qPCR.

5.2.2 Internalization of chimeras into HUVEC and MEC ³⁸⁹

We then proceeded to analyze the ability of the chimeras to be internalized into cells of the vasculature. Using qPCR we detected increased levels of TRA (Figure 4.2.3) and miR-126-3p and 5p (Figure 4.2.4) for HUVEC and MEC treated with all three chimeras in both total and internal RNA. Also, the stick or Pre-miR-126 do not significantly inhibit the ability of TRA to bind to HUVEC cells (Figure 4.2.2). The amount of detectable TRA varied depending on the chimera used. Attachment of constructs measured by TRA levels in total RNA were comparable in HUVEC for all chimeras, though after 1 h Ch1 showed a slightly elevated levels of binding (Figure 4.2.3a). TRA levels in HUVEC iRNA were most efficiently increased by Ch1 (Figure 4.2.3c). In MEC, Ch1 already showed less attachment measured by the levels in total RNA than the other chimeras and after 24 h there was hardly any TRA detectable in the iRNA (Figure 4.2.3d). Meanwhile Ch2 and 3 led to comparable levels of TRA in total and iRNA (Figure 4.2.3b+d). Taken together, these results indicate that TRA does not lose its ability to

bind to the transferrin receptor after annealing the mature form or precursor of miR-126 and the constructs are endocytosed as described in 5.1.2. It also shows that the internalization and attachment is probably not equally efficient for all cell types and chimeras.

5.2.3 Increase of miR levels after chimera treatment in EC ³⁸⁹

First it has to be pointed out here that the primers used for RT-qPCR cannot distinguish between processed or unprocessed chimera constructs. This can be deduced from the detectable levels of miR-126-3p and miR-126-5p when measuring the unprocessed chimeras in DPBS (Figure 4.2.1h+i). Chimeras taken up by the EC, but not processed by Dicer and/or incorporated into the RISC-complex would still be detectable by qPCR.

In HUVEC, the levels of miR-126-3p were increased in total and iRNA for all chimeras (Figure 4.2.4a+b). miR-126-5p levels were increased in total RNA for all chimeras after 1 h and for Ch2 and 3 after 24 h (Figure 4.2.4c). Interestingly, in the iRNA of HUVECs Ch2, but not Ch3 leads to significantly elevated levels of miR-126-5p after 1 h or 24 h (Figure 4.2.4d). Although this could be partially attributed to the comparably poorer ability of Ch3 to bind to the primers for miR-126-5p (Figure 4.2.1g), the detection was good enough to pick up an elevation in the total RNA. It has been reported that HUVEC cells in culture without laminar shear stress preferentially process Pre-miR-126 into the mature 3p strand ²⁷¹. Since Ch3 bears the Pre-miR, a possible explanation for the absence of increased miR-126-5p iRNA levels might be processing of Ch3 into the mature 3p strand by dicer in HUVEC due to the absence of laminar flow in culture flasks. In this case, the non-significant increase in miR-126-5p levels observed in the HUVEC iRNA is most likely be caused by trace amounts of unprocessed Ch3.

In MEC iRNA, we also observed no significant increase in miR-126-5p levels after Ch3 treatment (Figure 4.2.4h); although in this case the levels in total RNA were also not significantly increased either (Figure 4.2.4g). Furthermore, in MEC only Ch3 could induce a significant increase in miR-126-3p levels (Figure 4.2.4f). We also analyzed the actual amount of copies of miR-126-3p taken up by HUVEC and MEC (Figure 4.2.4i) to gain an insight into whether the delivery was likely to have a biological effect. Indeed, the copies of miR-126-3p that are carried into the internal RNA by Ch3 are substantial, indicating a possible functional effect of the delivery. It should be noted that for these initial experiments a higher amount

of miR-126-3p was detected in MEC than in HUVEC. However, when comparing the increase in copy number, we found no significant difference in the expression of miR-126-3p copies per ng RNA between HUVEC and MEC (Figure 4.2.4i).

In breast cancer cells the very low basal levels and the low copy number of miR-126-3p could be significantly increased by Ch3, as was expected (Figure 4.2.7a+c). In these cells Ch3 seemed not to be preferentially processed into the 3p over the 5p mature strand as the levels of miR-126-5p likewise increased dramatically (Figure 4.2.7b). This indicates that in the two EC cells used the absence of laminar flow might have indeed influence the processing of the Pre-miR-126 part of Ch3 towards a mature 3p instead of 5p strand. Although a preference for 3p to 5p was apparent for Ch3 in the EC, it is not clear whether Ch1 or 2 are also processed or incorporated into the RISC. Even for Ch3 processing the proof is indirect, which necessitated functional analysis of the chimeric constructs.

5.2.4 Functional effects of the chimeras in HUVEC ³⁸⁹

One role of miR-126-3p is the regulation of inflammation via targeting VCAM-1 on protein, but not mRNA level ²⁴⁶. We were able to show that not only conventional miR-126-3p mimics but also Ch3 reduce Tnf- α induced VCAM-1 protein expression by roughly 50% (Figure 4.2.5a). Ch1 and Ch2 treatment however had no effect on VCAM-1 protein levels. Another effect of miR-126-3p is enhancement of VEGF signaling (Figure 1.3.3.1) ²⁶⁸. Consequently, we found that miR-126-3p overexpression through conventional mimics does not increase basal sprouting of HUVEC (Figure 4.2.6a), but increases VEGF-mediated increases in HUVEC sprouting length (Figure 4.2.6b). Ch3 also significantly enhanced the VEGF-induced increase in sprouting while Ch1 and 2 had no effect. It should be noted that the miR-126-3p mimic shows a more pronounced effect on VEGF signaling than Ch3, which most likely can be attributed to the higher extent of miR-126-3p overexpression induced by the miR-126-3p mimics (Figure 4.2.5b). While for the suppression of VCAM-1 the overexpression of Ch3 seems to suffice to reach a similar effect as the conventional miR-126-3p mimic, the induction of sprouting is apparently more dependent on the degree of overexpression.

Neither Ch1 nor Ch2 have a significant effect on the expression of VCAM-1 and the VEGF induced sprouting although both chimeras competently raised the levels of miR-126-3p measured by qPCR. The likeliest explanation for the apparent dysfunction of Ch1 and 2 is an inability of the cell to incorporate the mature miR from the chimeras into the RISC. We

initially hypothesized that TRA and the mature miR strands would detach during the uptake in the endosomes. If the chimeras remain whole however, the TRA might prevent recognition of miR-126 by the RISC or dicer through steric hindrance. As both strands of miR-126 are annealed to another in Ch1 and 2, without further processing the strands might remain attached inside the cell, preventing their binding to any target mRNA. Ch3 on the other hand seems to be recognized and processed by dicer into functional forms, probably due to the two nucleotide overhang at the 3' end and the stem loop structure, which were designed to resemble endogenous Pre-miRs^{123,124,144,145}. This implies that the synthetic pre-miR-126 incorporated in Ch3 is probably processed like endogenous pre-miR-126. This processing, which as outlined before is preferential towards the 3p strand in EC in culture without laminar shear stress²⁷¹, results in mature strands which can be incorporated into the RISC and subsequently bind to and inhibit the transcription of their target mRNAs (Figure 5.2.4). We concluded that Ch1 and 2 are not recognized by the RNAi machinery of cells after treatment and can therefore not enact any functional effects. Ch3 on the other hand is recognized and processed correctly in EC and thus shows effects similar to miR-126-3p overexpression by traditional mimics. We therefore decided to only analyze Ch3 in other cell types to determine whether the chimera's functionality is limited to EC.

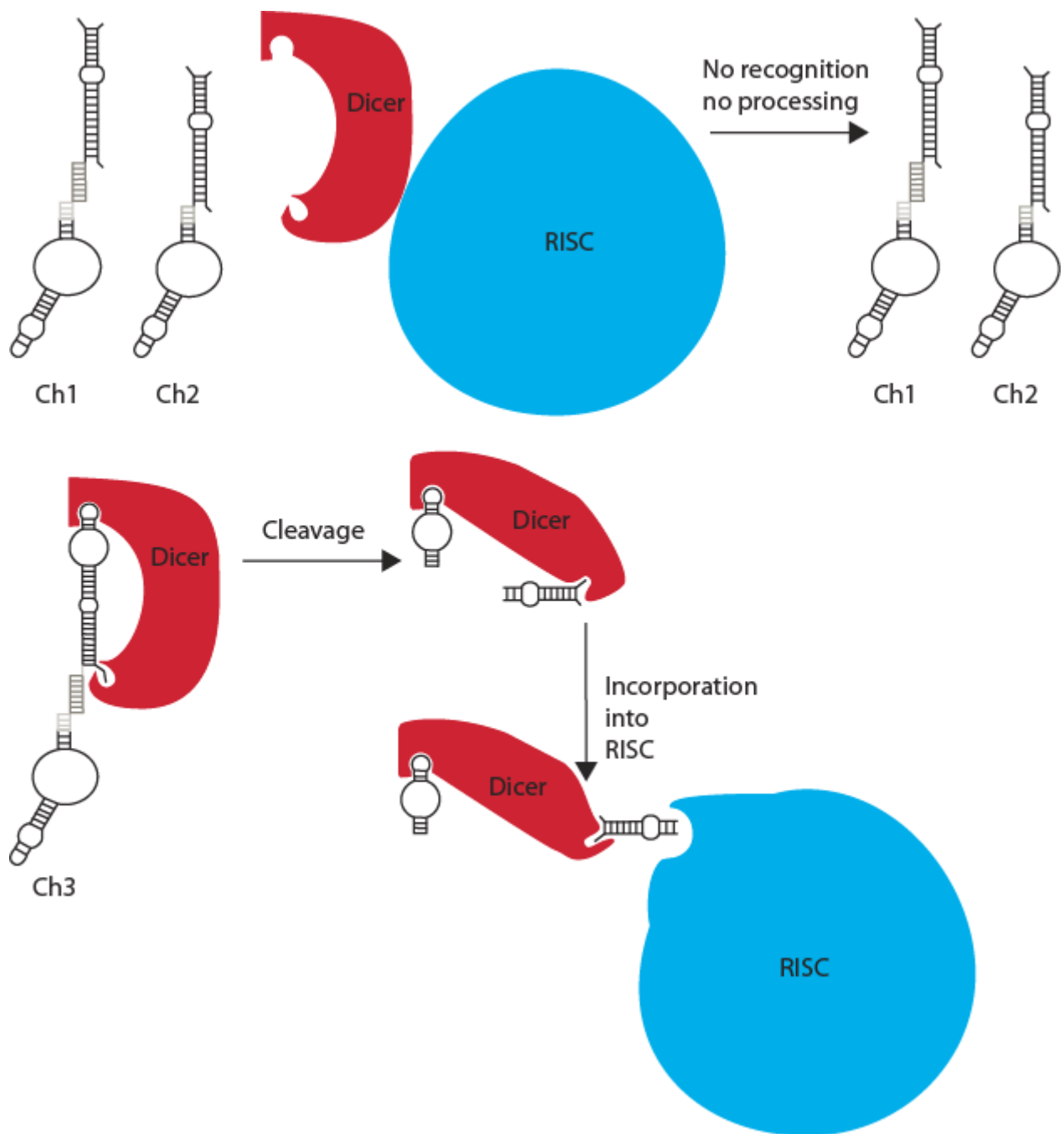


Figure 5.2.4 Proposed model for the processing of chimeras in cells

This tentative model is primarily based on the canonical processing of Pre-miRs in mammalian cells (see 1.3.1). Due to their lack of functional effects it appears that Ch1 and Ch2 are not recognized by dicer or the RNA-induced silencing complex (RISC). Ch3 on the other hand is probably processed similarly to endogenous Pre-miR-126. It is possibly first cleaved by dicer into the mature miR-126 and then incorporated into the RISC. In EC, shear stress preferentially leads to the use of miR-126-3p as the active strand (not shown).

5.2.5 Ch3 in breast cancer cell lines ³⁸⁹

For breast cancer cells it has been reported that reconstitution of miR-126-3p expression reduces the growth of the cells ^{253,297} and miR-126-3p overexpression reduces the

recruitment of EC to the tumor^{258,403}. We therefore decided to analyze the effects of Ch3 on two breast cancer cell lines. It should be noted that in breast cancer cells, Ch3 actually leads to a slightly larger overexpression than the conventional miR-126-3p mimics (Figure 4.2.7a).

5.2.5.1 Ch3 in SK-BR3 breast cancer cells

It has been reported before, that in the SK-BR3 cell line knockdown of miR-126-3p increases the recruitment of HUVECs in an *in vitro* assay comparable to the one we used²⁵⁸. Effects of miR-126-3p overexpression were not reported for this cell line and indeed, we found no effect of treatment with Ch3 or miR-126-3p mimics on the recruitment of HUVEC (Figure 4.2.9a). One explanation for this would be that the levels of miR-126-3p, although low (Figure 4.2.7a), are sufficient to inhibit HUVEC recruitment in untreated SK-BR3 cells. In this case, overexpression would have little influence while a knockdown would prevent the inhibition of recruitment via miR-126-3p and consequently increase HUVEC recruitment as reported previously²⁵⁸. However, overexpression of miR-126-3p was able to reduce the levels of its target mRNA SPRED-1, albeit not to statistically significant amount (Figure 4.2.7d). Also, both miR-126-3p mimics and Ch3 significantly reduced the viability of the SK-BR3 cells (Figure 4.2.8a). Together these data indicate that both Ch3 and miR-126-3p mimics are able to raise miR-126-3p levels to enact functional effects in SK-BR3 cells, but that the recruitment of HUVECs is not influenced by this overexpression.

5.2.5.2 Ch3 in MCF7 breast cancer cells

In the other cancer cell line we tested, the MCF7 breast cancer cell line, miR-126-3p mimic and Ch3 reduce the recruitment of HUVEC cells *in vitro* to a similar extent (Figure 4.2.9b). This has been described to be mediated mainly by a reduction in the secretion of cytokines to attract EC²⁵⁸. For MCF7, an overexpression of miR-126-3p, but not 5p was described to significantly reduce cell viability²⁵³. This was attributed to inhibition of Insulin receptor substrate 1 (IRS-1) translation and subsequent reduction in PIK3/Akt (Protein kinase B) signaling^{253,303}. We found no effect of mimic-based miR-126-3p overexpression on the viability of MCF7 cells (Figure 4.2.8b). Treatment of cells with miR-126-5p mimic, TRA or Ch3 on the other hand increased the viability of MCF7 cells in our hands (Figure 4.5.2b). It has been shown that extracellular transferrin can increase the proliferation of human breast cancer cells⁴⁰⁴ and antibody mediated blocking of TrfRc has the expected opposite effect⁴⁰⁵. Since TRA is competing with transferrin for binding and leads to the internalization of TrfRc (Figure 4.1.1-3)³⁵⁹, it can be surmised that it probably also mimics the other effects of

transferrin binding to TrfRc. This in turn would indicate an increase in proliferation and consequently viability of MCF7 cells, which is what we could observe. The results of miR-126-3p and 5p overexpression are more difficult to explain, since we not only observed the opposite effect that was described before, but also for the supposedly inactive strand²⁵³. In their publication, Zhang et al deduce the inactivity of the 5p strand from experiments done in Hek293 cells, which might behave differently from the MCF7 cell line. The reduced viability and inhibition of IRS-1 on protein level they observe in MCF7 cells are achieved by using a plasmid vector containing the Pre-miR-126 to generate overexpression, so it is not possible to determine which strand is responsible. Furthermore, overexpression of Pre-miR-126 is driven by a cytomegalovirus (CMV) promoter, which induces a very strong expression of its target. Since there is no data on the levels of miR-126-3p or 5p after treatment or description of vector dosage, the overexpression is probably larger than the overexpression we have achieved using Ch3 or mimics (Figure 4.2.7a-c). It has been reported that a high dose of vector containing shRNA driven by the U6 promoter can be lethal in murine hepatocytes independent of the specific shRNA sequence. This induction of cell death was attributed to an overload of the RNAi machinery, specifically exportin 5⁴⁰⁶. A possible explanation for the lethality observed in MCF7 cells treated with the CMV driven Pre-miR-126 vector would be a similar overload of the RNAi machinery. Since the negative control vector they use does not contain a recognizable miR sequence, it would not induce this RNAi-overload. As CMV was reported to lead to a very strong expression of its target in mammalian tumor cells⁴⁰⁷ and it was found that hybrid CMV promoters can outperform U6 in MCF7 cells^{408,409}, this explanation seems likely. The apoptosis attributed to a specific effect of miR-126 is therefore likely caused by unspecific RNAi overload. In Hek297 cells the authors show that miR-126-3p mimics reduce viability and proliferation, which led to the conclusion that it also mediates the apoptosis in MCF7 cells. However, the authors failed to analyze the miR-126-3p mimic's effects on MCF7 cells. Our contradictory results were caused by mimics specific for both strands at concentrations which resulted in levels of overexpression unlikely to cause an overload of the RNAi machinery (Figure 4.2.8a). This can be judged from the level of copy numbers reached in breast cancer cells after treatment (Figure 4.2.7c), which were still lower than those measured in untreated EC (Figure 4.2.4i). Also, if such an overload would take place both mimics would have the same effect, a reduction of viability, which was not the case. It should also be noted that neither the

mimics nor Ch3 require involvement of exportin 5 for their processing since they are present in the cytosol after internalization while vector based Pre-miR-126 has to be exported from the nucleus. We therefore propose that miR-126-3p actually has no effect on MCF7 cell viability while miR-126-5p increases viability, though whether this is by inducing proliferation or reducing apoptosis is not clear. Ch3 also increased the viability of MCF7 cells, which is probably mediated by both effects of the transferrin mimicry by TRA and the effects of miR-126-5p processed from the Pre-miR-126 sequence of Ch3. As we have not compared the increase of miR-126-5p caused by mimics to the overexpression induced by Ch3, it is difficult to judge how much of the viability increase is caused by either mechanism. It should also be noted that lipofection generally reduces cell viability^{410–412}, so a direct comparison between miR-126-5p mimic and Ch3 is difficult. Due to this, we have expressed the viability as percentage of corresponding control conditions. Ch3 induces a larger increase in viability as TRA however, which implies that its effects are at least partially mediated by miR-126-5p.

5.2.6 A chimera of TRA and miR-1³⁸⁹

We then designed a chimera of TRA and Pre-miR-1 to establish whether the design approach would be transferrable to miRs other than Pre-miR-126. Pre-miR-1 was chosen as a candidate due to its described ability to reprogram neonatal cardiac fibroblasts into CM³¹⁹. Indeed, we were able to show internalization of Ch4 into AMCF and saw an increase in miR-1-3p levels in qPCR analysis (Figure 4.3.3c+d). This suggests that attaching other Pre-miRs to TRA using a sticky bridge structure does not prevent binding and internalization of the chimera.

5.2.7 Implications for therapy and experimental work³⁸⁹

Taken together, the data on the chimeras suggests that Ch3 is recognized by the RNAi machinery of the cell and be processed by it. Because of this, Ch3 can cause the same effect as miR-126-3p and 5p overexpression using conventional mimics. Ch1 and 2 can competently enter the cells judged by the qPCR results. However, they do not influence the behavior of HUVEC, so it can be concluded that they are not recognized by the RNAi machinery as mature miRs, probably due to the attached TRA. For Ch4 we have also shown an uptake into cells, but as there are no well-established assays available to analyze the effects of miR-1a in fibroblasts we cannot eliminate the possibility that Ch4 is not recognized by the RNAi

machinery yet. Nevertheless, it appears likely that the chimera design can be adapted to incorporate other Pre-miRs than Pre-miR-126.

As stated before, target specific delivery of miRs is a promising emerging option for the therapy of numerous disorders^{88,326,356,413}. Our experiments show that it is not only possible to use aptamers to shuttle Pre-miRs into healthy cells of the cardiovascular system as well as breast cancer cells, but that the Pre-miR can be processed into functional mature miRs by the cells. We also show that the processing of the Chimera in endothelial cells is comparable to the processing of endogenous Pre-miR-126, at least in HUVEC cultured without laminar shear stress. This has to be considered when applying similar constructs for therapy, as the opposing strands of miRs often show different functions, as can be observed by the effect of miR-126-3p and 5p on MCF7 cells (Figure 4.2.8b and 4.2.9b). On the other hand, EC cleave Pre-miR-126 according to the level of shear stress they experience, so treatment with aptamers carrying Pre-miR-126 could positively influence EC both in the context of ischemia and atherosclerosis^{271,277,283}.

Since the design can be adapted to incorporate other Pre-miRs, it seems reasonable to assume that other aptamers than TRA would also be possible, provided the attached Pre-miR does not inhibit aptamer-target interactions. The adaptable chimera design could therefore also be used for specific delivery of possible every miR of interest. A possible example would be the use of an aptamer to HER2, overexpressed on many breast cancer cells,³⁵² and miR-126 for the treatment of breast cancer^{222,258,297}.

However, even if the design should prove to be unfeasible when applied to other aptamers, the TRA-based chimeras still have value outside of a proof-of-principle. Since the target of TRA is ubiquitously expressed by mammalian cells, the chimera design can be used to shuttle miRs into any cell type. While this is not an attractive approach for therapy due to the high chance of off-target effects of any such treatment, it might prove useful for research applications. Many cells are difficult to transfect with miR-mimics due to a high cytotoxicity of lipofection or electroporation in the specific cell type used⁴¹⁰⁻⁴¹². We have not observed effect on cell viability or change in phenotype upon treatment with the chimeras, which might make them a useful tool to achieve overexpression of miRs in cell types susceptible to transfection induced cytotoxicity, for example primary cells of the hematopoietic system. The chimeras might also be useful to treat cells which, while normally not susceptible to

transfection induced cytotoxicity, have to undergo other stressful treatments as part of more elaborate assays, for example live cell sorting.

5.3 Inefficient reprogramming of AMCF using a microRNA cocktail

We observed no significant changes in the proposed markers for reprogramming of CF to CM when we treated AMCF with a cocktail of miR-1a, 133a, 208a and 499 (Figure 4.3.4). It has been reported that this cocktail of miRs could efficiently lead to the reprogramming of neonatal murine CF to an iCM phenotype, although a cocktail using only miR-1a, 133a and 208a was almost equally effective and even treatment with only miR-1a was able to turn a small number of CF into an iCM phenotype³¹⁹. We tried to adapt the protocol in various ways to initiate the induction of CM markers. Changing the medium used had no significant impact on mRNA expressions. We also initiated co-treatment with JAK-inhibitor 1 and BMP4 to induce a change from CF to CM mRNA expression in the cells, but this also failed to produce the expected effects (Figure 4.3.4i+j).

It could be argued that we did not analyze all the markers mentioned by Jayawardena et al, but we did measure the levels of GATA4 and vimentin, which were described to be the earliest markers to show differences in expression. We also extended the incubation time for some of the experiments to ensure that we did not miss a later change in expression levels. There are several possible explanations for our failure to induce reprogramming.

5.3.1 Differences in cell types used for reprogramming

A possible problem with the replication of results would be use of improper cells or impurities in the cell pool used for reprogramming. We adapted two methods to isolate AMCF from the hearts of C57BL/6 mice to reliably produce viable primary fibroblasts. In our hands, the Langendorff-Perfusion³⁹⁰ method for the isolation of AMCF was able to isolate a higher number of cells more quickly than the extravasation method^{95,414}, but at the cost of a very high variance in yield. Both methods have been shown to isolate viable AMCF with purity sufficient to use for experimentation (~90%)^{95,390,414}. The major caveat would of course be the presence of mature cardiomyocytes in the AMCF culture. However, cardiomyocytes are prone to die during isolation and culture⁴¹⁵ and they do not spontaneously migrate out of tissue slices. It is therefore highly unlikely that the extravasation method yields any viable CM which could confuse reprogramming results later on. While the Langendorff perfusion method can be used to isolate viable CM for culture³⁹⁰

they are separated from other cells of the heart by centrifugation at low g-force, omitting them from our cell pool. We have addressed the purity with qPCR as well as light and fluorescent microscopy (Figure 4.3.1). In qPCR of AMCF RNA we saw levels of Myh6 and Myl2 mRNA barely above water controls (Figure 4.3.1c). During morphological analysis no spontaneous contractions characteristic for CM or cells having a CM-like morphology were observed (Figure 4.3.1a). The cells also showed a high expression of the fibroblast markers vimentin and fibroblast-specific-protein 1 (Figure 4.3.1e+f). Together, these results indicate that the isolated AMCF are of sufficient purity for the reprogramming experiments.

However, Jayawardena et al isolated CF from neonatal mice while we have isolated CF from adult specimen. It should be noted that Muraoka et al were also unable to induce reprogramming in murine embryonic fibroblasts using the miR-cocktail¹⁰³. It has been well described that neonatal mice hearts show a remarkable ability to regenerate after injury⁴⁷. It is likely that this regeneration is at least partially mediated by CF, so it is likely that CF show an increased plasticity in neonatal compared to adult mice. CF and CM share common progenitors⁴¹⁶, so shortly after birth the CF might be closer to a CM-progenitor state, enabling reprogramming when exposed to the miR-cocktail composed of mostly (cardio-) muscular miRs. This would also explain the inability to use the cocktail to induce an iCM phenotype in MEF, which are more distant in lineage to CM. Possibly, the mature AMCF are more stable in their fibroblastic phenotype and would require additional stimulation to transdifferentiate into iCM. It has been shown, that combinations of transcription factors can induce an iCM phenotype in AMCF^{95,96,101,108,417}, which may indicate that the miR-cocktail is an insufficiently strong stimulus to induce transdifferentiation *in vitro*. However, the studies by Jayawardena et al in a mouse model of AMI indicates that during cardiac ischemia, the miR-cocktail can induce a transdifferentiation of CF and enhance the recovery of the infarcted area^{119,319}. This might be due to the transdifferentiation of CF into myofibroblasts in the ischemic region^{56,57} before formation of scar tissue in the area⁵⁰. During this transdifferentiation, the fibroblasts might be more susceptible to the influences of the miR-cocktail, which then turns the transdifferentiation into MF into reprogramming into CM instead. During normal culture conditions however, it seems the miR-cocktail is unable to induce iCM in our hands

5.3.2 Possible methodological inaccuracies

Reprogramming of any cell type is usually an unstable, complex and precise procedure. In face of the rather limited space provided in the methods section of most papers, crucial information necessary to ensure a faithful reproduction of cell reprogramming data is often lost. It is possible that we simply lacked some crucial information necessary to enable us to reprogram AMCF into iCM. Even well described and robust reprogramming data sets often prove difficult to reproduce in other laboratories ¹⁰⁰.

5.3.3 Consideration for human use

It should be noted that human CF are usually more difficult to reprogram into an iCM phenotype and when transdifferentiation is induced it often appears to lead to more immature cell types than in murine CF ^{103,114,116}. Considering that even in murine fibroblasts the miR-cocktail is unable to induce an iCM phenotype if the conditions are not optimal, it seems unlikely that any significant amount of reprogramming could be induced in human fibroblasts. CF to iCM transdifferentiation using miRs is an exciting possible treatment for cardiac ischemia, but it appears clear that a substantial amount of further research and reproduction of the results by other research teams is necessary before it is possible to assess whether the approach is suitable for human use. It should be noted however, that miR-133 has been shown to also support iCM conversion in humans ¹⁰³, so even if the miR-cocktail proves to be insufficiently strong in humans, it might still prove useful to enhance reprogramming using other molecules, for example GMTMM ¹¹⁵.

5.4 Cell SELEX to select aptamers binding to AMCF

We were able to show that a cell-SELEX approach is able to select for specimen binding to primary adult cardiac fibroblasts isolated from healthy mice. Although with the initial pool of $\sim 10^{12}$ aptamers, we were unable to achieve a significant enrichment of the pool using both traditional and internalization cell SELEX ³⁵², when we applied a pool consisting of 2×10^{31} species containing a stem-loop sequence using a SELEX protocol less rigorous and not selecting for internalization, we were able to achieve a significant enrichment of the pool for species binding to AMCF and we were ultimately able to select the 10 most promising candidates after 7 rounds of SELEX.

5.4.1 Performance of the aptamer pool with 20 variable nucleotides

It is unclear why we were unable to achieve any significant enrichment of the 10^{12} aptamer pool when applying it to AMCF and using EC as the negative selector cell line. The pool has been used to successfully select aptamers binding various cells before^{339,352,373}. In these cases the cell line selected for was very closely related to the cell line used for negative selection, which might enhance the efficacy of the approach. It could be argued, that there might not be an aptamer in the pool that binds to AMCF, internalizes and does not bind to EC. However, there was little enrichment visible even when no RNase digestion was done (Figure 4.4.1a round 1-6) or no negative selection on EC was applied (Figure 4.4.1c round 1+2). This would imply that even only one of the two selection criteria was too strict to allow enrichment of the pool.

5.4.2 SELEX using an aptamer pool with 52 variable nucleotides

We then switched to using a larger pool containing 52 variable nucleotides, leading to a potential 2×10^{31} different species. It should be noted that not all possible species of the pool were used for the selection. We used 2 nanomoles, which by definition contain only a maximum of 2×10^{-9} times 6.02214×10^{23} , so 2×10^{14} different molecules, which is still 100 times more different species than for the shorter pool. Additionally, due to the increased size of the variable region, it is likely that the species differ more from another than the ones of the 10^{12} -pool. The longer sequence probably also allows folding into more complex three dimensional structures, which might increase the chance of binding to the target cells. Indeed, we were able to achieve enrichment of certain species using this larger pool. After 7 rounds of selection, we sent rounds 5-7 for sequencing. Bioinformatic analysis led us to pick the ten candidates that were most present in round 7, most highly amplified from round 5 until 7 and/or contained RNA motifs predicted by MEME Suite.

5.4.3 Evaluation of the 10 AMCF aptamer candidates

Since all 10 candidates could be detected in the total RNA of MEC, HUVEC and AMCF after treatment far above the levels detectable for treatment with an unselected pool (Figure 4.4.4). Also, all candidates we tested were able to internalize into AMCF and MEC. Judged from the levels and CN measured (Figure 4.4.4), the candidates show a higher affinity to fibroblasts than to EC. It is likely that the incubation steps on EC during the SELEX were not long enough to fish out unspecific binders. It appears that all the candidates most prevalent in the SELEX pool after round 7 can bind and internalize into AMCF, but do so to a lower

extent in EC as well. Candidate 2 shows the best binding capabilities of the selection. Because all candidates seem to bind and internalize into cells unspecifically with noticeable but not overly large differences and the secondary structures looking similar around the conserved stem loop sequence (Figure 4.4.3), it appears likely that the candidates bind to the same target. This target would presumably be expressed by fibroblasts and, to a lesser extent, EC. Since the levels measured in iRNA also appear to be higher than the levels of TRA measured after treatment using the same molarities, the candidates target is better suited for internalization than transferrin receptor or that the candidates bind with higher efficiency to their target than TRA. In either case, especially candidate 2 appears to be potentially more (cost-) efficient than TRA for the transport of miRs, although candidate 2 would first have to be researched more thoroughly. Future experiments would have to try to address the identity of its target and the strength and specificity of the interaction. This would also allow truncation of candidate 2, since most aptamers do not require their full length to interact with their targets^{326,327,368}. The potential cytotoxicity of candidate 2 at higher concentrations as well as its toxicity in living animals would have to be tested. Another issue that we have only addressed on the surface so far is the stability of candidate 2. While after 90 minutes it is still stable inside the cells, its stability in plasma would have to be examined as would its general resistance to RNase and the rate of its (renal) clearance *in vivo*. It would also have to be established, whether candidate 2 can be attached to Pre-miRs without impairing their processing by dicer and incorporation into the RISC.

Ultimately, we were unable to fish out non-specific binders from the pool during the SELEX. In hindsight, it might have been prudent to more strictly exclude these during the procedure. It might have helped to elongate the incubation on the EC to 90 minutes, use a larger number of cells for the counterselection, run two counterselection steps or include more competitor RNA during the selection. These steps would ideally have to be included relatively early during the SELEX to prevent the apparent rapid and efficient enrichment of non-specific binders we have observed in our sequencing results or rounds 5 to 7. It appears likely though, that it is theoretically possible to select specific aptamers using an adapted cell SELEX protocol. While we have focused on the cardiovascular system, such a selection would be therapeutically interesting for all tissues containing homogenous cell populations in which one particular cell type is to be targeted, for example glial cells in the brain.

6. Conclusion and Outlook

Taken together, our data shows that transport of functional miRs into cells of the cardiovascular system is feasible and that it is possible to select aptamers for this purpose. Although we have failed to isolate aptamers which are cell-specific, the candidates identified by the cell SELEX showed promising levels in both the total and internal RNA of the cells treated, indicating their potential suitability for miR transport. Although we have not been successful in achieving miR-mediated reprogramming of AMCF into iCM, there is a myriad of other applications for miRs in the cardiovascular system. An example would be the use of miR-1, which we have shown to be efficiently shuttled by TRA, to alleviate atrial fibrillations¹⁹⁶. Another possibility would be the use of miR-145 to alleviate atherosclerosis^{197–200}. The therapeutic possibilities of miR-126 have already been discussed (see 5.2.7).

While there are inhibitors for miRs already in clinical trials^{168,170,208,418,419}, the difficulties of delivering functional miR mimics *in vivo* have prevented the advent of miR-mimetics as therapeutics so far. This has also greatly influenced the research of the physiological effects of miRs as groups working on translational research have been focusing on miRs which have therapeutically relevant effects upon inhibition rather than overexpression. However, as can be judged from our results of miR-126 overexpression (see 4.2, 5.2), increasing miR levels can have dramatic effects on the behavior of cells. While this focus on inhibition has been born of technical limitations and is understandable, it sells miRs short. In many pathological states an upregulation of some and downregulation of other miRs has been reported, which indicates an interplay between various miRs in the pathogenesis^{193–196,212}. It stands to reason that ideally a therapeutic intervention would also use both the venues of up- and downregulation to initiate recovery of the healthy state. Therefore upregulation of miRs is a very promising therapeutic option as of now and more research into the role of miRs in the human body will only increase the potential applications. Although there are many other options for miR transport, aptamer chimeras appear to be among the most promising delivery agents so far, both based on the data present in this thesis and prior research^{360,362}. The TRA-miR-126 chimeras presented in this thesis are relatively easy to adapt to incorporate other miRs (e.g. miR-1) and probably also other aptamers. While they use 2'-F modified nucleotides, recent advances have shown that incorporating LNA might be more useful for *in vivo* applications^{326,346,367,420,421}. Regardless of the specific modifications, such chimeras would be comparatively cheap to synthesize on a large scale (although small scale

synthesis for experimental purposes is costly). Aptamers (including TRA) are usually non-toxicity and non-immunogenic (see 1.3)^{326,359} and so the chimeras are most likely also safe to use. One of the big selling points of aptamers is their ability to deliver targets specifically, which is of enormous usefulness for example when targeting cancer and omitting side effects on surrounding cells³⁶⁰.

Although we were unable to select aptamers specifically targeting AMCF, we were able to isolate candidates showing a strong ability to bind to and internalize into all cells. This indicates that the approach in general can be used to identify specific aptamers, although the protocol has to be adapted to exclude non-specific binders more effectively. While the aptamer research field has grown in recent years, it is still relatively small and many publications focus on optimization or modification of existing aptamers. So far, there have been very few publications aiming to specifically target non-tumorous cells for therapeutic purposes, although according to our data this seems to be a feasible approach. It should be noted that aptamers can of course be used to facilitate transport of all kinds of therapeutics, not only miRs or siRNA. While smaller molecules can be directly attached to the aptamers, nanoparticles coated with aptamers allow transport of larger molecules or mixtures of different therapeutics^{326,422}. This makes aptamers useful in basically every situation that would warrant a target (cell) specific treatment. Due to their high binding abilities aptamers are often also retained at their target site, so even if a specific delivery in the target tissue is not necessary, it might still be beneficial to use aptamers to increase local retention. Increased research to identify aptamers for therapeutic applications would appear to be a promising venue and it should be hoped that more groups focus their efforts in this direction.

7. Zusammenfassung

Erklärung: Teile dieser Doktorarbeit wurden bereits in (Rohde, J.-H., Weigand, J. E., Suess, B. & Dimmeler, S. A Universal Aptamer Chimera for the Delivery of Functional microRNA-126. Nucleic Acid Ther. 25, 141–51, 2015) veröffentlicht.

Aptamer-medierter zellspezifischer Transport von microRNA in Zellen des kardiovaskulären Systems

Ischämische Erkrankungen des Herz-Kreislaufsystems sind noch immer die häufigste Todesursache in Deutschland und weiten Teilen der westlichen Welt ²². Akuter Myokardinfarkt (AMI) ist eine der am weitesten verbreiteten ischämischen Erkrankungen des Herzens und geht meist mit einem erheblichen Verlust der Kontraktionsfähigkeit des Herzens einher. Die ischämisch bedingte Unterversorgung der Herzmuskelzellen, sogenannte Kardiomyozyten (KM), mit Sauer- und Nährstoffen führt ihrem Tod. Während dieser Verlust in Zebrafischen und neugeborenen Nagetieren komplett regeneriert werden kann ⁴⁷, führt er in erwachsenen Säugetieren zur Bildung von Narbengewebe im Herzen ⁵⁰. Das Narbengewebe kann allerdings nicht kontrahieren, daher müssen die verbleibenden Herzmuskeln stärker und/oder schneller kontrahieren um dieselbe Herzfunktion wie zuvor zu gewährleisten. Dieser erhöhte Stress prädisponiert das Herz für weiteren Schaden, verringert die Lebensqualität der Betroffenen und führt letztendlich oft zum Tode. Daher wäre eine Beeinflussung der Wundheilung, um die Funktion des Herzens aufrecht zu erhalten, ein vielversprechender Therapieansatz.

In den letzten Jahren wurde mit verschiedenen Methoden eine Transdifferenzierung von kardialen Fibroblasten zu Kardiomyozyten *in vitro* hervorgerufen. Einige dieser Methoden wurden auch in Mausmodellen von AMI getestet und führten zu einer verbesserten Wundheilung. Eine dieser Methoden benutzt einen Cocktail aus vier microRNAs (miRs), miR-1a, 133a, 208a und 499, um die Reprogrammierung hervorzurufen ^{119,319}. Bei miRs handelt es sich um endogene RNA-Stränge mit einer Länge von 22 Nukleotiden, welche durch komplementäre Basenpaarung an Messenger-RNA (mRNA) binden und deren Translation in Eiweiße verhindern können. Eine miR kann hunderte mRNAs beeinflussen und so Differenzierung und die meisten anderen Verhaltensweisen einer Zelle drastisch verändern. In der Zelle werden miRs im Zellkern als primäre miRs hergestellt, zu Precursor-miRs (Pre-miRs) prozessiert und dann ins Zellplasma transportiert. Im Zellplasma werden die

Pre-miRs dann zu maturen miRs prozessiert und in den RNA-induced silencing complex (RISC) integriert, in welchem sie nun ihre Ziel-mRNA binden und inhibieren können¹⁴⁶. Die meisten miRs besitzen zwei verschiedene mature Sequenzen genannt 3p und 5p, welche unterschiedliche Ziele haben können. Abhängig vom Zelltyp und Umgebungsfaktoren wird die Pre-miR meist preferentiell zu einer der beiden maturen miRs prozessiert. Auf Grund ihrer großen Anzahl Ziel-mRNAs sind miRs ein interessanter Ansatz für die Therapie von zahlreichen Erkrankungen. Da miRs allerdings verschiedene Effekte in verschiedenen Zelltypen haben, besteht die Gefahr von ernsthaften Nebenwirkungen. Diese könnten durch einen zielspezifischen Transport von miRs, z.B. durch die Verwendung von Aptameren, verhindert werden. Aptamere sind meist kurze DNA- oder RNA-Oligonukleotide welche sich zu spezifischen 3-dimensionalen Strukturen falten. Dadurch können sie durch räumliche Anziehung an Zielmoleküle binden. Aptamere werden gewöhnlich mittels systematischer Evolution von Liganden durch exponentielle Anreicherung (SELEX) aus einem großen Pool von Oligonukleotiden für ihre Fähigkeit an die Zielmoleküle zu binden selektiert. Aptamere wurden beispielsweise genutzt um in Mäusen miRs in Krebszellen zu transportieren ohne dass diese in gesunde Zellen gelangen^{326,360,361}.

Das Ziel dieser Doktorarbeit war die Verwendung von miRs und Aptameren um kardiale Fibroblasten zu Kardiomyozyten zu reprogrammieren. Dies beinhaltet drei Teilziele: der Transport von miRs mit Aptameren in Zellen des kardiovaskulären Systems, die Reprogrammierung von kardialen Fibroblasten zu Kardiomyozyten und die Selektion von Aptameren, welche spezifisch an kardiale Fibroblasten binden.

Aptamere können miRs in kardiovaskulären Zellen transportieren

Bisher wurden keine Aptamere beschrieben, welche spezifisch an gesunde Zellen aus dem kardiovaskulären System binden. Daher wurden zwei Oligonukleotide, welche als universal bindend beschrieben wurden, auf ihre Fähigkeit an Endothelzellen (EZ) und kardiale Fibroblasten zu binden und in zu internalisieren untersucht. Sowohl das Aptamer für den ubiquitär exprämierten Transferrin Rezeptor (TRA)³⁵⁹ als auch das generelle internalisierende RNA Motiv (GIRM)³⁵¹ konnten in der totalen und der intrazellulären RNA von humanen und murinen EZ sowie murinen kardialen Fibroblasten mittels quantitativer PCR (qPCR) nachgewiesen werden. Es war auch möglich fluoreszenz-markierte Versionen

von TRA und GIRM in den behandelten Zellen sichtbar zu machen. Dabei waren keine signifikanten Unterschiede zwischen TRA und GIRM ersichtlich. Da der Bindungspartner von GIRM unbekannt ist, haben wir uns entschieden für die weiteren Versuche das TRA zu benutzen. Zur Klärung der Frage, ob dieses Aptamer auch funktionelle miRs transportieren können, wurden drei verschiedene TRA-miR Chimären (Ch) entworfen und synthetisiert. Die Wahl der miR fiel hierbei zunächst auf miR-126, da diese eine gut beschriebene Rolle im vaskulären System und in Brustkrebszellen besitzt. Der Transport von miR-126 ist daher auch unabhängig von den anderen Resultaten der Doktorarbeit von therapeutischem Interesse, beispielsweise zur Behandlung von Atherosklerose oder (Brust-)Krebs. Ch1 und Ch2 beinhalten die maturen Sequenzen der miR-126, wobei im Falle von Ch2 der Aptamer und die miR mittels einer komplementären klebrigen Brückensequenz verbunden sind. Bei Ch3 wurde dieselbe Brückensequenz genutzt, allerdings wurde hier die Pre-miR-126 eingesetzt anstatt der maturen Formen. Bei der Analyse mittels qPCR konnte sowohl TRA als auch erhöhte Mengen von beiden Strängen der miR-126 in den behandelten humanen und murinen Zellen nachgewiesen werden. Auffällig hierbei war allerdings, dass Ch3 nicht zu einem langfristigen Anstieg von miR-126-5p in EZ führte. Dies kann dadurch erklärt werden, dass Pre-miR-126 in EZ in normalen Zellkulturbedingungen vorrangig zu miR-126-3p prozessiert wird²⁷¹. In einem anschließenden Test, welcher die gefäßformenden Fähigkeiten der behandelten EZ überprüft, zeigte nur Ch3 die erwartete Verstärkung der Gefäßformung unter Einfluß des Wachstumsfaktors VEGF. Auch konnte nur Ch3 die Eiweißexpression des entzündungsfördernden Eiweißes vascular cell adhesion molecule-1 in humanen EZ verringern. Damit hat Ch3 dieselben Effekte auf humane EZ wie klassische Überexpression von miR-126-3p, während weder Ch1 noch Ch2 die Funktionsweise der Zellen beeinflusst. Dies lässt darauf schließen, dass die maturen miR Sequenzen von Ch1 und 2 wahrscheinlich nicht erkannt werden, während Ch3 zu maturen miRs prozessiert und danach, wie endogene miRs, in den RISC eingebunden wird. Nachdem Ch3 also in EZ effektiv zu wirken scheint, wurde daraufhin der Effekt von Ch3 auf Brustkrebszellen untersucht um auszuschließen, dass Ch3 nur in EZ wirksam ist. In Brustkrebszellen führte eine Behandlung mit Ch3 zu einem drastischen Anstieg von miR-126-3p und -5p in den Zellen. In der SK-BR3 Brustkrebszelllinie war eine Reduktion der Viabilität nach der Behandlung mit Ch3 oder klassischen miR-126-3p Mimetika sichtbar, was mit vorherigen Publikationen übereinstimmt²⁵⁸. In einer anderen Brustkrebszelllinie hingegen war eine Steigerung der Viabilität nach der Behandlung mit Ch3,

TRA und mir-126-5p Mimetika offensichtlich. Die verbesserte Viabilität als Reaktion auf TRA ist wahrscheinlich darauf zurück zu führen, dass TRA in diesem Fall denselben Effekt hat wie der endogene Transferrin, für den eine Erhöhung der Viabilität für diverse Krebszellen bekannt ist^{404,405}. Der Effekt von miR-126-5p ist allerdings das Gegenteil von dem, der für die MCF7 Zelllinie zuvor beschrieben wurde. Bei einer Überexpression von Pre-miR-126 mittels eines viralen Vektors wurde eine Verminderung der Viabilität festgestellt²⁵³. Die wahrscheinlichste Erklärung hierfür ist, dass der virale Vektor zu einer so starken Überexpression der miR führte, dass die endogene RNA Maschinerie überlastet wurde und die Zellviabilität abnahm. Dieses Phänomen wurde bereits zuvor für vergleichbare Vektoren beschrieben⁴⁰⁶. Unsere Resultate lassen darauf schließen, dass Ch3 vergleichbare Effekte zeigt wie eine Überexpression von miR-126-3p oder 5p, abhängig vom Zelltyp und Test. Dies wiederum deutet darauf hin, dass Ch3 sowohl zu funktioneller miR-126-3p als auch miR-126-5p prozessiert werden kann. Um zu überprüfen, ob ein Transport von Pre-miRs auch für andere miRs möglich ist, wurde eine Chimäre aus TRA und miR-1a erstellt. Diese Chimäre führte bei Behandlung von murinen kardialen Fibroblasten zu einem drastischen Anstieg der Level von miR-1a-3p. Zusammen genommen deuten diese Resultate darauf hin, dass ein Transport von funktionellen miRs in Zellen des Gefäßsystems mittels Aptameren möglich ist.

Ein Cocktail aus miR-1a, 133a, 208a und 499 ist nicht ausreichend für die Reprogrammierung von adulten kardialen Fibroblasten

In kardialen Fibroblasten isoliert aus dem Herzen von neugeborenen Mäusen führt die Behandlung mit einem miR-Cocktail aus miR-1a, 133a, 208a und 499 zu einer Reprogrammierung zu einem herzmuskelzellähnlichen Phänotyp. Derselbe Cocktail verbesserte auch die Erholung der Herzfunktionen von Mäusen nach einem experimentellen Herzinfarkt. Wir behandelten kardiale Fibroblasten von erwachsenen Mäusen mit dem miR-Cocktail und kultivierten sie unter verschiedenen Zellkulturbedingungen für bis zu 21 Tagen. Es war jedoch zu keiner Zeit eine Veränderung in der Zellmorphologie und Genexpression der behandelten Fibroblasten sichtbar. Auch Inklusion diverser Wachstumsfaktoren in die Behandlung hatte nicht die gewünschte Reprogrammierung zur Folge. Daraus lässt sich schließen, dass murine kardiale Fibroblasten in der Zellkultur nicht mit den verwendeten miRs reprogrammiert werden können. Dies ist wahrscheinlich auf den höheren Differenzierungsstatus, im Vergleich zu Fibroblasten von neugeborenen Mäusen, zurück zu führen. Die publizierte Wirksamkeit des miR-Cocktails im

Falle eines Herzinfarktes in erwachsenen Mäusen könnte auf Faktoren im Infarktgebiet beruhen, welche die Fibroblasten empfindlicher für eine Reprogrammierung machen.

Auswahl von Aptameren für kardiale Fibroblasten mittels Zell-SELEX

Um einen spezifischen Transport von miRs in kardiale Fibroblasten zu ermöglichen, wurden zwei Pools aus 10^{12} und 10^{31} RNA-Aptameren mit einer variablen Sequenz von 20 oder 52 Nukleotiden für eine Zell-SELEX genutzt. Dazu wurden die Aptamer-Pools zu den Fibroblasten gegeben. Danach wurden die Aptamere, welche an den Zellen haften blieben, eluiert, aufgereinigt und amplifiziert. Dieser Prozedur wurde mehrmals wiederholt, wobei in späteren Runden die Aptamere erst auf EZ gegeben wurden um die Aptamere zu entfernen, welche an EZ binden. Für den Pool mit der kleineren variablen Sequenz war keine Anreicherung von RNA-Spezies sichtbar. Bei dem Pool mit 52 randomisierten Nukleotiden war allerdings nach wenigen Runden eine deutliche Anreicherung sichtbar, weshalb nach 5, 6 und 7 Runden der SELEX der jeweils verbleibende Pool sequenziert wurde. Die Sequenzierungsdaten wurden danach bioinformatisch nach konservierten Sequenzen durchsucht und zehn vielversprechende Kandidaten wurden synthetisiert. Diese Kandidaten wurden dann für die Behandlung von kardialen Fibroblasten und EZ benutzt. Danach waren bei allen Kandidaten signifikante Level in der totalen RNA von sowohl EZ als auch Fibroblasten detektierbar, was auf eine unspezifische Bindung hindeutet. Kandidaten 1,2,4 und 6 wurden außerdem auf ihre Fähigkeit in Zellen internalisiert zu werden untersucht. Überraschenderweise konnten alle vier Kandidaten in größeren Mengen als TRA in der internen RNA von murinen kardialen Fibroblasten und EZ detektiert werden. Dies deutet darauf hin, dass die Kandidaten effizienter als TRA in diese Zellen internalisiert werden. Allerdings sind die Kandidaten nicht spezifisch für Fibroblasten und können somit nur für unspezifischen Transport, vergleichbar mit TRA, genutzt werden. Es ist wahrscheinlich, dass das Zell-SELEX Protokoll bei einer Verschärfung der Selektionsbedingungen auch für die Selektion von spezifischen Aptameren genutzt werden kann.

Schlußfolgerung

Zusammen genommen war es möglich zu zeigen, dass Aptamere benutzt werden können um microRNAs in gesunde Zellen des kardiovaskulären Systems zu transportieren. Außerdem kann man einen Zell-SELEX Ansatz nutzen, um Aptamere zu selektieren welche unspezifisch an Zellen des kardiovaskulären Systems binden. Der Transport von miRs in Zellen des

kardiovaskulären Systems und die mögliche zukünftige Etablierung von zellspezifischen Aptameren zu diesem Zweck eröffnet vielfältige Möglichkeiten für die Behandlung von kardiovaskulären Erkrankungen, beispielsweise durch die Reduktion von Atherosklerose mittels miR-126-5p. Auf Grund der fehlenden Reprogrammierung von Fibroblasten zu herzmuskelzellähnlichen Zellen konnte der Ansatz des Aptamer basierten Transports von miRs für eine Reprogrammierung nicht weiter verfolgt werden.

8. References

1. Neil A. Campbell, Reece, J. B., Molles, M., Urry, L. A. & Heyden, R. *Campbell Biology, 7th edition*. (Benjamin Cummings, 2004).
2. Carmeliet, P. Mechanisms of angiogenesis and arteriogenesis. *Nat. Med.* **6**, 389–95 (2000).
3. Swift, M. R. & Weinstein, B. M. Arterial-venous specification during development. *Circ. Res.* **104**, 576–88 (2009).
4. Meisner, J. K. & Price, R. J. Spatial and temporal coordination of bone marrow-derived cell activity during arteriogenesis: regulation of the endogenous response and therapeutic implications. *Microcirculation* **17**, 583–99 (2010).
5. Folkman, J. & Shing, Y. Angiogenesis. *J. Biol. Chem.* **267**, 10931–4 (1992).
6. Geudens, I. & Gerhardt, H. Coordinating cell behaviour during blood vessel formation. *Development* **138**, 4569–83 (2011).
7. Carmeliet, P. Manipulating angiogenesis in medicine. *J. Intern. Med.* **255**, 538–561 (2004).
8. Potente, M., Gerhardt, H. & Carmeliet, P. Basic and therapeutic aspects of angiogenesis. *Cell* **146**, 873–87 (2011).
9. Phng, L.-K. & Gerhardt, H. Angiogenesis: a team effort coordinated by notch. *Dev. Cell* **16**, 196–208 (2009).
10. Roca, C. & Adams, R. H. Regulation of vascular morphogenesis by Notch signaling. *Genes Dev.* **21**, 2511–24 (2007).
11. Hellström, M. *et al.* Dll4 signalling through Notch1 regulates formation of tip cells during angiogenesis. *Nature* **445**, 776–80 (2007).
12. Siekmann, A. F. & Lawson, N. D. Notch signalling limits angiogenic cell behaviour in developing zebrafish arteries. *Nature* **445**, 781–4 (2007).
13. Adams, R. H. & Alitalo, K. Molecular regulation of angiogenesis and lymphangiogenesis. *Nat. Rev. Mol. Cell Biol.* **8**, 464–78 (2007).
14. Potente, M., Gerhardt, H. & Carmeliet, P. Basic and therapeutic aspects of angiogenesis. *Cell* **146**, 873–87 (2011).
15. Carmeliet, P. & Tessier-Lavigne, M. Common mechanisms of nerve and blood vessel wiring. *Nature* **436**, 193–200 (2005).
16. Eilken, H. M. & Adams, R. H. Dynamics of endothelial cell behavior in sprouting angiogenesis. *Curr. Opin. Cell Biol.* **22**, 617–25 (2010).
17. Jain, R. K. Molecular regulation of vessel maturation. *Nat. Med.* **9**, 685–93 (2003).
18. Gaengel, K., Genové, G., Armulik, A. & Betsholtz, C. Endothelial-mural cell signaling in vascular development and angiogenesis. *Arterioscler. Thromb. Vasc. Biol.* **29**, 630–8 (2009).
19. Dyer, L. A. & Patterson, C. Development of the endothelium: an emphasis on heterogeneity. *Semin. Thromb. Hemost.* **36**, 227–35 (2010).
20. Dekker, R. J. *et al.* Prolonged fluid shear stress induces a distinct set of endothelial cell genes, most specifically lung Krüppel-like factor (KLF2). *Blood* **100**, 1689–98 (2002).

21. Atkins, G. B. & Jain, M. K. Role of Krüppel-like transcription factors in endothelial biology. *Circ. Res.* **100**, 1686–95 (2007).
22. World Health Organization. *World Health Statistics 2014*. (World Health Organization, 2014).
23. Roger, V. L. *et al.* Heart disease and stroke statistics--2011 update: a report from the American Heart Association. *Circulation* **123**, e18–e209 (2011).
24. Krishnan, A., Yadav, K., Kaur, M. & Kumar, R. Epidemiology to public health intervention for preventing cardiovascular diseases: the role of translational research. *Indian J Med Res* **132**, 643–650 (2010).
25. Lusis, A. J. Atherosclerosis. *Nature* **407**, 233–41 (2000).
26. Gimbrone, M. A. Vascular endothelium, hemodynamic forces, and atherogenesis. *Am. J. Pathol.* **155**, 1–5 (1999).
27. Tabas, I., Williams, K. J. & Borén, J. Subendothelial lipoprotein retention as the initiating process in atherosclerosis: update and therapeutic implications. *Circulation* **116**, 1832–44 (2007).
28. Glagov, S., Weisenberg, E., Zarins, C. K., Stankunavicius, R. & Kolettis, G. J. Compensatory enlargement of human atherosclerotic coronary arteries. *N. Engl. J. Med.* **316**, 1371–5 (1987).
29. Sparrow, C. P. & Olszewski, J. Cellular oxidation of low density lipoprotein is caused by thiol production in media containing transition metal ions. *J. Lipid Res.* **34**, 1219–28 (1993).
30. Shih, D. M. *et al.* Combined serum paraoxonase knockout/apolipoprotein E knockout mice exhibit increased lipoprotein oxidation and atherosclerosis. *J. Biol. Chem.* **275**, 17527–35 (2000).
31. Ross, R. The pathogenesis of atherosclerosis: a perspective for the 1990s. *Nature* **362**, 801–9 (1993).
32. Libby, P., Ridker, P. M. & Hansson, G. K. Progress and challenges in translating the biology of atherosclerosis. *Nature* **473**, 317–25 (2011).
33. Newby, A. C., Southgate, K. M. & Davies, M. Extracellular matrix degrading metalloproteinases in the pathogenesis of arteriosclerosis. *Basic Res. Cardiol.* **89 Suppl 1**, 59–70 (1994).
34. Schönbeck, U. *et al.* CD40 ligation induces tissue factor expression in human vascular smooth muscle cells. *Am. J. Pathol.* **156**, 7–14 (2000).
35. Moreno, P. R. Vulnerable plaque: definition, diagnosis, and treatment. *Cardiol. Clin.* **28**, 1–30 (2010).
36. Virmani, R. *et al.* Atherosclerotic plaque progression and vulnerability to rupture: angiogenesis as a source of intraplaque hemorrhage. *Arterioscler. Thromb. Vasc. Biol.* **25**, 2054–61 (2005).
37. Libby, P. Changing concepts of atherogenesis. *J. Intern. Med.* **247**, 349–58 (2000).
38. Steinberg, D. Thematic review series: the pathogenesis of atherosclerosis: an interpretive history of the cholesterol controversy, part III: mechanistically defining the role of hyperlipidemia. *J. Lipid Res.* **46**, 2037–51 (2005).
39. Cannon, C. P. *et al.* Intensive versus moderate lipid lowering with statins after acute coronary

- syndromes. *N. Engl. J. Med.* **350**, 1495–504 (2004).
40. Vale, N. *et al.* Statins for acute coronary syndrome. *Cochrane database Syst. Rev.* **9**, CD006870 (2014).
 41. Keeley, E. C. & Hillis, L. D. Primary PCI for myocardial infarction with ST-segment elevation. *N. Engl. J. Med.* **356**, 47–54 (2007).
 42. Niccoli, G., Burzotta, F., Galiuto, L. & Crea, F. Myocardial no-reflow in humans. *J. Am. Coll. Cardiol.* **54**, 281–92 (2009).
 43. Heineke, J. & Molkenstin, J. D. Regulation of cardiac hypertrophy by intracellular signalling pathways. *Nat Rev Mol Cell Biol* **7**, 589–600 (2006).
 44. Engler, A. J. *et al.* Embryonic cardiomyocytes beat best on a matrix with heart-like elasticity: scar-like rigidity inhibits beating. *J. Cell Sci.* **121**, 3794–802 (2008).
 45. Laflamme, M. A. & Murry, C. E. Regenerating the heart. *Nat. Biotechnol.* **23**, 845–56 (2005).
 46. Esposito, G., Dellegrottaglie, S. & Chiariello, M. The extent of irreversible myocardial damage and the potential for left ventricular repair after primary percutaneous coronary intervention. *Am. Heart J.* **160**, S4–S10 (2010).
 47. Porrello, E. R. *et al.* Transient regenerative potential of the neonatal mouse heart. *Science* **331**, 1078–80 (2011).
 48. Poss, K. D., Wilson, L. G. & Keating, M. T. Heart regeneration in zebrafish. *Science* **298**, 2188–90 (2002).
 49. Berk, B. C., Fujiwara, K. & Lehoux, S. ECM remodeling in hypertensive heart disease. *J. Clin. Invest.* **117**, 568–75 (2007).
 50. Kong, P., Christia, P. & Frangogiannis, N. G. The pathogenesis of cardiac fibrosis. *Cell. Mol. Life Sci.* **71**, 549–74 (2014).
 51. Janicki, J. S. & Brower, G. L. The role of myocardial fibrillar collagen in ventricular remodeling and function. *J. Card. Fail.* **8**, S319–25 (2002).
 52. Nahrendorf, M. *et al.* The healing myocardium sequentially mobilizes two monocyte subsets with divergent and complementary functions. *J. Exp. Med.* **204**, 3037–47 (2007).
 53. Wynn, T. A. & Barron, L. Macrophages: master regulators of inflammation and fibrosis. *Semin. Liver Dis.* **30**, 245–57 (2010).
 54. Frangogiannis, N. G. *et al.* Stem cell factor induction is associated with mast cell accumulation after canine myocardial ischemia and reperfusion. *Circulation* **98**, 687–98 (1998).
 55. Zhang, W. *et al.* The development of myocardial fibrosis in transgenic mice with targeted overexpression of tumor necrosis factor requires mast cell-fibroblast interactions. *Circulation* **124**, 2106–16 (2011).
 56. Yano, T. *et al.* Intracardiac fibroblasts, but not bone marrow derived cells, are the origin of myofibroblasts in myocardial infarct repair. *Cardiovasc. Pathol.* **14**, 241–6 (2005).
 57. Frangogiannis, N. G., Michael, L. H. & Entman, M. L. Myofibroblasts in reperfused myocardial infarcts express the embryonic form of smooth muscle myosin heavy chain (SMemb). *Cardiovasc. Res.* **48**, 89–100 (2000).

58. Hill, J. A. & Olson, E. N. Cardiac plasticity. *N Engl J Med* **358**, 1370–1380 (2008).
59. Xin, M., Olson, E. N. & Bassel-Duby, R. Mending broken hearts: cardiac development as a basis for adult heart regeneration and repair. *Nat. Rev. Mol. Cell Biol.* **14**, 529–41 (2013).
60. Konstam, M. A., Kramer, D. G., Patel, A. R., Maron, M. S. & Udelson, J. E. Left ventricular remodeling in heart failure: Current concepts in clinical significance and assessment. *JACC Cardiovasc. Imaging* **4**, 98–108 (2011).
61. Laflamme, M. a & Murry, C. E. Heart regeneration. *Nature* **473**, 326–35 (2011).
62. Dimmeler, S., Burchfield, J. & Zeiher, A. M. Cell-based therapy of myocardial infarction. *Arter. Thromb Vasc Biol* **28**, 208–216 (2008).
63. Moonen, J.-R. a J. *et al.* Endothelial progenitor cells give rise to pro-angiogenic smooth muscle-like progeny. *Cardiovasc. Res.* **86**, 506–15 (2010).
64. Urbich, C. & Dimmeler, S. Endothelial progenitor cells: characterization and role in vascular biology. *Circ. Res.* **95**, 343–53 (2004).
65. Gneccchi, M., Zhang, Z., Ni, A. & Dzau, V. J. Paracrine mechanisms in adult stem cell signaling and therapy. *Circ Res* **103**, 1204–1219 (2008).
66. Burchfield, J. S. *et al.* Pharmacological priming of adipose-derived stem cells promotes myocardial repair. *J. Investig. Med.* **64**, 50–62 (2016).
67. Chong, J. J. H. & Murry, C. E. Cardiac regeneration using pluripotent stem cells--progression to large animal models. *Stem Cell Res.* **13**, 654–65 (2014).
68. Bolli, R. *et al.* Cardiac stem cells in patients with ischaemic cardiomyopathy (SCIPIO): initial results of a randomised phase 1 trial. *Lancet* **378**, 1847–1857 (2011).
69. Beltrami, A. P. *et al.* Adult cardiac stem cells are multipotent and support myocardial regeneration. *Cell* **114**, 763–776 (2003).
70. Shiba, Y. *et al.* Human ES-cell-derived cardiomyocytes electrically couple and suppress arrhythmias in injured hearts. *Nature* **489**, 322–5 (2012).
71. Chong, J. J. H. *et al.* Human embryonic-stem-cell-derived cardiomyocytes regenerate non-human primate hearts. *Nature* **510**, 273–7 (2014).
72. Fernandes, S. *et al.* Human embryonic stem cell-derived cardiomyocytes engraft but do not alter cardiac remodeling after chronic infarction in rats. *J. Mol. Cell. Cardiol.* **49**, 941–9 (2010).
73. Kawamura, M. *et al.* Feasibility, safety, and therapeutic efficacy of human induced pluripotent stem cell-derived cardiomyocyte sheets in a porcine ischemic cardiomyopathy model. *Circulation* **126**, S29–37 (2012).
74. Schächinger, V. *et al.* Intracoronary infusion of bone marrow-derived mononuclear cells abrogates adverse left ventricular remodelling post-acute myocardial infarction: insights from the reinfusion of enriched progenitor cells and infarct remodelling in acute myocardial infarcti. *Eur. J. Heart Fail.* **11**, 973–9 (2009).
75. Seeger, F. H., Tonn, T., Krzossok, N., Zeiher, A. M. & Dimmeler, S. Cell isolation procedures matter: a comparison of different isolation protocols of bone marrow mononuclear cells used for cell therapy in patients with acute myocardial infarction. *Eur. Heart J.* **28**, 766–72 (2007).

76. Chavakis, E., Koyanagi, M. & Dimmeler, S. Enhancing the outcome of cell therapy for cardiac repair: progress from bench to bedside and back. *Circulation* **121**, 325–35 (2010).
77. Iekushi, K., Seeger, F., Assmus, B., Zeiher, A. M. & Dimmeler, S. *Paracrine Regulation of Cardiac miRNAs by Bone Marrow Mononuclear Cell Therapy in Myocardial Infarction*. (2012).
78. Zimmet, H. *et al.* Short- and long-term outcomes of intracoronary and endogenously mobilized bone marrow stem cells in the treatment of ST-segment elevation myocardial infarction: a meta-analysis of randomized control trials. *Eur J Hear. Fail* **14**, 91–105 (2012).
79. Lipinski, M. J. *et al.* Impact of intracoronary cell therapy on left ventricular function in the setting of acute myocardial infarction: a collaborative systematic review and meta-analysis of controlled clinical trials. *J Am Coll Cardiol* **50**, 1761–1767 (2007).
80. Fisher, S. A., Zhang, H., Doree, C., Mathur, A. & Martin-Rendon, E. Stem cell treatment for acute myocardial infarction. *Cochrane database Syst. Rev.* **9**, CD006536 (2015).
81. Delewi, R. *et al.* Impact of intracoronary cell therapy on left ventricular function in the setting of acute myocardial infarction: a meta-analysis of randomised controlled clinical trials. *Heart* **99**, 225–32 (2013).
82. Burchfield, J. S. & Dimmeler, S. Role of paracrine factors in stem and progenitor cell mediated cardiac repair and tissue fibrosis. *Fibrogenesis Tissue Repair* **1**, 4 (2008).
83. Latet, S. C., Hoymans, V. Y., Van Herck, P. L. & Vrints, C. J. The cellular immune system in the post-myocardial infarction repair process. *Int. J. Cardiol.* **179**, 240–7 (2015).
84. Taylor, D. A. & Zenovich, A. G. Cardiovascular cell therapy and endogenous repair. *Diabetes. Obes. Metab.* **10 Suppl 4**, 5–15 (2008).
85. Seeger, F. H. *et al.* CXCR4 expression determines functional activity of bone marrow-derived mononuclear cells for therapeutic neovascularization in acute ischemia. *Arterioscler. Thromb. Vasc. Biol.* **29**, 1802–9 (2009).
86. Romaine, S. P. R., Tomaszewski, M., Condorelli, G. & Samani, N. J. MicroRNAs in cardiovascular disease: an introduction for clinicians. *Heart* 1–8 (2015). doi:10.1136/heartjnl-2013-305402
87. Piubelli, C. *et al.* microRNAs and Cardiac Cell Fate. *Cells* **3**, 802–23 (2014).
88. Jakob, P. & Landmesser, U. Role of microRNAs in stem/progenitor cells and cardiovascular repair. *Cardiovasc. Res.* **93**, 614–22 (2012).
89. Hunter, M. P. *et al.* Detection of microRNA expression in human peripheral blood microvesicles. *PLoS One* **3**, e3694 (2008).
90. Doebele, C. *et al.* Members of the microRNA-17-92 cluster exhibit a cell-intrinsic antiangiogenic function in endothelial cells. *Blood* **115**, 4944–4950 (2010).
91. Dimmeler, S. & Zeiher, A. M. Circulating microRNAs: novel biomarkers for cardiovascular diseases? *Eur Hear. J* **31**, 2705–2707 (2010).
92. Zimmermann, W.-H. *et al.* Engineered heart tissue grafts improve systolic and diastolic function in infarcted rat hearts. *Nat. Med.* **12**, 452–8 (2006).
93. Dvir, T. *et al.* Prevascularization of cardiac patch on the omentum improves its therapeutic outcome. *Proc. Natl. Acad. Sci. U. S. A.* **106**, 14990–5 (2009).

94. Zakharova, L. *et al.* Transplantation of cardiac progenitor cell sheet onto infarcted heart promotes cardiogenesis and improves function. *Cardiovasc. Res.* **87**, 40–9 (2010).
95. Ieda, M. *et al.* Direct reprogramming of fibroblasts into functional cardiomyocytes by defined factors. *Cell* **142**, 375–86 (2010).
96. Qian, L. *et al.* In vivo reprogramming of murine cardiac fibroblasts into induced cardiomyocytes. *Nature* **485**, 593–8 (2012).
97. Inagawa, K. *et al.* Induction of cardiomyocyte-like cells in infarct hearts by gene transfer of Gata4, Mef2c, and Tbx5. *Circ. Res.* **111**, 1147–56 (2012).
98. Wang, L. *et al.* Stoichiometry of Gata4, Mef2c, and Tbx5 influences the efficiency and quality of induced cardiac myocyte reprogramming. *Circ. Res.* **116**, 237–44 (2015).
99. Hirai, H., Katoku-Kikyo, N., Keirstead, S. a. & Kikyo, N. Accelerated direct reprogramming of fibroblasts into cardiomyocyte-like cells with the MyoD transactivation domain. *Cardiovasc. Res.* **100**, 105–113 (2013).
100. Chen, J. X. *et al.* Inefficient reprogramming of fibroblasts into cardiomyocytes using Gata4, Mef2c, and Tbx5. *Circ. Res.* **111**, 50–5 (2012).
101. Song, K. *et al.* Heart repair by reprogramming non-myocytes with cardiac transcription factors. *Nature* **485**, 599–604 (2012).
102. Nam, Y. *et al.* Induction of diverse cardiac cell types by reprogramming fibroblasts with cardiac transcription factors. *Development* 4267–4278 (2014). doi:10.1242/dev.114025
103. Muraoka, N. *et al.* MiR-133 promotes cardiac reprogramming by directly repressing Snai1 and silencing fibroblast signatures. *EMBO J.* **33**, 1565–81 (2014).
104. Addis, R. C. *et al.* Optimization of direct fibroblast reprogramming to cardiomyocytes using calcium activity as a functional measure of success. *J. Mol. Cell. Cardiol.* **60**, 97–106 (2013).
105. Ifkovits, J. L., Addis, R. C., Epstein, J. a & Gearhart, J. D. Inhibition of TGF β signaling increases direct conversion of fibroblasts to induced cardiomyocytes. *PLoS One* **9**, e89678 (2014).
106. Takahashi, M. *et al.* Cytokines produced by bone marrow cells can contribute to functional improvement of the infarcted heart by protecting cardiomyocytes from ischemic injury. *Am J Physiol Hear. Circ Physiol* **291**, H886–93 (2006).
107. Schenke-Layland, K. *et al.* Reprogrammed mouse fibroblasts differentiate into cells of the cardiovascular and hematopoietic lineages. *Stem Cells* **26**, 1537–1546 (2008).
108. Efe, J. a *et al.* Conversion of mouse fibroblasts into cardiomyocytes using a direct reprogramming strategy. *Nat. Cell Biol.* **13**, 215–22 (2011).
109. Talkhabi, M., Pahlavan, S., Aghdami, N. & Baharvand, H. Ascorbic acid promotes the direct conversion of mouse fibroblasts into beating cardiomyocytes. *Biochem. Biophys. Res. Commun.* **463**, 699–705 (2015).
110. Wang, H. *et al.* Small molecules enable cardiac reprogramming of mouse fibroblasts with a single factor, Oct4. *Cell Rep.* **6**, 951–60 (2014).
111. Hou, P. *et al.* Pluripotent Stem Cells Induced from Mouse Somatic Cells by Small-Molecule Compounds. *Science (80-.).* **341**, 651–654 (2013).

112. Long, Y., Wang, M., Gu, H. & Xie, X. Bromodeoxyuridine promotes full-chemical induction of mouse pluripotent stem cells. *Cell Res.* (2015). doi:10.1038/cr.2015.96
113. Fu, Y. *et al.* Direct reprogramming of mouse fibroblasts into cardiomyocytes with chemical cocktails. *Cell Res.* 1–12 (2015). doi:10.1038/cr.2015.99
114. Nam, Y.-J. *et al.* Reprogramming of human fibroblasts toward a cardiac fate. *Proc. Natl. Acad. Sci. U. S. A.* **110**, 5588–93 (2013).
115. Wada, R. *et al.* Induction of human cardiomyocyte-like cells from fibroblasts by defined factors. *Proc. Natl. Acad. Sci.* **110**, 12667–12672 (2013).
116. Fu, J.-D. *et al.* Direct Reprogramming of Human Fibroblasts toward a Cardiomyocyte-like State. *Stem cell reports* **1**, 235–47 (2013).
117. Bruneau, B. G. Direct reprogramming for cardiac regeneration: from dream to reality. *Circ. Res.* **110**, 1392–4 (2012).
118. Sadahiro, T., Yamanaka, S. & Ieda, M. Direct Cardiac Reprogramming: Progress and Challenges in Basic Biology and Clinical Applications. *Circ. Res.* **116**, 1378–1391 (2015).
119. Jayawardena, T. M. *et al.* MicroRNA Induced Cardiac Reprogramming In Vivo: Evidence for Mature Cardiac Myocytes and Improved Cardiac Function. *Circ. Res.* **116**, 418–24 (2015).
120. Doppler, S. A., Deutsch, M.-A., Lange, R. & Krane, M. Direct Reprogramming-The Future of Cardiac Regeneration? *Int. J. Mol. Sci.* **16**, 17368–93 (2015).
121. Bartel, D. P., Lee, R. & Feinbaum, R. MicroRNAs : Genomics , Biogenesis , Mechanism , and Function Genomics : The miRNA Genes. **116**, 281–297 (2004).
122. Lee, R. C. & Ambros, V. An extensive class of small RNAs in *Caenorhabditis elegans*. *Science* **294**, 862–4 (2001).
123. Kim, V. N., Han, J. & Siomi, M. C. Biogenesis of small RNAs in animals. *Nat. Rev. Mol. Cell Biol.* **10**, 126–39 (2009).
124. Ameres, S. L. & Zamore, P. D. Diversifying microRNA sequence and function. *Nat. Rev. Mol. Cell Biol.* **14**, 475–88 (2013).
125. Flynt, A. S. & Lai, E. C. Biological principles of microRNA-mediated regulation: shared themes amid diversity. *Nat. Rev. Genet.* **9**, 831–42 (2008).
126. Inui, M., Martello, G. & Piccolo, S. MicroRNA control of signal transduction. *Nat Rev Mol Cell Biol* **11**, 252–263 (2010).
127. Stark, A., Brennecke, J., Russell, R. B. & Cohen, S. M. Identification of *Drosophila* MicroRNA targets. *PLoS Biol.* **1**, E60 (2003).
128. Heinrich, E. M. & Dimmeler, S. MicroRNAs and stem cells: control of pluripotency, reprogramming, and lineage commitment. *Circ Res* **110**, 1014–1022 (2012).
129. Lee, Y., Jeon, K., Lee, J. T., Kim, S. & Kim, V. N. MicroRNA maturation: Stepwise processing and subcellular localization. *EMBO J.* **21**, 4663–4670 (2002).
130. Lee, Y. *et al.* MicroRNA genes are transcribed by RNA polymerase II. *EMBO J.* **23**, 4051–4060 (2004).

131. Borchert, G. M., Lanier, W. & Davidson, B. L. RNA polymerase III transcribes human microRNAs. *Nat. Struct. Mol. Biol.* **13**, 1097–1101 (2006).
132. Yang, J. S. & Lai, E. C. Alternative miRNA Biogenesis Pathways and the Interpretation of Core miRNA Pathway Mutants. *Molecular Cell* **43**, 892–903 (2011).
133. Lee, Y. *et al.* The nuclear RNase III Drosha initiates microRNA processing. *Nature* **425**, 415–9 (2003).
134. Gregory, R. I. *et al.* The Microprocessor complex mediates the genesis of microRNAs. *Nature* **432**, 235–240 (2004).
135. Landthaler, M., Yalcin, A. & Tuschl, T. The human DiGeorge syndrome critical region gene 8 and its *D. melanogaster* homolog are required for miRNA biogenesis. *Curr. Biol.* **14**, 2162–2167 (2004).
136. Han, J. *et al.* Molecular Basis for the Recognition of Primary microRNAs by the Drosha-DGCR8 Complex. *Cell* **125**, 887–901 (2006).
137. Zeng, Y. & Cullen, B. R. Efficient processing of primary microRNA hairpins by Drosha requires flanking nonstructured RNA sequences. *J. Biol. Chem.* **280**, 27595–27603 (2005).
138. Kim, Y.-K. & Kim, V. N. Processing of intronic microRNAs. *EMBO J.* **26**, 775–783 (2007).
139. Han, J. *et al.* Posttranscriptional Crossregulation between Drosha and DGCR8. *Cell* **136**, 75–84 (2009).
140. Lund, E., Güttinger, S., Calado, A., Dahlberg, J. E. & Kutay, U. Nuclear export of microRNA precursors. *Science* **303**, 95–98 (2004).
141. Zeng, Y. & Cullen, B. R. Structural requirements for pre-microRNA binding and nuclear export by Exportin 5. *Nucleic Acids Res.* **32**, 4776–4785 (2004).
142. Okada, C. *et al.* A high-resolution structure of the pre-microRNA nuclear export machinery. *Science* **326**, 1275–1279 (2009).
143. Bohnsack, M. T., Czaplinski, K. & Gorlich, D. Exportin 5 is a RanGTP-dependent dsRNA-binding protein that mediates nuclear export of pre-miRNAs. *RNA* **10**, 185–191 (2004).
144. Hutvagner, G. *et al.* A cellular function for the RNA-interference enzyme Dicer in the maturation of the let-7 small temporal RNA. *Science* **293**, 834–838 (2001).
145. Zhang, H., Kolb, F. a., Jaskiewicz, L., Westhof, E. & Filipowicz, W. Single processing center models for human Dicer and bacterial RNase III. *Cell* **118**, 57–68 (2004).
146. He, L. & Hannon, G. J. MicroRNAs: small RNAs with a big role in gene regulation. *Nat. Rev. Genet.* **5**, 522–31 (2004).
147. Parker, J. S., Parizotto, E. A., Wang, M., Roe, S. M. & Barford, D. Enhancement of the Seed-Target Recognition Step in RNA Silencing by a PIWI/MID Domain Protein. *Mol. Cell* **33**, 204–214 (2009).
148. Wang, Y. *et al.* Nucleation, propagation and cleavage of target RNAs in Ago silencing complexes. *Nature* **461**, 754–761 (2009).
149. Wee, L. M., Flores-Jasso, C. F., Salomon, W. E. & Zamore, P. D. Argonaute divides Its RNA guide into domains with distinct functions and RNA-binding properties. *Cell* **151**, 1055–1067

- (2012).
150. Grimson, A. *et al.* MicroRNA Targeting Specificity in Mammals: Determinants beyond Seed Pairing. *Mol. Cell* **27**, 91–105 (2007).
 151. Gu, S., Jin, L., Zhang, F., Sarnow, P. & Kay, M. A. Biological basis for restriction of microRNA targets to the 3' untranslated region in mammalian mRNAs. *Nat. Struct. Mol. Biol.* **16**, 144–150 (2009).
 152. Chatterjee, S. & Grosshans, H. Active turnover modulates mature microRNA activity in *Caenorhabditis elegans*. *Nature* **461**, 546–549 (2009).
 153. Ameres, S. L. *et al.* Target RNA-directed trimming and tailing of small silencing RNAs. *Science* **328**, 1534–1539 (2010).
 154. Yekta, S., Shih, I.-H. & Bartel, D. P. MicroRNA-directed cleavage of HOXB8 mRNA. *Science* **304**, 594–596 (2004).
 155. Karginov, F. V *et al.* Diverse endonucleolytic cleavage sites in the mammalian transcriptome depend upon microRNAs, Drosha, and additional nucleases. *Mol. Cell* **38**, 781–788 (2010).
 156. Guo, H., Ingolia, N. T., Weissman, J. S. & Bartel, D. P. Mammalian microRNAs predominantly act to decrease target mRNA levels. *Nature* **466**, 835–840 (2010).
 157. Baek, D. *et al.* The impact of microRNAs on protein output. *Nature* **455**, 64–71 (2008).
 158. Wu, L., Fan, J. & Belasco, J. G. MicroRNAs direct rapid deadenylation of mRNA. *Proc. Natl. Acad. Sci. U. S. A.* **103**, 4034–4039 (2006).
 159. Eulalio, A. *et al.* Deadenylation is a widespread effect of miRNA regulation. *RNA* **15**, 21–32 (2009).
 160. Lim, L. P. *et al.* Microarray analysis shows that some microRNAs downregulate large numbers of target mRNAs. *Nature* **433**, 769–773 (2005).
 161. Djuranovic, S., Nahvi, A. & Green, R. miRNA-mediated gene silencing by translational repression followed by mRNA deadenylation and decay. *Science* **336**, 237–40 (2012).
 162. Bazzini, A. A., Lee, M. T. & Giraldez, A. J. Ribosome profiling shows that miR-430 reduces translation before causing mRNA decay in zebrafish. *Science* **336**, 233–7 (2012).
 163. Hu, W. & Collier, J. What comes first: translational repression or mRNA degradation? The deepening mystery of microRNA function. *Cell Res.* **22**, 1322–1324 (2012).
 164. Stenvang, J., Petri, A., Lindow, M., Obad, S. & Kauppinen, S. Inhibition of microRNA function by anti-miR oligonucleotides. *Silence* **3**, 1 (2012).
 165. Lennox, K. A. & Behlke, M. A. Chemical modification and design of anti-miRNA oligonucleotides. *Gene Ther.* **18**, 1111–20 (2011).
 166. Thum, T. MicroRNA therapeutics in cardiovascular medicine. *EMBO Mol. Med.* **4**, 3–14 (2012).
 167. Krützfeldt, J. *et al.* Silencing of microRNAs in vivo with 'antagomirs'. *Nature* **438**, 685–9 (2005).
 168. Gebert, L. F. R. *et al.* Miravirsin (SPC3649) can inhibit the biogenesis of miR-122. *Nucleic Acids Res.* **42**, 609–21 (2014).

169. Janssen, H. LA *et al.* Treatment of HCV infection by targeting microRNA. *N. Engl. J. Med.* **368**, 1685–94 (2013).
170. Farooqi, A. A. *et al.* Is miR-34a a Well Equipped swordsman to Conquer Temple of Molecular Oncology? *Chem. Biol. Drug Des.* (2015). doi:10.1111/cbdd.12634
171. Urbich, C., Kuehbacher, A. & Dimmeler, S. Role of microRNAs in vascular diseases, inflammation, and angiogenesis. *Cardiovasc. Res.* **79**, 581–8 (2008).
172. Thum, T. *et al.* MicroRNAs in the human heart: a clue to fetal gene reprogramming in heart failure. *Circulation* **116**, 258–67 (2007).
173. Bernstein, E. *et al.* Dicer is essential for mouse development. *Nat. Genet.* **35**, 215–7 (2003).
174. Ohtani, K. & Dimmeler, S. Control of cardiovascular differentiation by microRNAs. *Basic Res Cardiol* **106**, 5–11 (2011).
175. Wystub, K., Besser, J., Bachmann, A., Boettger, T. & Braun, T. miR-1/133a Clusters Cooperatively Specify the Cardiomyogenic Lineage by Adjustment of Myocardin Levels during Embryonic Heart Development. *PLoS Genet.* **9**, e1003793 (2013).
176. Zhao, Y. *et al.* Dysregulation of cardiogenesis, cardiac conduction, and cell cycle in mice lacking miRNA-1-2. *Cell* **129**, 303–17 (2007).
177. da Costa Martins, P. A. *et al.* Conditional dicer gene deletion in the postnatal myocardium provokes spontaneous cardiac remodeling. *Circulation* **118**, 1567–76 (2008).
178. Landgraf, P. *et al.* A mammalian microRNA expression atlas based on small RNA library sequencing. *Cell* **129**, 1401–14 (2007).
179. Xu, Q. *et al.* Micro-RNA-34a contributes to the impaired function of bone marrow-derived mononuclear cells from patients with cardiovascular disease. *J. Am. Coll. Cardiol.* **59**, 2107–17 (2012).
180. Iekushi, K., Seeger, F., Assmus, B., Zeiher, A. M. & Dimmeler, S. Regulation of Cardiac MicroRNAs by Bone Marrow Mononuclear Cell Therapy in Myocardial Infarction. *Circulation* **125**, 1765–1773 (2012).
181. Boon, R. A. *et al.* MicroRNA-34a regulates cardiac ageing and function. *Nature* **495**, 107–10 (2013).
182. Hinkel, R. *et al.* Inhibition of microRNA-92a protects against ischemia/reperfusion injury in a large-animal model. *Circulation* **128**, 1066–75 (2013).
183. Bonauer, A. *et al.* MicroRNA-92a controls angiogenesis and functional recovery of ischemic tissues in mice. *Science* **324**, 1710–3 (2009).
184. Thum, T. *et al.* MicroRNA-21 contributes to myocardial disease by stimulating MAP kinase signalling in fibroblasts. *Nature* **456**, 980–984 (2008).
185. Fiedler, J. *et al.* MicroRNA-24 regulates vascularity after myocardial infarction. *Circulation* **124**, 720–30 (2011).
186. Wahlquist, C. *et al.* Inhibition of miR-25 improves cardiac contractility in the failing heart. *Nature* **508**, 531–5 (2014).
187. da Costa Martins, P. A. *et al.* MicroRNA-199b targets the nuclear kinase Dyrk1a in an auto-

- amplification loop promoting calcineurin/NFAT signalling. *Nat. Cell Biol.* **12**, 1220–7 (2010).
188. van Rooij, E. *et al.* Control of stress-dependent cardiac growth and gene expression by a microRNA. *Science* **316**, 575–9 (2007).
 189. Satoh, M., Minami, Y., Takahashi, Y., Tabuchi, T. & Nakamura, M. Expression of microRNA-208 is associated with adverse clinical outcomes in human dilated cardiomyopathy. *J. Card. Fail.* **16**, 404–10 (2010).
 190. Ikeda, S., He, A., Kong, S. & Lu, J. MicroRNA-1 negatively regulates expression of the hypertrophy-associated calmodulin and Mef2a genes. ... *Cell. Biol.* **29**, 2193–204 (2009).
 191. Li, Q. *et al.* Attenuation of microRNA-1 derepresses the cytoskeleton regulatory protein twinfilin-1 to provoke cardiac hypertrophy. *J. Cell Sci.* **123**, 2444–2452 (2010).
 192. Carè, A. *et al.* MicroRNA-133 controls cardiac hypertrophy. *Nat. Med.* **13**, 613–8 (2007).
 193. Yang, B. *et al.* The muscle-specific microRNA miR-1 regulates cardiac arrhythmogenic potential by targeting GJA1 and KCNJ2. *Nat. Med.* **13**, 486–91 (2007).
 194. Curcio, A. *et al.* MicroRNA-1 downregulation increases connexin 43 displacement and induces ventricular tachyarrhythmias in rodent hypertrophic hearts. *PLoS One* **8**, e70158 (2013).
 195. Lu, Y. *et al.* MicroRNA-328 contributes to adverse electrical remodeling in atrial fibrillation. *Circulation* **122**, 2378–87 (2010).
 196. Girmatsion, Z. *et al.* Changes in microRNA-1 expression and IK1 up-regulation in human atrial fibrillation. *Heart Rhythm* **6**, 1802–9 (2009).
 197. Boettger, T. *et al.* Acquisition of the contractile phenotype by murine arterial smooth muscle cells depends on the Mir143/145 gene cluster. *J. Clin. Invest.* **119**, 2634–47 (2009).
 198. Lovren, F. *et al.* MicroRNA-145 targeted therapy reduces atherosclerosis. *Circulation* **126**, S81–90 (2012).
 199. Cordes, K. R. *et al.* miR-145 and miR-143 regulate smooth muscle cell fate and plasticity. *Nature* **460**, 705–10 (2009).
 200. Cheng, Y. *et al.* MicroRNA-145, a novel smooth muscle cell phenotypic marker and modulator, controls vascular neointimal lesion formation. *Circ. Res.* **105**, 158–66 (2009).
 201. Hergenreider, E. *et al.* Atheroprotective communication between endothelial cells and smooth muscle cells through miRNAs. *Nat Cell Biol* **14**, 249–256 (2012).
 202. Marquart, T. J., Allen, R. M., Ory, D. S. & Baldán, A. miR-33 links SREBP-2 induction to repression of sterol transporters. *Proc. Natl. Acad. Sci. U. S. A.* **107**, 12228–32 (2010).
 203. Rayner, K. J. *et al.* MiR-33 contributes to the regulation of cholesterol homeostasis. *Science* **328**, 1570–3 (2010).
 204. Najafi-Shoushtari, S. H. *et al.* MicroRNA-33 and the SREBP host genes cooperate to control cholesterol homeostasis. *Science* **328**, 1566–9 (2010).
 205. Boon, R. A. *et al.* MicroRNA-29 in aortic dilation: implications for aneurysm formation. *Circ. Res.* **109**, 1115–9 (2011).
 206. Caporali, A. *et al.* Deregulation of microRNA-503 contributes to diabetes mellitus-induced

- impairment of endothelial function and reparative angiogenesis after limb ischemia. *Circulation* **123**, 282–91 (2011).
207. McArthur, K., Feng, B., Wu, Y., Chen, S. & Chakrabarti, S. MicroRNA-200b regulates vascular endothelial growth factor-mediated alterations in diabetic retinopathy. *Diabetes* **60**, 1314–23 (2011).
 208. Chan, Y. C., Roy, S., Khanna, S. & Sen, C. K. Downregulation of endothelial microRNA-200b supports cutaneous wound angiogenesis by desilencing GATA binding protein 2 and vascular endothelial growth factor receptor 2. *Arterioscler. Thromb. Vasc. Biol.* **32**, 1372–82 (2012).
 209. Mitchell, P. S. *et al.* Circulating microRNAs as stable blood-based markers for cancer detection. *Proc. Natl. Acad. Sci. U. S. A.* **105**, 10513–8 (2008).
 210. Tijssen, A. J. *et al.* MiR423-5p as a circulating biomarker for heart failure. *Circ Res* **106**, 1035–1039 (2010).
 211. Fichtlscherer, S. *et al.* Circulating microRNAs in patients with coronary artery disease. *Circ Res* **107**, 677–684 (2010).
 212. Zampetaki, A. *et al.* Prospective study on circulating MicroRNAs and risk of myocardial infarction. *J. Am. Coll. Cardiol.* **60**, 290–9 (2012).
 213. D’Alessandra, Y. *et al.* Circulating microRNAs are new and sensitive biomarkers of myocardial infarction. *Eur. Heart J.* **31**, 2765–73 (2010).
 214. Wang, G.-K. *et al.* Circulating microRNA: a novel potential biomarker for early diagnosis of acute myocardial infarction in humans. *Eur. Heart J.* **31**, 659–66 (2010).
 215. Ji, X. *et al.* Plasma miR-208 as a biomarker of myocardial injury. *Clin. Chem.* **55**, 1944–9 (2009).
 216. Parker, L. H. *et al.* The endothelial-cell-derived secreted factor Eglf7 regulates vascular tube formation. *Nature* **428**, 754–8 (2004).
 217. Kuehbacher, A., Urbich, C., Zeiher, A. M. & Dimmeler, S. Role of Dicer and Drosha for endothelial microRNA expression and angiogenesis. *Circ. Res.* **101**, 59–68 (2007).
 218. Musiyenko, A., Bitko, V. & Barik, S. Ectopic expression of miR-126*, an intronic product of the vascular endothelial EGF-like 7 gene, regulates prostein translation and invasiveness of prostate cancer LNCaP cells. *J. Mol. Med.* **86**, 313–322 (2008).
 219. Zhao, S. *et al.* MicroRNA-126 regulates DNA methylation in CD4+ T cells and contributes to systemic lupus erythematosus by targeting DNA methyltransferase 1. *Arthritis Rheum.* **63**, 1376–1386 (2011).
 220. Zhu, N. *et al.* Endothelial-specific intron-derived miR-126 is down-regulated in human breast cancer and targets both VEGFA and PIK3R2. *Mol. Cell. Biochem.* **351**, 157–164 (2011).
 221. Sun, Y. *et al.* miR-126 inhibits non-small cell lung cancer cells proliferation by targeting EGFL7. *Biochem. Biophys. Res. Commun.* **391**, 1483–1489 (2010).
 222. Zhang, Y. *et al.* miR-126 and miR-126* repress recruitment of mesenchymal stem cells and inflammatory monocytes to inhibit breast cancer metastasis. *Nat. Cell Biol.* **15**, 284–94 (2013).
 223. Li, Z. *et al.* Distinct microRNA expression profiles in acute myeloid leukemia with common translocations. *Proc. Natl. Acad. Sci. U. S. A.* **105**, 15535–15540 (2008).

224. Díaz, R., Silva, J. & García, J. Deregulated expression of miR-106a predicts survival in human colon cancer patients. ... *Cancer* **802**, 794–802 (2008).
225. Harris, T. A., Yamakuchi, M., Kondo, M., Oettgen, P. & Lowenstein, C. J. Ets-1 and Ets-2 regulate the expression of microRNA-126 in endothelial cells. *Arterioscler. Thromb. Vasc. Biol.* **30**, 1990–7 (2010).
226. Harnprasopwat, R. *et al.* Alteration of processing induced by a single nucleotide polymorphism in pri-miR-126. *Biochem. Biophys. Res. Commun.* **399**, 117–122 (2010).
227. McAuley, A. K. *et al.* A genetic variant regulating miR-126 is associated with sight threatening diabetic retinopathy. *Diabetes Vasc. Dis. Res.* **12**, 133–8 (2015).
228. Aguado-Fraile, E. *et al.* A Pilot Study Identifying a Set of microRNAs As Precise Diagnostic Biomarkers of Acute Kidney Injury. *PLoS One* **10**, e0127175 (2015).
229. Oglesby, I. K. *et al.* miR-126 is downregulated in cystic fibrosis airway epithelial cells and regulates TOM1 expression. *J. Immunol.* **184**, 1702–1709 (2010).
230. Chen, C., Wu, C.-Q., Zhang, Z.-Q., Yao, D.-K. & Zhu, L. Loss of expression of miR-335 is implicated in hepatic stellate cell migration and activation. *Exp. Cell Res.* **317**, 1714–25 (2011).
231. Gong, X.-H. *et al.* Overexpression of miR-126 Inhibits the Activation and Migration of HSCs through Targeting CRK. *Cell. Physiol. Biochem.* **33**, 97–106 (2014).
232. Guo, C.-J. *et al.* Dynamic expression of miR-126* and its effects on proliferation and contraction of hepatic stellate cells. *FEBS Lett.* **587**, 3792–801 (2013).
233. Feng, X. *et al.* Upregulation of microRNA-126 in Hepatic Stellate Cells May Affect Pathogenesis of Liver Fibrosis Through the NF- κ B Pathway. *DNA Cell Biol.* **34**, 470–80 (2015).
234. Nakano, M. *et al.* CYP2A7 pseudogene transcript affects CYP2A6 expression in human liver by acting as a decoy for miR-126. *Drug Metab. Dispos.* **43**, 703–12 (2015).
235. Liu, Y. *et al.* The Role of Circulating MicroRNA-126 (miR-126): A Novel Biomarker for Screening Prediabetes and Newly Diagnosed Type 2 Diabetes Mellitus. *Int. J. Mol. Sci.* **15**, 10567–10577 (2014).
236. Zampetaki, A. *et al.* Plasma microRNA profiling reveals loss of endothelial miR-126 and other microRNAs in type 2 diabetes. *Circ. Res.* **107**, 810–7 (2010).
237. Zhang, T. *et al.* Plasma miR-126 is a potential biomarker for early prediction of type 2 diabetes mellitus in susceptible individuals. *Biomed Res. Int.* **2013**, 761617 (2013).
238. Meng, S. *et al.* Downregulation of microRNA-126 in endothelial progenitor cells from diabetes patients, impairs their functional properties, via target gene Spred-1. *J. Mol. Cell. Cardiol.* **53**, 64–72 (2012).
239. Olivieri, F. *et al.* Age- and glycemia-related miR-126-3p levels in plasma and endothelial cells. *Aging (Albany, NY).* **6**, 771–87 (2014).
240. Hu, J., Zeng, L., Huang, J., Wang, G. & Lu, H. miR-126 promotes angiogenesis and attenuates inflammation after contusion spinal cord injury in rats. *Brain Res.* **1608**, 191–202 (2015).
241. Wang, S. *et al.* The endothelial-specific microRNA miR-126 governs vascular integrity and angiogenesis. *Dev. Cell* **15**, 261–71 (2008).

242. Guo, C. *et al.* The noncoding RNA, miR-126, suppresses the growth of neoplastic cells by targeting phosphatidylinositol 3-kinase signaling and is frequently lost in colon cancers. *Genes. Chromosomes Cancer* **47**, 939–46 (2008).
243. Sessa, R. *et al.* The miR-126 regulates angiopoietin-1 signaling and vessel maturation by targeting p85 β . *Biochim. Biophys. Acta* **1823**, 1925–35 (2012).
244. Meng, Q. *et al.* Upregulation of MicroRNA-126 Contributes to Endothelial Progenitor Cell Function in Deep Vein Thrombosis via Its Target PIK3R2. *J. Cell. Biochem.* **116**, 1613–1623 (2015).
245. Yan, T. *et al.* MicroRNA-126 regulates EPCs function: Implications for a role of miR-126 in preeclampsia. *J. Cell. Biochem.* **114**, 2148–2159 (2013).
246. Harris, T. a, Yamakuchi, M., Ferlito, M., Mendell, J. T. & Lowenstein, C. J. MicroRNA-126 regulates endothelial expression of vascular cell adhesion molecule 1. *Proc. Natl. Acad. Sci. U. S. A.* **105**, 1516–21 (2008).
247. Asgeirsdóttir, S. a *et al.* MicroRNA-126 contributes to renal microvascular heterogeneity of VCAM-1 protein expression in acute inflammation. *Am. J. Physiol. Renal Physiol.* **302**, F1630–9 (2012).
248. Bijkerk, R. *et al.* Silencing of miRNA-126 in kidney ischemia reperfusion is associated with elevated SDF-1 levels and mobilization of Sca-1+/Lin- progenitor cells. *MicroRNA (Shāriqah, United Arab Emirates)* **3**, 144–9 (2014).
249. Taverna, S. *et al.* Exosomal shuttling of miR-126 in endothelial cells modulates adhesive and migratory abilities of chronic myelogenous leukemia cells. *Mol. Cancer* **13**, 169 (2014).
250. Tan, T. W. *et al.* Naringin suppress chondrosarcoma migration through inhibition vascular adhesion molecule-1 expression by modulating miR-126. *Int. Immunopharmacol.* **22**, 107–114 (2014).
251. Sun, C. *et al.* IRF-1 and miRNA126 modulate VCAM-1 expression in response to a high-fat meal. *Circ. Res.* **111**, 1054–64 (2012).
252. Okuyama, K. *et al.* MicroRNA-126-mediated control of cell fate in B-cell myeloid progenitors as a potential alternative to transcriptional factors. *Proc. Natl. Acad. Sci. U. S. A.* **110**, 13410–5 (2013).
253. Zhang, J. *et al.* The cell growth suppressor, mir-126, targets IRS-1. *Biochem. Biophys. Res. Commun.* **377**, 136–140 (2008).
254. Ryu, H. S., Park, S. Y., Ma, D., Zhang, J. & Lee, W. The induction of microrna targeting IRS-1 is involved in the development of insulin resistance under conditions of mitochondrial dysfunction in hepatocytes. *PLoS One* **6**, (2011).
255. Li, X., Shen, Y., Ichikawa, H., Antes, T. & Goldberg, G. S. Regulation of miRNA expression by Src and contact normalization: effects on nonanchored cell growth and migration. *Oncogene* **28**, 4272–4283 (2009).
256. Zhao, C., Li, Y., Zhang, M., Yang, Y. & Chang, L. miR-126 inhibits cell proliferation and induces cell apoptosis of hepatocellular carcinoma cells partially by targeting Sox2. *Hum. Cell* **28**, 91–99 (2015).
257. Otsubo, T. *et al.* Microrna-126 inhibits sox2 expression and contributes to gastric

- carcinogenesis. *PLoS One* **6**, (2011).
258. Png, K. J., Halberg, N., Yoshida, M. & Tavazoie, S. F. A microRNA regulon that mediates endothelial recruitment and metastasis by cancer cells. *Nature* **481**, 190–4 (2012).
259. Felli, N. *et al.* miR-126&126* Restored Expressions Play a Tumor Suppressor Role by Directly Regulating ADAM9 and MMP7 in Melanoma. *PLoS One* **8**, (2013).
260. Huang, X. *et al.* Regulated expression of microRNAs-126/126* inhibits erythropoiesis from human embryonic stem cells. *Blood* **117**, 2157–2165 (2011).
261. Shen, W.-F., Hu, Y.-L., Uttarwar, L., Passegue, E. & Largman, C. MicroRNA-126 regulates HOXA9 by binding to the homeobox. *Mol. Cell. Biol.* **28**, 4609–4619 (2008).
262. Jiao, L. R. *et al.* Micrnas targeting oncogenes are down-regulated in pancreatic malignant transformation from benign tumors. *PLoS One* **7**, (2012).
263. Hsu, S. Da *et al.* MiRTarBase update 2014: An information resource for experimentally validated miRNA-target interactions. *Nucleic Acids Res.* **42**, 78–85 (2014).
264. Xu, J. Q., Liu, P., Si, M. J. & Ding, X. Y. MicroRNA-126 inhibits osteosarcoma cells proliferation by targeting Sirt1. *Tumor Biol.* **34**, 3871–3877 (2013).
265. Wu, Z. *et al.* MiR-126-5p regulates osteoclast differentiation and bone resorption in giant cell tumor through inhibition of MMP-13. *Biochem. Biophys. Res. Commun.* **443**, 944–949 (2014).
266. Zhou, W. *et al.* MiR-126-5p regulates osteolysis formation and stromal cell proliferation in giant cell tumor through inhibition of PTHrP. *Bone* **66**, 267–276 (2014).
267. Shibayama, Y. *et al.* Upregulation of microRNA-126-5p is associated with drug resistance to cytarabine and poor prognosis in AML patients. *Oncol. Rep.* 2176–2182 (2015). doi:10.3892/or.2015.3839
268. Fish, J. E. *et al.* miR-126 Regulates Angiogenic Signaling and Vascular Integrity. *Dev. Cell* **15**, 272–284 (2008).
269. Wang, S. *et al.* The endothelial-specific microRNA miR-126 governs vascular integrity and angiogenesis. *Dev. Cell* **15**, 261–71 (2008).
270. Nicoli, S. *et al.* MicroRNA-mediated integration of haemodynamics and Vegf signalling during angiogenesis. *Nature* **464**, 1196–200 (2010).
271. Schober, A. *et al.* MicroRNA-126-5p promotes endothelial proliferation and limits atherosclerosis by suppressing Dlk1. *Nat. Med.* (2014). doi:10.1038/nm.3487
272. Fichtlscherer, S. *et al.* Circulating microRNAs in patients with coronary artery disease. *Circ. Res.* **107**, 677–84 (2010).
273. Fichtlscherer, S., Zeiher, A. M. & Dimmeler, S. Circulating microRNAs: biomarkers or mediators of cardiovascular diseases? *Arterioscler. Thromb. Vasc. Biol.* **31**, 2383–90 (2011).
274. Long, G. *et al.* Human circulating microRNA-1 and microRNA-126 as potential novel indicators for acute myocardial infarction. *Int. J. Biol. Sci.* **8**, 811–8 (2012).
275. Jiang, C. *et al.* The effects and mechanism of miR-92a and miR-126 on myocardial apoptosis in mouse ischemia-reperfusion model. *Cell Biochem. Biophys.* **70**, 1901–6 (2014).

276. Chen, J.-J. & Zhou, S.-H. Mesenchymal stem cells overexpressing MiR-126 enhance ischemic angiogenesis via the AKT/ERK-related pathway. *Cardiol. J.* **18**, 675–81 (2011).
277. Bijkerk, R. *et al.* Hematopoietic MicroRNA-126 Protects against Renal Ischemia/Reperfusion Injury by Promoting Vascular Integrity. *J. Am. Soc. Nephrol.* (2014). doi:10.1681/ASN.2013060640
278. van Solingen, C. *et al.* MicroRNA-126 modulates endothelial SDF-1 expression and mobilization of Sca-1(+)/Lin(-) progenitor cells in ischaemia. *Cardiovasc. Res.* **92**, 449–55 (2011).
279. Hu, J.-Z. *et al.* Anti-apoptotic effect of microRNA-21 after contusion spinal cord injury in rats. *J. Neurotrauma* **30**, 1349–60 (2013).
280. Arroyo, J. D. *et al.* Argonaute2 complexes carry a population of circulating microRNAs independent of vesicles in human plasma. *Proc. Natl. Acad. Sci. U. S. A.* **108**, 5003–8 (2011).
281. Zhou, J. *et al.* Regulation of vascular smooth muscle cell turnover by endothelial cell-secreted microRNA-126: role of shear stress. *Circ. Res.* **113**, 40–51 (2013).
282. Schmidt, Y. *et al.* miR-126 regulates platelet-derived growth factor receptor- α expression and migration of primary human osteoblasts. *Biol. Chem.* **396**, 61–70 (2015).
283. Togliatto, G. *et al.* Obesity reduces the pro-angiogenic potential of adipose tissue stem cell-derived extracellular vesicles (EVs) by impairing miR-126 content: impact on clinical applications. *Int. J. Obes. (Lond)*. (2015). doi:10.1038/ijo.2015.123
284. Zhang, Q., Kandic, I. & Kutryk, M. J. Dysregulation of angiogenesis-related microRNAs in endothelial progenitor cells from patients with coronary artery disease. *Biochem. Biophys. Res. Commun.* **405**, 42–46 (2011).
285. Heeschen, C. *et al.* Profoundly Reduced Neovascularization Capacity of Bone Marrow Mononuclear Cells Derived from Patients with Chronic Ischemic Heart Disease. *Circulation* **109**, 1615–1622 (2004).
286. Vasa, M. *et al.* Number and migratory activity of circulating endothelial progenitor cells inversely correlate with risk factors for coronary artery disease. *Circ Res* **89**, E1–7 (2001).
287. Tamarat, R. *et al.* Impairment in ischemia-induced neovascularization in diabetes: bone marrow mononuclear cell dysfunction and therapeutic potential of placenta growth factor treatment. *Am. J. Pathol.* **164**, 457–466 (2004).
288. Luppi, P. *et al.* Maternal circulating CD34+VEGFR-2+ and CD133+VEGFR-2+ progenitor cells increase during normal pregnancy but are reduced in women with preeclampsia. *Reprod. Sci.* **17**, 643–652 (2010).
289. Modarai, B., Burnand, K. G., Sawyer, B. & Smith, A. Endothelial progenitor cells are recruited into resolving venous thrombi. *Circulation* **111**, 2645–2653 (2005).
290. Li, X., Meng, Q. & Wu, H. Effects of bone marrow-derived endothelial progenitor cell transplantation on vein microenvironment in a rat model of chronic thrombosis. *Chin. Med. J. (Engl)*. **120**, 2245–2249 (2007).
291. Lechman, E. R. *et al.* Attenuation of miR-126 activity expands HSC in vivo without exhaustion. *Cell Stem Cell* **11**, 799–811 (2012).

292. Santulli, G. *et al.* A selective microRNA-based strategy inhibits restenosis while preserving endothelial function. *J. Clin. Invest.* **124**, 4102–14 (2014).
293. Tanner, F. C. *et al.* Differential effects of the cyclin-dependent kinase inhibitors p27(Kip1), p21(Cip1), and p16(Ink4) on vascular smooth muscle cell proliferation. *Circulation* **101**, 2022–2025 (2000).
294. Meister, J. & Schmidt, M. H. H. miR-126 and miR-126*: new players in cancer. *ScientificWorldJournal.* **10**, 2090–100 (2010).
295. Ebrahimi, F., Gopalan, V., Smith, R. A. & Lam, A. K.-Y. miR-126 in human cancers: clinical roles and current perspectives. *Exp. Mol. Pathol.* **96**, 98–107 (2014).
296. Wang, X. *et al.* Aberrant expression of oncogenic and tumor-suppressive microRNAs in cervical cancer is required for cancer cell growth. *PLoS One* **3**, e2557 (2008).
297. Tavazoie, S. F. *et al.* Endogenous human microRNAs that suppress breast cancer metastasis. *Nature* **451**, 147–52 (2008).
298. Feng, R. *et al.* miR-126 functions as a tumour suppressor in human gastric cancer. *Cancer Lett.* **298**, 50–63 (2010).
299. Yanaihara, N. *et al.* Unique microRNA molecular profiles in lung cancer diagnosis and prognosis. *Cancer Cell* **9**, 189–98 (2006).
300. Yin, J. *et al.* Differential expression of serum miR-126, miR-141 and miR-21 as novel biomarkers for early detection of liver metastasis in colorectal cancer. *Chin. J. Cancer Res.* **26**, 95–103 (2014).
301. Saito, Y. *et al.* Epigenetic therapy upregulates the tumor suppressor microRNA-126 and its host gene EGFL7 in human cancer cells. *Biochem. Biophys. Res. Commun.* **379**, 726–31 (2009).
302. Frame, M. C. Newest findings on the oldest oncogene; how activated src does it. *J. Cell Sci.* **117**, 989–98 (2004).
303. Cesarone, G. *et al.* RNAi-mediated silencing of insulin receptor substrate 1 (IRS-1) enhances tamoxifen-induced cell death in MCF-7 breast cancer cells. *J. Cell. Biochem.* **98**, 440–50 (2006).
304. Wong, Q. W. L. *et al.* MicroRNA-223 Is Commonly Repressed in Hepatocellular Carcinoma and Potentiates Expression of Stathmin1. *Gastroenterology* **135**, 257–269 (2008).
305. White, N. M. a *et al.* miRNA profiling in metastatic renal cell carcinoma reveals a tumour-suppressor effect for miR-215. *Br. J. Cancer* **105**, 1741–9 (2011).
306. Khella, H. W. Z. *et al.* Low Expression of miR-126 Is a Prognostic Marker for Metastatic Clear Cell Renal Cell Carcinoma. *Am. J. Pathol.* **185**, 693–703 (2015).
307. Vergho, D. *et al.* Combination of expression levels of miR-21 and miR-126 is associated with cancer-specific survival in clear-cell renal cell carcinoma. *BMC Cancer* **14**, 25 (2014).
308. Lin, N., Zhou, Y., Lian, X. & Tu, Y. Down-regulation of tissue microRNA-126 was associated with poor prognosis in patients with cutaneous melanoma. **8**, 4297–4301 (2015).
309. Wuelling, M. *et al.* Histogenesis of giant cell tumors. *Pathologe* **23**, 332–339 (2002).
310. Mak, I. W. Y. *et al.* Evidence for the role of matrix metalloproteinase-13 in bone resorption by giant cell tumor of bone. *Hum. Pathol.* **41**, 1320–1329 (2010).

311. Mak, I. W. Y., Cowan, R. W., Turcotte, R. E., Singh, G. & Ghert, M. PTHrP Induces Autocrine/Paracrine Proliferation of Bone Tumor Cells through Inhibition of Apoptosis. *PLoS One* **6**, e19975 (2011).
312. Yang, C. *et al.* miR-126 Functions as a Tumor Suppressor in Osteosarcoma by Targeting Sox2. *Int. J. Mol. Sci.* **15**, 423–437 (2013).
313. Jiang, L., He, A., Zhang, Q. & Tao, C. miR-126 inhibits cell growth, invasion, and migration of osteosarcoma cells by downregulating ADAM-9. *Tumor Biol.* **35**, 12645–12654 (2014).
314. Jiang, L., Tao, C., He, A. & He, X. Overexpression of miR-126 sensitizes osteosarcoma cells to apoptosis induced by epigallocatechin-3-gallate. *World J. Surg. Oncol.* **12**, 383 (2014).
315. Chen, H. *et al.* Reduced miR-126 expression facilitates angiogenesis of gastric cancer through its regulation on VEGF-A. *Oncotarget* **5**, 11873–85 (2014).
316. Li, X., Wang, F. & Qi, Y. MiR-126 inhibits the invasion of gastric cancer cell in part by targeting Crk. *Eur. Rev. Med. Pharmacol. Sci.* **18**, 2031–7 (2014).
317. de Leeuw, D. C. *et al.* Attenuation of microRNA-126 Expression That Drives CD34+38-Stem/Progenitor Cells in Acute Myeloid Leukemia Leads to Tumor Eradication. *Cancer Res.* (2014). doi:10.1158/0008-5472.CAN-13-1733
318. Dorrance, A. M. *et al.* Targeting leukemia stem cells in vivo with ANTAGOMIR-126 nanoparticles in acute myeloid leukemia. *Leukemia* (2015). doi:10.1038/leu.2015.139
319. Jayawardena, T. M. *et al.* MicroRNA-mediated in vitro and in vivo direct reprogramming of cardiac fibroblasts to cardiomyocytes. *Circ. Res.* **110**, 1465–1473 (2012).
320. Cerchia, L., Giangrande, P. H., McNamara, J. O. & de Franciscis, V. Cell-specific aptamers for targeted therapies. *Methods Mol. Biol.* **535**, 59–78 (2009).
321. Hicke, B. J. & Stephens, A. W. Escort aptamers: a delivery service for diagnosis and therapy. *J Clin Invest* **106**, 923–928 (2000).
322. Zhou, J. & Rossi, J. J. Cell-specific aptamer-mediated targeted drug delivery. *Oligonucleotides* **21**, 1–10 (2011).
323. Tuerk, C. & Gold, L. Systematic evolution of ligands by exponential enrichment: RNA ligands to bacteriophage T4 DNA polymerase. *Science (80-.)*. **249**, 505–510 (1990).
324. Ellington, A. D. & Szostak, J. W. In vitro selection of RNA molecules that bind specific ligands. *Nature* **346**, 818–22 (1990).
325. Burnett, J. C. & Rossi, J. J. RNA-based therapeutics: current progress and future prospects. *Chem. Biol.* **19**, 60–71 (2012).
326. Sun, H. & Zu, Y. A Highlight of Recent Advances in Aptamer Technology and Its Application. *Molecules* **20**, 11959–11980 (2015).
327. Proske, D., Blank, M., Buhmann, R. & Resch, A. Aptamers--basic research, drug development, and clinical applications. *Appl. Microbiol. Biotechnol.* **69**, 367–74 (2005).
328. Gragoudas, E. S., Adamis, A. P., Cunningham, E. T., Feinsod, M. & Guyer, D. R. Pegaptanib for neovascular age-related macular degeneration. *N. Engl. J. Med.* **351**, 2805–16 (2004).
329. Ireson, C. R. & Kelland, L. R. Discovery and development of anticancer aptamers. *Mol. Cancer*

- Ther.* **5**, 2957–62 (2006).
330. Rakic, J.-M., Blaise, P. & Foidart, J.-M. Pegaptanib and age-related macular degeneration. *The New England journal of medicine* **352**, 1720–1721; author reply 1720–1721 (2005).
 331. Katz, B. & Goldbaum, M. Macugen (pegaptanib sodium), a novel ocular therapeutic that targets vascular endothelial growth factor (VEGF). *Int. Ophthalmol. Clin.* **46**, 141–54 (2006).
 332. Ruckman, J. *et al.* 2'-Fluoropyrimidine RNA-based aptamers to the 165-amino acid form of vascular endothelial growth factor (VEGF165). Inhibition of receptor binding and VEGF-induced vascular permeability through interactions requiring the exon 7-encoded domain. *J. Biol. Chem.* **273**, 20556–67 (1998).
 333. Martin, J. *a et al.* Selection of an aptamer antidote to the anticoagulant drug bivalirudin. *PLoS One* **8**, e57341 (2013).
 334. Nie, H., Chen, Y., Lü, C. & Liu, Z. Efficient selection of glycoprotein-binding DNA aptamers via boronate affinity monolithic capillary. *Anal. Chem.* **85**, 8277–83 (2013).
 335. Sun, W., Du, L. & Li, M. Aptamer-based carbohydrate recognition. *Curr. Pharm. Des.* **16**, 2269–78 (2010).
 336. Darmostuk, M., Rimpelova, S., Gbelcova, H. & Ruml, T. Current approaches in SELEX: An update to aptamer selection technology. *Biotechnol. Adv.* **33**, 1141–61 (2015).
 337. Weigand, J. E. & Suess, B. Aptamers and riboswitches: perspectives in biotechnology. *Appl. Microbiol. Biotechnol.* **85**, 229–36 (2009).
 338. Jenison, R. D., Gill, S. C., Pardi, A. & Polisky, B. High-resolution molecular discrimination by RNA. *Science* **263**, 1425–9 (1994).
 339. Thiel, W. H. *et al.* Rapid identification of cell-specific, internalizing RNA aptamers with bioinformatics analyses of a cell-based aptamer selection. *PLoS One* **7**, e43836 (2012).
 340. Schutze, T. *et al.* Probing the SELEX process with next-generation sequencing. *PLoS One* **6**, e29604 (2011).
 341. Alam, K. K., Chang, J. L. & Burke, D. H. FASTAptamer: A Bioinformatic Toolkit for High-throughput Sequence Analysis of Combinatorial Selections. *Mol. Ther. Acids* **4**, e230 (2015).
 342. Dausse, E. *et al.* HAPIScreen, a method for high-throughput aptamer identification. *J Nanobiotechnology* **9**, 25 (2011).
 343. Berezovski, M. *et al.* Nonequilibrium capillary electrophoresis of equilibrium mixtures: a universal tool for development of aptamers. *J. Am. Chem. Soc.* **127**, 3165–71 (2005).
 344. Ashley, J., Ji, K. & Li, S. F. Y. Selection of bovine catalase aptamers using non-SELEX. *Electrophoresis* **33**, 2783–9 (2012).
 345. Blank, M., Weinschenk, T., Priemer, M. & Schluesener, H. Systematic evolution of a DNA aptamer binding to rat brain tumor microvessels. selective targeting of endothelial regulatory protein pigpen. *J Biol Chem* **276**, 16464–16468 (2001).
 346. Elle, I. C. *et al.* Selection of LNA-containing DNA aptamers against recombinant human CD73. *Mol. Biosyst.* **11**, 1260–70 (2015).
 347. Shangguan, D. *et al.* Aptamers evolved from live cells as effective molecular probes for cancer

- study. *Proc Natl Acad Sci U S A* **103**, 11838–11843 (2006).
348. Zhou, J. & Rossi, J. J. The therapeutic potential of cell-internalizing aptamers. *Curr Top Med Chem* **9**, 1144–1157 (2009).
 349. McNamara, J. O. *et al.* Cell type-specific delivery of siRNAs with aptamer-siRNA chimeras. *Nat. Biotechnol.* **24**, 1005–15 (2006).
 350. Sefah, K., Shangguan, D., Xiong, X., O'Donoghue, M. B. & Tan, W. Development of DNA aptamers using Cell-SELEX. *Nat Protoc* **5**, 1169–1185 (2010).
 351. Magalhães, M. L. B. *et al.* A general RNA motif for cellular transfection. *Mol. Ther.* **20**, 616–24 (2012).
 352. Thiel, K. W. *et al.* Delivery of chemo-sensitizing siRNAs to HER2+-breast cancer cells using RNA aptamers. *Nucleic Acids Res* **40**, 6319–6337 (2012).
 353. Mi, J. *et al.* In vivo selection of tumor-targeting RNA motifs. *Nat. Chem. Biol.* **6**, 22–4 (2010).
 354. Cheng, C., Chen, Y. H., Lennox, K. a, Behlke, M. a & Davidson, B. L. In vivo SELEX for Identification of Brain-penetrating Aptamers. *Mol. Ther. Nucleic Acids* **2**, e67 (2013).
 355. Guo, S., Tschammer, N., Mohammed, S. & Guo, P. Specific delivery of therapeutic RNAs to cancer cells via the dimerization mechanism of phi29 motor pRNA. *Hum. Gene Ther.* **16**, 1097–109 (2005).
 356. Thiel, K. W. & Giangrande, P. H. Intracellular delivery of RNA-based therapeutics using aptamers. *Ther. Deliv.* **1**, 849–61 (2010).
 357. Zhou, J. & Rossi, J. J. Cell-specific aptamer-mediated targeted drug delivery. *Oligonucleotides* **21**, 1–10 (2011).
 358. Zhou, J., Li, H., Zhang, J., Piotr, S. & Rossi, J. Development of cell-type specific anti-HIV gp120 aptamers for siRNA delivery. *J. Vis. Exp.* 1–9 (2011). doi:10.3791/2954
 359. Wilner, S. E. *et al.* An RNA alternative to human transferrin: a new tool for targeting human cells. *Mol. Ther. Nucleic Acids* **1**, e21 (2012).
 360. Dai, F., Zhang, Y., Zhu, X., Shan, N. & Chen, Y. Anticancer role of MUC1 aptamer-miR-29b chimera in epithelial ovarian carcinoma cells through regulation of PTEN methylation. *Target. Oncol.* **7**, 217–25 (2012).
 361. Dai, F., Zhang, Y., Zhu, X., Shan, N. & Chen, Y. The anti-chemoresistant effect and mechanism of MUC1 aptamer-miR-29b chimera in ovarian cancer. *Gynecol. Oncol.* **131**, 451–9 (2013).
 362. Esposito, C. L. *et al.* Multifunctional Aptamer-miRNA Conjugates for Targeted Cancer Therapy. *Mol. Ther.* (2014). doi:10.1038/mt.2014.5
 363. Mallikaratchy, P. *et al.* Aptamer directly evolved from live cells recognizes membrane bound immunoglobulin heavy mu chain in Burkitt's lymphoma cells. *Mol. Cell. Proteomics* **6**, 2230–8 (2007).
 364. Wu, Y., Sefah, K., Liu, H., Wang, R. & Tan, W. DNA aptamer-micelle as an efficient detection/delivery vehicle toward cancer cells. *Proc Natl Acad Sci U S A* **107**, 5–10 (2010).
 365. Osborne, S. E., Matsumura, I. & Ellington, A. D. Aptamers as therapeutic and diagnostic reagents: problems and prospects. *Curr. Opin. Chem. Biol.* **1**, 5–9 (1997).

366. Stovall, G. M. *et al.* In vitro selection using modified or unnatural nucleotides. *Curr. Protoc. Nucleic Acid Chem.* **56**, 9.6.1–9.6.33 (2014).
367. Edwards, S. L. *et al.* Targeting VEGF with LNA-stabilized G-rich oligonucleotide for efficient breast cancer inhibition. *Chem. Commun.* 9499–9502 (2015). doi:10.1039/C5CC02756J
368. Kong, H. Y. & Byun, J. Nucleic acid aptamers: New methods for selection, stabilization, and application in biomedical science. *Biomol. Ther.* **21**, 423–434 (2013).
369. Yu, D. *et al.* Modifications incorporated in CpG motifs of oligodeoxynucleotides lead to antagonist activity of toll-like receptors 7 and 9. *J. Med. Chem.* **52**, 5108–14 (2009).
370. Burmeister, P. E. *et al.* Direct in vitro selection of a 2'-O-methyl aptamer to VEGF. *Chem. Biol.* **12**, 25–33 (2005).
371. Healy, J. M. *et al.* Pharmacokinetics and biodistribution of novel aptamer compositions. *Pharm. Res.* **21**, 2234–46 (2004).
372. Zhou, J. *et al.* Functional in vivo delivery of multiplexed anti-HIV-1 siRNAs via a chemically synthesized aptamer with a sticky bridge. *Mol. Ther.* **21**, 192–200 (2013).
373. Zhou, J. *et al.* Cell-specific RNA aptamer against human CCR5 specifically targets HIV-1 susceptible cells and inhibits HIV-1 infectivity. *Chem. Biol.* **22**, 379–90 (2015).
374. Zhou, J. *et al.* Selection, characterization and application of new RNA HIV gp 120 aptamers for facile delivery of Dicer substrate siRNAs into HIV infected cells. *Nucleic Acids Res.* **37**, 3094–109 (2009).
375. Zhou, J. *et al.* Dual functional BAFF receptor aptamers inhibit ligand-induced proliferation and deliver siRNAs to NHL cells. *Nucleic Acids Res.* **41**, 4266–83 (2013).
376. Williams, K. P. *et al.* Bioactive and nuclease-resistant L-DNA ligand of vasopressin. *Proc. Natl. Acad. Sci. U. S. A.* **94**, 11285–90 (1997).
377. Klussmann, S., Nolte, A., Bald, R., Erdmann, V. A. & Fürste, J. P. Mirror-image RNA that binds D-adenosine. *Nat. Biotechnol.* **14**, 1112–5 (1996).
378. Nolte, A., Klussmann, S., Bald, R., Erdmann, V. A. & Fürste, J. P. Mirror-design of L-oligonucleotide ligands binding to L-arginine. *Nat. Biotechnol.* **14**, 1116–9 (1996).
379. Vater, A. & Klussmann, S. Turning mirror-image oligonucleotides into drugs: the evolution of Spiegelmer[®] therapeutics. *Drug Discov. Today* **20**, 147–55 (2015).
380. Schmidt, K. S. *et al.* Application of locked nucleic acids to improve aptamer in vivo stability and targeting function. *Nucleic Acids Res.* **32**, 5757–65 (2004).
381. Keefe, A. D., Pai, S. & Ellington, A. Aptamers as therapeutics. *Nat. Rev. Drug Discov.* **9**, 537–50 (2010).
382. Macugen AMD Study Group *et al.* Pegaptanib 1-year systemic safety results from a safety-pharmacokinetic trial in patients with neovascular age-related macular degeneration. *Ophthalmology* **114**, 1702–12 (2007).
383. Floege, J. *et al.* Novel approach to specific growth factor inhibition in vivo: antagonism of platelet-derived growth factor in glomerulonephritis by aptamers. *Am. J. Pathol.* **154**, 169–79 (1999).

384. Tan, L., Neoh, K. G., Kang, E.-T., Choe, W. S. & Su, X. PEGylated anti-MUC1 aptamer-doxorubicin complex for targeted drug delivery to MCF7 breast cancer cells. *Macromol. Biosci.* **11**, 1331–5 (2011).
385. Diener, J. L. *et al.* Inhibition of von Willebrand factor-mediated platelet activation and thrombosis by the anti-von Willebrand factor A1-domain aptamer ARC1779. *J. Thromb. Haemost.* **7**, 1155–62 (2009).
386. Wu, Y., Sefah, K., Liu, H., Wang, R. & Tan, W. DNA aptamer-micelle as an efficient detection/delivery vehicle toward cancer cells. *Proc. Natl. Acad. Sci. U. S. A.* **107**, 5–10 (2010).
387. Shiang, Y.-C. *et al.* Highly efficient inhibition of human immunodeficiency virus type 1 reverse transcriptase by aptamers functionalized gold nanoparticles. *Nanoscale* **5**, 2756–64 (2013).
388. Kasahara, Y. & Kuwahara, M. Artificial specific binders directly recovered from chemically modified nucleic acid libraries. *J. Nucleic Acids* **2012**, 156482 (2012).
389. Rohde, J.-H., Weigand, J. E., Suess, B. & Dimmeler, S. A Universal Aptamer Chimera for the Delivery of Functional microRNA-126. *Nucleic Acid Ther.* **25**, 141–51 (2015).
390. Buitrago, M. *et al.* The transcriptional repressor Nab1 is a specific regulator of pathological cardiac hypertrophy. *Nat. Med.* **11**, 837–44 (2005).
391. Barbas, C. F., Burton, D. R., Scott, J. K. & Silverman, G. J. Quantitation of DNA and RNA. *CSH Protoc.* **2007**, pdb.ip47 (2007).
392. Schindelin, J. *et al.* Fiji: an open-source platform for biological-image analysis. *Nat. Methods* **9**, 676–82 (2012).
393. Efe, J. a *et al.* Conversion of mouse fibroblasts into cardiomyocytes using a direct reprogramming strategy. *Nat. Cell Biol.* **13**, 215–22 (2011).
394. Snyder, A., Fraser, S. T. & Baron, M. H. Bone morphogenetic proteins in vertebrate hematopoietic development. *J. Cell. Biochem.* **93**, 224–232 (2004).
395. Bailey, T. L. *et al.* MEME SUITE: tools for motif discovery and searching. *Nucleic Acids Res.* **37**, W202–8 (2009).
396. Bailey, T. L. DREME: motif discovery in transcription factor ChIP-seq data. *Bioinformatics* **27**, 1653–9 (2011).
397. Bailey, T. L. & Elkan, C. Fitting a mixture model by expectation maximization to discover motifs in biopolymers. *Proc. Int. Conf. Intell. Syst. Mol. Biol.* **2**, 28–36 (1994).
398. Reuter, J. S. & Mathews, D. H. RNAstructure: software for RNA secondary structure prediction and analysis. *BMC Bioinformatics* **11**, 129 (2010).
399. Korff, T. & Augustin, H. G. Tensional forces in fibrillar extracellular matrices control directional capillary sprouting. *J. Cell Sci.* **112** (Pt 1, 3249–58 (1999).
400. Fish, J. E. *et al.* miR-126 regulates angiogenic signaling and vascular integrity. *Dev Cell* **15**, 272–284 (2008).
401. Smith, A. W. *et al.* Direct reprogramming of mouse fibroblasts to cardiomyocyte-like cells using Yamanaka factors on engineered poly(ethylene glycol) (PEG) hydrogels. *Biomaterials* **34**, 6559–71 (2013).

402. Harding, C., Heuser, J. & Stahl, P. Receptor-mediated endocytosis of transferrin and recycling of the transferrin receptor in rat reticulocytes. *J. Cell Biol.* **97**, 329–39 (1983).
403. Zhang, J. *et al.* microRNA 126 inhibits the transition of endothelial progenitor cells to mesenchymal cells via the PIK3R2-PI3K/Akt signalling pathway. *PLoS One* **8**, e83294 (2013).
404. Park, S. *et al.* Interleukin-18 induces transferrin expression in breast cancer cell line MCF-7. *Cancer Lett.* **286**, 189–95 (2009).
405. Jones, D. T., Trowbridge, I. S. & Harris, A. L. Effects of transferrin receptor blockade on cancer cell proliferation and hypoxia-inducible factor function and their differential regulation by ascorbate. *Cancer Res.* **66**, 2749–56 (2006).
406. Grimm, D. *et al.* Fatality in mice due to oversaturation of cellular microRNA/short hairpin RNA pathways. *Nature* **441**, 537–41 (2006).
407. Qin, J. Y. *et al.* Systematic comparison of constitutive promoters and the doxycycline-inducible promoter. *PLoS One* **5**, e10611 (2010).
408. Su, J., Zhu, Z., Xiong, F. & Wang, Y. Hybrid cytomegalovirus-U6 promoter-based plasmid vectors improve efficiency of RNA interference in zebrafish. *Mar. Biotechnol. (NY)*. **10**, 511–7 (2008).
409. Weiwei, M., Zhenhua, X., Feng, L., Hang, N. & Yuyang, J. A significant increase of RNAi efficiency in human cells by the CMV enhancer with a tRNAlys promoter. *J. Biomed. Biotechnol.* **2009**, 514287 (2009).
410. Kiefer, K., Clement, J., Garidel, P. & Peschka-Süss, R. Transfection efficiency and cytotoxicity of nonviral gene transfer reagents in human smooth muscle and endothelial cells. *Pharm. Res.* **21**, 1009–17 (2004).
411. McLenachan, S., Sarsero, J. P. & Ioannou, P. A. Flow-cytometric analysis of mouse embryonic stem cell lipofection using small and large DNA constructs. *Genomics* **89**, 708–20 (2007).
412. Dalby, B. *et al.* Advanced transfection with Lipofectamine 2000 reagent: primary neurons, siRNA, and high-throughput applications. *Methods* **33**, 95–103 (2004).
413. Fang, X. & Tan, W. Aptamers generated from cell-SELEX for molecular medicine: a chemical biology approach. *Acc. Chem. Res.* **43**, 48–57 (2010).
414. Stacy, L. B., Yu, Q., Horak, K. & Larson, D. F. Effect of angiotensin II on primary cardiac fibroblast matrix metalloproteinase activities. *Perfusion* **22**, 51–55 (2007).
415. Graham, E. L. *et al.* Isolation, culture, and functional characterization of adult mouse cardiomyocytes. *J. Vis. Exp.* e50289 (2013). doi:10.3791/50289
416. Hill, J. & Olson, E. Cardiac plasticity. *N. Engl. J. Med.* **358**, 1370–1380 (2008).
417. Protze, S. *et al.* A new approach to transcription factor screening for reprogramming of fibroblasts to cardiomyocyte-like cells. *J. Mol. Cell. Cardiol.* **53**, 323–32 (2012).
418. Janssen, H. L. A. *et al.* Treatment of HCV infection by targeting microRNA. *N. Engl. J. Med.* **368**, 1685–94 (2013).
419. Miravirsen works against hepatitis C virus. *BMJ* **346**, f2069 (2013).
420. Mallikaratchy, P. R. *et al.* A multivalent DNA aptamer specific for the B-cell receptor on human

- lymphoma and leukemia. *Nucleic Acids Res.* **39**, 2458–2469 (2011).
421. Subramanian, N. *et al.* EpCAM aptamer mediated cancer cell specific delivery of EpCAM siRNA using polymeric nanocomplex. *J. Biomed. Sci.* **22**, 4 (2015).
422. Zhou, J., Bobbin, M. L., Burnett, J. C. & Rossi, J. J. Current progress of RNA aptamer-based therapeutics. *Front. Genet.* **3**, 234 (2012).

9. Glossary

Abbreviation	Meaning
2'-F	2'-deoxy-2'-fluoro modified RNA
°C	Degree Celsius
AGO	Argonaut
AMCF	Adult murine cardiac fibroblast
ATP	Adenosine triphosphate
BMP4	Bone morphogenic protein 4
BSA	Bovine serum albumine
C	CHIR99021
CA	Control aptamer
Cand	Candidate
CASD	Cell activation and signaling-directed
CF	Cardiac fibroblasts
Ch1-4	TRA-microRNA chimera 1-4
CM	Cardiomyocytes
cm	Centimeters
CMV	Cytomegalovirus
CN	Copy number
Cy3	Cyanine 3
cTnT	Cardiac Troponin T
CTP	Cytidine triphosphate
ctrl	Control; usually scramble or negmiR
DAPI	4',6-diamidino-2-phenylindole
DDR2	Discoidin domain-containing receptor 2
DMEM	Dulbecco's modified Eagle medium
DMPC	1,2-dimyristoyl-sn-glycero-3-phosphocholine
DNA	Deoxyribonucleic acid
dNTP	Deoxy-nucleoside triphosphates
DPBS	Dulbecco's phosphate buffered solution
DPBS+	Dulbecco's phosphate buffered solution with MgCl ₂ and CaCl ₂
dsDNA/RNA	Double stranded DNA/RNA
DTT	Dithiothreitol
EBM	Endothelial cell basal medium
EBSS	Earle's balanced salt solution
ECM	Extracellular Matrix
EGM	Endothelial cell growth medium
EC	Endothelial cells
EEA1	Early Endosome antigen 1
EGFL7	EGF-like domain-containing protein 7
F	Forskolin
FA	Formaldehyde
FBS	Fetal bovine serum
FSP-1	Fibroblast specific protein-1
GHT	Combination of the transcription factors Gata4, Hand2 and Tbx5
GHMT	Combination of the transcription factors Gata4, Hand2, Mef2c and Tbx5
GIRM	General internalizing RNA motif
GMT	Combination of the transcription factors Gata4, Mef2c and Tbx5

GMTMM	Combination of the transcription factors Gata4, Mef2c, Tbx5, MyocD and Mesp1
GTP	Guanosine triphosphate
h	Hours
HNGMT	Combination of the transcription factors Gata4, Hand2, Mef2c, Tbx5 and Nkx 2.5
HRP	Horseradish peroxidase
hsa	Homo sapiens
HSC	Hematopoietic stem cells
HUVEC	Human umbilical vein endothelial cells
iCM	Induced Cardiomyocytes
IRS-1	Insulin receptor substrate-1
Jl1	Jak-Inhibitor 1
Klf2	Krüppel-like factor 2
LB	Lithium tetraborate
LDL	Low-density lipid particles
µg	Microgram
µm	Micrometer
µM	Micromolar
M-199	Medium-199
MAP	Mitogen-activated protein
MCF7	MCF7 human breast cancer line
MEC	Murine endothelial cells
MEF	Murine embryonic fibroblasts
mg	Milligram
min	Minutes
miR	MicroRNA
ml	Milliliters
mM	Millimolar
MMP	Matrix metalloproteinase
mmu	Mus musculus
MSC	Mesenchymal stem cells
MTT	3-[4,5-dimethylthiazol-2-yl]-2,5- diphenyltetrazolium bromide
Myh6	Myosin heavy chain 6, also called α -myosin heavy chain
Myl2	Myosin light chain 2
MyocD	Myocardin
NF-κB	Nuclear factor kappa-light-chain-enhancer of activated B cells
ng	Nanogram
nm	Nanometer
nM	Nanomolar
nt	Nucleotides
Oct4	octamer-binding transcription factor 4
ORF	Open reading frame
P	Parnate
PIK3	Phosphatidylinositol-4,5-bisphosphate 3-kinase
PIK3R2	Phosphatidylinositol-4,5-bisphosphate 3-kinase regulatory subunit β
Pre-miR	Precursor of microRNA
Pri-miR	Primary microRNA
P/S	Penicillin and streptomycin solution

qPCR	Quantitative PCR
RISC	RNA induced silencing complex
RNA	Ribonucleic acid
RNAi	RNA-interference
ROS	Reactive oxygen species
RPLP0	60S acidic ribosomal protein P0
RT	Reverse transcription
S	SB431542
scr	Scramble control
SDF-1	Stromal cell-derived growth factor 1
sec	seconds
SELEX	Systematic evolution of ligands by exponential enrichment
siRNA	Small inhibitory RNA
shRNA	Small hairpin RNA
SOX2	Sex determining region Y-box 2
ssDNA/RNA	Single stranded DNA/RNA
SK-BR3	SK-BR3 human breast cancer line
SMC	smooth muscle cell
SPRED-1	Sprouty-related, EVH1 domain-containing protein 1
TBST	Tris-buffered saline solution containing 1% Tween20
Tfs	Transcription factors
TGF-β	Transforming growth factor- β 1
TNF-α	Tumor necrosis factor- α
TRA	Transferrin receptor aptamer
TrfRc	Transferrin receptor c
tRNA	Transfer RNA
TTP	Thymidine triphosphate
U	Units of protein activity, defined and measured by the manufacturer
untr	Untreated
UTP	Uridine triphosphate
UTR	3' untranslated region
V	Volt
Vol	Volume, usually used to denote how many volumes of another solution is added
VEGF	Vascular endothelial cell growth factor
VCAM-1	Vascular cell adhesion molecule 1
VSMC	Vascular smooth muscle cells
x g	Times gravity (as in centrifuged at 200 times the force of gravity)

10. Eidesstattliche Erklärung

Ich erkläre ehrenwörtlich, dass ich die dem Fachbereich Biologie der Johann Wolfgang Goethe-Universität Frankfurt am Main zur Promotionsprüfung eingereichte Dissertation mit dem Titel

„Aptamer-mediierter Transport von microRNAs in Zellen des kardiovaskulären Systems“

in dem Institut für kardiovaskuläre Regeneration an der Universitätsklinik der Goethe Universität unter Betreuung und Anleitung von Prof. Dr. Stefanie Dimmeler mit Unterstützung durch Prof. Dr. Beatrix Süß und Dr. Julia E. Weigand ohne sonstige Hilfe selbst durchgeführt und bei der Abfassung der Arbeit keine anderen als die in der Dissertation angeführten Hilfsmittel benutzt habe. Darüber hinaus versichere ich, nicht die Hilfe einer kommerziellen Promotionsvermittlung in Anspruch genommen zu haben.

Ich habe bisher an keiner in- oder ausländischen Universität ein Gesuch um Zulassung zur Promotion eingereicht. Die vorliegende Arbeit wurde bisher nicht als Dissertation eingereicht.

Einige vorliegende Ergebnisse der Arbeit wurden in folgendem Publikationsorgan veröffentlicht:

Rohde J-H, Weigand JE, Suess B, Dimmeler S. A Universal Aptamer Chimera for the Delivery of Functional microRNA-126. *Nucleic Acid Ther.* 2015;25(3):141–51. doi:10.1089/nat.2014.0501.

(Ort, Datum)

(Unterschrift)

11. Copyright permission

Dear Jan:

Copyright permission is granted for this request.

Kind regards,

Karen Ballen

Manager

NUCLEIC ACID THERAPEUTICS

From: jan.h.rohde@gmail.com [mailto:jan.h.rohde@gmail.com]

Sent: Wednesday, June 22, 2016 5:50 AM

To: Ballen, Karen

Subject: LiebertPub Website Customer Question

Name - Jan-H. Rohde

Position -

Department -

Institution/affiliation -

Address Line1 -

City -

State -

Country - GER

Zip -

Email - jan.h.rohde@gmail.com

Phone -

Regarding - Reprints and permissions

For Publication - Nucleic Acid Therapeutics

Questions/Comments - I have had the luck to be able to publish an article in Nucleic Acid Therapeutics last year, titled A Universal Aptamer Chimera for the Delivery of Functional microRNA-126 (2015 Jun;25(3):141-51). As I am finishing my PhD I would like permission to use some of the figures in my thesis as well.